REPORT DOCUMENTATION PAGE

Form Approved OMB No. 0704-0188

1. AGENCY USE ONLY (Leave blank)	2. REPORT DATE	3. REPORT TYPE AND DATES COVERED
	1994	Final Report

4. TITLE AND SUBTITLE

Wide Range Equation of State for Large Computer Codes: User Guide

5. FUNDING NUMBERS

F6170893W1082

6. AUTHOR(S)

I.V. Lomonosov, V.E. Fortov, K.V. Khishchenko

7. PERFORMING ORGANIZATION NAME(S) AND ADDRESS(ES)

High Energy Density Research Center
Russian Academy of Sciences
Izhorskaya Str. 14/19
Moscow 127412, Russia

8. PERFORMING ORGANIZATION REPORT NUMBER

SPC-93-4074

9. SPONSORING/MONITORING AGENCY NAME(S) AND ADDRESS(ES)

EOARD
PSC 802 BOX 14
FPO AE 09499-0200

10. SPONSORING/MONITORING AGENCY REPORT NUMBER

SPC-93-4074

11. SUPPLEMENTARY NOTES

12a. DISTRIBUTION/AVAILABILITY STATEMENT

Approved for public release; distribution is unlimited.

12b. DISTRIBUTION CODE

A

13. ABSTRACT (Maximum 200 words)

The goal of the report is description of work of the EOS code. It requires minimum knowledges in hydrodynamics, thermodynamics, and programming. The manual is devoted to typical hypercode user with an experience in numerical modeling of such processes, as high-velocity impact, for example.

14. SUBJECT TERMS	15. NUMBER OF PAGES
	141
	16. PRICE CODE
	N/A

17. SECURITY CLASSIFICATION OF REPORT	18. SECURITY CLASSIFICATION OF THIS PAGE	19. SECURITY CLASSIFICATION OF ABSTRACT	20. LIMITATION OF ABSTRACT
UNCLASSIFIED	UNCLASSIFIED	UNCLASSIFIED	UL

HEDRC REPORT

Printed November 1994

WIDE-RANGE EQUATION OF STATE FOR LARGE COMPUTER CODES: USER GUIDE

I. V. Lomonosov, V. E. Fortov, and K. V. Khishchenko

Prepared by
High Energy Density Research Center
Russian Academy of Sciences
Izhorskaya Str. 14/19, Moscow 127412, Russia
for USAF
by contract SPC-93-4074

WIDE-RANGE EQUATION OF STATE FOR LARGE COMPUTER CODES: USER GUIDE

I. V. Lomonosov, V. E. Fortov, and K. V. Khishchenko

High Energy Density Research Center
Russian Academy of Sciences
Izhorskaya Str. 14/19, Moscow 127412, Russia

Abstract

This is fourth (12-month) report performed for USAF by contract SPC-93-4074. Described are the generation of output tables, prepared by the multi-phase equation-of-state (EOS) code, their internal structure and utilization. Regimes of calculations for different cases are discussed with typical examples. Possible code problems, errors are also given. Appendix contents useful thermodynamical calculations for all metals.

1. Introduction

The goal of the report is description of work of the EOS code. It requires minimum knowledges in hydrodynamics, thermodynamics and programming. The manual is devoted to typical hydrocode user with an experience in numerical modeling of such processes, as high-velocity impact, for example.

The code is oriented to users which utilize different numerical schemes and methods. The output tables can be obtained in dependence of 3 pairs of input data, viz. *(volume, temperature), (volume, internal energy)* and *(volume, pressure).*

Discussed are also such necessary things, as normilizing conditions, structure of tables, possible problems, mistakes and code errors.

2. About the EOS code

The multi-phase EOS (file **tabeos.exe**) is computer code which has been developed to use real thermodynamical data of metals in solid, liquid, gas, plasma states, solid-liquid and liquid-gas regions in hydrocodes.

2.1. Region of applicability

The EOS provides for an accurate calculation of all equilibrium thermodynamical functions in following range of the phase diagram:

1. to 100-fold compressions at T=0 K;

2. at high temperature the limits are:

up to about 100 Mbar point on the principal Hugoniot and all states which lie down the release isentrope, originating in the 100 Mbar point, i.e $0.001<V_0 / V<3\text{-}4$.

2.2. Phase boundaries

The EOS code can not be used directly in hydrocodes as it calculates correctly by solving numerically the equation for Gibb's energy in different phase states. It is possible to use only output tabular data. Each point in these tables has its own phase identificator.

The nomencalture of the identificators is given in Table 1 (file **physid.tab**).

Table 1. Nomenclature of the phase identificatores.

Identificator value	Physical state
0	unphysical region
1	solid
2	solid + liquid, melting
3	liquid
4	liquid + gas, evaporation
5	plasma

2.3. Input and output

The code calculates tables of thermodynamical functions with maximum dimension 256*256 in linear, logarithm ore arbitrary grid.

Users dealing with hydrocodes need different dependencies, such as *pressure(volume, temperature), pressure(volume, internal energy)* or *internal energy(volume,pressure).* The code provides for calculations in the three regimes, i.e. when input pairs are *(volume, temperature)*, *(volume, internal energy)*, and *(volume,pressure)*.

The scale of the input greed (let's suppose, *volume*, for instance) can be linear, logarithm or arbitrary. Details are described below.

As output, generated are following tables: *pressure, entropy, enthalpy, internal energy, isentropical and isothermal sound velocities, temperature, heat capacities at constant volume and pressure, phase identificators.*

3. How it works?

This section contents the details of organizing calculations, structure of input and output data.

3.1. Load

All manipulations with regime of calculations, dimension of grid, and others, are made by editing managing file **data.man**. So if you need to calculate new tables, you should correct the file.

data.man must be placed in the same directory, as **tabeos.exe** (the EOS code) and **tt50.dat** (coefficients for EOS code). The output files with thermodynamic tables will be placed also in this work directory.

So, you work directory will contain following files:

tabeos.exe - the EOS code;
tt50.dat - internal data for EOS code;
data.man - managing file;
volume.in - file containing data for arbitrary-volume grid;
temper.in - file containing data for arbitrary-temperature grid;
pressu.in - file containing data for arbitrary-pressure grid;
energy.in - file containing data for arbitrary-internal_energy grid.

You may calculate tables of different dimension in different grids for any one of available ten metals: ***Li, Al, Fe, Ni, Cu, Mo, Ta, W, Au, Pb***.

At first you should clearly understand, what region of the phase diagram is of the most interst and significance for your calculations and introduce the limits and dimension of input grid into managing file **data.man**. After completing the edition of file **data.man** you may run the calculations.

3.2. Structure of managing file **data.man**

The typical contents of the file **data.man** is following:

Parameter	Unit	Comment
01	[-]	number of material used
0.300E-03	10**3 [K]	initial temperature
0.100E+03	10**3 [K]	final temperature
0.200E-00	[cc/g]	initial volume
0.100E+02	[cc/g]	final volume
256	[-]	number of points in temperature grid
256	[-]	number of points in volume grid
+0	[-]	scale identificator (linear grid)
+0	[-]	scale identificator (linear grid)
+0	[-]	output identificator
+0	[-]	regime identificator

In this file only 1-st column is used; the others contain only comments.

Let's clarify each value in the column:

- number of material used (note, that only I2 format *must be used*):

Number	01	02	03	04	05	06	07	08	09	10
Metal	Li	Al	Fe	Ni	Cu	Mo	Ta	W	Au	Pb

- values of initial temperature, final temperature (*temperature* grid) or initial and final energy (*energy* grid) or initial and final pressure (*pressure* grid) are introduced by format E9.3;
- dimension of grid is limited to 256*256 and is introduced by format I3;
- scale identificator allows to calculate linear (+0), logarithm (+1) or arbitrary (-1) grid. The first scale identificator manages *energy, temperature, pressure* grids, while second always manages the *volume* grid. If scale identificator equals -1, the data are read from file and in this case the previously read data are not significant;

- output identificator manages the format of output tables, they can be written in fixed (+0) or binary (+1) format;
- regime identificator (ri) forces the code to calculate output tables using as input pairs *volume-temperature* (ri = +0), *volume-internal_energy* (ri = +1) or *volume-pressure* (ri = -1).

3.3. Structure of input and output data

As it has been written in Section 3.1, you should have in your work directory special files for calculation tables in arbitrary grids. It is possible to have such arbitrary data for both X (volume) and Y (temperature, pressure, internal_energy) grids.

Note, that units for input data are following: pressure [GPa], temperature [10^3 K], internal energy [kJ/g], volume [cc/g]; all thermodynamical functions are given per 1 g of metal.

See in Appendies a simple FORTRAN file **make$tab.f** (it is also included in EOS Kit) created especially for producing files ***.in.**

Also given in Appendies is file **read.f**, which allows to load tables and find any desired point.

Correspondence between output files and thermodynamical functions is following:

Filename	Function	Unit
temper.tab	temperature	10^3 K
pressu.tab	pressure	GPa
energy.tab	internal energy	kJ/g
entropy.tab	entropy	J/(gK)
sndvls.tab	isentropic sound velocity	km/s
sndvlt.tab	isothermal sound velocity	km/s
hcapap.tab	heat capacity at constant pressure	J/(gK)
hcapav.tab	heat capacity at constant volume	J/(gK)
physid.tab	physical-state (solid, liquid,...) identificator	dimensionless

3.4 Normilizing conditions

Obviously, the knowledge of normilizing conditions is of importance in hydrocalculations. In the EOS they are following:

ar room temperature (293 K), normal volume ($V=V_0$) pressure p=1 bar (± 0.001%), internal energy E=0 kJ/(gK) ($\pm 10^{-8}$, computer zero), entropy s=0 J/(gK) ($\pm 10^{-8}$, computer zero).

4. Running calculations

A model test of calculation thermodynamical tables for a typical problem is given in this section.

4.1. Problem setup

Let's suppose that we should generate correct tables for calculation high-velocity (22 km/s) impact with aluminum as impactor (1 cm thickness) and target (also 1 cm) material. Our goal is to match the velocity, form and mass of debris clouds. Our code needs *volume-temperature* calcualtions.

I choose 22 km/s to have a large amount of evaporated metal and all physical states during the process - solid, liquid, gas and plasma.

4.2. Determination of grid limits

At first, we should to determine the maximum value of pressure and entropy. Given in Appendies shock Hugoniot and saturation curve for aluminum indicate, that under conditions of our impact realized will be following states:

- in shocked material: p<5.78 Mbar, s<4.57 J/(gK), V>0.161 cc/g, T<33500 K;
- aluminum will be evaporated on release isentrope with s=4.57 J(gK), so final value of volume will be V=8.69E+03 cc/g, of temperature T=300 K.

4.3. Choosing of grids

It is reasonable to make a detailed logarithm grid for volume, i.e. to have about 150-200 points; as for temperature, 100 points in logarithm grid is enough.

Execution **make$tab.exe** will make any desired grid. For instance, we may pay more attention to evaporation and divide the volume grid into 3 regions:

- 0.161<V<0.369 - 30 points from shocked metal to normal volume;
- 0.369<V<1.188 - 100 points from normal volume to critical one;
- 1.88<V<8.69E+03 - 70 points from critical volume to full evaporation.

4.4. Managing file

Finally, file **data.man** is following:

Parameter	Unit	Comment
02	[-]	number of material used
0.300E-00	10**3 [K]	initial temperature
0.350E+03	10**3 [K]	final temperature
0.160E-00	[cc/g]	initial volume
0.100E+05	[cc/g]	final volume
100	[-]	number of points in temperature grid
200	[-]	number of points in volume grid
+1	[-]	scale identificator (linear grid)
+1	[-]	scale identificator (linear grid)
+0	[-]	output identificator
+0	[-]	regime identificator

5. Possible errors

The code can stop calculations in 2 following sitiations:

- p=const, T=const functions are near critical point. In this case sometimes (when T or P are less then critical-point parameters in 0.1-0.5%) the code can not find numerical soluion in 2-phase liquid-gas region, as the liquid-gas equilibrium curve is approximately horizontal.

Recommendation: match the values of T and P and avoid this sutuation.

- the logical scheme of the code requires to begin calculations from condensed phase; they must begin from $V_{initial} \leq V_0$, otherwise the code can not find correctly the phase boundaries.

Recommendation: introduce initial volume less or of the order of V_0 then increase volume on the volume grid. Never start calculations inside liquid-gas mixture.

6. References

Utilizing the code, refer to [1] for EOS of Al, Cu, Pb, Li and to [2] for Fe, Ni, Mo, Ta, W metals:

[1] A. V. Bushman, G. I. Kanel', A. L. Ni, and V. E. Fortov, *Intense Dynamic Loading of Condensed Matter,* New York: Taylor&Francis, 1993.

[2] V. E. Fortov and I. V. Lomonosov, High Pressure Research (1995) [in press].

7. Servise office

Call for help Igor Lomonosov:

Address	Fax/Phone	E-mail
Institute of Chemical Physics in Chernogolovka RAS P.O. 142432 Chernogolovka Moscow region Russia	(7-095)485-7988 (7-096)517-1870	*ivl@ficp.ac.ru* *ivl@hedric.msk.su*

(e-mail is preferred).

Send briff description of your problem with file **data.man.**

Appendixes

Placed in appendixes are results of phase-diagram calcualtions for metals and few useful FORTRAN programs for preparing, reading and manipulating the input and output data.

Appendix A. Phase diagrams of metals

Given in the Appenidxes A1-A10 are calculations of phase diagrams for Li, Al, Fe, Ni, Cu, Mo, Ta, W, Au, Pb.

Nomenclature:

Symbol	Name	Unit
P	pressure	GPa
T	temperature	10^3 K
VS	volume of solid phase	cc/g
VL	volume of liquid phase	cc/g
VG	volume of gas phase	cc/g
SS	entropy of solid phase	J/(gK)
SL	entropy of liquid phase	J/(gK)
SG	entropy of gase phase	J/(gK)
ES	energy of solid phase	kJ/g
EL	energy of liquid phase	kJ/g
EG	energy of gas phase	kJ/g
E	internal energy	kJ/g
S	entropy	J/(gK)
V	volume	cc/g
D	shock velocity	km/s
U	mass velocity	km/s
CS	sound velocity	km/s
CV	heat capacity	J/(gK)

Empty lines in the shock adiabat tables mark the position of melting.

Appendix A1

Lithium

MELTING CURVE

P	T	VS/VS0	VS	VL	ES	EL	DV/VS	DS/R
1.000-4	4.540-1	1.000 0	1.909 0	1.948 0	6.184-1	1.052 0	2.041-2	7.901-1
1.000 0	4.849-1	9.242-1	1.765 0	1.786 0	6.785-1	1.110 0	1.211-2	7.711-1
1.500 0	4.948-1	8.937-1	1.707 0	1.723 0	7.346-1	1.171 0	9.436-3	7.687-1
2.000 0	5.024-1	8.668-1	1.655 0	1.667 0	8.035-1	1.247 0	7.326-3	7.686-1
2.500 0	5.080-1	8.427-1	1.609 0	1.618 0	8.828-1	1.334 0	5.628-3	7.702-1
3.000 0	5.122-1	8.210-1	1.568 0	1.574 0	9.705-1	1.430 0	4.240-3	7.728-1
4.000 0	5.174-1	7.832-1	1.495 0	1.499 0	1.166 0	1.641 0	2.123-3	7.801-1
5.000 0	5.194-1	7.513-1	1.434 0	1.435 0	1.381 0	1.873 0	6.007-4	7.888-1
6.000 0	5.194-1	7.237-1	1.382 0	1.381 0	1.611 0	2.117 0	-5.368-4	7.982-1
8.000 0	5.156-1	6.782-1	1.295 0	1.292 0	2.102 0	2.634 0	-2.106-3	8.176-1
1.000 1	5.090-1	6.417-1	1.225 0	1.221 0	2.618 0	3.172 0	-3.130-3	8.373-1
1.500 1	4.872-1	5.743-1	1.097 0	1.091 0	3.963 0	4.561 0	-4.605-3	8.863-1
2.000 1	4.632-1	5.267-1	1.006 0	1.000 0	5.333 0	5.967 0	-5.415-3	9.357-1
2.500 1	4.395-1	4.906-1	9.367-1	9.312-1	6.700 0	7.364 0	-5.935-3	9.866-1
3.000 1	4.168-1	4.618-1	8.817-1	8.762-1	8.053 0	8.743 0	-6.282-3	1.039 0
4.000 1	3.758-1	4.179-1	7.980-1	7.927-1	1.070 1	1.143 1	-6.587-3	1.149 0
5.000 1	3.413-1	3.856-1	7.362-1	7.314-1	1.326 1	1.402 1	-6.454-3	1.261 0
6.000 1	3.134-1	3.603-1	6.879-1	6.838-1	1.574 1	1.651 1	-5.985-3	1.369 0
8.000 1	2.741-1	3.227-1	6.161-1	6.133-1	2.049 1	2.124 1	-4.609-3	1.556 0
1.000 2	2.504-1	2.955-1	5.641-1	5.623-1	2.500 1	2.570 1	-3.318-3	1.695 0
1.500 2	2.233-1	2.504-1	4.781-1	4.774-1	3.537 1	3.598 1	-1.441-3	1.892 0
2.000 2	2.138-1	2.217-1	4.234-1	4.231-1	4.475 1	4.532 1	-6.438-4	1.983 0
2.500 2	2.102-1	2.014-1	3.845-1	3.844-1	5.340 1	5.394 1	-2.462-4	2.030 0
3.000 2	2.093-1	1.858-1	3.548-1	3.548-1	6.147 1	6.199 1	-1.655-5	2.059 0
4.000 2	2.109-1	1.634-1	3.119-1	3.120-1	7.629 1	7.679 1	2.298-4	2.089 0
5.000 2	2.143-1	1.475-1	2.817-1	2.818-1	8.977 1	9.027 1	3.561-4	2.105 0

SATURATION CURVE

P	T	T/TC	VL	VG	SL	SG	EL	EG
1.058-1	3.942 0	1.000 0	9.760 0	9.760 0	1.297 1	1.297 1	2.132 1	2.132 1
1.000-1	3.907 0	9.911-1	7.399 0	1.360 1	1.247 1	1.347 1	1.961 1	2.289 1
8.000-2	3.770 0	9.564-1	5.600 0	2.242 1	1.187 1	1.410 1	1.745 1	2.452 1
6.000-2	3.600 0	9.132-1	4.695 0	3.554 1	1.140 1	1.460 1	1.580 1	2.544 1
5.000-2	3.496 0	8.868-1	4.345 0	4.583 1	1.117 1	1.485 1	1.498 1	2.577 1
4.000-2	3.373 0	8.555-1	4.029 0	6.108 1	1.091 1	1.512 1	1.411 1	2.603 1
3.000-2	3.221 0	8.170-1	3.731 0	8.608 1	1.062 1	1.544 1	1.315 1	2.620 1
2.500-2	3.129 0	7.938-1	3.584 0	1.057 2	1.044 1	1.562 1	1.261 1	2.625 1
2.000-2	3.022 0	7.665-1	3.434 0	1.347 2	1.025 1	1.584 1	1.200 1	2.627 1
1.500-2	2.891 0	7.334-1	3.275 0	1.819 2	1.001 1	1.610 1	1.130 1	2.625 1
1.000-2	2.721 0	6.903-1	3.101 0	2.733 2	9.695 0	1.647 1	1.042 1	2.615 1
8.000-3	2.634 0	6.683-1	3.022 0	3.398 2	9.534 0	1.666 1	9.996 0	2.608 1
6.000-3	2.529 0	6.416-1	2.934 0	4.479 2	9.337 0	1.691 1	9.488 0	2.598 1
5.000-3	2.467 0	6.257-1	2.885 0	5.323 2	9.218 0	1.707 1	9.189 0	2.592 1
4.000-3	2.393 0	6.071-1	2.831 0	6.564 2	9.076 0	1.727 1	8.847 0	2.583 1
3.000-3	2.305 0	5.846-1	2.769 0	8.580 2	8.902 0	1.751 1	8.438 0	2.572 1
2.500-3	2.252 0	5.711-1	2.734 0	1.016 3	8.796 0	1.767 1	8.196 0	2.565 1
2.000-3	2.190 0	5.554-1	2.694 0	1.247 3	8.670 0	1.787 1	7.916 0	2.556 1
1.500-3	2.114 0	5.363-1	2.648 0	1.624 3	8.514 0	1.812 1	7.581 0	2.545 1
1.000-3	2.016 0	5.114-1	2.591 0	2.351 3	8.306 0	1.847 1	7.151 0	2.530 1
8.000-4	1.966 0	4.987-1	2.562 0	2.881 3	8.197 0	1.867 1	6.933 0	2.522 1
6.000-4	1.905 0	4.831-1	2.529 0	3.743 3	8.060 0	1.893 1	6.669 0	2.513 1
5.000-4	1.868 0	4.738-1	2.510 0	4.419 3	7.977 0	1.909 1	6.512 0	2.506 1
4.000-4	1.824 0	4.628-1	2.487 0	5.413 3	7.877 0	1.929 1	6.328 0	2.499 1
3.000-4	1.771 0	4.493-1	2.461 0	7.033 3	7.753 0	1.956 1	6.105 0	2.490 1
2.500-4	1.739 0	4.412-1	2.445 0	8.303 3	7.677 0	1.972 1	5.971 0	2.485 1
2.000-4	1.702 0	4.317-1	2.427 0	1.018 4	7.586 0	1.993 1	5.814 0	2.478 1
1.500-4	1.656 0	4.200-1	2.405 0	1.323 4	7.472 0	2.020 1	5.623 0	2.470 1
1.000-4	1.595 0	4.045-1	2.377 0	1.916 4	7.318 0	2.057 1	5.373 0	2.460 1

Lithium

SHOCK ADIABAT M= 1.000

P	T	V	S	E	D	U	CS	CV
1.000-4	2.930-1	1.860 0	-9.537-7	-8.382-8	.000 0	.000 0	4.662 0	3.633 0
5.000 0	4.291-1	1.424 0	5.397-1	1.091 0	6.297 0	1.477 0	6.146 0	3.683 0
6.000 0	4.688-1	1.376 0	7.639-1	1.451 0	6.552 0	1.703 0	6.347 0	3.692 0
7.103 0	5.178-1	1.331 0	1.032 0	1.878 0	6.818 0	1.938 0	6.551 0	3.701 0
7.103 0	5.178-1	1.331 0	1.031 0	1.878 0	6.818 0	1.938 0	6.423 0	5.401 3
8.000 0	5.157-1	1.294 0	1.235 0	2.264 0	6.993 0	2.128 0	6.545 0	2.652 3
9.898 0	5.094-1	1.225 0	1.744 0	3.144 0	7.342 0	2.508 0	6.783 0	1.183 3
9.898 0	5.094-1	1.225 0	1.744 0	3.144 0	7.342 0	2.508 0	6.913 0	3.463 0
1.000 1	5.160-1	1.222 0	1.783 0	3.192 0	7.363 0	2.526 0	6.927 0	3.465 0
1.500 1	8.586-1	1.108 0	3.334 0	5.638 0	8.309 0	3.358 0	7.529 0	3.547 0
2.000 1	1.265 0	1.028 0	4.557 0	8.324 0	9.118 0	4.080 0	7.975 0	3.615 0
2.500 1	1.718 0	9.651-1	5.544 0	1.119 1	9.831 0	4.730 0	8.315 0	3.669 0
3.000 1	2.205 0	9.140-1	6.364 0	1.419 1	1.047 1	5.327 0	8.582 0	3.710 0
4.000 1	3.264 0	8.334-1	7.674 0	2.053 1	1.161 1	6.408 0	8.985 0	3.757 0
5.000 1	4.420 0	7.716-1	8.700 0	2.721 1	1.261 1	7.377 0	9.366 0	3.765 0
6.000 1	5.671 0	7.238-1	9.548 0	3.409 1	1.352 1	8.257 0	9.869 0	3.747 0
8.000 1	8.474 0	6.598-1	1.091 1	4.801 1	1.519 1	9.799 0	1.122 1	3.675 0
1.000 2	1.162 1	6.224-1	1.197 1	6.189 1	1.672 1	1.113 1	1.255 1	3.601 0
1.500 2	2.039 1	5.759-1	1.382 1	9.631 1	2.010 1	1.388 1	1.499 1	3.492 0
2.000 2	2.974 1	5.539-1	1.505 1	1.306 2	2.302 1	1.616 1	1.670 1	3.473 0
2.500 2	3.926 1	5.407-1	1.596 1	1.649 2	2.561 1	1.816 1	1.809 1	3.512 0
3.000 2	4.872 1	5.317-1	1.669 1	1.992 2	2.795 1	1.996 1	1.930 1	3.589 0
4.000 2	6.710 1	5.196-1	1.781 1	2.681 2	3.213 1	2.316 1	2.142 1	3.813 0
5.000 2	8.449 1	5.113-1	1.868 1	3.372 2	3.581 1	2.597 1	2.329 1	4.074 0
6.000 2	1.009 2	5.049-1	1.939 1	4.065 2	3.914 1	2.851 1	2.499 1	4.331 0
8.000 2	1.315 2	4.956-1	2.054 1	5.458 2	4.504 1	3.304 1	2.806 1	4.776 0
1.000 3	1.597 2	4.893-1	2.146 1	6.854 2	5.024 1	3.702 1	3.084 1	5.117 0

Appendix A2

Aluminum

MELTING CURVE

P	T	VS/VS0	VS	VL	SS	SL	ES	EL
1.000-4	9.330-1	1.000 0	3.904-1	4.230-1	1.201 0	1.629 0	6.740-1	1.073 0
5.000 0	1.259 0	9.487-1	3.704-1	3.967-1	1.378 0	1.842 0	9.139-1	1.367 0
6.000 0	1.314 0	9.395-1	3.668-1	3.924-1	1.400 0	1.872 0	9.619-1	1.428 0
8.000 0	1.418 0	9.220-1	3.600-1	3.843-1	1.437 0	1.923 0	1.059 0	1.554 0
1.000 1	1.515 0	9.057-1	3.536-1	3.770-1	1.466 0	1.966 0	1.159 0	1.684 0
1.500 1	1.733 0	8.694-1	3.394-1	3.611-1	1.519 0	2.051 0	1.422 0	2.019 0
2.000 1	1.925 0	8.385-1	3.274-1	3.477-1	1.557 0	2.115 0	1.702 0	2.369 0
2.500 1	2.099 0	8.117-1	3.169-1	3.362-1	1.585 0	2.166 0	1.993 0	2.730 0
3.000 1	2.259 0	7.882-1	3.077-1	3.261-1	1.607 0	2.207 0	2.293 0	3.097 0
4.000 1	2.544 0	7.485-1	2.922-1	3.090-1	1.640 0	2.271 0	2.912 0	3.844 0
5.000 1	2.795 0	7.160-1	2.795-1	2.950-1	1.664 0	2.318 0	3.544 0	4.598 0
6.000 1	3.020 0	6.886-1	2.688-1	2.832-1	1.682 0	2.356 0	4.183 0	5.353 0
8.000 1	3.411 0	6.444-1	2.516-1	2.642-1	1.707 0	2.410 0	5.465 0	6.851 0
1.000 2	3.746 0	6.097-1	2.380-1	2.493-1	1.724 0	2.449 0	6.740 0	8.326 0
1.500 2	4.418 0	5.470-1	2.136-1	2.225-1	1.749 0	2.510 0	9.855 0	1.188 1
2.000 2	4.942 0	5.036-1	1.966-1	2.040-1	1.761 0	2.546 0	1.285 1	1.526 1
2.500 2	5.372 0	4.709-1	1.839-1	1.902-1	1.766 0	2.570 0	1.574 1	1.848 1
3.000 2	5.738 0	4.449-1	1.737-1	1.793-1	1.769 0	2.587 0	1.854 1	2.156 1
4.000 2	6.339 0	4.056-1	1.583-1	1.628-1	1.769 0	2.609 0	2.387 1	2.741 1
5.000 2	6.822 0	3.765-1	1.470-1	1.508-1	1.765 0	2.623 0	2.893 1	3.289 1
6.000 2	7.227 0	3.538-1	1.381-1	1.414-1	1.760 0	2.633 0	3.375 1	3.810 1
8.000 2	7.883 0	3.199-1	1.249-1	1.275-1	1.748 0	2.644 0	4.286 1	4.785 1
1.000 3	8.405 0	2.952-1	1.152-1	1.174-1	1.736 0	2.650 0	5.139 1	5.691 1

SATURATION CURVE

P	T	T/TC	VL	VG	SL	SG	EL	EG
4.452-1	6.388 0	1.000 0	1.169 0	1.169 0	4.525 0	4.525 0	1.072 1	1.072 1
4.000-1	6.299 0	9.861-1	9.711-1	1.481 0	4.394 0	4.648 0	9.968 0	1.137 1
3.000-1	6.089 0	9.532-1	8.493-1	1.949 0	4.267 0	4.761 0	9.226 0	1.190 1
2.500-1	5.974 0	9.351-1	8.088-1	2.247 0	4.212 0	4.811 0	8.903 0	1.213 1
2.000-1	5.848 0	9.155-1	7.734-1	2.645 0	4.156 0	4.864 0	8.582 0	1.235 1
1.500-1	5.707 0	8.934-1	7.405-1	3.251 0	4.097 0	4.924 0	8.245 0	1.259 1
1.000-1	5.538 0	8.670-1	7.075-1	4.423 0	4.028 0	5.002 0	7.866 0	1.289 1
8.000-2	5.456 0	8.541-1	6.932-1	5.383 0	3.996 0	5.046 0	7.688 0	1.304 1
6.000-2	5.355 0	8.383-1	6.769-1	7.464 0	3.956 0	5.113 0	7.474 0	1.326 1
5.000-2	5.289 0	8.280-1	6.668-1	1.004 1	3.930 0	5.169 0	7.336 0	1.342 1
4.000-2	5.197 0	8.135-1	6.536-1	1.608 1	3.894 0	5.256 0	7.147 0	1.361 1
3.000-2	5.053 0	7.911-1	6.348-1	2.782 1	3.838 0	5.360 0	6.863 0	1.374 1
2.500-2	4.953 0	7.754-1	6.230-1	3.692 1	3.800 0	5.415 0	6.671 0	1.377 1
2.000-2	4.826 0	7.555-1	6.094-1	5.006 1	3.752 0	5.477 0	6.436 0	1.377 1
1.500-2	4.661 0	7.297-1	5.935-1	7.115 1	3.690 0	5.552 0	6.142 0	1.376 1
1.000-2	4.436 0	6.944-1	5.744-1	1.116 2	3.605 0	5.651 0	5.756 0	1.372 1
8.000-3	4.317 0	6.758-1	5.653-1	1.409 2	3.560 0	5.704 0	5.559 0	1.369 1
6.000-3	4.170 0	6.528-1	5.549-1	1.887 2	3.504 0	5.773 0	5.321 0	1.365 1
5.000-3	4.081 0	6.388-1	5.489-1	2.260 2	3.469 0	5.816 0	5.179 0	1.363 1
4.000-3	3.976 0	6.224-1	5.422-1	2.809 2	3.429 0	5.868 0	5.015 0	1.359 1
3.000-3	3.847 0	6.023-1	5.345-1	3.704 2	3.378 0	5.936 0	4.818 0	1.355 1
2.500-3	3.770 0	5.901-1	5.300-1	4.404 2	3.347 0	5.980 0	4.700 0	1.352 1
2.000-3	3.679 0	5.759-1	5.249-1	5.436 2	3.310 0	6.033 0	4.563 0	1.349 1
1.500-3	3.567 0	5.584-1	5.189-1	7.118 2	3.265 0	6.101 0	4.398 0	1.345 1
1.000-3	3.421 0	5.355-1	5.114-1	1.038 3	3.204 0	6.199 0	4.185 0	1.339 1
8.000-4	3.345 0	5.237-1	5.077-1	1.276 3	3.172 0	6.253 0	4.077 0	1.336 1
6.000-4	3.252 0	5.092-1	5.033-1	1.665 3	3.132 0	6.323 0	3.945 0	1.332 1
5.000-4	3.196 0	5.004-1	5.007-1	1.970 3	3.107 0	6.367 0	3.866 0	1.330 1
4.000-4	3.130 0	4.900-1	4.977-1	2.420 3	3.078 0	6.422 0	3.774 0	1.327 1
3.000-4	3.049 0	4.774-1	4.941-1	3.155 3	3.042 0	6.493 0	3.661 0	1.324 1
2.500-4	3.000 0	4.697-1	4.920-1	3.732 3	3.019 0	6.538 0	3.594 0	1.322 1
2.000-4	2.942 0	4.606-1	4.895-1	4.584 3	2.993 0	6.594 0	3.514 0	1.319 1
1.500-4	2.871 0	4.494-1	4.865-1	5.976 3	2.959 0	6.665 0	3.417 0	1.316 1
1.000-4	2.776 0	4.346-1	4.826-1	8.687 3	2.914 0	6.767 0	3.290 0	1.312 1

Aluminum

SHOCK ADIABAT M= 1.000

P	T	V	S	E	D	U	CS	CV
1.000-4	2.930-1	3.690-1	-3.576-7	-1.281-7	.000 0	.000 0	5.266 0	9.305-1
1.000 1	3.832-1	3.322-1	4.785-2	1.841-1	6.083 0	6.067-1	6.186 0	9.339-1
1.500 1	4.454-1	3.195-1	1.196-1	3.711-1	6.426 0	8.614-1	6.533 0	9.368-1
2.000 1	5.235-1	3.091-1	2.145-1	5.994-1	6.741 0	1.095 0	6.836 0	9.400-1
2.500 1	6.179-1	3.002-1	3.228-1	8.601-1	7.034 0	1.312 0	7.107 0	9.433-1
3.000 1	7.282-1	2.925-1	4.368-1	1.147 0	7.309 0	1.515 0	7.353 0	9.465-1
4.000 1	9.941-1	2.798-1	6.639-1	1.784 0	7.815 0	1.889 0	7.789 0	9.529-1
5.000 1	1.315 0	2.696-1	8.758-1	2.485 0	8.276 0	2.229 0	8.169 0	9.596-1
6.000 1	1.683 0	2.611-1	1.068 0	3.237 0	8.702 0	2.544 0	8.507 0	9.664-1
8.000 1	2.541 0	2.476-1	1.394 0	4.855 0	9.474 0	3.116 0	9.093 0	9.808-1
1.000 2	3.530 0	2.372-1	1.661 0	6.589 0	1.017 1	3.630 0	9.595 0	9.953-1
1.057 2	3.833 0	2.347-1	1.728 0	7.102 0	1.035 1	3.769 0	9.727 0	9.994-1
1.057 2	3.833 0	2.347-1	1.728 0	7.102 0	1.035 1	3.769 0	9.714 0	9.953 0
1.500 2	4.418 0	2.195-1	2.258 0	1.121 1	1.169 1	4.735 0	1.057 1	1.389 1
1.726 2	4.668 0	2.134-1	2.528 0	1.342 1	1.229 1	5.181 0	1.095 1	1.595 1
1.726 2	4.668 0	2.134-1	2.528 0	1.342 1	1.229 1	5.181 0	1.097 1	1.236 0
2.000 2	6.050 0	2.061-1	2.811 0	1.629 1	1.293 1	5.707 0	1.140 1	1.258 0
2.500 2	8.770 0	1.954-1	3.222 0	2.170 1	1.400 1	6.589 0	1.209 1	1.268 0
3.000 2	1.175 1	1.869-1	3.544 0	2.732 1	1.498 1	7.392 0	1.269 1	1.253 0
4.000 2	1.849 1	1.742-1	4.032 0	3.896 1	1.672 1	8.827 0	1.372 1	1.201 0
5.000 2	2.613 1	1.651-1	4.392 0	5.098 1	1.827 1	1.010 1	1.460 1	1.168 0
6.000 2	3.436 1	1.581-1	4.673 0	6.327 1	1.968 1	1.125 1	1.537 1	1.175 0
8.000 2	5.118 1	1.476-1	5.098 0	8.858 1	2.218 1	1.331 1	1.667 1	1.285 0
1.000 3	6.720 1	1.396-1	5.421 0	1.147 2	2.436 1	1.515 1	1.775 1	1.456 0
1.500 3	1.025 2	1.256-1	6.021 0	1.825 2	2.897 1	1.911 1	1.996 1	1.888 0
2.000 3	1.333 2	1.165-1	6.481 0	2.525 2	3.284 1	2.247 1	2.180 1	2.214 0
2.500 3	1.618 2	1.101-1	6.867 0	3.236 2	3.626 1	2.544 1	2.343 1	2.428 0
3.000 3	1.891 2	1.057-1	7.205 0	3.950 2	3.939 1	2.811 1	2.498 1	2.554 0
4.000 3	2.426 2	1.003-1	7.781 0	5.375 2	4.502 1	3.279 1	2.803 1	2.633 0
5.000 3	2.958 2	9.791-2	8.264 0	6.777 2	5.011 1	3.682 1	3.119 1	2.614 0
6.000 3	3.486 2	9.733-2	8.682 0	8.150 2	5.484 1	4.037 1	3.447 1	2.603 0
8.000 3	4.488 2	9.832-2	9.373 0	1.083 3	6.344 1	4.653 1	4.055 1	2.749 0
1.000 4	5.391 2	9.959-2	9.932 0	1.347 3	7.109 1	5.191 1	4.535 1	3.060 0

Appendix A3

Iron

MELTING CURVE

P	T	VS/VS0	VS	VL	SS	SL	ES	EL
1.000-4	1.810 0	1.000 0	1.306-1	1.359-1	9.474-1	1.105 0	8.194-1	1.105 0
1.000 1	2.116 0	9.441-1	1.233-1	1.273-1	9.794-1	1.122 0	9.165-1	1.178 0
1.500 1	2.252 0	9.222-1	1.205-1	1.241-1	9.919-1	1.129 0	9.793-1	1.233 0
2.000 1	2.381 0	9.030-1	1.179-1	1.213-1	1.003 0	1.135 0	1.048 0	1.297 0
2.500 1	2.505 0	8.858-1	1.157-1	1.188-1	1.013 0	1.141 0	1.123 0	1.368 0
3.000 1	2.624 0	8.704-1	1.137-1	1.166-1	1.022 0	1.147 0	1.201 0	1.443 0
4.000 1	2.850 0	8.433-1	1.101-1	1.128-1	1.037 0	1.158 0	1.368 0	1.605 0
5.000 1	3.065 0	8.202-1	1.071-1	1.096-1	1.052 0	1.168 0	1.545 0	1.779 0
6.000 1	3.271 0	8.000-1	1.045-1	1.068-1	1.064 0	1.177 0	1.730 0	1.963 0
8.000 1	3.660 0	7.660-1	1.001-1	1.021-1	1.086 0	1.194 0	2.116 0	2.348 0
1.000 2	4.028 0	7.381-1	9.640-2	9.827-2	1.106 0	1.210 0	2.517 0	2.751 0
1.500 2	4.873 0	6.845-1	8.941-2	9.101-2	1.145 0	1.244 0	3.554 0	3.799 0
2.000 2	5.639 0	6.450-1	8.425-2	8.567-2	1.175 0	1.272 0	4.609 0	4.874 0
2.500 2	6.339 0	6.138-1	8.017-2	8.147-2	1.198 0	1.295 0	5.665 0	5.955 0
3.000 2	6.982 0	5.881-1	7.681-2	7.801-2	1.217 0	1.314 0	6.712 0	7.031 0
4.000 2	8.120 0	5.475-1	7.151-2	7.255-2	1.245 0	1.344 0	8.764 0	9.151 0
5.000 2	9.099 0	5.161-1	6.742-2	6.833-2	1.263 0	1.364 0	1.075 1	1.122 1
6.000 2	9.948 0	4.908-1	6.411-2	6.493-2	1.275 0	1.379 0	1.268 1	1.322 1
8.000 2	1.135 1	4.517-1	5.900-2	5.968-2	1.289 0	1.397 0	1.638 1	1.706 1
1.000 3	1.248 1	4.223-1	5.516-2	5.573-2	1.295 0	1.407 0	1.988 1	2.072 1

SATURATION CURVE

P	T	T/TC	VL	VG	SL	SG	EL	EG
1.025 0	1.095 1	1.000 0	5.223-1	5.223-1	2.815 0	2.815 0	1.011 1	1.011 1
1.000 0	1.082 1	9.875-1	4.647-1	5.879-1	2.795 0	2.818 0	9.945 0	1.007 1
8.000-1	9.849 0	8.991-1	3.691-1	7.616-1	2.700 0	2.788 0	9.045 0	9.605 0
6.000-1	9.018 0	8.232-1	3.240-1	9.295-1	2.612 0	2.765 0	8.250 0	9.270 0
5.000-1	8.629 0	7.877-1	3.064-1	1.042 0	2.567 0	2.758 0	7.865 0	9.146 0
4.000-1	8.244 0	7.526-1	2.904-1	1.200 0	2.520 0	2.755 0	7.476 0	9.048 0
3.000-1	7.848 0	7.164-1	2.751-1	1.454 0	2.469 0	2.757 0	7.066 0	8.975 0
2.500-1	7.638 0	6.972-1	2.673-1	1.663 0	2.440 0	2.761 0	6.844 0	8.946 0
2.000-1	7.410 0	6.764-1	2.591-1	2.000 0	2.407 0	2.767 0	6.600 0	8.923 0
1.500-1	7.146 0	6.523-1	2.499-1	2.676 0	2.367 0	2.780 0	6.314 0	8.898 0
1.000-1	6.790 0	6.199-1	2.379-1	4.681 0	2.311 0	2.808 0	5.922 0	8.850 0
8.000-2	6.586 0	6.013-1	2.314-1	6.618 0	2.277 0	2.827 0	5.695 0	8.809 0
6.000-2	6.317 0	5.766-1	2.230-1	9.987 0	2.230 0	2.854 0	5.393 0	8.746 0
5.000-2	6.146 0	5.611-1	2.179-1	1.264 1	2.199 0	2.870 0	5.202 0	8.705 0
4.000-2	5.943 0	5.425-1	2.121-1	1.652 1	2.162 0	2.891 0	4.975 0	8.656 0
3.000-2	5.693 0	5.197-1	2.053-1	2.276 1	2.114 0	2.918 0	4.697 0	8.597 0
2.500-2	5.543 0	5.060-1	2.013-1	2.760 1	2.084 0	2.935 0	4.531 0	8.562 0
2.000-2	5.368 0	4.901-1	1.968-1	3.469 1	2.049 0	2.957 0	4.339 0	8.521 0
1.500-2	5.158 0	4.709-1	1.917-1	4.616 1	2.005 0	2.985 0	4.110 0	8.472 0
1.000-2	4.888 0	4.462-1	1.853-1	6.821 1	1.948 0	3.026 0	3.819 0	8.410 0
8.000-3	4.751 0	4.337-1	1.823-1	8.423 1	1.918 0	3.049 0	3.674 0	8.379 0
6.000-3	4.586 0	4.187-1	1.787-1	1.102 2	1.881 0	3.080 0	3.502 0	8.341 0
5.000-3	4.488 0	4.097-1	1.766-1	1.305 2	1.858 0	3.099 0	3.401 0	8.319 0
4.000-3	4.374 0	3.993-1	1.743-1	1.604 2	1.832 0	3.124 0	3.284 0	8.293 0
3.000-3	4.237 0	3.867-1	1.715-1	2.090 2	1.800 0	3.155 0	3.145 0	8.262 0
2.500-3	4.154 0	3.792-1	1.699-1	2.470 2	1.780 0	3.176 0	3.063 0	8.243 0
2.000-3	4.058 0	3.704-1	1.681-1	3.030 2	1.757 0	3.201 0	2.968 0	8.221 0
1.500-3	3.941 0	3.598-1	1.659-1	3.942 2	1.728 0	3.234 0	2.854 0	8.195 0
1.000-3	3.789 0	3.459-1	1.632-1	5.711 2	1.691 0	3.280 0	2.708 0	8.160 0
8.000-4	3.711 0	3.387-1	1.618-1	7.005 2	1.671 0	3.306 0	2.634 0	8.142 0
6.000-4	3.615 0	3.300-1	1.602-1	9.115 2	1.647 0	3.340 0	2.544 0	8.121 0
5.000-4	3.557 0	3.247-1	1.592-1	1.077 3	1.632 0	3.362 0	2.491 0	8.107 0
4.000-4	3.489 0	3.185-1	1.581-1	1.322 3	1.614 0	3.389 0	2.429 0	8.092 0
3.000-4	3.406 0	3.109-1	1.568-1	1.721 3	1.592 0	3.423 0	2.354 0	8.073 0
2.500-4	3.355 0	3.063-1	1.560-1	2.035 3	1.579 0	3.445 0	2.309 0	8.062 0
2.000-4	3.296 0	3.009-1	1.550-1	2.499 3	1.563 0	3.472 0	2.256 0	8.048 0
1.500-4	3.222 0	2.942-1	1.539-1	3.258 3	1.543 0	3.507 0	2.191 0	8.031 0
1.000-4	3.125 0	2.853-1	1.524-1	4.738 3	1.517 0	3.557 0	2.107 0	8.009 0

Iron

SHOCK ADIABAT M= 1.050

P	T	V	S	E	D	U	CS	CV
1.000-4	2.930-1	1.210-1	-7.153-7	-2.331-7	.000 0	.000 0	4.436 0	4.597-1
1.000 1	3.944-1	1.150-1	9.322-2	6.019-2	3.662 0	3.470-1	4.950 0	4.653-1
1.500 1	4.503-1	1.126-1	1.368-1	1.081-1	4.098 0	4.650-1	5.163 0	4.678-1
2.000 1	5.105-1	1.105-1	1.793-1	1.651-1	4.422 0	5.747-1	5.357 0	4.703-1
2.500 1	5.758-1	1.087-1	2.211-1	2.298-1	4.686 0	6.779-1	5.534 0	4.730-1
3.000 1	6.461-1	1.070-1	2.619-1	3.010-1	4.912 0	7.759-1	5.697 0	4.756-1
4.000 1	8.017-1	1.040-1	3.406-1	4.601-1	5.298 0	9.592-1	5.993 0	4.813-1
5.000 1	9.760-1	1.016-1	4.145-1	6.372-1	5.627 0	1.129 0	6.255 0	4.873-1
6.000 1	1.168 0	9.940-2	4.835-1	8.294-1	5.919 0	1.288 0	6.492 0	4.935-1
8.000 1	1.597 0	9.582-2	6.076-1	1.249 0	6.430 0	1.581 0	6.907 0	5.063-1
1.000 2	2.079 0	9.291-2	7.154-1	1.707 0	6.877 0	1.848 0	7.266 0	5.190-1
1.500 2	3.455 0	8.746-2	9.324-1	2.969 0	7.821 0	2.437 0	8.005 0	5.474-1
2.000 2	5.013 0	8.354-2	1.100 0	4.351 0	8.614 0	2.950 0	8.602 0	5.694-1
2.326 2	6.103 0	8.150-2	1.191 0	5.298 0	9.078 0	3.255 0	8.941 0	5.804-1
2.326 2	6.103 0	8.150-2	1.191 0	5.298 0	9.078 0	3.255 0	8.837 0	2.723 0
2.500 2	6.339 0	8.073-2	1.240 0	5.790 0	9.334 0	3.403 0	9.021 0	2.828 0
2.731 2	6.643 0	7.979-2	1.305 0	6.453 0	9.659 0	3.593 0	9.248 0	2.979 0
2.731 2	6.643 0	7.979-2	1.305 0	6.453 0	9.659 0	3.593 0	9.332 0	6.565-1
3.000 2	7.514 0	7.854-2	1.370 0	7.278 0	9.991 0	3.815 0	9.557 0	6.700-1
4.000 2	1.086 1	7.467-2	1.574 0	1.048 1	1.110 1	4.578 0	1.029 1	7.080-1
5.000 2	1.436 1	7.167-2	1.735 0	1.385 1	1.207 1	5.262 0	1.090 1	7.338-1
6.000 2	1.797 1	6.922-2	1.870 0	1.735 1	1.294 1	5.890 0	1.142 1	7.534-1
8.000 2	2.543 1	6.537-2	2.086 0	2.467 1	1.447 1	7.025 0	1.229 1	7.859-1
1.000 3	3.309 1	6.236-2	2.257 0	3.235 1	1.580 1	8.043 0	1.300 1	8.154-1
1.500 3	5.259 1	5.686-2	2.577 0	5.264 1	1.857 1	1.026 1	1.444 1	8.768-1
2.000 3	7.241 1	5.304-2	2.814 0	7.402 1	2.089 1	1.217 1	1.565 1	9.161-1
2.500 3	9.262 1	5.023-2	3.005 0	9.603 1	2.292 1	1.386 1	1.674 1	9.401-1
3.000 3	1.132 2	4.813-2	3.167 0	1.184 2	2.477 1	1.539 1	1.778 1	9.597-1
4.000 3	1.548 2	4.527-2	3.432 0	1.636 2	2.810 1	1.809 1	1.973 1	1.020 0
5.000 3	1.948 2	4.343-2	3.646 0	2.091 2	3.107 1	2.045 1	2.148 1	1.126 0
6.000 3	2.318 2	4.209-2	3.826 0	2.549 2	3.376 1	2.258 1	2.301 1	1.265 0
8.000 3	2.966 2	4.009-2	4.126 0	3.478 2	3.854 1	2.638 1	2.555 1	1.559 0
1.000 4	3.525 2	3.861-2	4.376 0	4.422 2	4.272 1	2.974 1	2.767 1	1.818 0

Appendix A4
Nickel

MELTING CURVE

P	T	VS/VS0	VS	VL	SS	SL	ES	EL
1.000-4	1.730 0	1.000 0	1.201-1	1.276-1	8.263-1	9.983-1	6.874-1	9.849-1
5.000 0	1.941 0	9.733-1	1.169-1	1.239-1	8.549-1	1.026 0	7.475-1	1.045 0
6.000 0	1.982 0	9.685-1	1.163-1	1.232-1	8.601-1	1.031 0	7.608-1	1.059 0
8.000 0	2.062 0	9.594-1	1.152-1	1.220-1	8.699-1	1.041 0	7.883-1	1.088 0
1.000 1	2.140 0	9.508-1	1.142-1	1.208-1	8.791-1	1.051 0	8.170-1	1.118 0
1.500 1	2.328 0	9.313-1	1.119-1	1.182-1	9.002-1	1.072 0	8.931-1	1.198 0
2.000 1	2.508 0	9.140-1	1.098-1	1.159-1	9.187-1	1.091 0	9.741-1	1.285 0
2.500 1	2.681 0	8.985-1	1.079-1	1.138-1	9.353-1	1.109 0	1.059 0	1.377 0
3.000 1	2.848 0	8.843-1	1.062-1	1.120-1	9.503-1	1.125 0	1.147 0	1.472 0
4.000 1	3.168 0	8.594-1	1.032-1	1.087-1	9.766-1	1.153 0	1.331 0	1.671 0
5.000 1	3.469 0	8.378-1	1.006-1	1.059-1	9.989-1	1.178 0	1.521 0	1.879 0
6.000 1	3.755 0	8.189-1	9.835-2	1.034-1	1.018 0	1.199 0	1.715 0	2.092 0
8.000 1	4.284 0	7.866-1	9.448-2	9.912-2	1.050 0	1.234 0	2.111 0	2.529 0
1.000 2	4.765 0	7.598-1	9.126-2	9.556-2	1.074 0	1.262 0	2.511 0	2.974 0
1.500 2	5.795 0	7.078-1	8.501-2	8.860-2	1.116 0	1.311 0	3.505 0	4.093 0
2.000 2	6.632 0	6.688-1	8.033-2	8.337-2	1.142 0	1.342 0	4.478 0	5.197 0
2.500 2	7.326 0	6.379-1	7.661-2	7.921-2	1.158 0	1.363 0	5.425 0	6.275 0
3.000 2	7.911 0	6.123-1	7.354-2	7.579-2	1.169 0	1.377 0	6.347 0	7.323 0
4.000 2	8.841 0	5.719-1	6.869-2	7.042-2	1.180 0	1.395 0	8.125 0	9.335 0
5.000 2	9.550 0	5.408-1	6.495-2	6.633-2	1.183 0	1.404 0	9.830 0	1.125 1
6.000 2	1.011 1	5.157-1	6.194-2	6.307-2	1.183 0	1.408 0	1.148 1	1.308 1
8.000 2	1.095 1	4.771-1	5.730-2	5.811-2	1.176 0	1.410 0	1.463 1	1.654 1
1.000 3	1.155 1	4.481-1	5.382-2	5.444-2	1.167 0	1.407 0	1.765 1	1.980 1

SATURATION CURVE

P	T	T/TC	VL	VG	SL	SG	EL	EG
1.049 0	7.585 0	1.000 0	4.785-1	4.785-1	2.526 0	2.526 0	7.734 0	7.734 0
1.000 0	7.504 0	9.893-1	3.950-1	5.955-1	2.461 0	2.581 0	7.329 0	8.034 0
8.000-1	7.156 0	9.435-1	3.160-1	8.449-1	2.356 0	2.646 0	6.634 0	8.287 0
6.000-1	6.769 0	8.924-1	2.749-1	1.144 0	2.268 0	2.689 0	6.052 0	8.376 0
5.000-1	6.554 0	8.641-1	2.585-1	1.349 0	2.223 0	2.709 0	5.758 0	8.396 0
4.000-1	6.318 0	8.330-1	2.436-1	1.625 0	2.174 0	2.729 0	5.450 0	8.403 0
3.000-1	6.052 0	7.979-1	2.293-1	2.035 0	2.119 0	2.751 0	5.116 0	8.397 0
2.500-1	5.903 0	7.782-1	2.222-1	2.333 0	2.088 0	2.763 0	4.933 0	8.387 0
2.000-1	5.737 0	7.564-1	2.150-1	2.746 0	2.054 0	2.776 0	4.734 0	8.372 0
1.500-1	5.549 0	7.316-1	2.074-1	3.380 0	2.014 0	2.792 0	4.511 0	8.350 0
1.000-1	5.322 0	7.016-1	1.990-1	4.540 0	1.965 0	2.811 0	4.248 0	8.314 0
8.000-2	5.212 0	6.872-1	1.952-1	5.373 0	1.942 0	2.821 0	4.123 0	8.294 0
6.000-2	5.083 0	6.702-1	1.910-1	6.757 0	1.913 0	2.835 0	3.977 0	8.267 0
5.000-2	5.007 0	6.602-1	1.886-1	7.896 0	1.896 0	2.844 0	3.892 0	8.250 0
4.000-2	4.919 0	6.485-1	1.859-1	9.695 0	1.877 0	2.856 0	3.794 0	8.229 0
3.000-2	4.809 0	6.340-1	1.826-1	1.300 1	1.852 0	2.873 0	3.674 0	8.202 0
2.500-2	4.740 0	6.250-1	1.807-1	1.592 1	1.836 0	2.887 0	3.599 0	8.184 0
2.000-2	4.657 0	6.139-1	1.783-1	2.068 1	1.817 0	2.905 0	3.509 0	8.163 0
1.500-2	4.547 0	5.995-1	1.754-1	2.920 1	1.792 0	2.931 0	3.392 0	8.137 0
1.000-2	4.392 0	5.790-1	1.714-1	4.699 1	1.755 0	2.971 0	3.229 0	8.101 0
8.000-3	4.306 0	5.677-1	1.693-1	6.042 1	1.735 0	2.994 0	3.140 0	8.081 0
6.000-3	4.197 0	5.533-1	1.667-1	8.260 1	1.708 0	3.024 0	3.029 0	8.057 0
5.000-3	4.129 0	5.443-1	1.651-1	1.002 2	1.692 0	3.044 0	2.960 0	8.042 0
4.000-3	4.047 0	5.336-1	1.633-1	1.262 2	1.672 0	3.068 0	2.879 0	8.024 0
3.000-3	3.945 0	5.201-1	1.610-1	1.688 2	1.647 0	3.099 0	2.779 0	8.001 0
2.500-3	3.882 0	5.118-1	1.597-1	2.024 2	1.631 0	3.119 0	2.717 0	7.987 0
2.000-3	3.808 0	5.020-1	1.582-1	2.521 2	1.613 0	3.144 0	2.646 0	7.971 0
1.500-3	3.715 0	4.898-1	1.563-1	3.334 2	1.589 0	3.175 0	2.558 0	7.950 0
1.000-3	3.591 0	4.735-1	1.539-1	4.920 2	1.558 0	3.221 0	2.442 0	7.922 0
8.000-4	3.526 0	4.649-1	1.527-1	6.085 2	1.541 0	3.246 0	2.382 0	7.908 0
6.000-4	3.446 0	4.543-1	1.512-1	7.991 2	1.520 0	3.279 0	2.309 0	7.890 0
5.000-4	3.397 0	4.479-1	1.503-1	9.492 2	1.507 0	3.299 0	2.265 0	7.879 0
4.000-4	3.339 0	4.402-1	1.493-1	1.171 3	1.492 0	3.325 0	2.213 0	7.866 0
3.000-4	3.267 0	4.307-1	1.481-1	1.535 3	1.473 0	3.358 0	2.150 0	7.850 0
2.500-4	3.223 0	4.250-1	1.473-1	1.821 3	1.461 0	3.379 0	2.112 0	7.840 0
2.000-4	3.171 0	4.181-1	1.465-1	2.245 3	1.447 0	3.405 0	2.067 0	7.829 0
1.500-4	3.107 0	4.096-1	1.454-1	2.940 3	1.429 0	3.439 0	2.012 0	7.814 0
1.000-4	3.020 0	3.982-1	1.441-1	4.298 3	1.405 0	3.487 0	1.939 0	7.795 0

Nickel

SHOCK ADIABAT M= 1.000

P	T	V	S	E	D	U	CS	CV
1.000-4	2.930-1	1.120-1	-7.749-7	-2.346-7	.000 0	.000 0	4.556 0	4.264-1
1.000 1	3.235-1	1.068-1	4.165-3	2.579-2	4.931 0	2.272-1	5.055 0	4.268-1
1.500 1	3.415-1	1.048-1	1.190-2	5.431-2	5.097 0	3.296-1	5.264 0	4.271-1
2.000 1	3.631-1	1.029-1	2.422-2	9.089-2	5.253 0	4.264-1	5.454 0	4.275-1
2.500 1	3.885-1	1.012-1	4.073-2	1.344-1	5.401 0	5.184-1	5.629 0	4.279-1
3.000 1	4.180-1	9.975-2	6.086-2	1.838-1	5.542 0	6.063-1	5.791 0	4.284-1
4.000 1	4.904-1	9.711-2	1.095-1	2.979-1	5.804 0	7.719-1	6.085 0	4.295-1
5.000 1	5.802-1	9.485-2	1.647-1	4.289-1	6.047 0	9.261-1	6.347 0	4.308-1
6.000 1	6.871-1	9.287-2	2.228-1	5.738-1	6.273 0	1.071 0	6.584 0	4.322-1
8.000 1	9.493-1	8.957-2	3.376-1	8.973-1	6.689 0	1.340 0	7.004 0	4.351-1
1.000 2	1.271 0	8.687-2	4.440-1	1.257 0	7.065 0	1.585 0	7.369 0	4.381-1
1.500 2	2.288 0	8.176-2	6.637-1	2.268 0	7.888 0	2.130 0	8.126 0	4.465-1
2.000 2	3.549 0	7.805-2	8.315-1	3.395 0	8.597 0	2.606 0	8.739 0	4.557-1
2.500 2	4.994 0	7.517-2	9.646-1	4.603 0	9.228 0	3.034 0	9.262 0	4.654-1
3.000 2	6.579 0	7.283-2	1.074 0	5.875 0	9.802 0	3.428 0	9.721 0	4.755-1
3.553 2	8.458 0	7.068-2	1.176 0	7.341 0	1.039 1	3.832 0	1.017 1	4.871-1
3.553 2	8.458 0	7.068-2	1.176 0	7.341 0	1.039 1	3.832 0	1.016 1	4.934 0
4.000 2	8.841 0	6.928-2	1.254 0	8.543 0	1.084 1	4.134 0	1.042 1	6.040 0
4.870 2	9.468 0	6.681-2	1.403 0	1.100 1	1.163 1	4.691 0	1.088 1	8.567 0
4.870 2	9.468 0	6.681-2	1.403 0	1.100 1	1.163 1	4.691 0	1.089 1	7.084-1
5.000 2	9.812 0	6.644-2	1.424 0	1.139 1	1.173 1	4.773 0	1.096 1	7.125-1
6.000 2	1.251 1	6.393-2	1.573 0	1.442 1	1.251 1	5.371 0	1.151 1	7.374-1
8.000 2	1.822 1	5.999-2	1.813 0	2.081 1	1.389 1	6.451 0	1.244 1	7.648-1
1.000 3	2.431 1	5.700-2	2.003 0	2.750 1	1.510 1	7.417 0	1.323 1	7.763-1
1.500 3	4.094 1	5.184-2	2.356 0	4.512 1	1.769 1	9.500 0	1.486 1	7.941-1
2.000 3	5.870 1	4.844-2	2.610 0	6.356 1	1.987 1	1.128 1	1.617 1	8.351-1
2.500 3	7.652 1	4.595-2	2.809 0	8.257 1	2.179 1	1.285 1	1.729 1	9.012-1
3.000 3	9.379 1	4.399-2	2.975 0	1.020 2	2.352 1	1.428 1	1.828 1	9.803-1
4.000 3	1.261 2	4.106-2	3.246 0	1.419 2	2.659 1	1.685 1	1.999 1	1.146 0
5.000 3	1.558 2	3.892-2	3.468 0	1.827 2	2.930 1	1.912 1	2.146 1	1.300 0
6.000 3	1.833 2	3.730-2	3.660 0	2.241 2	3.174 1	2.117 1	2.278 1	1.437 0
8.000 3	2.340 2	3.498-2	3.986 0	3.081 2	3.610 1	2.482 1	2.511 1	1.668 0
1.000 4	2.803 2	3.342-2	4.262 0	3.929 2	3.996 1	2.803 1	2.716 1	1.856 0

Appendix A5

Copper

MELTING CURVE

P	T	VS/VS0	VS	VL	SS	SL	ES	EL
1.000-4	1.360 0	1.000 0	1.205-1	1.271-1	6.599-1	8.089-1	4.701-1	6.727-1
5.000 0	1.547 0	9.564-1	1.153-1	1.202-1	6.781-1	8.325-1	5.088-1	7.230-1
6.000 0	1.578 0	9.494-1	1.144-1	1.191-1	6.806-1	8.359-1	5.173-1	7.342-1
8.000 0	1.635 0	9.366-1	1.129-1	1.172-1	6.850-1	8.419-1	5.350-1	7.574-1
1.000 1	1.687 0	9.253-1	1.115-1	1.155-1	6.886-1	8.471-1	5.533-1	7.813-1
1.500 1	1.801 0	9.009-1	1.086-1	1.120-1	6.951-1	8.575-1	6.013-1	8.425-1
2.000 1	1.901 0	8.793-1	1.060-1	1.093-1	6.994-1	8.666-1	6.548-1	9.072-1
2.500 1	1.997 0	8.599-1	1.036-1	1.068-1	7.031-1	8.748-1	7.144-1	9.771-1
3.000 1	2.089 0	8.424-1	1.015-1	1.047-1	7.065-1	8.821-1	7.792-1	1.052 0
4.000 1	2.262 0	8.118-1	9.784-2	1.009-1	7.125-1	8.946-1	9.207-1	1.211 0
5.000 1	2.426 0	7.858-1	9.471-2	9.769-2	7.181-1	9.053-1	1.074 0	1.379 0
6.000 1	2.581 0	7.633-1	9.200-2	9.492-2	7.232-1	9.145-1	1.236 0	1.555 0
8.000 1	2.876 0	7.259-1	8.748-2	9.032-2	7.333-1	9.308-1	1.578 0	1.919 0
1.000 2	3.157 0	6.956-1	8.384-2	8.661-2	7.434-1	9.450-1	1.935 0	2.295 0
1.500 2	3.820 0	6.392-1	7.704-2	7.971-2	7.684-1	9.758-1	2.862 0	3.253 0
2.000 2	4.452 0	5.989-1	7.219-2	7.480-2	7.931-1	1.003 0	3.807 0	4.220 0
2.500 2	5.066 0	5.680-1	6.846-2	7.102-2	8.170-1	1.028 0	4.756 0	5.187 0
3.000 2	5.664 0	5.431-1	6.546-2	6.797-2	8.397-1	1.052 0	5.701 0	6.149 0
4.000 2	6.819 0	5.047-1	6.083-2	6.323-2	8.807-1	1.094 0	7.564 0	8.057 0
5.000 2	7.916 0	4.758-1	5.734-2	5.963-2	9.159-1	1.130 0	9.383 0	9.937 0
6.000 2	8.951 0	4.528-1	5.457-2	5.673-2	9.456-1	1.161 0	1.115 1	1.178 1
8.000 2	1.083 1	4.177-1	5.035-2	5.225-2	9.914-1	1.209 0	1.454 1	1.537 1
1.000 3	1.245 1	3.915-1	4.719-2	4.885-2	1.023 0	1.243 0	1.774 1	1.882 1

SATURATION CURVE

P	T	T/TC	VL	VG	SL	SG	EL	EG
9.375-1	7.946 0	1.000 0	4.353-1	4.353-1	1.979 0	1.979 0	5.554 0	5.554 0
8.000-1	7.664 0	9.645-1	3.229-1	6.485-1	1.896 0	2.050 0	5.002 0	5.919 0
6.000-1	7.215 0	9.080-1	2.752-1	9.122-1	1.830 0	2.096 0	4.542 0	6.080 0
5.000-1	6.966 0	8.767-1	2.581-1	1.090 0	1.797 0	2.117 0	4.319 0	6.134 0
4.000-1	6.693 0	8.423-1	2.428-1	1.330 0	1.762 0	2.139 0	4.088 0	6.175 0
3.000-1	6.384 0	8.034-1	2.285-1	1.685 0	1.723 0	2.162 0	3.838 0	6.203 0
2.500-1	6.211 0	7.816-1	2.214-1	1.943 0	1.701 0	2.175 0	3.702 0	6.211 0
2.000-1	6.019 0	7.574-1	2.143-1	2.300 0	1.677 0	2.188 0	3.554 0	6.214 0
1.500-1	5.799 0	7.298-1	2.067-1	2.845 0	1.648 0	2.203 0	3.388 0	6.209 0
1.000-1	5.534 0	6.965-1	1.985-1	3.834 0	1.614 0	2.221 0	3.192 0	6.192 0
8.000-2	5.406 0	6.804-1	1.947-1	4.538 0	1.597 0	2.231 0	3.099 0	6.179 0
6.000-2	5.256 0	6.615-1	1.906-1	5.702 0	1.576 0	2.242 0	2.991 0	6.159 0
5.000-2	5.168 0	6.504-1	1.882-1	6.656 0	1.564 0	2.249 0	2.928 0	6.145 0
4.000-2	5.065 0	6.375-1	1.855-1	8.167 0	1.550 0	2.259 0	2.855 0	6.127 0
3.000-2	4.938 0	6.215-1	1.823-1	1.098 1	1.532 0	2.273 0	2.766 0	6.101 0
2.500-2	4.859 0	6.114-1	1.804-1	1.352 1	1.521 0	2.283 0	2.711 0	6.083 0
2.000-2	4.760 0	5.991-1	1.780-1	1.774 1	1.507 0	2.298 0	2.643 0	6.060 0
1.500-2	4.631 0	5.828-1	1.751-1	2.546 1	1.488 0	2.320 0	2.554 0	6.030 0
1.000-2	4.444 0	5.593-1	1.710-1	4.168 1	1.460 0	2.354 0	2.428 0	5.988 0
8.000-3	4.341 0	5.463-1	1.688-1	5.387 1	1.444 0	2.374 0	2.360 0	5.966 0
6.000-3	4.209 0	5.297-1	1.662-1	7.390 1	1.424 0	2.400 0	2.273 0	5.939 0
5.000-3	4.127 0	5.194-1	1.645-1	8.967 1	1.411 0	2.417 0	2.220 0	5.922 0
4.000-3	4.029 0	5.070-1	1.627-1	1.129 2	1.396 0	2.438 0	2.156 0	5.903 0
3.000-3	3.907 0	4.917-1	1.604-1	1.509 2	1.376 0	2.465 0	2.079 0	5.878 0
2.500-3	3.832 0	4.823-1	1.591-1	1.807 2	1.364 0	2.482 0	2.031 0	5.864 0
2.000-3	3.744 0	4.711-1	1.575-1	2.246 2	1.349 0	2.503 0	1.976 0	5.846 0
1.500-3	3.635 0	4.574-1	1.557-1	2.961 2	1.331 0	2.531 0	1.908 0	5.825 0
1.000-3	3.490 0	4.392-1	1.533-1	4.349 2	1.306 0	2.570 0	1.820 0	5.797 0
8.000-4	3.415 0	4.297-1	1.521-1	5.364 2	1.293 0	2.592 0	1.774 0	5.782 0
6.000-4	3.322 0	4.181-1	1.506-1	7.020 2	1.276 0	2.621 0	1.718 0	5.764 0
5.000-4	3.266 0	4.110-1	1.498-1	8.319 2	1.266 0	2.639 0	1.685 0	5.753 0
4.000-4	3.200 0	4.027-1	1.488-1	1.024 3	1.254 0	2.662 0	1.646 0	5.740 0
3.000-4	3.118 0	3.924-1	1.476-1	1.337 3	1.239 0	2.691 0	1.598 0	5.724 0
2.500-4	3.069 0	3.862-1	1.469-1	1.583 3	1.230 0	2.709 0	1.569 0	5.715 0
2.000-4	3.010 0	3.788-1	1.460-1	1.946 3	1.219 0	2.732 0	1.535 0	5.703 0
1.500-4	2.938 0	3.697-1	1.450-1	2.539 3	1.205 0	2.762 0	1.494 0	5.689 0
1.000-4	2.842 0	3.577-1	1.437-1	3.695 3	1.186 0	2.804 0	1.439 0	5.670 0

Copper

SHOCK ADIABAT M= 1.000

P	T	V	S	E	D	U	CS	CV
1.000-4	2.930-1	1.120-1	3.368-6	9.800-7	.000 0	.000 0	3.867 0	3.903-1
1.000 1	3.354-1	1.054-1	6.367-3	3.323-2	4.347 0	2.577-1	4.423 0	3.907-1
1.500 1	3.614-1	1.027-1	1.658-2	6.952-2	4.507 0	3.728-1	4.595 0	3.911-1
2.000 1	3.929-1	1.004-1	3.230-2	1.157-1	4.656 0	4.811-1	4.754 0	3.915-1
2.500 1	4.307-1	9.838-2	5.295-2	1.703-1	4.798 0	5.836-1	4.901 0	3.919-1
3.000 1	4.751-1	9.654-2	7.759-2	2.320-1	4.933 0	6.811-1	5.040 0	3.925-1
4.000 1	5.846-1	9.336-2	1.347-1	3.728-1	5.189 0	8.634-1	5.295 0	3.938-1
5.000 1	7.211-1	9.070-2	1.967-1	5.325-1	5.427 0	1.032 0	5.526 0	3.953-1
6.000 1	8.836-1	8.843-2	2.591-1	7.073-1	5.650 0	1.189 0	5.737 0	3.972-1
8.000 1	1.279 0	8.471-2	3.765-1	1.092 0	6.064 0	1.478 0	6.114 0	4.022-1
1.000 2	1.755 0	8.175-2	4.802-1	1.512 0	6.440 0	1.739 0	6.445 0	4.088-1
1.500 2	3.201 0	7.636-2	6.855-1	2.673 0	7.266 0	2.312 0	7.133 0	4.308-1
1.805 2	4.209 0	7.391-2	7.836-1	3.438 0	7.711 0	2.622 0	7.485 0	4.459-1
1.805 2	4.209 0	7.391-2	7.836-1	3.438 0	7.711 0	2.622 0	7.405 0	2.647 0
2.000 2	4.452 0	7.286-2	8.474-1	3.914 0	8.006 0	2.798 0	7.660 0	2.606 0
2.500 2	5.065 0	7.080-2	1.010 0	5.150 0	8.725 0	3.209 0	8.279 0	2.526 0
2.566 2	5.144 0	7.058-2	1.031 0	5.313 0	8.815 0	3.260 0	8.357 0	2.518 0
2.566 2	5.144 0	7.058-2	1.031 0	5.313 0	8.815 0	3.260 0	8.477 0	5.373-1
3.000 2	6.581 0	6.871-2	1.145 0	6.493 0	9.324 0	3.604 0	8.878 0	5.651-1
4.000 2	9.997 0	6.533-2	1.348 0	9.335 0	1.037 1	4.321 0	9.657 0	6.066-1
5.000 2	1.358 1	6.277-2	1.504 0	1.231 1	1.129 1	4.962 0	1.030 1	6.247-1
6.000 2	1.734 1	6.073-2	1.631 0	1.538 1	1.212 1	5.546 0	1.085 1	6.298-1
8.000 2	2.539 1	5.765-2	1.831 0	2.174 1	1.359 1	6.594 0	1.176 1	6.276-1
1.000 3	3.402 1	5.536-2	1.985 0	2.832 1	1.488 1	7.527 0	1.249 1	6.265-1
1.500 3	5.700 1	5.132-2	2.259 0	4.551 1	1.761 1	9.541 0	1.389 1	6.475-1
2.000 3	8.042 1	4.853-2	2.451 0	6.347 1	1.988 1	1.127 1	1.494 1	6.987-1
2.500 3	1.031 2	4.638-2	2.601 0	8.203 1	2.186 1	1.281 1	1.578 1	7.674-1
3.000 3	1.247 2	4.462-2	2.726 0	1.011 2	2.363 1	1.422 1	1.646 1	8.421-1
4.000 3	1.647 2	4.181-2	2.931 0	1.404 2	2.674 1	1.676 1	1.750 1	9.927-1
4.590 3	1.865 2	4.043-2	3.033 0	1.642 2	2.836 1	1.812 1	1.797 1	1.081 0
5.000 3	2.010 2	3.955-2	3.099 0	1.811 2	2.942 1	1.903 1	1.825 1	1.142 0
6.000 3	2.342 2	3.762-2	3.243 0	2.232 2	3.181 1	2.113 1	1.885 1	1.291 0
8.000 3	2.934 2	3.443-2	3.489 0	3.103 2	3.597 1	2.491 1	1.997 1	1.580 0
1.000 4	3.453 2	3.199-2	3.702 0	4.001 2	3.960 1	2.829 1	2.124 1	1.843 0

Appendix A6

Molibdenum

MELTING CURVE

P	T	VS/VS0	VS	VL	SS	SL	ES	EL
1.000-4	2.890 0	1.000 0	1.020-1	1.066-1	6.213-1	7.573-1	7.195-1	1.113 0
5.000 0	3.053 0	9.820-1	1.002-1	1.043-1	6.295-1	7.592-1	7.486-1	1.124 0
6.000 0	3.084 0	9.786-1	9.982-2	1.038-1	6.311-1	7.597-1	7.553-1	1.128 0
8.000 0	3.146 0	9.720-1	9.916-2	1.030-1	6.341-1	7.605-1	7.692-1	1.136 0
1.000 1	3.206 0	9.657-1	9.851-2	1.022-1	6.369-1	7.615-1	7.840-1	1.146 0
1.500 1	3.354 0	9.509-1	9.700-2	1.005-1	6.436-1	7.638-1	8.248-1	1.176 0
2.000 1	3.497 0	9.371-1	9.559-2	9.889-2	6.497-1	7.664-1	8.705-1	1.212 0
2.500 1	3.637 0	9.242-1	9.427-2	9.743-2	6.555-1	7.690-1	9.206-1	1.254 0
3.000 1	3.775 0	9.120-1	9.303-2	9.607-2	6.610-1	7.716-1	9.748-1	1.301 0
4.000 1	4.046 0	8.899-1	9.077-2	9.360-2	6.711-1	7.768-1	1.093 0	1.408 0
5.000 1	4.310 0	8.700-1	8.875-2	9.140-2	6.804-1	7.819-1	1.223 0	1.528 0
6.000 1	4.569 0	8.520-1	8.691-2	8.942-2	6.889-1	7.869-1	1.362 0	1.659 0
8.000 1	5.072 0	8.205-1	8.369-2	8.598-2	7.040-1	7.964-1	1.659 0	1.945 0
1.000 2	5.559 0	7.935-1	8.094-2	8.306-2	7.171-1	8.055-1	1.976 0	2.255 0
1.500 2	6.727 0	7.395-1	7.543-2	7.730-2	7.442-1	8.262-1	2.823 0	3.095 0
2.000 2	7.838 0	6.980-1	7.120-2	7.293-2	7.656-1	8.448-1	3.715 0	3.991 0
2.500 2	8.903 0	6.646-1	6.779-2	6.942-2	7.835-1	8.616-1	4.630 0	4.918 0
3.000 2	9.926 0	6.366-1	6.494-2	6.651-2	7.988-1	8.768-1	5.556 0	5.860 0
4.000 2	1.186 1	5.919-1	6.038-2	6.185-2	8.239-1	9.033-1	7.414 0	7.767 0
5.000 2	1.364 1	5.571-1	5.683-2	5.822-2	8.435-1	9.253-1	9.257 0	9.672 0
6.000 2	1.528 1	5.288-1	5.394-2	5.527-2	8.594-1	9.436-1	1.107 1	1.156 1
8.000 2	1.820 1	4.848-1	4.945-2	5.065-2	8.832-1	9.721-1	1.459 1	1.524 1
1.000 3	2.072 1	4.515-1	4.606-2	4.714-2	9.000-1	9.929-1	1.795 1	1.879 1

SATURATION CURVE

P	T	T/TC	VL	VG	SL	SG	EL	EG
5.878-1	1.521 1	1.000 0	6.358-1	6.358-1	1.617 0	1.617 0	8.320 0	8.320 0
5.000-1	1.442 1	9.480-1	3.738-1	1.163 0	1.559 0	1.646 0	7.607 0	8.471 0
4.000-1	1.351 1	8.878-1	2.880-1	1.689 0	1.510 0	1.660 0	6.956 0	8.422 0
3.000-1	1.254 1	8.243-1	2.326-1	2.466 0	1.453 0	1.674 0	6.243 0	8.344 0
2.500-1	1.202 1	7.900-1	2.108-1	3.052 0	1.421 0	1.683 0	5.847 0	8.297 0
2.000-1	1.145 1	7.528-1	1.915-1	3.900 0	1.384 0	1.695 0	5.419 0	8.243 0
1.500-1	1.081 1	7.109-1	1.744-1	5.256 0	1.341 0	1.710 0	4.947 0	8.178 0
1.000-1	1.005 1	6.605-1	1.587-1	7.839 0	1.289 0	1.733 0	4.412 0	8.096 0
8.000-2	9.678 0	6.362-1	1.526-1	9.701 0	1.265 0	1.745 0	4.168 0	8.054 0
6.000-2	9.244 0	6.076-1	1.465-1	1.270 1	1.236 0	1.762 0	3.896 0	8.004 0
5.000-2	8.991 0	5.910-1	1.433-1	1.504 1	1.219 0	1.772 0	3.743 0	7.974 0
4.000-2	8.701 0	5.720-1	1.400-1	1.846 1	1.200 0	1.786 0	3.575 0	7.938 0
3.000-2	8.357 0	5.493-1	1.364-1	2.399 1	1.178 0	1.803 0	3.383 0	7.896 0
2.500-2	8.154 0	5.360-1	1.345-1	2.830 1	1.164 0	1.814 0	3.273 0	7.870 0
2.000-2	7.920 0	5.206-1	1.324-1	3.463 1	1.149 0	1.828 0	3.149 0	7.840 0
1.500-2	7.640 0	5.022-1	1.301-1	4.487 1	1.130 0	1.846 0	3.005 0	7.804 0
1.000-2	7.279 0	4.785-1	1.274-1	6.462 1	1.106 0	1.872 0	2.827 0	7.756 0
8.000-3	7.096 0	4.665-1	1.261-1	7.898 1	1.094 0	1.887 0	2.740 0	7.732 0
6.000-3	6.875 0	4.519-1	1.246-1	1.023 2	1.079 0	1.906 0	2.636 0	7.703 0
5.000-3	6.743 0	4.432-1	1.237-1	1.206 2	1.071 0	1.918 0	2.575 0	7.685 0
4.000-3	6.588 0	4.331-1	1.228-1	1.474 2	1.060 0	1.932 0	2.505 0	7.664 0
3.000-3	6.400 0	4.207-1	1.216-1	1.911 2	1.047 0	1.952 0	2.421 0	7.638 0
2.500-3	6.287 0	4.133-1	1.210-1	2.253 2	1.039 0	1.964 0	2.372 0	7.623 0
2.000-3	6.154 0	4.045-1	1.203-1	2.757 2	1.030 0	1.979 0	2.314 0	7.605 0
1.500-3	5.992 0	3.939-1	1.194-1	3.579 2	1.019 0	1.999 0	2.245 0	7.583 0
1.000-3	5.779 0	3.799-1	1.183-1	5.174 2	1.003 0	2.027 0	2.156 0	7.554 0
8.000-4	5.668 0	3.726-1	1.177-1	6.341 2	9.955-1	2.043 0	2.110 0	7.538 0
6.000-4	5.533 0	3.637-1	1.170-1	8.247 2	9.856-1	2.063 0	2.055 0	7.520 0
5.000-4	5.450 0	3.583-1	1.166-1	9.744 2	9.796-1	2.076 0	2.022 0	7.509 0
4.000-4	5.353 0	3.519-1	1.162-1	1.195 3	9.724-1	2.091 0	1.983 0	7.495 0
3.000-4	5.233 0	3.440-1	1.156-1	1.557 3	9.635-1	2.112 0	1.936 0	7.479 0
2.500-4	5.160 0	3.392-1	1.153-1	1.841 3	9.580-1	2.125 0	1.907 0	7.469 0
2.000-4	5.074 0	3.335-1	1.149-1	2.261 3	9.514-1	2.141 0	1.873 0	7.457 0
1.500-4	4.967 0	3.265-1	1.144-1	2.949 3	9.432-1	2.162 0	1.832 0	7.443 0
1.000-4	4.824 0	3.171-1	1.138-1	4.291 3	9.321-1	2.191 0	1.778 0	7.423 0

Molibdenum

SHOCK ADIABAT M= 1.000

P	T	V	S	E	D	U	CS	CV
1.000-4	2.930-1	9.780-2	7.153-7	2.082-7	.000 0	.000 0	5.117 0	2.610-1
1.000 1	3.117-1	9.445-2	1.552-3	1.674-2	5.344 0	1.830-1	5.378 0	2.610-1
1.500 1	3.238-1	9.297-2	4.782-3	3.622-2	5.451 0	2.692-1	5.496 0	2.610-1
2.000 1	3.388-1	9.160-2	1.025-2	6.200-2	5.554 0	3.522-1	5.608 0	2.610-1
2.500 1	3.574-1	9.032-2	1.821-2	9.350-2	5.654 0	4.324-1	5.714 0	2.610-1
3.000 1	3.801-1	8.913-2	2.854-2	1.301-1	5.752 0	5.101-1	5.815 0	2.610-1
4.000 1	4.389-1	8.695-2	5.543-2	2.170-1	5.939 0	6.587-1	6.004 0	2.610-1
5.000 1	5.172-1	8.502-2	8.847-2	3.195-1	6.118 0	7.993-1	6.179 0	2.611-1
6.000 1	6.159-1	8.329-2	1.252-1	4.353-1	6.289 0	9.331-1	6.342 0	2.614-1
8.000 1	8.750-1	8.030-2	2.012-1	7.002-1	6.612 0	1.183 0	6.636 0	2.631-1
1.000 2	1.212 0	7.778-2	2.738-1	1.001 0	6.912 0	1.415 0	6.898 0	2.668-1
1.500 2	2.343 0	7.286-2	4.259-1	1.870 0	7.585 0	1.934 0	7.454 0	2.773-1
2.000 2	3.826 0	6.922-2	5.428-1	2.859 0	8.181 0	2.391 0	7.921 0	2.857-1
2.500 2	5.597 0	6.637-2	6.356-1	3.929 0	8.722 0	2.803 0	8.326 0	2.930-1
3.000 2	7.600 0	6.405-2	7.117-1	5.062 0	9.221 0	3.182 0	8.683 0	3.002-1
3.912 2	1.169 1	6.073-2	8.219-1	7.251 0	1.005 1	3.808 0	9.245 0	3.146-1
3.912 2	1.169 1	6.073-2	8.219-1	7.251 0	1.005 1	3.808 0	9.064 0	1.506 0
4.000 2	1.186 1	6.054-2	8.325-1	7.452 0	1.013 1	3.861 0	9.124 0	1.519 0
4.745 2	1.320 1	5.908-2	9.200-1	9.187 0	1.083 1	4.286 0	9.592 0	1.641 0
4.745 2	1.320 1	5.908-2	9.200-1	9.187 0	1.083 1	4.286 0	9.769 0	3.849-1
5.000 2	1.428 1	5.844-2	9.451-1	9.840 0	1.102 1	4.436 0	9.890 0	3.909-1
6.000 2	1.860 1	5.622-2	1.032 0	1.247 1	1.175 1	4.995 0	1.033 1	4.112-1
8.000 2	2.756 1	5.271-2	1.168 0	1.804 1	1.303 1	6.006 0	1.106 1	4.419-1
1.000 3	3.684 1	5.002-2	1.276 0	2.389 1	1.415 1	6.912 0	1.169 1	4.663-1
1.500 3	6.065 1	4.531-2	1.478 0	3.937 1	1.653 1	8.873 0	1.296 1	5.262-1
2.000 3	8.412 1	4.214-2	1.627 0	5.566 1	1.854 1	1.055 1	1.399 1	5.952-1
2.500 3	1.065 2	3.979-2	1.749 0	7.251 1	2.030 1	1.204 1	1.487 1	6.699-1
3.000 3	1.275 2	3.794-2	1.854 0	8.979 1	2.189 1	1.340 1	1.565 1	7.455-1
4.000 3	1.661 2	3.517-2	2.030 0	1.253 2	2.472 1	1.583 1	1.701 1	8.901-1
5.000 3	2.010 2	3.316-2	2.179 0	1.616 2	2.720 1	1.798 1	1.819 1	1.021 0
6.000 3	2.331 2	3.162-2	2.311 0	1.985 2	2.945 1	1.993 1	1.926 1	1.138 0
8.000 3	2.912 2	2.944-2	2.539 0	2.735 2	3.346 1	2.339 1	2.116 1	1.338 0
1.000 4	3.437 2	2.796-2	2.736 0	3.492 2	3.701 1	2.643 1	2.287 1	1.502 0

Appendix A7

Tantalum

MELTING CURVE

P	T	VS/VS0	VS	VL	SS	SL	ES	EL
1.000-4	3.290 0	1.000 0	6.423-2	6.797-2	3.624-1	4.234-1	4.730-1	6.737-1
5.000 0	3.585 0	9.740-1	6.256-2	6.589-2	3.714-1	4.302-1	5.080-1	7.020-1
6.000 0	3.641 0	9.692-1	6.225-2	6.552-2	3.731-1	4.315-1	5.158-1	7.088-1
8.000 0	3.751 0	9.600-1	6.166-2	6.481-2	3.763-1	4.341-1	5.319-1	7.234-1
1.000 1	3.859 0	9.513-1	6.110-2	6.414-2	3.794-1	4.366-1	5.487-1	7.390-1
1.500 1	4.118 0	9.311-1	5.981-2	6.263-2	3.866-1	4.427-1	5.934-1	7.820-1
2.000 1	4.364 0	9.128-1	5.863-2	6.129-2	3.930-1	4.483-1	6.413-1	8.294-1
2.500 1	4.600 0	8.960-1	5.755-2	6.008-2	3.989-1	4.536-1	6.917-1	8.802-1
3.000 1	4.827 0	8.806-1	5.656-2	5.898-2	4.042-1	4.585-1	7.440-1	9.335-1
4.000 1	5.256 0	8.530-1	5.479-2	5.701-2	4.134-1	4.671-1	8.521-1	1.045 0
5.000 1	5.655 0	8.291-1	5.325-2	5.529-2	4.210-1	4.742-1	9.629-1	1.162 0
6.000 1	6.024 0	8.078-1	5.189-2	5.378-2	4.273-1	4.801-1	1.074 0	1.279 0
8.000 1	6.692 0	7.717-1	4.957-2	5.120-2	4.368-1	4.892-1	1.296 0	1.516 0
1.000 2	7.277 0	7.416-1	4.763-2	4.907-2	4.433-1	4.955-1	1.515 0	1.752 0
1.500 2	8.470 0	6.833-1	4.389-2	4.497-2	4.519-1	5.041-1	2.045 0	2.325 0
2.000 2	9.391 0	6.399-1	4.110-2	4.195-2	4.548-1	5.072-1	2.556 0	2.877 0
2.500 2	1.012 1	6.056-1	3.890-2	3.959-2	4.549-1	5.078-1	3.051 0	3.411 0
3.000 2	1.072 1	5.775-1	3.709-2	3.767-2	4.537-1	5.070-1	3.533 0	3.930 0
4.000 2	1.165 1	5.335-1	3.427-2	3.469-2	4.494-1	5.037-1	4.466 0	4.927 0
5.000 2	1.234 1	5.001-1	3.212-2	3.246-2	4.443-1	4.996-1	5.364 0	5.880 0
6.000 2	1.288 1	4.736-1	3.042-2	3.069-2	4.391-1	4.954-1	6.232 0	6.795 0
8.000 2	1.368 1	4.335-1	2.784-2	2.804-2	4.296-1	4.877-1	7.895 0	8.535 0
1.000 3	1.425 1	4.040-1	2.595-2	2.610-2	4.213-1	4.809-1	9.477 0	1.018 1

SATURATION CURVE

P	T	T/TC	VL	VG	SL	SG	EL	EG
7.756-1	1.426 1	1.000 0	2.592-1	2.592-1	9.528-1	9.528-1	5.099 0	5.099 0
6.000-1	1.354 1	9.491-1	1.823-1	4.081-1	9.130-1	9.668-1	4.599 0	5.190 0
5.000-1	1.311 1	9.192-1	1.667-1	4.815-1	8.962-1	9.686-1	4.382 0	5.174 0
4.000-1	1.267 1	8.879-1	1.541-1	5.730-1	8.788-1	9.703-1	4.164 0	5.155 0
3.000-1	1.219 1	8.546-1	1.431-1	7.016-1	8.601-1	9.723-1	3.936 0	5.136 0
2.500-1	1.193 1	8.366-1	1.379-1	7.923-1	8.498-1	9.736-1	3.813 0	5.126 0
2.000-1	1.166 1	8.173-1	1.327-1	9.163-1	8.386-1	9.750-1	3.682 0	5.116 0
1.500-1	1.135 1	7.960-1	1.274-1	1.105 0	8.260-1	9.769-1	3.538 0	5.105 0
1.000-1	1.100 1	7.711-1	1.217-1	1.462 0	8.109-1	9.795-1	3.370 0	5.090 0
8.000-2	1.083 1	7.592-1	1.191-1	1.744 0	8.035-1	9.810-1	3.289 0	5.082 0
6.000-2	1.062 1	7.449-1	1.161-1	2.320 0	7.945-1	9.836-1	3.193 0	5.069 0
5.000-2	1.050 1	7.358-1	1.142-1	2.994 0	7.887-1	9.860-1	3.132 0	5.059 0
4.000-2	1.032 1	7.234-1	1.118-1	4.684 0	7.807-1	9.914-1	3.049 0	5.040 0
3.000-2	1.004 1	7.037-1	1.081-1	8.378 0	7.678-1	1.001 0	2.918 0	5.008 0
2.500-2	9.838 0	6.897-1	1.057-1	1.124 1	7.585-1	1.007 0	2.826 0	4.989 0
2.000-2	9.585 0	6.720-1	1.027-1	1.532 1	7.467-1	1.014 0	2.711 0	4.966 0
1.500-2	9.259 0	6.491-1	9.924-2	2.181 1	7.313-1	1.023 0	2.566 0	4.938 0
1.000-2	8.819 0	6.183-1	9.496-2	3.416 1	7.103-1	1.035 0	2.376 0	4.903 0
8.000-3	8.591 0	6.023-1	9.293-2	4.310 1	6.994-1	1.043 0	2.281 0	4.885 0
6.000-3	8.311 0	5.826-1	9.061-2	5.759 1	6.859-1	1.052 0	2.167 0	4.863 0
5.000-3	8.142 0	5.708-1	8.929-2	6.892 1	6.778-1	1.058 0	2.100 0	4.851 0
4.000-3	7.945 0	5.570-1	8.783-2	8.559 1	6.683-1	1.065 0	2.024 0	4.836 0
3.000-3	7.705 0	5.402-1	8.615-2	1.127 2	6.567-1	1.075 0	1.933 0	4.818 0
2.500-3	7.561 0	5.301-1	8.519-2	1.340 2	6.497-1	1.081 0	1.880 0	4.808 0
2.000-3	7.392 0	5.182-1	8.412-2	1.653 2	6.415-1	1.089 0	1.818 0	4.796 0
1.500-3	7.186 0	5.038-1	8.287-2	2.163 2	6.315-1	1.099 0	1.746 0	4.781 0
1.000-3	6.916 0	4.849-1	8.134-2	3.154 2	6.184-1	1.113 0	1.653 0	4.761 0
8.000-4	6.777 0	4.751-1	8.060-2	3.880 2	6.116-1	1.121 0	1.606 0	4.751 0
6.000-4	6.607 0	4.632-1	7.972-2	5.064 2	6.032-1	1.132 0	1.551 0	4.739 0
5.000-4	6.504 0	4.560-1	7.921-2	5.995 2	5.982-1	1.138 0	1.517 0	4.732 0
4.000-4	6.383 0	4.475-1	7.862-2	7.370 2	5.922-1	1.147 0	1.479 0	4.723 0
3.000-4	6.234 0	4.371-1	7.792-2	9.617 2	5.848-1	1.157 0	1.432 0	4.713 0
2.500-4	6.144 0	4.307-1	7.751-2	1.138 3	5.803-1	1.164 0	1.405 0	4.706 0
2.000-4	6.037 0	4.233-1	7.704-2	1.400 3	5.750-1	1.172 0	1.372 0	4.699 0
1.500-4	5.906 0	4.140-1	7.648-2	1.827 3	5.684-1	1.183 0	1.333 0	4.690 0
1.000-4	5.731 0	4.018-1	7.575-2	2.662 3	5.596-1	1.199 0	1.282 0	4.677 0

Tantalum

SHOCK ADIABAT M= 1.000

P	T	V	S	E	D	U	CS	CV
1.000-4	2.930-1	6.000-2	-1.252-6	-3.731-7	.000 0	.000 0	3.410 0	1.380-1
1.000 1	3.222-1	5.724-2	1.659-3	1.378-2	3.612 0	1.661-1	3.637 0	1.380-1
1.500 1	3.420-1	5.607-2	4.959-3	2.950-2	3.706 0	2.429-1	3.739 0	1.380-1
2.000 1	3.675-1	5.501-2	1.035-2	4.994-2	3.797 0	3.161-1	3.835 0	1.380-1
2.500 1	3.995-1	5.404-2	1.770-2	7.455-2	3.885 0	3.861-1	3.925 0	1.380-1
3.000 1	4.388-1	5.315-2	2.681-2	1.028-1	3.970 0	4.535-1	4.011 0	1.380-1
4.000 1	5.411-1	5.157-2	4.879-2	1.687-1	4.132 0	5.809-1	4.172 0	1.381-1
5.000 1	6.757-1	5.020-2	7.348-2	2.451-1	4.285 0	7.001-1	4.318 0	1.386-1
6.000 1	8.419-1	4.900-2	9.879-2	3.301-1	4.431 0	8.125-1	4.453 0	1.402-1
8.000 1	1.253 0	4.696-2	1.467-1	5.215-1	4.700 0	1.021 0	4.692 0	1.464-1
1.000 2	1.747 0	4.528-2	1.895-1	7.360-1	4.946 0	1.213 0	4.907 0	1.538-1
1.500 2	3.289 0	4.210-2	2.771-1	1.342 0	5.493 0	1.638 0	5.391 0	1.660-1
2.000 2	5.239 0	3.988-2	3.447-1	2.012 0	5.982 0	2.006 0	5.810 0	1.719-1
2.500 2	7.539 0	3.823-2	3.985-1	2.722 0	6.430 0	2.333 0	6.175 0	1.751-1
3.000 2	1.012 1	3.695-2	4.425-1	3.457 0	6.845 0	2.630 0	6.498 0	1.779-1
3.137 2	1.087 1	3.665-2	4.532-1	3.663 0	6.954 0	2.707 0	6.581 0	1.787-1
3.137 2	1.087 1	3.665-2	4.532-1	3.663 0	6.954 0	2.707 0	6.573 0	3.120 0
3.830 2	1.151 1	3.514-2	5.044-1	4.761 0	7.447 0	3.086 0	6.835 0	4.403 0
3.830 2	1.151 1	3.514-2	5.044-1	4.761 0	7.447 0	3.086 0	6.844 0	2.156-1
4.000 2	1.234 1	3.483-2	5.172-1	5.034 0	7.564 0	3.173 0	6.923 0	2.177-1
5.000 2	1.735 1	3.327-2	5.817-1	6.682 0	8.207 0	3.656 0	7.341 0	2.298-1
6.000 2	2.250 1	3.202-2	6.333-1	8.395 0	8.786 0	4.098 0	7.699 0	2.421-1
8.000 2	3.291 1	3.006-2	7.142-1	1.198 1	9.807 0	4.894 0	8.305 0	2.670-1
1.000 3	4.320 1	2.855-2	7.775-1	1.572 1	1.070 1	5.608 0	8.821 0	2.919-1
1.500 3	6.766 1	2.589-2	8.973-1	2.559 1	1.258 1	7.154 0	9.883 0	3.544-1
2.000 3	9.012 1	2.407-2	9.887-1	3.593 1	1.416 1	8.477 0	1.075 1	4.141-1
2.500 3	1.109 2	2.272-2	1.065 0	4.660 1	1.554 1	9.654 0	1.151 1	4.679-1
3.000 3	1.304 2	2.167-2	1.131 0	5.749 1	1.679 1	1.072 1	1.218 1	5.151-1
4.000 3	1.666 2	2.016-2	1.246 0	7.969 1	1.901 1	1.262 1	1.339 1	5.925-1
5.000 3	2.003 2	1.912-2	1.343 0	1.022 2	2.098 1	1.430 1	1.446 1	6.542-1
6.000 3	2.322 2	1.838-2	1.429 0	1.249 2	2.278 1	1.580 1	1.544 1	7.073-1
8.000 3	2.913 2	1.741-2	1.578 0	1.704 2	2.600 1	1.846 1	1.723 1	8.028-1
1.000 4	3.451 2	1.683-2	1.705 0	2.159 2	2.888 1	2.078 1	1.882 1	8.923-1

Appendix A8

Tungsten

MELTING CURVE

P	T	VS/VS0	VS	VL	SS	SL	ES	EL
1.000-4	3.690 0	1.000 0	5.459-2	5.999-2	3.597-1	4.307-1	4.952-1	7.572-1
5.000 0	4.067 0	9.870-1	5.387-2	5.909-2	3.711-1	4.408-1	5.411-1	7.985-1
6.000 0	4.142 0	9.845-1	5.374-2	5.893-2	3.732-1	4.427-1	5.506-1	8.073-1
8.000 0	4.291 0	9.796-1	5.347-2	5.860-2	3.773-1	4.465-1	5.699-1	8.254-1
1.000 1	4.439 0	9.749-1	5.322-2	5.829-2	3.813-1	4.501-1	5.896-1	8.441-1
1.500 1	4.805 0	9.636-1	5.260-2	5.756-2	3.907-1	4.588-1	6.404-1	8.933-1
2.000 1	5.167 0	9.530-1	5.202-2	5.688-2	3.993-1	4.669-1	6.933-1	9.454-1
2.500 1	5.524 0	9.430-1	5.148-2	5.626-2	4.072-1	4.745-1	7.478-1	1.000 0
3.000 1	5.878 0	9.335-1	5.096-2	5.567-2	4.145-1	4.816-1	8.039-1	1.057 0
4.000 1	6.572 0	9.157-1	4.999-2	5.460-2	4.277-1	4.948-1	9.199-1	1.176 0
5.000 1	7.253 0	8.995-1	4.910-2	5.363-2	4.394-1	5.067-1	1.040 0	1.302 0
6.000 1	7.919 0	8.846-1	4.829-2	5.275-2	4.498-1	5.174-1	1.164 0	1.432 0
8.000 1	9.209 0	8.578-1	4.682-2	5.114-2	4.676-1	5.361-1	1.418 0	1.703 0
1.000 2	1.044 1	8.342-1	4.554-2	4.971-2	4.822-1	5.516-1	1.677 0	1.985 0
1.500 2	1.326 1	7.853-1	4.287-2	4.662-2	5.095-1	5.806-1	2.330 0	2.710 0
2.000 2	1.573 1	7.458-1	4.071-2	4.405-2	5.281-1	6.003-1	2.974 0	3.442 0
2.500 2	1.790 1	7.127-1	3.890-2	4.185-2	5.412-1	6.140-1	3.600 0	4.166 0
3.000 2	1.979 1	6.840-1	3.734-2	3.994-2	5.506-1	6.239-1	4.206 0	4.875 0
4.000 2	2.293 1	6.365-1	3.475-2	3.679-2	5.623-1	6.362-1	5.356 0	6.235 0
5.000 2	2.539 1	5.983-1	3.266-2	3.429-2	5.681-1	6.428-1	6.432 0	7.512 0
6.000 2	2.735 1	5.668-1	3.094-2	3.226-2	5.708-1	6.461-1	7.447 0	8.712 0
8.000 2	3.026 1	5.172-1	2.823-2	2.916-2	5.710-1	6.480-1	9.332 0	1.092 1
1.000 3	3.232 1	4.798-1	2.619-2	2.688-2	5.683-1	6.469-1	1.108 1	1.292 1

SATURATION CURVE

P	T	T/TC	VL	VG	SL	SG	EL	EG
1.074 0	1.512 1	1.000 0	2.105-1	2.105-1	9.040-1	9.040-1	5.073 0	5.073 0
1.000 0	1.492 1	9.866-1	1.706-1	2.701-1	8.838-1	9.194-1	4.809 0	5.242 0
8.000-1	1.434 1	9.481-1	1.421-1	3.683-1	8.574-1	9.317-1	4.449 0	5.334 0
6.000-1	1.369 1	9.053-1	1.255-1	4.968-1	8.332-1	9.403-1	4.122 0	5.366 0
5.000-1	1.333 1	8.814-1	1.187-1	5.920-1	8.202-1	9.447-1	3.950 0	5.372 0
4.000-1	1.292 1	8.547-1	1.122-1	7.320-1	8.059-1	9.495-1	3.765 0	5.373 0
3.000-1	1.245 1	8.235-1	1.059-1	9.699-1	7.892-1	9.555-1	3.555 0	5.367 0
2.000-1	1.185 1	7.839-1	9.899-2	1.490 0	7.677-1	9.644-1	3.296 0	5.349 0
1.500-1	1.145 1	7.575-1	9.502-2	2.073 0	7.532-1	9.715-1	3.128 0	5.331 0
1.000-1	1.091 1	7.218-1	9.024-2	3.350 0	7.333-1	9.825-1	2.906 0	5.299 0
8.000-2	1.063 1	7.027-1	8.793-2	4.342 0	7.225-1	9.890-1	2.790 0	5.280 0
6.000-2	1.026 1	6.788-1	8.527-2	6.000 0	7.090-1	9.976-1	2.649 0	5.256 0
5.000-2	1.004 1	6.642-1	8.374-2	7.317 0	7.007-1	1.003 0	2.564 0	5.241 0
4.000-2	9.781 0	6.469-1	8.203-2	9.268 0	6.907-1	1.010 0	2.466 0	5.223 0
3.000-2	9.459 0	6.256-1	8.006-2	1.246 1	6.784-1	1.019 0	2.347 0	5.201 0
2.000-2	9.035 0	5.975-1	7.768-2	1.866 1	6.621-1	1.032 0	2.197 0	5.171 0
1.500-2	8.755 0	5.790-1	7.621-2	2.468 1	6.512-1	1.042 0	2.100 0	5.152 0
1.000-2	8.388 0	5.547-1	7.443-2	3.637 1	6.369-1	1.056 0	1.977 0	5.126 0
8.000-3	8.199 0	5.422-1	7.356-2	4.491 1	6.295-1	1.063 0	1.916 0	5.113 0
6.000-3	7.968 0	5.270-1	7.255-2	5.883 1	6.204-1	1.073 0	1.842 0	5.097 0
5.000-3	7.829 0	5.177-1	7.196-2	6.976 1	6.149-1	1.079 0	1.799 0	5.087 0
4.000-3	7.665 0	5.069-1	7.129-2	8.588 1	6.084-1	1.087 0	1.748 0	5.076 0
3.000-3	7.465 0	4.937-1	7.050-2	1.122 2	6.004-1	1.097 0	1.688 0	5.062 0
2.500-3	7.344 0	4.857-1	7.004-2	1.328 2	5.955-1	1.104 0	1.652 0	5.054 0
2.000-3	7.201 0	4.762-1	6.951-2	1.633 2	5.897-1	1.112 0	1.610 0	5.044 0
1.500-3	7.026 0	4.647-1	6.888-2	2.132 2	5.826-1	1.122 0	1.559 0	5.032 0
1.000-3	6.795 0	4.494-1	6.808-2	3.102 2	5.732-1	1.137 0	1.494 0	5.016 0
8.000-4	6.674 0	4.414-1	6.767-2	3.813 2	5.682-1	1.145 0	1.461 0	5.007 0
6.000-4	6.526 0	4.316-1	6.719-2	4.977 2	5.621-1	1.156 0	1.420 0	4.997 0
5.000-4	6.436 0	4.256-1	6.690-2	5.893 2	5.584-1	1.163 0	1.396 0	4.991 0
4.000-4	6.329 0	4.186-1	6.657-2	7.248 2	5.539-1	1.171 0	1.367 0	4.983 0
3.000-4	6.197 0	4.098-1	6.616-2	9.466 2	5.483-1	1.182 0	1.333 0	4.974 0
2.500-4	6.116 0	4.045-1	6.592-2	1.121 3	5.449-1	1.189 0	1.312 0	4.969 0
2.000-4	6.021 0	3.982-1	6.564-2	1.380 3	5.409-1	1.197 0	1.287 0	4.962 0
1.500-4	5.902 0	3.904-1	6.530-2	1.804 3	5.358-1	1.208 0	1.257 0	4.954 0
1.000-4	5.744 0	3.799-1	6.485-2	2.633 3	5.290-1	1.223 0	1.217 0	4.943 0

Tungsten

SHOCK ADIABAT M= 1.000

P	T	V	S	E	D	U	CS	CV
1.000-4	2.930-1	5.190-2	-1.416-6	-4.109-7	.000 0	.000 0	4.014 0	1.360-1
1.000 1	3.097-1	5.034-2	6.262-4	7.781-3	4.162 0	1.247-1	4.180 0	1.360-1
1.500 1	3.200-1	4.964-2	1.913-3	1.692-2	4.232 0	1.840-1	4.256 0	1.360-1
2.000 1	3.326-1	4.899-2	4.156-3	2.913-2	4.301 0	2.413-1	4.329 0	1.360-1
2.500 1	3.479-1	4.837-2	7.458-3	4.413-2	4.368 0	2.971-1	4.399 0	1.360-1
3.000 1	3.665-1	4.779-2	1.180-2	6.166-2	4.433 0	3.512-1	4.467 0	1.360-1
4.000 1	4.149-1	4.672-2	2.361-2	1.036-1	4.560 0	4.553-1	4.594 0	1.360-1
5.000 1	4.793-1	4.575-2	3.863-2	1.536-1	4.681 0	5.543-1	4.713 0	1.360-1
6.000 1	5.613-1	4.488-2	5.585-2	2.106-1	4.798 0	6.490-1	4.824 0	1.360-1
8.000 1	7.796-1	4.335-2	9.299-2	3.420-1	5.020 0	8.271-1	5.029 0	1.363-1
1.000 2	1.070 0	4.205-2	1.297-1	4.928-1	5.228 0	9.928-1	5.213 0	1.370-1
1.500 2	2.084 0	3.947-2	2.089-1	9.326-1	5.701 0	1.366 0	5.612 0	1.406-1
2.000 2	3.450 0	3.752-2	2.706-1	1.438 0	6.121 0	1.696 0	5.951 0	1.444-1
2.500 2	5.107 0	3.599-2	3.196-1	1.989 0	6.506 0	1.995 0	6.250 0	1.485-1
3.000 2	6.997 0	3.473-2	3.599-1	2.575 0	6.861 0	2.269 0	6.518 0	1.529-1
4.000 2	1.128 1	3.278-2	4.234-1	3.824 0	7.507 0	2.765 0	6.983 0	1.628-1
5.000 2	1.600 1	3.130-2	4.724-1	5.149 0	8.086 0	3.209 0	7.382 0	1.739-1
6.000 2	2.093 1	3.012-2	5.125-1	6.534 0	8.615 0	3.615 0	7.731 0	1.862-1
7.818 2	3.004 1	2.845-2	5.712-1	9.167 0	9.476 0	4.282 0	8.276 0	2.102-1
7.818 2	3.004 1	2.845-2	5.712-1	9.167 0	9.476 0	4.282 0	8.273 0	2.291 0
8.000 2	3.026 1	2.830-2	5.763-1	9.441 0	9.555 0	4.345 0	8.302 0	2.416 0
1.000 3	3.232 1	2.675-2	6.321-1	1.257 1	1.035 1	5.015 0	8.616 0	4.012 0
1.052 3	3.276 1	2.639-2	6.464-1	1.342 1	1.054 1	5.180 0	8.698 0	4.489 0
1.052 3	3.276 1	2.639-2	6.464-1	1.342 1	1.054 1	5.180 0	8.703 0	2.684-1
1.500 3	5.136 1	2.401-2	7.548-1	2.092 1	1.204 1	6.468 0	9.554 0	3.085-1
2.000 3	7.152 1	2.219-2	8.469-1	2.971 1	1.347 1	7.708 0	1.034 1	3.563-1
2.500 3	9.057 1	2.085-2	9.224-1	3.881 1	1.473 1	8.810 0	1.101 1	4.051-1
3.000 3	1.085 2	1.981-2	9.874-1	4.814 1	1.587 1	9.812 0	1.160 1	4.519-1
4.000 3	1.416 2	1.827-2	1.098 0	6.726 1	1.790 1	1.160 1	1.265 1	5.349-1
5.000 3	1.721 2	1.719-2	1.192 0	8.677 1	1.970 1	1.317 1	1.357 1	6.035-1
6.000 3	2.007 2	1.640-2	1.274 0	1.065 2	2.134 1	1.459 1	1.440 1	6.609-1
8.000 3	2.540 2	1.533-2	1.417 0	1.463 2	2.427 1	1.711 1	1.592 1	7.553-1
1.000 4	3.031 2	1.466-2	1.539 0	1.862 2	2.689 1	1.930 1	1.730 1	8.360-1

Appendix A9

Gold

MELTING CURVE

P	T	VS/VS0	VS	VL	SS	SL	ES	EL
1.000-4	1.340 0	1.000 0	5.444-2	5.743-2	2.118-1	2.592-1	1.486-1	2.121-1
5.000 0	1.625 0	9.789-1	5.329-2	5.575-2	2.285-1	2.760-1	1.760-1	2.408-1
6.000 0	1.676 0	9.749-1	5.307-2	5.545-2	2.309-1	2.785-1	1.812-1	2.467-1
8.000 0	1.773 0	9.670-1	5.264-2	5.489-2	2.351-1	2.830-1	1.914-1	2.584-1
1.000 1	1.864 0	9.594-1	5.223-2	5.436-2	2.387-1	2.869-1	2.016-1	2.702-1
1.500 1	2.070 0	9.414-1	5.125-2	5.316-2	2.453-1	2.947-1	2.269-1	3.004-1
2.000 1	2.253 0	9.247-1	5.034-2	5.210-2	2.500-1	3.006-1	2.528-1	3.318-1
2.500 1	2.419 0	9.092-1	4.950-2	5.114-2	2.534-1	3.054-1	2.798-1	3.643-1
3.000 1	2.571 0	8.947-1	4.871-2	5.027-2	2.560-1	3.093-1	3.079-1	3.981-1
4.000 1	2.844 0	8.686-1	4.729-2	4.871-2	2.597-1	3.156-1	3.676-1	4.693-1
5.000 1	3.086 0	8.456-1	4.603-2	4.736-2	2.622-1	3.204-1	4.313-1	5.443-1
6.000 1	3.304 0	8.251-1	4.492-2	4.617-2	2.640-1	3.243-1	4.983-1	6.222-1
8.000 1	3.688 0	7.900-1	4.301-2	4.415-2	2.663-1	3.303-1	6.394-1	7.840-1
1.000 2	4.024 0	7.609-1	4.142-2	4.248-2	2.677-1	3.348-1	7.870-1	9.507-1
1.500 2	4.730 0	7.049-1	3.837-2	3.930-2	2.690-1	3.419-1	1.169 0	1.375 0
2.000 2	5.314 0	6.638-1	3.614-2	3.697-2	2.687-1	3.456-1	1.556 0	1.799 0
2.500 2	5.818 0	6.317-1	3.439-2	3.514-2	2.676-1	3.475-1	1.942 0	2.218 0
3.000 2	6.263 0	6.054-1	3.296-2	3.365-2	2.661-1	3.482-1	2.325 0	2.632 0
4.000 2	7.021 0	5.643-1	3.072-2	3.131-2	2.625-1	3.479-1	3.079 0	3.444 0
5.000 2	7.652 0	5.329-1	2.901-2	2.952-2	2.586-1	3.464-1	3.817 0	4.235 0
6.000 2	8.188 0	5.076-1	2.763-2	2.808-2	2.547-1	3.444-1	4.540 0	5.007 0
8.000 2	9.057 0	4.688-1	2.552-2	2.588-2	2.473-1	3.400-1	5.943 0	6.500 0
1.000 3	9.740 0	4.397-1	2.394-2	2.423-2	2.405-1	3.357-1	7.298 0	7.934 0

SATURATION CURVE

P	T	T/TC	VL	VG	SL	SG	EL	EG
7.568-1	9.007 0	1.000 0	1.514-1	1.514-1	6.336-1	6.336-1	1.933 0	1.933 0
6.000-1	8.653 0	9.607-1	1.149-1	2.256-1	6.079-1	6.548-1	1.731 0	2.070 0
5.000-1	8.408 0	9.335-1	1.069-1	2.674-1	5.980-1	6.612-1	1.651 0	2.102 0
4.000-1	8.142 0	9.040-1	1.006-1	3.208-1	5.883-1	6.669-1	1.573 0	2.125 0
3.000-1	7.843 0	8.708-1	9.516-2	3.987-1	5.778-1	6.725-1	1.491 0	2.143 0
2.500-1	7.676 0	8.522-1	9.255-2	4.562-1	5.720-1	6.754-1	1.447 0	2.149 0
2.000-1	7.489 0	8.315-1	8.994-2	5.391-1	5.656-1	6.785-1	1.399 0	2.154 0
1.500-1	7.273 0	8.075-1	8.722-2	6.779-1	5.581-1	6.821-1	1.344 0	2.157 0
1.000-1	6.997 0	7.768-1	8.414-2	1.002 0	5.485-1	6.873-1	1.276 0	2.155 0
8.000-2	6.848 0	7.603-1	8.262-2	1.333 0	5.433-1	6.909-1	1.240 0	2.151 0
6.000-2	6.643 0	7.375-1	8.068-2	2.126 0	5.360-1	6.975-1	1.191 0	2.141 0
5.000-2	6.499 0	7.215-1	7.941-2	2.889 0	5.308-1	7.024-1	1.157 0	2.132 0
4.000-2	6.310 0	7.006-1	7.788-2	4.057 0	5.240-1	7.086-1	1.113 0	2.119 0
3.000-2	6.060 0	6.728-1	7.601-2	5.943 0	5.149-1	7.164-1	1.057 0	2.102 0
2.500-2	5.901 0	6.552-1	7.493-2	7.396 0	5.090-1	7.213-1	1.022 0	2.091 0
2.000-2	5.711 0	6.341-1	7.371-2	9.508 0	5.019-1	7.272-1	9.809-1	2.079 0
1.500-2	5.476 0	6.080-1	7.232-2	1.290 1	4.930-1	7.349-1	9.311-1	2.063 0
1.000-2	5.167 0	5.737-1	7.063-2	1.937 1	4.810-1	7.459-1	8.671-1	2.043 0
8.000-3	5.009 0	5.561-1	6.983-2	2.405 1	4.747-1	7.521-1	8.350-1	2.033 0
6.000-3	4.817 0	5.348-1	6.890-2	3.160 1	4.669-1	7.602-1	7.967-1	2.020 0
5.000-3	4.702 0	5.220-1	6.837-2	3.749 1	4.622-1	7.654-1	7.741-1	2.013 0
4.000-3	4.568 0	5.071-1	6.777-2	4.612 1	4.565-1	7.719-1	7.481-1	2.004 0
3.000-3	4.405 0	4.891-1	6.707-2	6.012 1	4.496-1	7.803-1	7.170-1	1.994 0
2.500-3	4.308 0	4.783-1	6.667-2	7.104 1	4.454-1	7.857-1	6.986-1	1.987 0
2.000-3	4.195 0	4.657-1	6.621-2	8.708 1	4.404-1	7.925-1	6.773-1	1.980 0
1.500-3	4.057 0	4.505-1	6.567-2	1.131 2	4.342-1	8.012-1	6.518-1	1.971 0
1.000-3	3.878 0	4.306-1	6.498-2	1.635 2	4.259-1	8.138-1	6.191-1	1.960 0
8.000-4	3.787 0	4.204-1	6.464-2	2.001 2	4.216-1	8.208-1	6.026-1	1.954 0
6.000-4	3.675 0	4.080-1	6.424-2	2.598 2	4.163-1	8.299-1	5.826-1	1.947 0
5.000-4	3.607 0	4.005-1	6.400-2	3.065 2	4.130-1	8.357-1	5.706-1	1.942 0
4.000-4	3.528 0	3.917-1	6.372-2	3.754 2	4.091-1	8.429-1	5.567-1	1.937 0
3.000-4	3.432 0	3.810-1	6.339-2	4.875 2	4.042-1	8.523-1	5.399-1	1.931 0
2.500-4	3.373 0	3.745-1	6.319-2	5.755 2	4.013-1	8.582-1	5.298-1	1.927 0
2.000-4	3.305 0	3.669-1	6.296-2	7.053 2	3.977-1	8.656-1	5.179-1	1.923 0
1.500-4	3.220 0	3.575-1	6.268-2	9.170 2	3.933-1	8.751-1	5.035-1	1.917 0
1.000-4	3.109 0	3.451-1	6.232-2	1.329 3	3.874-1	8.887-1	4.847-1	1.910 0

Gold

SHOCK ADIABAT M= 1.000

P	T	V	S	E	D	U	CS	CV
1.000-4	2.930-1	5.180-2	-2.846-6	-8.327-7	.000 0	.000 0	3.019 0	1.270-1
1.000 1	3.454-1	4.930-2	2.013-3	1.250-2	3.277 0	1.581-1	3.353 0	1.270-1
1.500 1	3.780-1	4.830-2	5.600-3	2.625-2	3.392 0	2.291-1	3.492 0	1.270-1
2.000 1	4.173-1	4.742-2	1.109-2	4.380-2	3.500 0	2.960-1	3.619 0	1.270-1
2.500 1	4.642-1	4.664-2	1.822-2	6.456-2	3.604 0	3.593-1	3.736 0	1.270-1
3.000 1	5.193-1	4.593-2	2.659-2	8.805-2	3.703 0	4.197-1	3.845 0	1.270-1
4.000 1	6.551-1	4.471-2	4.577-2	1.418-1	3.891 0	5.326-1	4.044 0	1.270-1
5.000 1	8.250-1	4.368-2	6.620-2	2.029-1	4.066 0	6.371-1	4.223 0	1.272-1
6.000 1	1.028 0	4.280-2	8.647-2	2.699-1	4.230 0	7.347-1	4.384 0	1.280-1
8.000 1	1.511 0	4.135-2	1.238-1	4.181-1	4.532 0	9.144-1	4.658 0	1.331-1
1.000 2	2.061 0	4.015-2	1.559-1	5.824-1	4.800 0	1.079 0	4.882 0	1.416-1
1.500 2	3.603 0	3.784-2	2.203-1	1.047 0	5.369 0	1.447 0	5.359 0	1.588-1
1.974 2	5.286 0	3.624-2	2.687-1	1.536 0	5.835 0	1.753 0	5.769 0	1.657-1
1.974 2	5.286 0	3.624-2	2.687-1	1.536 0	5.835 0	1.753 0	5.769 0	1.767 0
2.000 2	5.314 0	3.617-2	2.711-1	1.564 0	5.859 0	1.768 0	5.788 0	1.784 0
2.500 2	5.818 0	3.487-2	3.181-1	2.117 0	6.294 0	2.058 0	6.132 0	2.115 0
2.812 2	6.101 0	3.418-2	3.480-1	2.477 0	6.543 0	2.226 0	6.320 0	2.326 0
2.812 2	6.101 0	3.418-2	3.480-1	2.477 0	6.543 0	2.226 0	6.321 0	1.812-1
3.000 2	6.836 0	3.380-2	3.654-1	2.701 0	6.687 0	2.324 0	6.443 0	1.820-1
4.000 2	1.118 1	3.217-2	4.403-1	3.926 0	7.394 0	2.802 0	7.017 0	1.798-1
5.000 2	1.623 1	3.101-2	4.959-1	5.198 0	8.033 0	3.224 0	7.490 0	1.747-1
6.000 2	2.185 1	3.011-2	5.391-1	6.508 0	8.615 0	3.608 0	7.884 0	1.718-1
8.000 2	3.407 1	2.873-2	6.031-1	9.230 0	9.645 0	4.296 0	8.509 0	1.744-1
1.000 3	4.675 1	2.763-2	6.498-1	1.209 1	1.054 1	4.917 0	9.001 0	1.845-1
1.500 3	7.737 1	2.550-2	7.316-1	1.972 1	1.237 1	6.281 0	9.958 0	2.242-1
2.000 3	1.051 2	2.390-2	7.908-1	2.790 1	1.387 1	7.470 0	1.073 1	2.703-1
2.500 3	1.302 2	2.264-2	8.395-1	3.646 1	1.517 1	8.539 0	1.142 1	3.162-1
3.000 3	1.531 2	2.162-2	8.821-1	4.527 1	1.633 1	9.516 0	1.204 1	3.602-1
4.000 3	1.942 2	2.008-2	9.560-1	6.345 1	1.839 1	1.126 1	1.315 1	4.409-1
5.000 3	2.308 2	1.896-2	1.020 0	8.210 1	2.021 1	1.281 1	1.413 1	5.120-1
6.000 3	2.641 2	1.811-2	1.078 0	1.011 2	2.186 1	1.422 1	1.500 1	5.746-1
8.000 3	3.240 2	1.691-2	1.181 0	1.396 2	2.481 1	1.671 1	1.655 1	6.790-1
1.000 4	3.780 2	1.610-2	1.271 0	1.785 2	2.742 1	1.889 1	1.791 1	7.621-1

Appendix A10

Lead

MELTING CURVE

P	T	VS/VS0	VS	VL	SS	SL	ES	EL
1.000-4	6.020-1	1.000 0	9.152-2	9.494-2	1.003-1	1.385-1	4.343-2	6.643-2
1.000 1	1.009 0	8.526-1	7.803-2	7.966-2	1.156-1	1.731-1	1.106-1	1.524-1
2.000 1	1.263 0	7.771-1	7.112-2	7.266-2	1.188-1	1.851-1	2.153-1	2.683-1
3.000 1	1.481 0	7.261-1	6.645-2	6.792-2	1.223-1	1.932-1	3.354-1	3.965-1
4.000 1	1.678 0	6.880-1	6.297-2	6.436-2	1.260-1	1.993-1	4.626-1	5.300-1
5.000 1	1.861 0	6.578-1	6.020-2	6.152-2	1.297-1	2.043-1	5.931-1	6.661-1
6.000 1	2.033 0	6.328-1	5.791-2	5.917-2	1.331-1	2.086-1	7.252-1	8.031-1
7.000 1	2.195 0	6.116-1	5.597-2	5.718-2	1.364-1	2.124-1	8.578-1	9.404-1
8.000 1	2.350 0	5.933-1	5.430-2	5.545-2	1.394-1	2.157-1	9.905-1	1.077 0
9.000 1	2.498 0	5.771-1	5.282-2	5.392-2	1.423-1	2.186-1	1.123 0	1.214 0
1.000 2	2.640 0	5.628-1	5.150-2	5.256-2	1.449-1	2.213-1	1.254 0	1.350 0
1.100 2	2.776 0	5.498-1	5.032-2	5.134-2	1.474-1	2.238-1	1.385 0	1.485 0
1.200 2	2.907 0	5.381-1	4.924-2	5.023-2	1.497-1	2.261-1	1.516 0	1.620 0
1.300 2	3.034 0	5.273-1	4.826-2	4.921-2	1.519-1	2.282-1	1.645 0	1.753 0
1.400 2	3.156 0	5.174-1	4.736-2	4.827-2	1.539-1	2.301-1	1.773 0	1.885 0
1.500 2	3.274 0	5.083-1	4.652-2	4.740-2	1.558-1	2.319-1	1.901 0	2.017 0
1.600 2	3.389 0	4.998-1	4.574-2	4.660-2	1.576-1	2.336-1	2.027 0	2.148 0
1.700 2	3.500 0	4.919-1	4.501-2	4.584-2	1.593-1	2.352-1	2.153 0	2.277 0
1.800 2	3.608 0	4.844-1	4.433-2	4.514-2	1.609-1	2.367-1	2.278 0	2.406 0
1.900 2	3.712 0	4.774-1	4.369-2	4.447-2	1.624-1	2.381-1	2.401 0	2.534 0
2.000 2	3.814 0	4.708-1	4.309-2	4.385-2	1.638-1	2.394-1	2.524 0	2.661 0
2.100 2	3.912 0	4.646-1	4.252-2	4.326-2	1.651-1	2.407-1	2.646 0	2.787 0
2.200 2	4.008 0	4.587-1	4.198-2	4.269-2	1.663-1	2.418-1	2.767 0	2.913 0
2.300 2	4.102 0	4.531-1	4.147-2	4.216-2	1.675-1	2.430-1	2.888 0	3.037 0
2.400 2	4.193 0	4.478-1	4.098-2	4.165-2	1.686-1	2.440-1	3.007 0	3.161 0
2.500 2	4.281 0	4.427-1	4.051-2	4.117-2	1.697-1	2.450-1	3.126 0	3.283 0
2.600 2	4.368 0	4.378-1	4.007-2	4.071-2	1.707-1	2.460-1	3.243 0	3.405 0
2.700 2	4.452 0	4.331-1	3.964-2	4.027-2	1.716-1	2.469-1	3.361 0	3.526 0
2.800 2	4.535 0	4.287-1	3.923-2	3.984-2	1.725-1	2.477-1	3.477 0	3.647 0
2.900 2	4.615 0	4.244-1	3.884-2	3.944-2	1.734-1	2.486-1	3.592 0	3.766 0
3.000 2	4.693 0	4.203-1	3.846-2	3.905-2	1.742-1	2.493-1	3.707 0	3.885 0
3.100 2	4.770 0	4.163-1	3.810-2	3.867-2	1.749-1	2.501-1	3.821 0	4.003 0
3.200 2	4.845 0	4.125-1	3.775-2	3.831-2	1.757-1	2.508-1	3.935 0	4.121 0
3.300 2	4.918 0	4.088-1	3.742-2	3.796-2	1.764-1	2.515-1	4.048 0	4.237 0
3.400 2	4.990 0	4.053-1	3.709-2	3.762-2	1.770-1	2.521-1	4.160 0	4.354 0
3.500 2	5.060 0	4.018-1	3.678-2	3.730-2	1.777-1	2.528-1	4.271 0	4.469 0
3.600 2	5.129 0	3.985-1	3.647-2	3.698-2	1.783-1	2.534-1	4.382 0	4.584 0
3.700 2	5.196 0	3.953-1	3.618-2	3.668-2	1.788-1	2.539-1	4.492 0	4.698 0
3.800 2	5.262 0	3.922-1	3.589-2	3.638-2	1.794-1	2.545-1	4.602 0	4.811 0
3.900 2	5.326 0	3.892-1	3.562-2	3.610-2	1.799-1	2.550-1	4.711 0	4.924 0
4.000 2	5.389 0	3.863-1	3.535-2	3.582-2	1.804-1	2.555-1	4.820 0	5.036 0
4.100 2	5.451 0	3.834-1	3.509-2	3.555-2	1.809-1	2.560-1	4.927 0	5.148 0
4.200 2	5.512 0	3.807-1	3.484-2	3.529-2	1.813-1	2.565-1	5.035 0	5.259 0
4.300 2	5.572 0	3.780-1	3.459-2	3.504-2	1.818-1	2.569-1	5.142 0	5.370 0
4.400 2	5.630 0	3.754-1	3.435-2	3.479-2	1.822-1	2.574-1	5.248 0	5.480 0
4.500 2	5.688 0	3.728-1	3.412-2	3.455-2	1.826-1	2.578-1	5.354 0	5.589 0
4.600 2	5.744 0	3.703-1	3.389-2	3.431-2	1.829-1	2.582-1	5.459 0	5.698 0
4.700 2	5.800 0	3.679-1	3.367-2	3.408-2	1.833-1	2.586-1	5.564 0	5.806 0
4.800 2	5.854 0	3.656-1	3.346-2	3.386-2	1.837-1	2.590-1	5.668 0	5.914 0
4.900 2	5.907 0	3.633-1	3.325-2	3.365-2	1.840-1	2.593-1	5.772 0	6.021 0
5.000 2	5.960 0	3.610-1	3.304-2	3.343-2	1.843-1	2.597-1	5.875 0	6.128 0

Lead

SATURATION CURVE

P	T	T/TC	VL	VG	SL	SG	EL	EG
2.316-1	5.524 0	1.000 0	3.228-1	3.228-1	5.513-1	5.513-1	1.110 0	1.110 0
2.000-1	5.329 0	9.647-1	2.463-1	4.531-1	5.311-1	5.640-1	1.017 0	1.151 0
1.000-1	4.639 0	8.398-1	1.867-1	8.419-1	4.927-1	5.760-1	8.349-1	1.156 0
8.000-2	4.475 0	8.100-1	1.783-1	9.904-1	4.840-1	5.785-1	7.960-1	1.154 0
6.000-2	4.293 0	7.771-1	1.701-1	1.213 0	4.742-1	5.814-1	7.537-1	1.151 0
5.000-2	4.191 0	7.587-1	1.659-1	1.377 0	4.687-1	5.830-1	7.306-1	1.149 0
4.000-2	4.079 0	7.385-1	1.616-1	1.611 0	4.625-1	5.849-1	7.053-1	1.147 0
3.000-2	3.952 0	7.154-1	1.570-1	1.988 0	4.554-1	5.872-1	6.766-1	1.143 0
2.000-2	3.795 0	6.869-1	1.516-1	2.771 0	4.464-1	5.906-1	6.419-1	1.137 0
1.500-2	3.693 0	6.685-1	1.484-1	3.695 0	4.404-1	5.935-1	6.196-1	1.132 0
1.000-2	3.550 0	6.426-1	1.440-1	6.328 0	4.318-1	5.996-1	5.884-1	1.122 0
8.000-3	3.465 0	6.272-1	1.415-1	8.932 0	4.265-1	6.044-1	5.701-1	1.116 0
6.000-3	3.347 0	6.058-1	1.383-1	1.362 1	4.192-1	6.114-1	5.450-1	1.107 0
5.000-3	3.269 0	5.918-1	1.362-1	1.736 1	4.142-1	6.159-1	5.287-1	1.102 0
4.000-3	3.174 0	5.746-1	1.338-1	2.286 1	4.081-1	6.215-1	5.089-1	1.095 0
3.000-3	3.053 0	5.526-1	1.308-1	3.173 1	4.001-1	6.288-1	4.840-1	1.087 0
2.000-3	2.890 0	5.231-1	1.271-1	4.873 1	3.890-1	6.392-1	4.511-1	1.077 0
1.000-3	2.639 0	4.776-1	1.218-1	9.643 1	3.711-1	6.575-1	4.016-1	1.061 0
8.000-4	2.565 0	4.644-1	1.204-1	1.192 2	3.657-1	6.636-1	3.875-1	1.057 0
6.000-4	2.476 0	4.483-1	1.187-1	1.562 2	3.589-1	6.716-1	3.706-1	1.051 0
5.000-4	2.423 0	4.386-1	1.177-1	1.850 2	3.548-1	6.767-1	3.605-1	1.048 0
4.000-4	2.360 0	4.273-1	1.166-1	2.275 2	3.499-1	6.830-1	3.488-1	1.044 0
3.000-4	2.284 0	4.135-1	1.153-1	2.964 2	3.439-1	6.913-1	3.347-1	1.039 0
2.000-4	2.185 0	3.955-1	1.136-1	4.298 2	3.357-1	7.031-1	3.165-1	1.033 0
1.500-4	2.120 0	3.837-1	1.125-1	5.590 2	3.303-1	7.116-1	3.047-1	1.029 0
1.000-4	2.034 0	3.683-1	1.112-1	8.093 2	3.229-1	7.238-1	2.895-1	1.024 0

SHOCK ADIABAT M= 1.000

P	T	V	S	E	D	U	CS	CV
1.000-4	2.930-1	8.820-2	4.470-7	1.300-7	.000 0	.000 0	1.882 0	1.213-1
1.000 1	5.026-1	7.629-2	2.186-2	5.954-2	2.556 0	3.451-1	2.652 0	1.236-1
1.500 1	6.674-1	7.292-2	4.463-2	1.146-1	2.763 0	4.788-1	2.857 0	1.248-1
2.000 1	8.750-1	7.028-2	6.896-2	1.792-1	2.947 0	5.986-1	3.030 0	1.262-1
2.500 1	1.121 0	6.814-2	9.258-2	2.508-1	3.113 0	7.082-1	3.180 0	1.278-1
3.000 1	1.400 0	6.633-2	1.146-1	3.281-1	3.267 0	8.100-1	3.314 0	1.295-1
3.204 1	1.523 0	6.567-2	1.231-1	3.610-1	3.326 0	8.497-1	3.364 0	1.302-1
3.204 1	1.523 0	6.567-2	1.231-1	3.610-1	3.326 0	8.497-1	3.358 0	1.421 0
4.000 1	1.679 0	6.358-2	1.584-1	4.924-1	3.555 0	9.924-1	3.558 0	1.493 0
4.984 1	1.858 0	6.156-2	2.043-1	6.639-1	3.815 0	1.152 0	3.780 0	1.572 0
4.984 1	1.858 0	6.156-2	2.043-1	6.639-1	3.815 0	1.152 0	3.799 0	1.432-1
5.000 1	1.870 0	6.153-2	2.051-1	6.670-1	3.819 0	1.155 0	3.803 0	1.433-1
6.000 1	2.558 0	5.962-2	2.441-1	8.575-1	4.041 0	1.310 0	3.992 0	1.493-1
8.000 1	4.070 0	5.663-2	3.046-1	1.263 0	4.440 0	1.589 0	4.314 0	1.592-1
1.000 2	5.707 0	5.433-2	3.510-1	1.693 0	4.793 0	1.840 0	4.585 0	1.669-1
1.500 2	1.016 1	5.026-2	4.350-1	2.846 0	5.546 0	2.386 0	5.126 0	1.802-1
2.000 2	1.492 1	4.745-2	4.948-1	4.075 0	6.179 0	2.855 0	5.553 0	1.909-1
2.500 2	1.984 1	4.533-2	5.415-1	5.359 0	6.736 0	3.274 0	5.912 0	2.025-1
3.000 2	2.475 1	4.363-2	5.802-1	6.686 0	7.236 0	3.657 0	6.222 0	2.161-1
4.000 2	3.427 1	4.097-2	6.428-1	9.446 0	8.117 0	4.347 0	6.741 0	2.488-1
5.000 2	4.312 1	3.891-2	6.934-1	1.232 1	8.884 0	4.964 0	7.166 0	2.856-1
6.000 2	5.128 1	3.723-2	7.367-1	1.529 1	9.569 0	5.530 0	7.529 0	3.237-1
8.000 2	6.589 1	3.456-2	8.104-1	2.145 1	1.077 1	6.551 0	8.135 0	3.976-1
1.000 3	7.879 1	3.252-2	8.734-1	2.784 1	1.182 1	7.462 0	8.643 0	4.647-1
1.500 3	1.066 2	2.899-2	1.005 0	4.441 1	1.404 1	9.424 0	9.699 0	5.966-1
2.000 3	1.312 2	2.676-2	1.116 0	6.144 1	1.591 1	1.109 1	1.062 1	6.838-1
2.500 3	1.542 2	2.529-2	1.214 0	7.864 1	1.758 1	1.254 1	1.150 1	7.387-1
3.000 3	1.764 2	2.431-2	1.302 0	9.584 1	1.911 1	1.384 1	1.237 1	7.737-1
4.000 3	2.190 2	2.328-2	1.456 0	1.298 2	2.189 1	1.611 1	1.415 1	8.237-1
5.000 3	2.586 2	2.292-2	1.589 0	1.632 2	2.441 1	1.807 1	1.588 1	8.815-1
6.000 3	2.946 2	2.284-2	1.707 0	1.961 2	2.672 1	1.980 1	1.745 1	9.555-1
8.000 3	3.572 2	2.290-2	1.908 0	2.612 2	3.087 1	2.286 1	2.001 1	1.125 0
1.000 4	4.108 2	2.296-2	2.079 0	3.262 2	3.453 1	2.554 1	2.202 1	1.290 0

Appendix B

Reference volumes of metals

Metal	Li	Al	Fe	Ni	Cu	Mo	Ta	W	Au	Pb
Volume [cc/g]	1.86	0.369	0.121	0.112	0.112	0.0978	0.0600	0.0519	0.0518	0.0882

Appendix C

make$tab.f program - source text

```
      PROGRAM MAKE$TAB
      DIMENSION V(256)
      OPEN(99, FILE='OUT.IN', STATUS='UNKNOWN',
     *FORM='FORMATTED')
      WRITE(*,*)'Input data:initial, intermediate and final'
      WRITE(*,*)' VI           V1           V2           VF'
      READ(*,*) VI,V1,V2,VF
      WRITE(*,*)'Number of points in regions and scale(IL-0lin,1log)'
      WRITE(*,*)'in VI-V1(I1,IL1)  V1-V2(I2,IL2)   V2-VF(I3,IL3)'
      READ(*,*)I1,IL1,I2,IL2,I3,IL3
C     --- Tabular data output
C     - Region Vm<Vh for I1 points:
      DO 13 I=1,I1
      IF(IL1) 12,11,12
   11 X=VH+(V1-VH*(I-1.)/I1)
      GO TO 13
   12 X=VH*((V1/VH)**((I-1.)/I1))
   13 V(I)=X
C     - Region V1<V2 for I2 points:
      DO 23 I=1,I2
      IF(IL2) 22,21,22
   21 X=V1+(V2-V1*FLOAT(I-1)/I2)
      GO TO 23
   22 X=V1*((V2/V1)**(FLOAT(I-1)/I2))
   23 V(I1+I)=X
C     - Region V2<VK for I3 points:
      DO 33 I=1,I3
      IF(IL3) 32,31,32
   31 X=V2+(VK-V2*FLOAT(I-1)/I3)
      GO TO 33
   32 X=V2*((VK/V2)**(FLOAT(I-1)/I3))
   33 V(I2+I1+I)=X
C     --- Print output
      WRITE(*,*)(V(J),J=1,I1+I2+I3)
      WRITE(99,*)(V(J),J=1,I1+I2+I3)
      CLOSE(99)
      STOP
      END
```

Appendix D

read.f program - sorce text

```
      PROGRAM READ$TAB
      COMMON /RT/V(256),T(256),P(256,256),E(256,256),S(256,256),
     ,H(256,256),F(256,256),CS(256,256),CT(256,256),
     ,CP(256,256),CV(256,256),IPS(256,256)
      CALL RE$TAB
      STOP
      END
      SUBROUTINE RE$TAB
C-----------------------------------------------------------------------
C (C) I.V.Lomonosov, 1993
C Purpose: RE$TAB is small subroutine to read and manage EOS data
C          generated by TABEOS program. Parameters for TABEOS are
C          placed in file DATA.MAN
C Used:
C       files: DATA.MAN - TABEOS managing file
C              VOLUME.IN - data for volume scale (L2=-1)
C              TEMPER.IN - data for temperature scale (L1=-1)
C
C       parameters: NV - dimension of volume scale (256 max)
C                   NT - dimension of temperature scale (256 max)
C                V(NV) - volume array, calculated or in file  VOLUME.IN
C                T(NT) - temper. array, calculated or in file TEMPER.IN
C              P(NT,NV) - pressure table in file              PRESSU.TAB
C              E(NT,NV) - energy table in file                ENERGY.TAB
C              S(NT,NV) - entropy table in file               ENTROP.TAB
C              H(NT,NV) - enthalpy table in file              ENTHAL.TAB
C             CP(NT,NV) - heat capacity p=const table in file HCAPAP.TAB
C             CT(NT,NV) - heat capacity v=const table in file HCAPAV.TAB
C             CS(NT,NV) - sound velocity s=const table in file SNDVLS.TAB
C             CT(NT,NV) - sound velocity T=const table in file SNDVLT.TAB
C            IPS(NT,NV) - identifier of phase state in file   PHYSID.TAB
C                   L1 - identifier of V-scale (log or linear)
C                   L2 - identifier of T-scale (log or linear)
C                   L3 - identifier of table (fixed or binary)
C-----------------------------------------------------------------------
      COMMON /RT/V(256),T(256),P(256,256),E(256,256),S(256,256),
     ,H(256,256),F(256,256),CS(256,256),CT(256,256),
     ,CP(256,256),CV(256,256),IPS(256,256)
C
C +-- Open managing file and read scaling parameters from it
      OPEN(50,NAME='DATA.MAN',STATUS='OLD',FORM='FORMATTED',READONLY)
      READ(50,1001) TI,TF,VI,VF,NT,NV,L1,L2,L3
 1001 FORMAT(//E9.3/E9.3/E9.3/E9.3/I3/I3/I2/I2/I2)
      CLOSE(50)
C
C +-- Determination of volume- and temperature arrays
      IF(L1) 10,11,13
   10 OPEN(51,NAME='TEMPER.IN',STATUS='OLD',FORM='FORMATTED',READONLY)
      READ(51,*) (T(I),I=1,NT)
      CLOSE(51)
      GO TO 15
   11 DO 12 I=1,NT
      T(I)=TI+(TF-TI)*(I-1.)/(NT-1.)
   12 CONTINUE
      GO TO 15
   13 DO 14 I=1,NT
      T(I)=TI*EXP(ALOG(TF/TI)*(I-1.)/(NT-1.))
   14 CONTINUE
   15 CONTINUE
```

```
C     --- end of filling T-array
      IF(L1) 20,21,23
   20 OPEN(52,NAME='VOLUME.IN',STATUS='OLD',FORM='FORMATTED',READONLY)
      READ(52,*) (V(I),I=1,NV)
      CLOSE(52)
      GO TO 25
   21 DO 22 I=1,NV
      V(I)=VI+(VF-VI)*(I-1.)/(NV-1.)
   22 CONTINUE
      GO TO 25
   23 DO 24 I=1,NV
      V(I)=VI*EXP(ALOG(VF/VI)*(I-1.)/(NV-1.))
   24 CONTINUE
   25 CONTINUE
C     --- End of V(olume) array
C +--- Arrays V and T have been determinated
C
C +-- Reading data and phase ident-s arrays
      IF(L3) 31,31,33
   31 OPEN(99,FILE='PRESSU.TAB',STATUS='UNKNOWN',FORM='FORMATTED')
      OPEN(98,FILE='ENERGY.TAB',STATUS='UNKNOWN',FORM='FORMATTED')
      OPEN(97,FILE='SNDVLS.TAB',STATUS='UNKNOWN',FORM='FORMATTED')
      OPEN(96,FILE='SNDVLT.TAB',STATUS='UNKNOWN',FORM='FORMATTED')
      OPEN(95,FILE='ENTROP.TAB',STATUS='UNKNOWN',FORM='FORMATTED')
      OPEN(94,FILE='HCAPAP.TAB',STATUS='UNKNOWN',FORM='FORMATTED')
      OPEN(93,FILE='HCAPAV.TAB',STATUS='UNKNOWN',FORM='FORMATTED')
      OPEN(92,FILE='ENTHAL.TAB',STATUS='UNKNOWN',FORM='FORMATTED')
      OPEN(91,FILE='FRENER.TAB',STATUS='UNKNOWN',FORM='FORMATTED')
      OPEN(90,FILE='PHYSID.TAB',STATUS='UNKNOWN',FORM='FORMATTED')
      DO 32 I=1,NT
C     --- Thermodynamical data:
      READ(99,1002) (P(I,J), J=1,NV)
      READ(98,1002) (E(I,J), J=1,NV)
      READ(97,1002) (CS(I,J), J=1,NV)
      READ(96,1002) (CT(I,J), J=1,NV)
      READ(95,1002) (S(I,J), J=1,NV)
      READ(94,1002) (CP(I,J), J=1,NV)
      READ(93,1002) (CV(I,J), J=1,NV)
      READ(92,1002) (H(I,J), J=1,NV)
      READ(91,1002) (F(I,J), J=1,NV)
 1002 FORMAT(6E10.3)
C     --- Phase ident-s
      READ(90,1003) (IPS(I,J),J=1,NV)
 1003 FORMAT(60I1)
   32 CONTINUE
      WRITE(*,*)P(1,1),IPS(1,1),E(1,1),CS(1,1)
      GO TO 35
   33 OPEN(99,FILE='PRESSU.TAB',STATUS='UNKNOWN',FORM='UNFORMATTED')
      OPEN(98,FILE='ENERGY.TAB',STATUS='UNKNOWN',FORM='UNFORMATTED')
      OPEN(97,FILE='SNDVLS.TAB',STATUS='UNKNOWN',FORM='UNFORMATTED')
      OPEN(96,FILE='SNDVLT.TAB',STATUS='UNKNOWN',FORM='UNFORMATTED')
      OPEN(95,FILE='ENTROP.TAB',STATUS='UNKNOWN',FORM='UNFORMATTED')
      OPEN(94,FILE='HCAPAP.TAB',STATUS='UNKNOWN',FORM='UNFORMATTED')
      OPEN(93,FILE='HCAPAV.TAB',STATUS='UNKNOWN',FORM='UNFORMATTED')
      OPEN(92,FILE='ENTHAL.TAB',STATUS='UNKNOWN',FORM='UNFORMATTED')
      OPEN(91,FILE='FRENER.TAB',STATUS='UNKNOWN',FORM='UNFORMATTED')
      OPEN(90,FILE='PHYSID.TAB',STATUS='UNKNOWN',FORM='UNFORMATTED')
      DO 34 I=1,NT
C     --- Thermodynamical data:
      READ(99) (P(I,J), J=1,NV)
      READ(98) (E(I,J), J=1,NV)
      READ(97) (CS(I,J), J=1,NV)
      READ(96) (CT(I,J), J=1,NV)
      READ(95) (S(I,J), J=1,NV)
```

```
      READ(94) (CP(I,J), J=1,NV)
      READ(93) (CV(I,J), J=1,NV)
      READ(92) (H(I,J), J=1,NV)
      READ(91) (F(I,J), J=1,NV)
C     --- Phase ident-s
      READ(90) (IPS(I,J),J=1,NV)
      WRITE(*,*)P(1,1),IPS(1,1),E(1,1),CS(1,1)
   34 CONTINUE
   35 WRITE(*,*)'Data are loaded in arrays. Test is for (I,J) point:'
      WRITE(*,*)'Enter I, J (I OR J =0 --> EXIT'
      READ(*,*) I,J
      IF(I.LE.0.OR.J.LE.0) GO TO 36
      WRITE(*,*)'P=',P(I,J),' E=',E(I,J),' Cs=',CS(I,J),' I=',IPS(I,J)
      GO TO 35
   36 CLOSE(99)
      CLOSE(98)
      CLOSE(97)
      CLOSE(96)
      CLOSE(95)
      CLOSE(94)
      CLOSE(93)
      CLOSE(92)
      CLOSE(91)
      CLOSE(90)
      RETURN
      END
```

HEDRC REPORT

Printed October 1994

WIDE-RANGE EQUATION OF STATE FOR LARGE COMPUTER CODES: EQUATIONS OF STATE OF MOLYBDENUM, TANTALUM, NICKEL AND GOLD

I. V. Lomonosov, V. E. Fortov, and K. V. Khishchenko

Prepared by
High Energy Density Research Center
Russian Academy of Sciences
Izhorskaya Str. 14/19, Moscow 127412, Russia
for USAF
by contract SPC-93-4074

WIDE-RANGE EQUATION OF STATE FOR LARGE COMPUTER CODES: EQUATIONS OF STATE OF MOLYBDENUM, TANTALUM, NICKEL AND GOLD

I. V. Lomonosov, V. E. Fortov, and K. V. Khishchenko

High Energy Density Research Center
Russian Academy of Sciences
Izhorskaya Str. 14/19, Moscow 127412, Russia

Abstract

This is third (9-months) report performed for USAF by contract SPC-93-4074. Described is comparison between calculated by multi-phase equation of state (EOS) thermodynamical properties for molybdenum, tantalum, nickel and gold metals and available experimental data. For each metal we carried out a construction of EOS on the base of the model and procedure given in previous report and, after it, a calculation of metal's phase diagram. The comparison was made for: principal and porous Hugoniots, release isentropes, static compression data, phase-diagram data, and isobaric expansion data. The comparison and discussion with predictions of critical points are also done.

1. Introduction

Each section of the report is devoted to a selected metal. Discussed are measurements under static conditions, such diamond-anvil-cells (DAC) data, measurements of melting curve with use of high-pressure vessels, isobaric expansion investigations along with predictions of critical point and, finally, dynamic studies. They are explorations of shock Hugoniots and release isentropes. We supply the discussion by correspondent figures, shown on which are both our calculated characteristics and experimental data with theoretical predictions.

2. Molybdenum

Molybdenum is characterized by large values of melting and evaporation temperature. This fact explains a wide use of the metal in modern nuclear, aviation and space technologies. Along with aluminum and iron, molybdenum also serves as an etalon material on carrying out shock-wave measurements at extreme pressures.

2.1. Cold curve

Calculated cold curve for molybdenum is compared with theoretical calculations and the semiempirical cold curve [1] on Fig. 1.

As it was shown previously for large number of metals [3], the developed procedure of determination of the cold curve allows to describe thermodynamical properties of metals at T=0 K in a broad range of densities up to 100-fold compression. Fig. 1 confirms the fact for such metal, as molybdenum.

2.2. Static compression and melting curve

Molybdenum is bcc at ambient conditions. Diamond-Anvil-Cell (DAC) data [4,5] show no phase transition in Mo at room temperature up to 2.8 Mbar.

Carried out comparison between calculated with the use of EOS T=298 K isotherm and results of DAC experiment [4] proved their excellent agreement.

The initial slope of molybdenum melting curve dT/dp=0.8 K/kbar [6] measured with the use of an optical technique to 90 kbar differs significantly from those one 3.4±0.6 K/kbar measured on isobaric-expansion (IEX) experiment [7]. Note, that the value dT/dp=3.5±0.2 K/kbar obtained on the base of reduction of static data for solid and liquid molybdenum [8] is also more realistic then the one given in [6]. The developed EOS for molybdenum gives the value for dT/dp=3.34 K/kbar, which should be considered in very good agreement with results [7,8].

Note, that the calculated melting region in the high-pressure range corresponds to an intersection with the shock adiabat in the 3.91-4.75 Mbar pressure range. The result of determination of sound velocity in shocked molybdenum, obtained with the use of optical-analyzer technique, shows a disappearing of transverse component, which corresponds to melting, at p=3.9 Mbar [9]. This very good agreement proves the reliability of calculation of molybdenum melting curve at high pressure.

2.3. Shock-wave data

The shock compressibility of molybdenum have been studied thoroughly in megabar-pressure range with the use of different traditional shock-wave generators [10,11,12,13]. Experiments on light-gas gun increased the investigated range of pressure to 5 Mbar [14], higher pressures to 10 Mbar have been explored with the use of special powerful systems [15,16]. The region of high pressures and reduced (with respect to normal) densities for molybdenum has been subjected to intensive studies using the method of shock compression of porous samples [17,18].

The use of nuclear explosives made it possible to determine the shock compressibility of molybdenum at extreme high pressures. Absolute measurement of the principle Hugoniot at p≈20 Mbar [19] and impedance-match data [14,20,21] determined from aluminum standard at tens of megabars are available.

Sound velocity in shocked molybdenum has measured with use of overctacken technique, while bromoform serves as an optical etalon material [9]. These results [9] revealed a solid-solid phase transition at p≈2.1 Mbar and melting

in shocked metal at p≈3.9 Mbar. Taken into account shock-wave data at pressure higher then 2.1 Mbar and static data [5], it can be concluded that the solid-solid phase transition is corresponded by small change of density and leads to no breaks in principal Hugoniot. Therefore, it is possible for molybdenum to describe the complete set of high-pressure data by one solid phase.

A comparison of shock-wave data on the compression of solid and porous samples with calculated shock adiabats is presented on Fig. 2; also plotted in the figure are the results of isotherm calculations and the boundary of the high-temperature melting region. It is worth to note, that for molybdenum is a full correspondence between numerous shock-wave data, obtained with the use of high-explosive systems [10-13,15,16], light-gas gun [14] and nuclear explosions [14,19,20,21]. As it is seen from Fig. 2, the developed EOS describes with high accuracy all principle-Hugoniot data and measurements of porous Hugoniots, including high-porous (m=8) data [18] to pressures of the order of 10 Mbar. The carried out comparison for extreme-high-pressure data [14,19,20,21] also proved the fact.

Fig. 2,a demonstrates an agreement between calculated and measured isentropic sound velocity in shocked molybdenum.

2.4. High-pressure, low-density data

The region of high pressure and reduced (with respect to normal conditions) density has been studied with the use of IEX technique. Available are density-temperature data on the isobar p=0.2 GPa to 4450 K [22], 7000 K [23] and 4100 K [24]. Calculated isobars are compared with IEX data on Fig. 3.

The developed EOS for molybdenum describes with very good accuracy the melting on the isobars; calculated values are, as it is seen from Fig. 3, in agreement with measurements [22]. The calculated value of the evaporation temperature at p=1 bar T_v=4824 K is in agreement with the tabular [30] one 4910 K. Note, that for molybdenum the value of evaporation temperature differs in ca. 10% from different references.

Obtained from this EOS critical point parameters are following: p_c =5.878 kbar, T_c=15210 K, V_c=0.636 cc/g and s_c=1.617 J/gK. The analysis of evaluations

of critical point from [25-29] shows, that the data are in range 5.46 [29] - 12.6 kbar [27], 8000 [26] - 16140 K [27], 0.97 [26] - 3.18 [27] g/cc. This discrepancy is relatively large; the slope of the experimental $\rho(T)$ curves [22,23,24] does not coincide with calculated one. Nevertheless, for IEX measurements [22,23,24] calculated isobar to 5000 K is within experimental errors , which are typically of the order of ±0.3 g/cc for density and ±250 K for temperature.

The slope of experimental isobars indicates to larger value of Gruneisen coefficient or less value of isothermal sound velocity in liquid molybdenum, then those values calculated by EOS. It is well seen from formula $(\partial\rho/\partial T)_p = (\partial p/\partial T)_V/V^2(\partial p/\partial V)_T$. It is doubtful that molybdenum has very large value of Gruneisen coefficient in liquid state (to describe IEX data, it must be ca. 3.5) - it will contradict to shock-wave data for porous specimens. Note, that IEX data [22] leads to a very large value for the specific heat c_p=8.5R near melting point. It also indicates to dramatic decrease of sound velocity in liquid molybdenum.

Finally, it is possible to conclude that developed EOS for molybdenum provides for a reasonable description of available experimental and theoretical data in liquid state. It should be revised, nevertheless, that more accurate conclusions for liquid molybdenum properties can be made only having sound velocity measurements.

2.5. Discussion

The developed EOS for molybdenum, as it is shown by Figs. 1-3, provides for an accurate and reliable description of thermodynamical properties of the metal at high pressures and temperatures. The calculated Hugoniots agree with all available shock-wave data, as well as p(T=298 K) isotherm with static data; in region of low densities the EOS provides for a reasonable description of IEX data and evaluations of critical point parameters.

3. Tantalum

Tantalum is a component of alloys which are of wide use in modern air- and spacecraft technique, as well as in nuclear reactors. Tantalum is also used as a suitable material for impactors on shock-wave experiments.

3.1. Cold curve

Theoretical calculations of tantalum cold curve have been done in work [2]; available are also results for semiempirical cold curves [1,31]. The comparison between obtained for tantalum cold curve and results [1,2,31] are plotted to 100-fold compressions on Fig. 4. The analysis of the picture proves the fact, that obtained in the work cold curve agrees with semiempirical ones [1,31] at moderate pressures and with Thomas-Fermi calculations [2] at extreme high pressure, while the other semiempirical curves [1,31] have unphysical oscillations at high pressure and density $\rho \approx 20\rho_0$.

3.2. Static compression and melting curve

Tantalum is bcc at ambient conditions. Results of isothermal compressibility measurements at T=298 K in DAC with the ruby etalon to 100 kbar [4] and to 800 kbar [32] found no phase transitions. Data [32] are of the most interest as they have been obtained at hydrostatic conditions with use of argon as pressure-transmitting medium. Calculated isotherm is compared with the data [32] on Fig. 5, which demonstrates their good agreement.

The calculated value of the initial slope of molybdenum melting curve dT/dp=6.12 K/kbar agrees with those one 5.4 K/kbar determined by optical method to 90 kbar [6], and 5.8±1 K/kbar obtained from IEX measurements [22].

The calculated melting region at high pressure corresponds to an intersection with the principal Hugoniot in the 3.14-3.83 Mbar pressure range. The result of determination of sound velocity in shocked tantalum, obtained with the use of optical-analyzer technique, shows a disappearing of transverse

component, which corresponds to melting, at p=2.95 Mbar [33]. Our result is in agreement (within experimental error) with [33]. It proves the reliability of calculation of tantalum melting curve at high pressure.

3.3. Shock-wave data

The principle Hugoniot of tantalum has been investigated with the use of different explosive systems to fee megabars in works [10,12,13]. The usage of light-gas guns increased the region of studied pressure to 4.3 Mbar [34,35]. Higher pressure to 10 Mbar has been explored with use of powerful explosive systems [15,16]. These drivers have also been used on investigation of states of liquid tantalum by method of shock compression of porous samples [18]. The sound velocity in shocked tantalum has been measured, as it mentioned previously, in work [33].

To begin with, no discontinuities have been observed on tantalum principle Hugoniot and all available data obtained with the use of different experimental methods are self-consistent. As it is seen from Fig. 6, the developed EOS describes solid and liquid states of tantalum on the principal shock adiabat with high accuracy and reliability. The region of decreased, with respect to the principal Hugoniot, densities corresponding to porous Hugoniots, is also described by the EOS (see Fig. 6).

The developed EOS for tantalum describes also measurements of sound velocity in shocked metals, which is proved by Fig. 6,a.

Therefore, tantalum EOS is in very good agreement with all available shock-wave data for this metal.

3.4. High-pressure, low-density data

IEX data at p=2 kbar to 6200 K [36] and to 7400 K [37] are available for tantalum. Sound velocity measurements have been done in liquid tantalum under condition of the fast isobaric expansion from 14.49 g/cc to 11.49 g/cc in work [38]. Shown on Fig. 7 are calculated the liquid-gas coexistence curve with critical point and selected isobars in comparison with IEX data and evaluations of critical point for this metal.

The developed EOS provides for a good agreement with experimental data on melting along the isobar and with the experimental $\rho(T)$ dependence [36] in the neighborhood of evaporation region (see Fig. 7). Note, that the slope $\rho(T)$ for data [37] does not agree with the one from [36], measurements of sound velocity [38] and evaluations of the critical point [25,26].

Calculated sound velocity in liquid tantalum is compared with experimental data on Fig. 7,a. There is a good (within experimental error) agreement between calculated and measured values.

The EOS gives following parameters of tantalum critical point: p_c =7.756 kbar, T_c=14260 K, V_c=0.259 cc/g and s_c=0.953 J/gK. These values are in reasonable agreement with analogous evaluations [25,26,27]. The value of evaporation temperature at normal pressure, T_v=5731 K coincides with the tabular one [30].

Finally, the tantalum EOS provides for very agreement with all liquid-state data at moderate pressure.

3.5. Discussion

The developed EOS for tantalum, as it is seen from Figs. 4-7, describes with very high accuracy and reliability thermodynamical properties of the metal in solid, liquid and gas states. The calculated thermodynamical characteristics are in agreement with all available experimental data. It is worth to notice very good agreement of the EOS with theoretical and experimental data in the region of the liquid state both at moderate (IEX) and high-pressure (shock-wave) data, which is usually of the most difficulty for theoretical calculations.

So the EOS for tantalum can be used in hydrocodes in the most difficult situations, when the reliability and accuracy of modeling results are defining namely by EOS.

4. Nickel

Nickel due to its anti-oxidizing properties is of use in large amount of technological alloys. This fact helped to carry out very interesting experiments on shock compression of ultra-low-density nickel specimens [39].

4.1. Cold curve

Thermodynamical properties of nickel at T=0 K have been calculated with the use Thomas-Fermi model with quantum adjustments [2] and method of augmented plane waves [40]. Approximating semiempirical cold curves for this metal have been published in works [1,31,41,42]. The comparison between obtained in the work cold curve, results of theoretical calculation [2,40] and other semiempirical cold curves is given on Fig. 8.

The obtained in the work cold curve of nickel, as it is seen from Fig. 8, agrees with theoretical calculations [2,40] overall range of pressure, while the other semiempirical cold curves have unphysical oscillations at pressure higher then 400 Mbar. Note, that all these curves coincide with each other to $p<400$ Mbar.

4.2. Static compression and melting

According to [43], nickel is fcc at ambient conditions and the structure is stable at room temperature to 650 kbar.

The calculated value of the initial slope of the melting curve $dT/dp=4.38$ K/kbar is in satisfactory agreement with the one 3.3 K/kbar given in compendium [44], which has been determined to 60 kbar.

4.3. Shock-wave data

The principal Hugoniot of nickel has been studied by virtue of traditional shock-wave generators to 1.5 Mbar in works [10,11,13] and light-gas gun to 5

Mbar [45]. Usage of special powerful high-explosive systems increased the limit of investigated pressure to ca. 10 Mbar [16,41,46]. Data on shock compression of porous [18,41] and ultra porous [39] nickel samples in a megabar-pressure range significantly expanded the region of the investigated phase diagram. Results of work [39] are of especial interest as they occupy region of strongly heated liquid metal and, for the most porous shock Hugoniot $\rho_0 / \rho_{00}=20$ correspond to the state of weakly-ionized non-ideal plasma.

The calculated phase diagram of nickel is shown on Fig. 9 in comparison with available shock-wave data. Note, that results [41] for porosity m=1.73 does not agree with those one from recent work [18], while for m=3.0 their position on the phase diagram corresponds to the position of porous shock Hugoniots m=4.58, 2.72, 2.32 from [18]. The analysis of experimental data on shock compression of porous specimens shows, that the position of porous and ultra porous Hugoniots is reasonable (see Fig. 9). The principle Hugoniot data for nickel, obtained with the use of different shock-wave generators, are also in a good agreement with each other.

This unique set of data embraces the region of density $0.2<\rho / \rho_0<2$ to pressure ca. 10 Mbar and gives an opportunity to account for precisely thermal contribution of electrons and ions in EOS. Calculated shock adiabats of different initial densities describe with very high accuracy all available for nickel shock-wave data.

4.4. High-pressure, low-density data

Density-temperature measurements have been done for liquid nickel at p=2 kbar to 4300 K [47] along with determination of sound velocity. Evaluations of critical point for nickel are given in works [25,27].

Shown on Fig. 10 are calculated phase boundary liquid-gas with critical point CP, rectilinear diameter D and selected isobars in comparison with these data. Additionally given on Fig. 10,a are experimental and calculated sound velocity in liquid nickel.

Analogous to shock-wave data, there is a good correspondence for nickel between all available experimental data and theoretical predictions in the region of

lower densities and moderate temperatures. The nickel EOS describes with very good accuracy results of experimental work [47]. Calculated parameters of the critical point p_c =10.49 kbar, T_c=7585 K, V_c=0.479 cc/g and s_c=2.526 J/gK are in agreement with available evaluations [25,27]. Note, that given by the nickel EOS value of critical temperature is less, then the one from [25,27]. It is reasonable as for tantalum, for instance, the value of critical temperature has been changed from 17330 K [25] to 9284 K [26], when the hard-spheres model was substituted for soft-spheres one. The value of evaporation temperature at normal pressure, T_v=3020 K agrees with the tabular one 3190 K from [30] (note, that it can differ from other references in ±10%).

4.5. Discussion

Nickel is one of the most investigated metals. Both theoretical and experimental high-pressure data agree for nickel in a broad range of density and pressure. It made it possible to construct very reliable precise EOS for this metal.

The analysis of Figs. 7-10 proves the fact.

5. Gold

Gold is well-compressed metal with no phase transitions at high pressure. By this reason it is using very often as standard material for DAC measurements. Due to high density and large nuclear charge it is also used in producing targets for controlled-inertial-fusion experiments.

5.1. Cold curve

Theoretical calculations of themodynamical properties of gold at T=0 K have been done by Thomas-Fermi model with quantum corrections [2]. Semiempirical cold curves for gold have been obtained in works [1,31]. Results of these calculations are comparing with obtained in this work cold curve on Fig. 11. This picture shows a good agreement between our cold curve and [2] at high

pressure. At moderate pressure obtained cold curve agrees with both semiempirical cold curves from [1,31].

5.2. Static compression and melting

Gold is fcc at ambient conditions. According to DAC measurements to 3 Mbar [48,49,50] it remains fcc on room-temperature isotherm. Calculated T=298 K isotherm agrees with DAC data.

The calculated value of the initial slope of the melting curve dT/dp=6.3 K/kbar agrees the one 6 K/kbar given in compendium [44], which has been determined to 60 kbar.

5.3. Shock-wave data

The principal Hugoniot of gold has been studied by virtue of traditional shock-wave generators to 1.9 Mbar in works [10,11,13] and light-gas gun to 5.8 Mbar [51]. Data, obtained with the usage of special powerful high-explosive systems, also are in the pressure range to 5.1 Mbar [16,52].

The calculated phase diagram for gold is shown on Fig. 12. All available shock-wave data are in agreement with each other and described by developed EOS for gold with high accuracy, as it is seen from Fig. 12.

5.4. High-pressure, low-density data

Presented on Fig. 13 are calculated phase boundary liquid-gas with critical point, rectilinear diameter, selected isobars in comparison with IEX data, calculated by approximating relationships from review [24] and evaluations of critical point [25,27]. The IEX data for Au-5Cu alloy [24] are the only available; they are put on the figure only for estimations.

Calculated parameters of the critical point p_c =7.568 kbar, T_c=9007 K, V_c=0.151 cc/g and s_c=0.636 J/gK are in agreement with available evaluations [25,27]. The value of evaporation temperature at normal pressure, T_v=3110 K agrees with the tabular one 3150 K from [30].

5.5. Discussion

The developed EOS for gold provides for accurate and reliable description all non-numerous high-pressure data.

It will be possible to revise the EOS when new interesting results, especially in liquid state, appear.

6. Conclusion

Described in the report results of construction multi-phase EOS for molybdenum, tantalum and gold demonstrate the efficiency of the approach. Developed EOS for these metals provides for reliable and accurate calculation of thermodynamical properties in solid, liquid and gas states.

Figs. 1-13 prove the fact, so these EOS can be used in hydrocodes for numerical modeling high-energy-density processes.

References

[1] S. B. Kormer, V. D. Urlin, L. T. Popova, Fizika tverd. tela, 3, 2131-2140 (1961) [in Russian].

[2] N. N. Kalitkin, L. V. Kuz'mina, Preprint Inst. Prikl. Matem. Akad. Nauk SSSR N35: Moskva, 1975 [in Russian].

[3] A. V. Bushman, I. V. Lomonosov, V. E. Fortov, *Equation of State for Metals at High Energy Densities,* Chernogolovka: Inst. Chem. Phys., 1992 [in Russian].

[4] L. C. Ming, M. H. Manghnani, J. Appl. Phys., 48, 208-212 (1978).

[5] Y. K. Vohra, A. L. Ruoff, Phys. Rev. Ser. B, 42, 8651-8654 (1990).

[6] L. F. Vereshchagin, N. S. Fateeva, High Temp. - High Press., 9, 619-628 (1977).

[7] G. R. Gathers, J. W. Shaner, W. M. Hodgson, High Temp. - High Press., 11, 529-538 (1979).

[8] A. F. Guillermet, Int. J. Thermophys., 6, 367-393 (1985).

[9] R. S. Hixson, D. A. Boness, J. W. Shaner, Phys. Rev. Lett., 62, 637-640 (1989).

[10] J. M. Walsh, M. H. Rice, R. G. McQueen, F. L. Yarger, Phys.Rev., 108, 196-216 (1957).

[11] R. G. McQueen, S. P. Marsh, J. Appl. Phys., 1960, 31, 1253-1269 (1960).

[12] R. G. McQueen, S. P. Marsh, J. W. Taylor, J. N. Fritz, W. J. Carter, - In: *High Velocity Impact Phenomena* / Ed. R. Kinslow. - New-York: Academic Press, p.293-417; appendies on pp. 515-568 (1970).

[13] LASL Shock Hugoniot Data / Ed. S. P. Marsh. - Berkeley: Univ. of California Press, 1980.

[14] A. C. Mitchell, W. J. Nellis, J. A. Moriarty, R. A. Heinle, N. C. Holmes, R. E. Tipton, G. W. Repp, J. Appl. Phys., 69, 2981-2986 (1991).

[15] K. K. Krupnikov, A. A. Bakanova, M. I. Brazhnik, R. F. Trunin, Dokl. Akad. Nauk SSSR, 148, 1302-1305 (1963) [in Russian] (Sov. Phys. - Dokl. 8, 205 (1963)).

[16] L. V. Al'tshuler, A. A. Bakanova, I. P. Dudoladov, E. A. Dynin, R. F. Trunin, B. S. Chekin, Sov. J. Appl. Mech. Tech. Phys., 22, 145 (1981).

[17] A. A. Bakanova, I. P. Dudoladov, Yu. N. Sutulov, Zh. Prikl. Mekh. Tekhn. Fiz. 2, 117-122 (1974) [in Russian] (J. Appl. Mech. Techn. Phys. 15, 241 (1974)).

[18] R. F. Trunin, G. V. Simakov, Yu. N. Sutulov, A. B. Medvedev, B. D. Rogozkin, Yu. E. Fedorov, Zh. Eksp. Teor. Fiz. 96(9), 1024-1038 (1989) [in Russian] (Sov. Phys. - JETP 69(3), 580-588 (1989)).

[19] C. E. Ragan, M. G. Silbert, B. C. Diven, J. Appl. Phys., 48, 2860-2870 (1977).

[20] C. E. Ragan, Phys. Rev. Ser.A, 25, 3360-3375 (1982).

[21] A. C. Mitchell, W. J. Nellis, R. A. Heinle, G. W. Repp, J. A. Moriarty, M. Ross, N. C. Holmes, Physica Ser. B., 139&140, 591-594 (1986).

[22] J. W. Shaner, G. R. Gathers, C. A. Minichino, High Temp. - High Press., 8, 425-429 (1976).

[23] U. Seydel, W. Kitzel, J. Phys. F: Metal Phys., 9(9), L153-L160 (1979).

[24] G. R. Gathers, Rep. Progr. Phys., 49, 341-396 (1986).

[25] D. A. Young, B. J. Alder, Phys. Rev. A, 1971, 3, 364-371 (1971).

[26] D. A. Young, UCRL-52352 (Lawrence Livermore Laboratory, 1977)

[27] V. E. Fortov, I. T. Yakubov, *Physics of Non-Ideal Plasmas,* Chernogolovka: Inst. Chem. Phys., 1983 [in Russian].

[28] U. Seydel, H. Bauhof, W. Fucke, H. Wadle, High Temper. - High Pressures, 9, 635-642 (1979).

[29] U. Seydel, W. Fucke, J. Phys. F: Metal Phys., 8(7), L157-L151 (1978).

[30] R. Hultgren, P. D. Desai, D. T. Hawkins, M. Gleiser, K. K. Kelley, D. D. Wagman, *Selected Values of the Thermodynamic Properties of the Elements.* - Metals Park, Ohio: ASME, 1973.

[31] S. B. Kormer, V. D. Urlin, Dokl. Akad. Nauk SSSR, 131, 542-545 (1960) [in Russian].

[32] J. Xu, H. K. Mao, P. M. Bell, High Temp. - High Press., 16, 495-499 (1984).

[33] J. M. Brown, J. W. Shaner, - In: *Shock Waves in Condensed Matter - 83 /* Eds. J. R. Asay, R. A. Graham, G. K. Straub - Amsterdam: North Holland, 91-94 (1984).

[34] A. C. Mitchell, W. J. Nellis, J. Appl. Phys., 52, 3363-3374 (1981).

[35] N. C. Holmes, J. A. Moriarty, G. R. Gathers, W. J. Nellis, J. Appl. Phys., 66, 2962-2967 (1989).

[36] J. W. Shaner, G. R. Gathers, C. Minichino, High Temp. - High Press., 9, 331-343 (1977).

[37] A. Berthault, L. Arles, J. Matricon, Intern. J. of Thermophys., 7(1), 167-179 (1986).

[38] R. S. Hixson, M. A. Winkler, J. W. Shaner, High Temp. - High Press., 18, 635-638 (1986).

[39] R. F. Trunin, G. V. Simakov, Zh. Eksp. Teor. Fiz. 103(6), 2180-2188 (1993) [in Russian] (Sov. Phys. - JETP 76(6), 1090-1094 (1993)).

[40] A. K. McMahan, R. C. Albers, Phys. Rev. Lett., 49, 1198-1201 (1982).

[41] S. B. Kormer, A. I. Funtikov, V. D. Urlin, A. N. Kolesnikova, Zh. Eksper. Teor. Fiz., 42, 686-701 (1962) [in Russian].

[42] V. D. Urlin, Zh. Eksper. Teor. Fiz., 49, 485-492 (1962) [in Russian].

[43] D. A. Young, *Phase Diagrams of the Elements,* Berkeley: Univ. of California Press, 1991.

[44] E. Yu. Tonkov, *Phase Diagrams of Elements at High Pressure,* Moscow: Nauka, 1977 [in Russian].

[45] W. H. Isbell, F. H. Shipman, A. H. Jones, General Motors Corp.: Mat. Sci. Lab. Report MSL-68-13, 1968.

[46] L. V. Al'tshuler, A. A. Bakanova, R. F. Trunin, Zh. Eksp. Teor. Fiz. 42, 91-104 (1962) [in Russian] (Sov. Phys. - JETP 15, 65-74 (1962)).

[47] R. S. Hixson, M. A. Winkler, M. L. Hodgson, Phys. Rev. Ser. B, 32(10), 6485-6491 (1990).

[48] D. L. Heinz, R. Jeanloz, J. Appl. Phys., 55, 885-893 (1984).

[49] L. C. Ming, D. Xiong, M. H. Manghnani, Physica Ser. B, 139&140, 174-176 (1986).

[50] H. K. Mao, Y. Wu, R. J. Hemley, L. C. Chen, L. C. Shu, L. Finger, Science, 246, 649 (1989).

[51] A. H. Jones, W. H. Isbell, C. J. Maiden, J. Appl. Phys., 37, 3493-3499 (1966).

[52] L. V. Al'tshuler, K. K. Krupnikov, M. I. Brazhnik, Zh. Eksp. Teor. Fiz. 34, 886-893 (1958) [in Russian] (Sov. Phys. - JETP 7, 614-618 (1958)).

Appendix: Pictures to Report

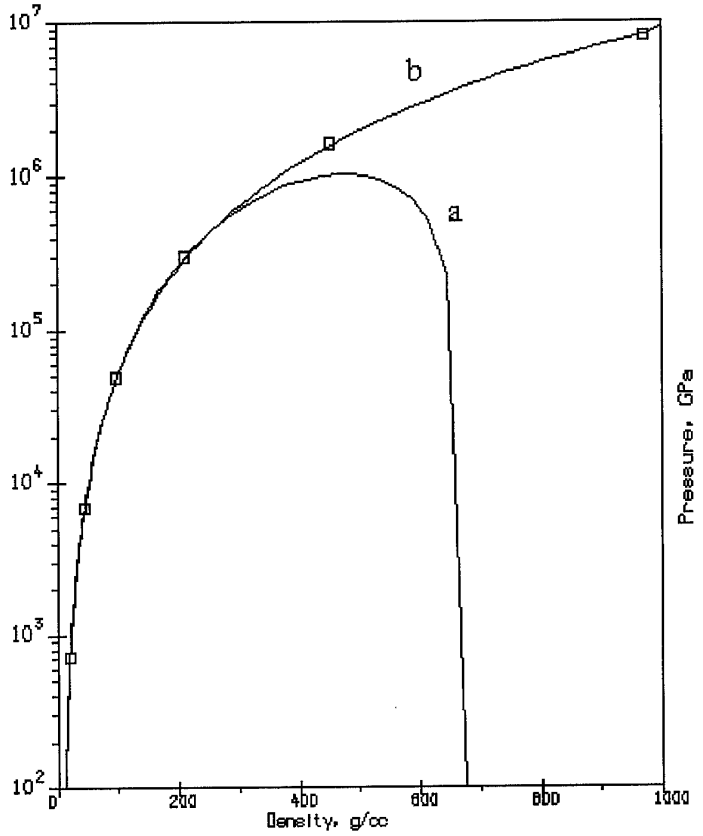

Fig. 1. Cold pressure (p(T=0 K)) in molibdenum. Curves: a - [1], b - this work; points - Thomas-Fermi calculations [2].

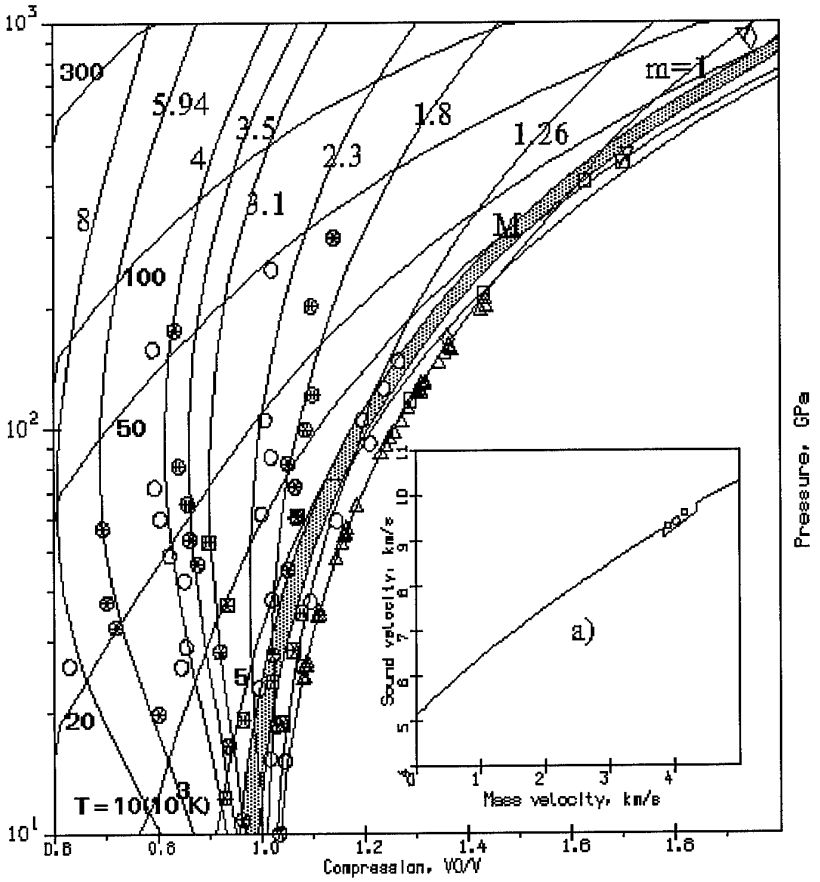

Fig. 2. Phase diagram for molybdenum. T, isotherms; m, porous Hugoniots; M, melting region. Experimental data: □ - [15], Δ - [10-13], ∇ - [14], ■ - [17], ○,⊗ - [18], ◊ - [16]. a) Sound velocity in shocked molybdenum. Points - experimental data [9].

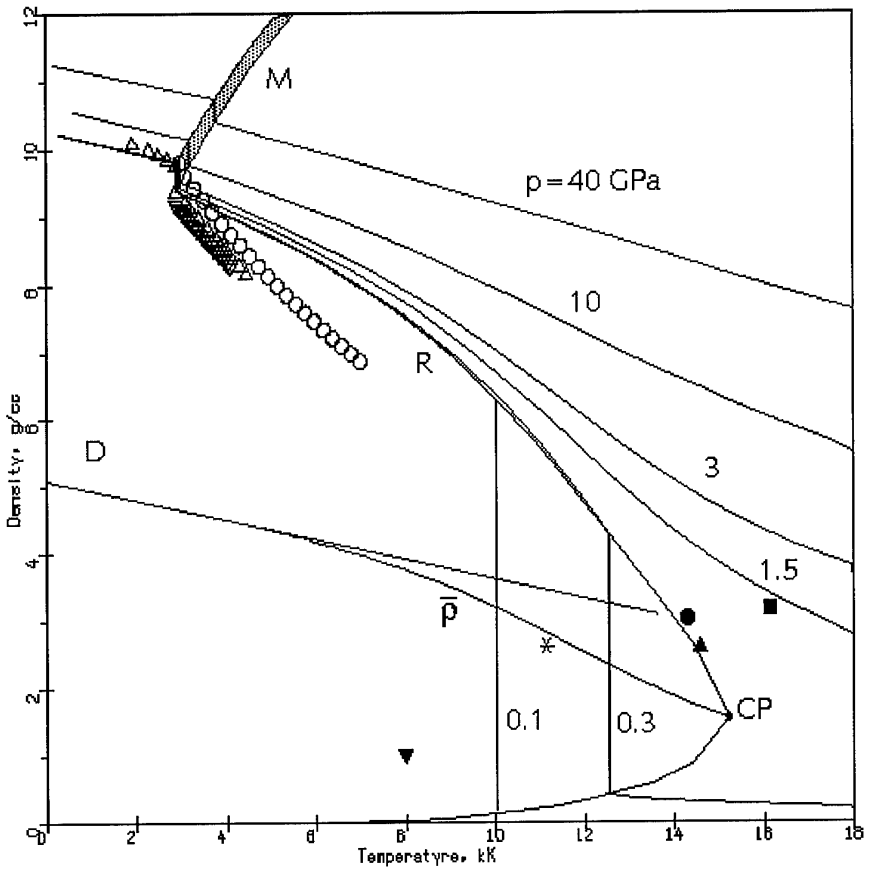

Fig. 3. Phase diagram for molybdenum in the region of lower temperatures. P, isobars; M, melting region; R, liquid-vapor equilibrium curve; D, rectilinear diameter; $\bar{\rho}$, half-sum of liquid and vapor densities. Isobaric expansion data: Δ - [22], O - [23], ∇ - [24]; evaluations of the critical-point parameters: Δ - [25], ∇ - [26], ■ - [27], ● - [28], * - [29], • - this work.

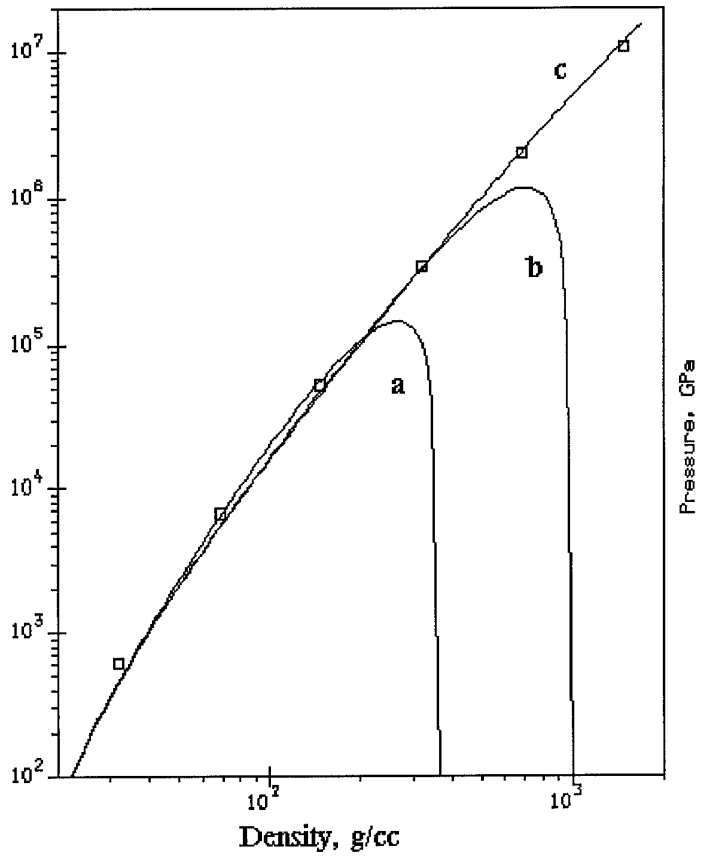

Fig. 4. Cold pressure (p(T=0 K)) in tantalum. Curves: a - [31], b - [1], c - this work; points - Thomas-Fermi calculations [2].

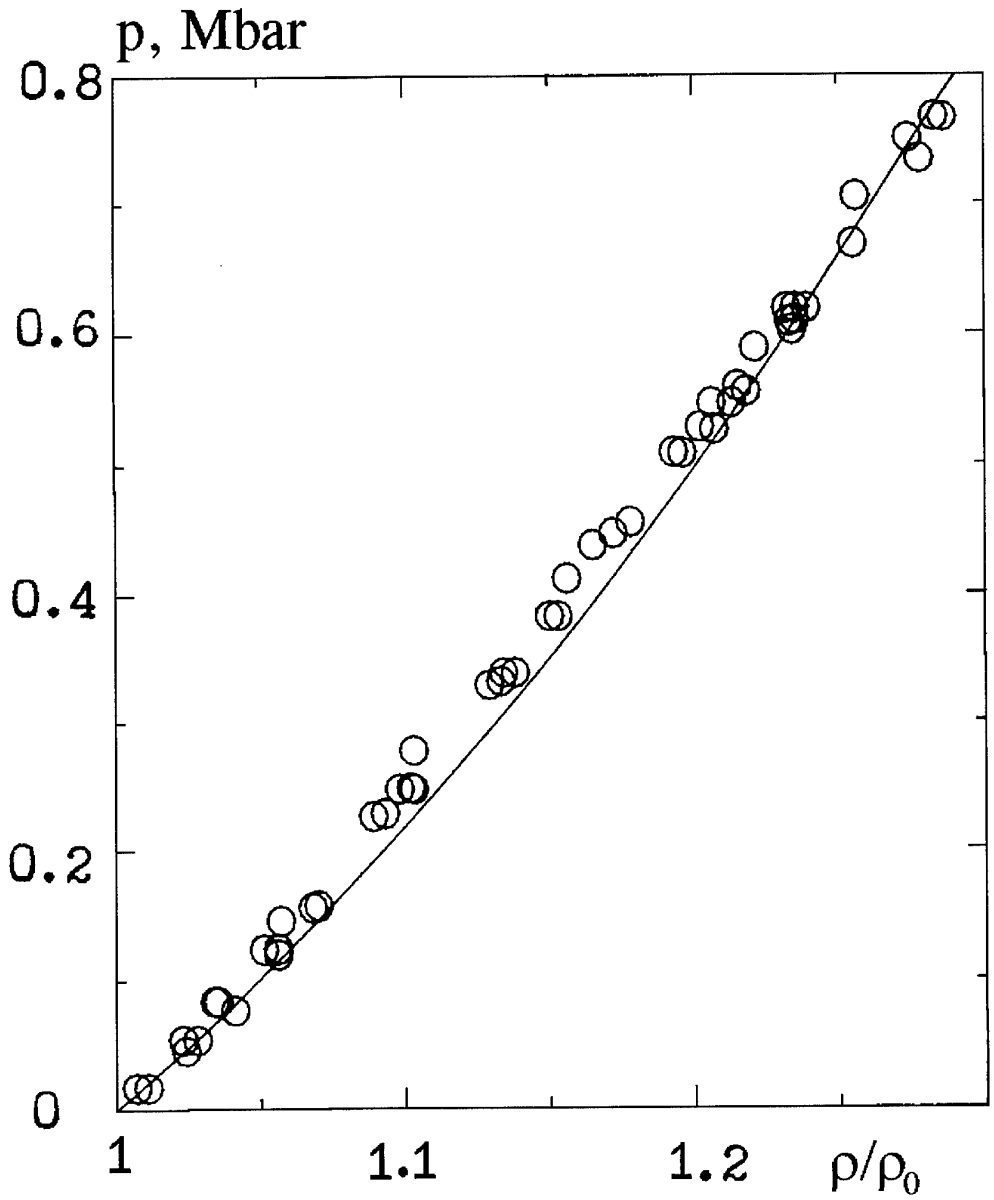

Fig. 5. Tantalum compressibility at T=298 K.
Solid line - EOS calculation, points - experimental data [32].

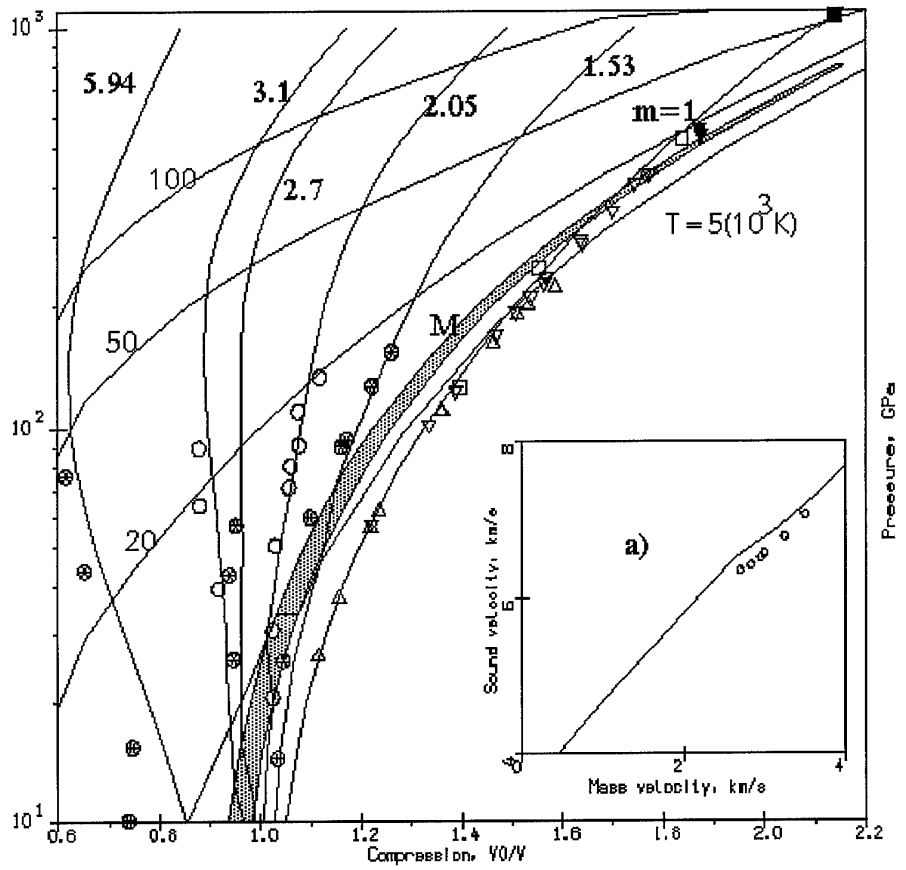

Fig. 6. Phase diagram for tantalum. T, isotherms; m, porous Hugoniots; M, melting region. Experimental data: □ - [15], ■ - [16], Δ - [34], ∇ - [11,12,13], ∇ - [35], ❍,⊗ - [18].
a) Sound velocity in shocked tantalum. Points - experimental data [33].

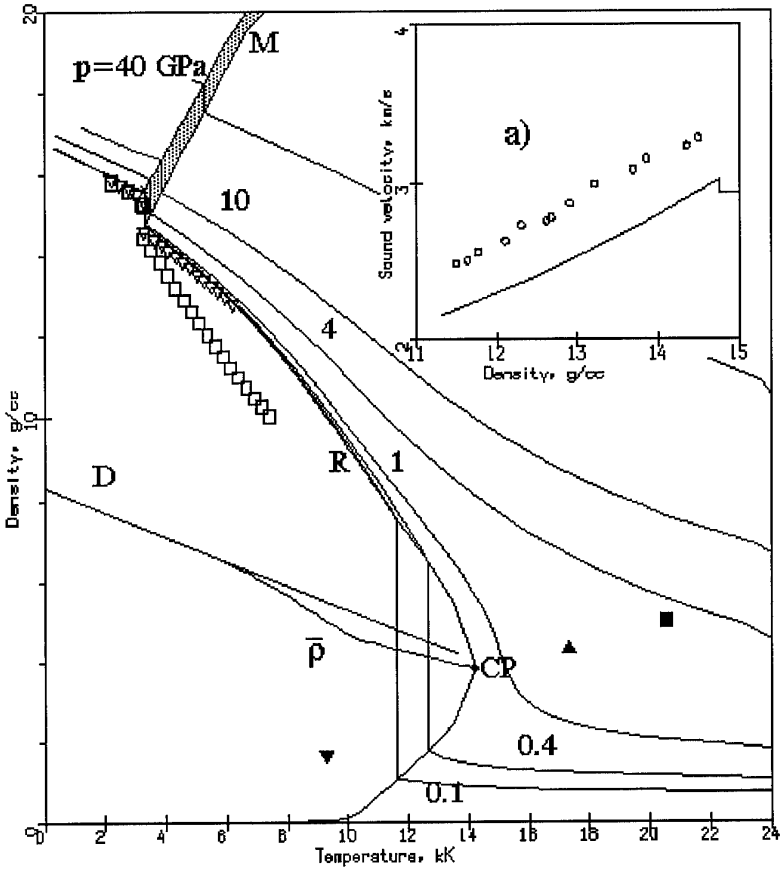

Fig. 7. Phase diagram for tantalum in the region of lower temperatures. P, isobars; M, melting region; R, liquid-vapor equilibrium curve; D, rectilinear diameter; $\bar{\rho}$, half-sum of liquid and vapor densities. Points: isobaric expansion measurements: ∇ - [36], □ - [37]; evaluations of the critical-point parameters: Δ - [25], ∇ - [26], ■ - [27], • - this work.
a) sound velocity in liquid tantalum; points - experimental data [38].

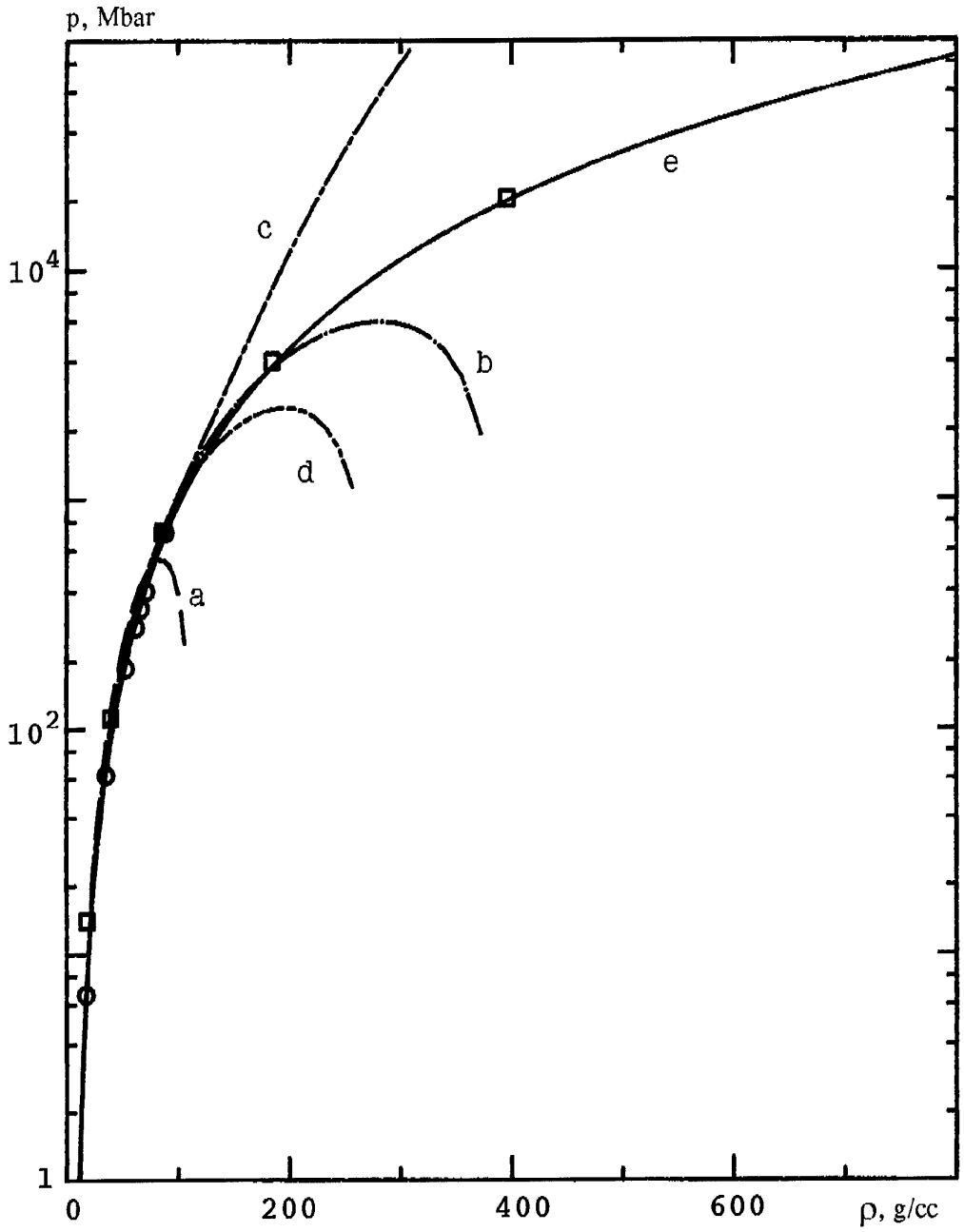

Fig. 8. Cold pressure in nickel. Theory: □ - [2], ○ - [40]; semiempirical cold curves: a - [31], b - [1], c - [41], d - [42], e - this work.

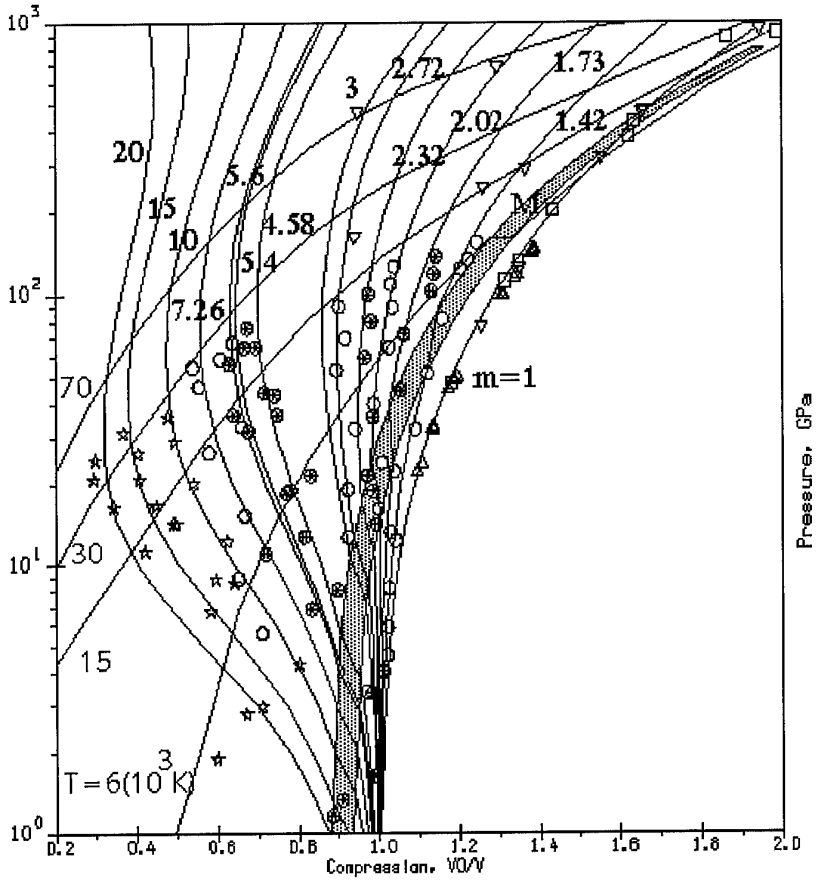

Fig. 9. Phase diagram for nickel. T, isotherms; m, porous Hugoniots; M, melting region. Experimental data: □ - [16,41,46], Δ - [10,11,13], ∇ - [45], ∇ - [41], ❍,⊗ - [18], ★ - [39].

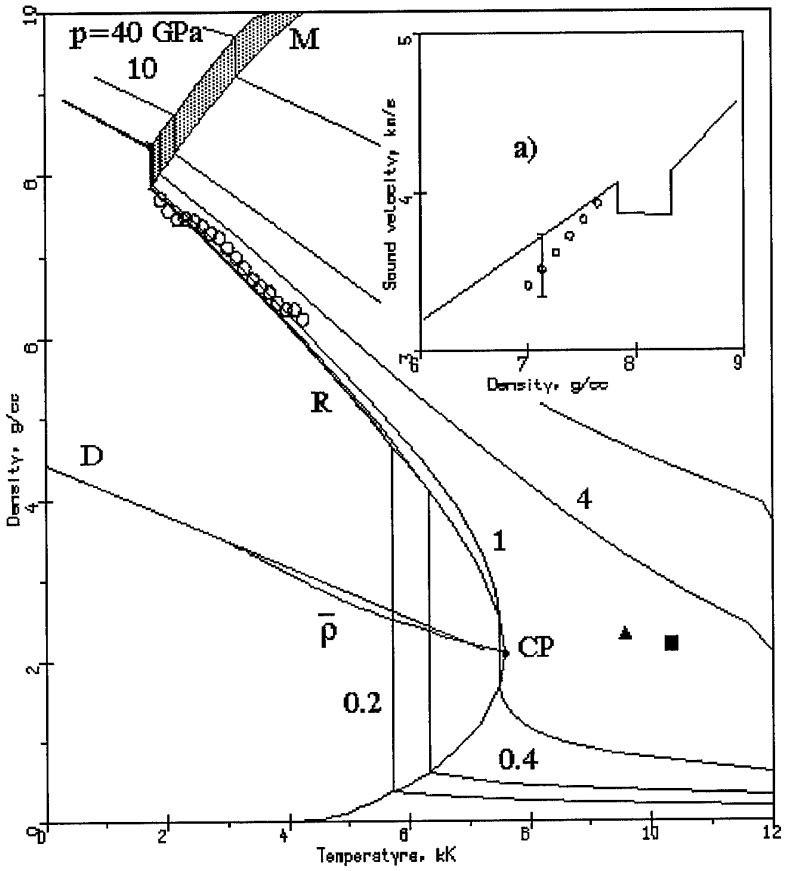

Fig. 10. Phase diagram for tungsten in the region of lower temperatures. P, isobars; M, melting region; R, liquid-vapor equilibrium curve; D, rectilinear diameter; $\bar{\rho}$, half-sum of liquid and vapor densities. Points: isobaric expansion measurements O - [47]; evaluations of the critical-point parameters: Δ - [25], ■ - [27], • - this work. a) sound velocity in liquid nickel; points - experimental data [47].

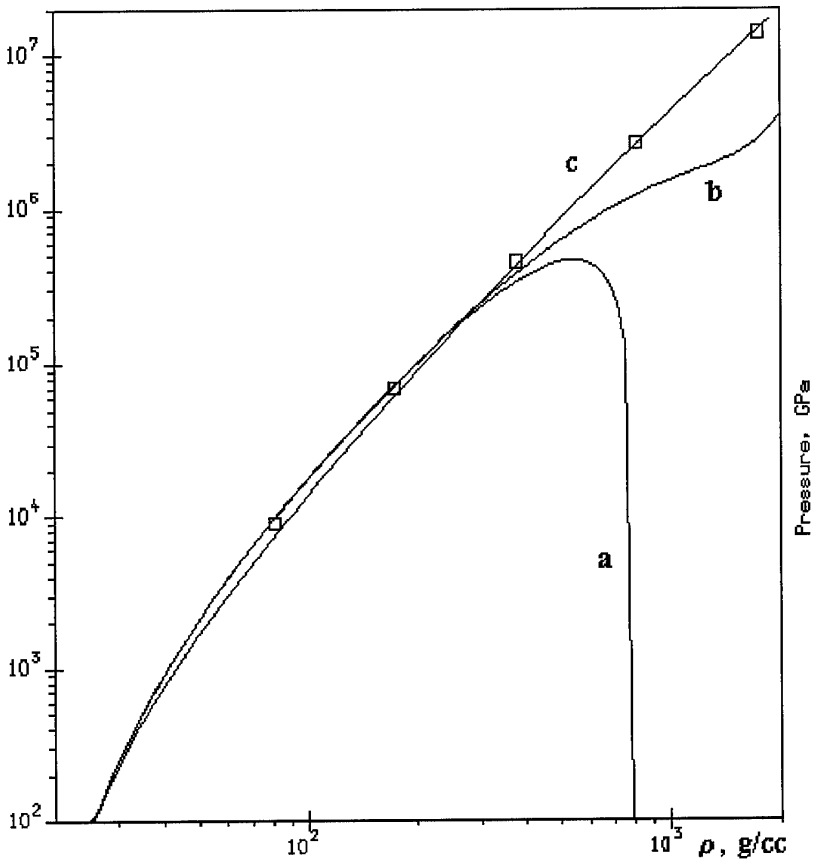

Fig. 11. Cold pressure in gold. Points - Thomas-Fermi calculations [2]; semiempirical curves: a - [31], b - [1], c - this work.

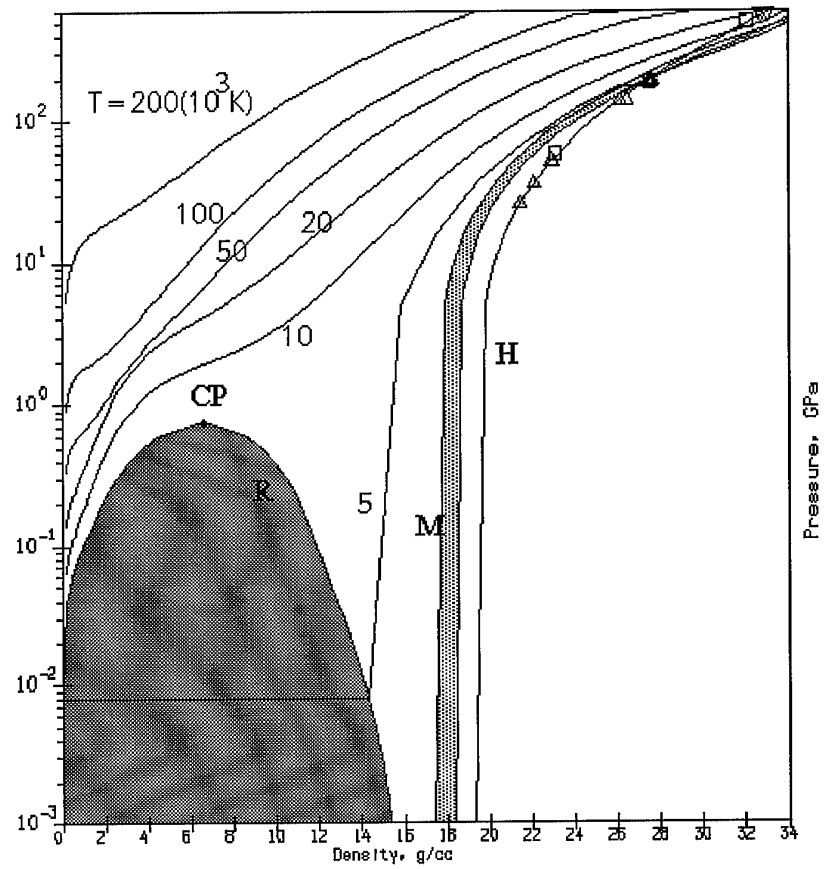

Fig. 12. Phase diagram of gold. M, melting region; R, liquid-vapor equilibrium curve with critical point CP; H - principal Hugoniot. Experimental data: □ - [16,52], Δ - [10,11,13], ∇ - [51].

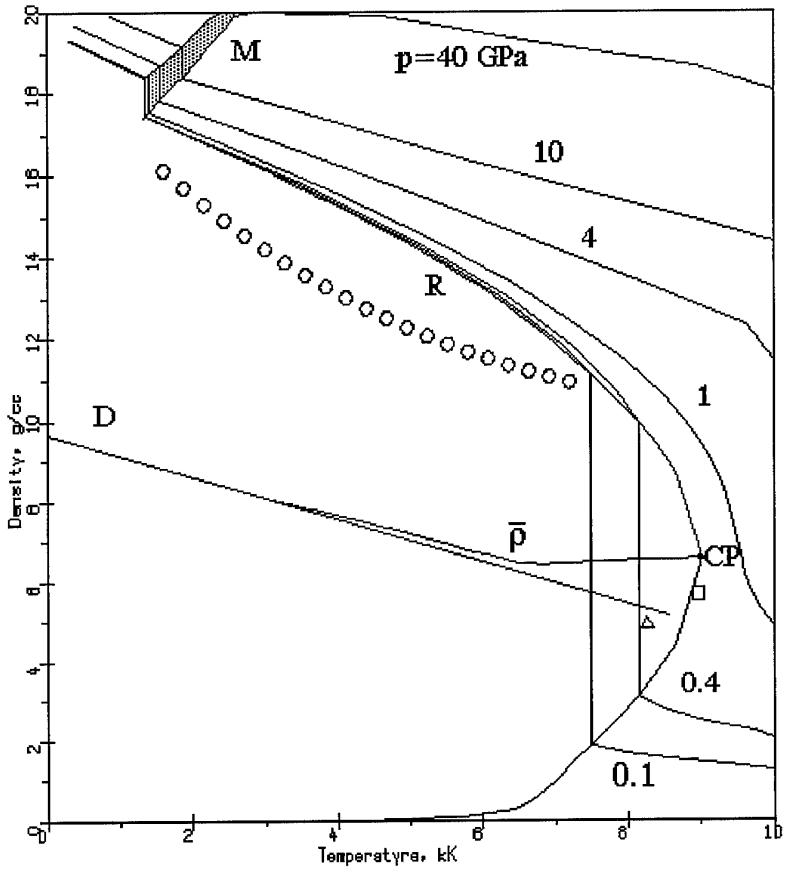

Fig. 13. Phase diagram for gold in the region of lower temperatures. P, isobars; M, melting region; R, liquid-vapor equilibrium curve; D, rectilinear diameter; $\bar{\rho}$, half-sum of liquid and vapor densities. Points: isobaric expansion measurements O - [24]; evaluations of the critical-point parameters: Δ - [25], □ - [27], • - this work.

HEDRC REPORT

Printed October 1994

WIDE-RANGE EQUATION OF STATE FOR LARGE COMPUTER CODES: EQUATIONS OF STATE OF LEAD, IRON AND TUNGSTEN

I. V. Lomonosov, V. E. Fortov, and K. V. Khishchenko

Prepared by
High Energy Density Research Center
Russian Academy of Sciences
Izhorskaya Str. 14/19, Moscow 127412, Russia
for USAF
by contract SPC-93-4074

WIDE-RANGE EQUATION OF STATE FOR LARGE COMPUTER CODES: EQUATIONS OF STATE OF LEAD, IRON AND TUNGSTEN

I. V. Lomonosov, V. E. Fortov, and K. V. Khishchenko

High Energy Density Research Center
Russian Academy of Sciences
Izhorskaya Str. 14/19, Moscow 127412, Russia

Abstract

This is second (6-months) report performed for USAF by contract SPC-93-4074. Described is comparison between calculated by multi-phase equation of state (EOS) thermodynamical properties for lead, iron and tungsten metals and available experimental data. For each metal we carried out a construction of EOS on the base of the model and procedure given in previous report and, after it, a calculation of metal's phase diagram. The comparison was made for: principal and porous Hugoniots, release isentropes, static compression data, phase-diagram data, and isobaric expansion data. The comparison and discussion with predictions of critical points are also done.

1. Introduction

Each section of the report is devoted to a selected metal. Discussed are measurements under static conditions, such diamond-anvil-cells (DAC) data, measurements of melting curve with use of high-pressure vessels, isobaric expansion investigations along with predictions of critical point and, finally, dynamic studies. They are explorations of shock Hugoniots and release isentropes. We supply the discussion by correspondent figures, shown on which are both our calculated characteristics and experiment with theoretical predictions.

2. Lead

Along with aluminum and copper, lead is one of the best investigated metals. Apart from the traditional shock-wave experiments at high and ultrahigh pressures, unique measurements on the liquid-phase characteristics at supercritical pressures were perfumed for lead, in view of its relatively low critical parameters. All this lends urgesy to the problem of the applicability of the scheme developed for constructing a wide-range semiemphirical equation of state to describe such an extensive set of heterogeneous experimental data. The lead characteristics were calculated using the coefficients obtained by procedure described previously; the results and their comparison with the available experimental data are discussed in this section.

2.1. Cold curve

Calculated cold curve for lead is compared with theoretical calculations and other semiempirical cold curves on Fig. 1.

It is well seen from the picture, that developed cold curve provide a very description of Thomas-Fermi calculations up to 100-fold compressions. At moderate densities and compressions it is in good agreement with semiempirical cold curves [1-4], obtained with analogous procedure.

2.2. Static compression and melting curve

Lead is subjected to phase transitions under condition of the static compression [6,7] - from fcc phase to hcp at 130 kbar and bcc at 1.09 Mbar. The volume changes are relatively small and are expanded with respect to pressure, so it is possible to regard that the static compression isotherm has a monotonic behavior.

These effects are accounted in the lead EOS by changing of the tabular values of the bulk compression modulus and its pressure derivative. The comparison with static and shock-wave data proved the validity of the treatment.

Shown on Fig. 2,a is a calculated by lead EOS isotherm T=298 K, which demonstrates a very good agreement with experimental data [6,7] up to highest pressures (of the order of 4 Mbar) achieved on experiment. Fig. 2,b urges such agreement in 1-10 Mbar pressure range also with theoretical calculations [8], which have been done with use of MT-orbital method.

The melting curve for lead is plotted in Fig. 3 together with the static measurement data and shows good agreement with the latter. Note, that the calculated melting line in the high-pressure region corresponds to an intersection with the shock adiabat in the 320-500 kbar pressure range, which is in a good agreement with a series of estimates obtained from shock-wave experiments [10,11].

2.3. Shock-wave data

Fig. 4, which illustrates experiments in double-shock compression for determining the characteristics of lead near the cold curve, points to the agreement between the calculated adiabats and experimental data. However, as can be seen from Fig. 4, even a simple increase of the normal velocity of sound makes it possible to allow for the phase transition which affects both the experimental data on single-shock-loading and the double-shock adiabats.

The region of high pressures and reduced (with respect to normal) densities for lead has been subjected to intensive studies using the method of shock compression of porous samples. A comparison of shock-wave data on the

compression of solid and porous samples with calculated shock adiabats is presented in Fig. 5; also plotted in the figure are the results of isotherm calculations and the boundaries of the high-temperature melting and boiling regions. The complete set of experimental measurements [13-16] is described by developed EOS with an accuracy which is not much then the experimental uncertainty. Note that here is a very good correspondence between shock-wave data obtained with the use of traditional high-explosives techniques [13,14,16] and nuclear-impedance measurements (NIM) [15]. Fig. 5,a demonstrates a quality of developed EOS on description of the isentropic sound velocity in shocked lead. In the ultrahigh-pressure region of $p>10$ Mbar, the results of calculations of the principal shock adiabat are in good agreement with the NIM data of lead compressibility measurements with a molybdenum standard [19] and iron standard [20].

The other possibility to study thermodynamical properties of metals at high pressures and low densities is provided by the isentropic expansion technique [21-23] which enables one to determine the characteristics of metal in the states of highly heated liquid and dense plasma and to record the point of entry of the release isentropes into the two-phase liquid-vapor region. Fig. 6 illustrates the quality of shock-compressed solid [22,23] and porous [21] samples using the semiempirical equation of state developed. As for lead, a divergence between the calculated curves and experimental data due to the nonequilibrium character of the process of heating a diffuse system, which is just within the experimental error (3-5%), is observed in the low-pressure region near the evaporation curve and inside the two-phase region upon expansion of porous samples; upon expansion of solid samples of the metal, full agreement of theory with experiment is observed.

The measurements of temperature and pressure on the release isentrope [22] give an unique possibility to determine the boiling curve of lead. Note, that the achieved on the dynamic experiment values of pressure exceed in 100 times the pressure obtained with use of static high-pressure vessels. The comparison between calculated release isentropes, evaporation curve and experimental data is given on Fig. 7, shown on which are also prediction of critical points for lead. It is seen from the figure, that developed EOS describes with very high accuracy and reliability all carried out experiments [22] and agrees with estimations of critical points.

2.4. High-pressure, low-density data

The same is demonstrated (Fig. 8) by an agreement between the calculated characteristics of high-temperature expansion of lead in the slow electric explosion of wires under pressure along the p=0.013 [29], 0.1, 0.2, 0.3, 0.4 [30] GPa isobar. Note, that shown on Fig. 8 are smoothed results of isobaric expansion measurements [30], calculated by approximating relationships presented in the work. The calculated curve both reproduces the general behavior of the experimental data over a correct description of a fine effect of the elbow in the experimental $\rho(T)$ curve towards low densities near the critical point, corresponding to an anomalously high value of the coefficient of volume expansion. The agreement between the temperature dependence of density and velocity of sound of the liquid phase of lead also points to the high reliability of description of thermodynamic characteristics in the region adjoining the evaporation curve. Calculations yielded the critical-point parameters of lead p_c =2.38 kbar, T_c=5540 K, V_c=0.32 cc/g and s_c=0.56 J/gK, and the evaporation temperature at normal pressure, T_v=2031 K. This value of the temperature coincides with the experimental value, while the critical-point parameters correspond, as can be seen from the figure, to their estimated values.

2.5. Discussion

The thermodynamic calculations of lead based on the wide-range semiempirical equation of state provide an example of efficient utilization of the scheme developed for constructing and determining the coefficients of the thermodynamic potential using a large heterogeneous set of initial experimental data. Note, that the developed EOS describe the available data with accuracy which does not exceed the typical experimental errors.

3. Iron

Iron is, probably, the material of the most use in modern technique, science and numerous applications. Iron serves also as standard material in modern physics of high dynamic pressure. These facts define the role of reliable and accurate calculation of its phase diagram at high pressures and temperatures.

Unlike simple metals, iron has very complicated phase diagram which includes, at least, 5 phases (α, β, ε, γ, θ) [31]. Developed was EOS for high-pressure phase of iron, namely ε-iron. The phase transition from α to ε–iron, occurring at normal temperature and pressure 13 GPa, is the most significant for practical calculations. The next ε-γ phase transition is following with small change of density, so it is possible to describe in the same monotonic manner this high-pressure phases. The generalized high-pressure phase was considered as ε–iron with initial density ρ=8.28 g/cc, which corresponds to reduction of static [32] and dynamic [33] data.

3.1. Cold curve

Calculated cold curve for lead is compared with theoretical calculations, based on the Thomas-Fermi model [5], on Fig. 9. The good correspondence between semiempirical cold curve and theoretical data conserves in range from 3-fold to 100-fold compression. This fact for iron (good agreement of Thomas-Fermi calculations and experimental shock Hugoniot data at pressures of the order of 20 Mbar) was used previously on revision on Russian NIM data [20].

3.2. Static compression and melting curve

The calculated isotherm T=298 K for ε–iron is compared with results of measurements of iron compressibility in diamond-anvil cell [32] on Fig. 10. This picture demonstrates their full agreement which confirms the reliability of developed EOS at normal temperature.

The calculated value of the initial slope of iron melting curve dT/dp=3.35 K/kbar agrees with those one given in [31] 3.85 K/kbar, which was determined at static conditions up to 200 kbar. As these values are very similar for both γ- and ε–phase, the agreement confirms an adequacy of description the solid-liquid phase transition.

3.3. Shock-wave data

The shock compressibility of iron was studied with the use traditional high-explosive drivers to 2.5 Mbar [14,35]. The region of more high pressures to 14 Mbar was investigated with use of special powerful explosive systems [13,34]. The region of high pressures and lower with respect to principal Hugoniot density was studied by measurement of the porous Hugoniots [14,35-37].

The extreme high pressures were generated in iron by nuclear explosions. There are absolute [38] and impedance-match principal Hugoniot data [39-41]. Results of determination of high-porous ($m=\rho_0 / \rho_{00}=3.3$) shock Hugoniots at pressure $p \approx 14$ Mbar [37] are of great interest as the state on Hugoniot corresponds to slightly-degenerated electron gas with very large value of energy concentration.

The phase diagram for iron is given on Fig. 11. As it is seen from the picture, developed EOS for iron provides very good and reliable description of principle- and porous-Hugoniot data overall range of investigated pressures. That is right for both situations of liquid (moderate temperatures) and plasma ($100<T<200$ kK [37]) states, which are occurred on shock compression of porous samples. Note, that the full set of data [13,14,34,36,37] which were obtained with use of different methods of generating and measuring of shock waves, is described in correct self-consistent manner.

Fig. 11, a demonstrates a very good agreement between calculated by the EOS and measured in works [17,33] the of sound velocity in shocked iron.

The melting in shocked iron was determined in [33] by disappearing of transverse component of isentropic sound velocity. Recent temperature measurements [42] revised the position of melting on the principle Hugoniot: p=2.4 Mbar, T=5.8 kK (estimated from the shock energy) [33]; p=2.35 Mbar,

T=6.35 kK [42]. Calculated by developed iron EOS values are: p=2.33 Mbar, T=6.1 kK. The temperature calculations describe with very good accuracy (within experimental bars) results [42].

3.4. High-pressure, low-density data

Shown on Fig. 12 are results of calculation of liquid-vapor coexistence curve with the critical point, and selected isobars. They are compared with isobaric-expansion (p=0.2 GPa) data [43] and evaluations of critical points. The results of calculations by developed EOS give slightly higher values of critical point: p_c=10.25 kbar, T_c=10.95 kK, V_c=0.0522 cc/g and s_c=2.815 J/gK; the evaporation temperature at normal pressure, T_v=3.125 kK is in very good agreement with tabular one [44]. The p=0.2 GPa isobar also deviates from experimental data [43] (see Fig. 12). Note, that this deviation is of the order of the experimental error; the slope of liquid-gas equilibrium curve is the same as from [43] and calculated sound velocity on the experimental isobar is in good agreement with the one from [43]. So it is possible to conclude, that the iron EOS provides for a necessary accuracy in the region of low densities and can be used in hydrocodes.

3.5. Discussion

The developed EOS for iron does not reflect correctly the very complicated phase diagram of real metal. It accounts only for a high-pressure phase, namely ε–iron. Obviously, due to only this reason there is no absolute agreement between EOS calculations and experimental and theoretical data at low densities. Nevertheless, it should be mentioned, that this discrepancy is not very large and does not effect on correct description of sound velocity.

The analysis of Fig. 9-12 allows to make a conclusion, that this iron EOS provides for a good accuracy and reliability on calculation in solid, liquid and plasma states and can be used in hydrocodes.

4. Tungsten

Along with iron, tungsten is of great use in numerous practical applications. It has large values of melting and evaporation temperatures which explains its usage on developing new structural materials for aviation and space technique.

4.1. Cold curve

T=0 K compression curve for tungsten is shown on Fig. 13 as well as semiempirical cold curve from [2] and results of Thomas-Fermi calculations [5]. It is interesting to mention, that cold curve [2], obtained with similar procedure, does not allow to run correct calculations of thermodynamic parameters at 10-fold and larger compressions. It can be explained by the fact, that in method [2] used were requirements $p_c(V = 0.1V_{0c}) = p^{TFC}, c_c(V = 0.1V_{0c}) = c^{TFC}$, where p and c are cold pressure and sound velocity, respectively. It leads to unphysical oscillations and even negative values of pressure at $V=0.02V_{0c}$, while the cold curve obtained in the work provides for a correct description of cold pressure up to 100-fold compression and agrees with Thomas-Fermi calculations [5].

4.2. Static compression and melting

According to [31], there is no phase transitions in tungsten at room temperature up to 60 kbar. The results [45] also does not reveal anomalies for the isothermal compressibility of tungsten up to 100 kbar. The comparison between calculated and experimental [45] dependencies p(T=298 K) showed their good agreement overall investigated range of pressure.

The value of the initial slope of the melting curve dT/dp significantly differs and depends upon the experimental technique. Optical measurements [46] gives dT/dp=7.5 K/kbar, while data obtained with the use of isobaric expansion methods lead to value 4.4 K/kbar [47]. The isobaric expansion data will be discussed below, as for calculation of the melting curve parameters, the EOS agrees with the result of optical measurements [46]: tungsten is melting at p=50 kbar, T=4050±200 K.

4.3. Shock-wave data

The shock compressibility of tungsten has been investigated thoroughly in megabar-pressure range with the use of various high-explosive systems [14,35,48] and two-stage light-gas gun [49]. Porous Hugoniots up to 3 Mbar have been studied in [36,48,50,51] also with use of high-explosive drivers. Impedance-match measurements were done at 60 Mbar [19] under condition of nuclear explosion. Data on shock compressibility of porous (m=3.06) samples [31] at p<22 Mbar are analogous to those one for iron and allow to determine the thermal electrons contribution with high accuracy.

The calculated with tungsten EOS phase diagram is shown on Fig. 14 in comparison with available shock-wave data. It is interesting to note, that tungsten has a large value of melting enthalpy. This fact leads to broad, with respect to density, melting region, which significantly effects to position of porous Hugoniots (see Fig. 14). The analysis of Fig. 14 allows to conclude, that developed EOS for tungsten provides an accurate and reliable description of all available shock-wave data. Carried out comparison with NIM data [19] also proves this fact.

The isentropic sound velocity has been measured in shocked porous (m=1.8) tungsten with use of overtaken technique [48]. Fig. 14,a demonstrates a good agreement between calculated and measured in experiment [48] sound velocity.

4.4. High-pressure, low-density data

Shown on Fig. 15 are calculated phase boundary liquid-gas with critical point CP, rectilinear diameter D and isobars in comparison with isobaric-expansion measurements [52,53,54] and evaluations of the critical point [24,27,52,55].

The thermodynamical situation for tungsten looks sophisticated as critical point estimations and isobaric expansion measurements do not agree with each other. The developed EOS for tungsten, as it is seen from Fig. 15, agrees with position of melting at moderate density and temperature given by results of measurements [52,53,54]. Calculated parameter of evaporation temperature at

normal pressure, T_v=5.744 kK, agrees with tabular data [44]; critical point parameters p_c=10.74 kbar, T_c=15.12 kK, V_c=0.2105 cc/g and s_c=0.904 J/gK are in good agreement with approximation of experimental data [52,55].

The discrepancy between position of calculated liquid-gas coexistence curve, isobars and isobaric expansion data can be explained only by difficulty of correct measurement density of liquid metal. It should to mention, that reduction of experimental data gives values for heat capacity at constant pressure c_p=0.28-0.31 J/(gK) [47,52,53,54] at melting temperature T=3690 K. Near-melting point value for solid tungsten is also of the order of 0.26-0.28 J/(gK) [30]. This exceeds in 2 or more times the one c_p=0.137 J/(gK) at ambient conditions. The value for heat capacity at melting temperature from the experimental data is too large. Note also, that typical error bars are of the order of ±250 K and ±2 g/cc (from recent publication [54]). Calculated sound velocity in liquid tungsten is in agreement with the measured one [54]. The slope of expansion curve for liquid tungsten in energy-density coordinates from [56] is less then from [47,52], so finally it is possible to conclude that developed EOS for tungsten is in satisfactory agreement with experimental and theoretical data in liquid state at moderate temperatures.

4.5. Discussion

The accuracy and reliability of developed EOS is very high at high pressures and temperatures. It describes all available static-compression and shock-wave data with accuracy which does not exceed the experimental error.

Thermodynamical data for tungsten are not in full agreement with each other in the region of liquid state at moderate temperatures. So developed EOS for tungsten describes by alternative way the set of isobaric expansion measurements and evaluations of critical point.

As the EOS describes high-pressure, high temperature data, provides for tabular value of evaporation temperature at p=1 bar and is in reasonable agreement with isobaric expansion data and evaluations of critical point, it can be resumed, that the EOS can be used in hydrocodes to calculate thermodynamical properties in solid, liquid, and gas states.

5. Conclusion

It is very difficult to satisfy simultaneously the condition of the best description of numerous high-pressure data. They have their own accuracy, occupy different regions of the phase diagram. Note also, that such information, as principal, porous Hugoniots and pressure-expansion velocity measurements on release isentropes is not thermodynamically complete.

On developing EOS for lead, iron and tungsten, the most attention was paid on correct description of dynamic, i.e. shock-wave, data. The accuracy and reliability of the EOS have been proved by comparison with the most significant experimental data. Pictures given in Appendix demonstrate this fact. The liquid state of metals is region of the greatest problems both for experimental and theoretical methods. Nevertheless, developed EOS provide for a reasonable description of metals thermodynamics at high and moderate temperatures.

Calculated with use of these EOS thermodynamical functions can be used in hydrocodes with great efficiency.

References

[1] S. B. Kormer, V. D. Urlin, Dokl. Akad. Nauk SSSR, 131, 542-545 (1960) [in Russian].

[2] S. B. Kormer, V. D. Urlin, L. T. Popova, Fizika tverd. tela, 3, 2131-2140 (1961) [in Russian].

[3] S. B. Kormer, A. I. Funtikov, V. D. Urlin, A. N. Kolesnikova, Zh. Eksper. Teor. Fiz., 42, 686-701 (1962) [in Russian].

[4] V. D. Urlin, Zh. Eksper. Teor. Fiz., 49, 485-492 (1962) [in Russian].

[5] N. N. Kalitkin, L. V. Kuz'mina, Preprint Inst. Prikl. Matem. Akad. Nauk SSSR N35: Moskva, 1975 [in Russian].

[6] C. A. Vanderborgh, Y. K. Vohra, H. Xia, A. L. Ruoff, Phys. Rev. Ser. B, 41, 7338-7340 (1990).

[7] Y. K. Vohra, A. L. Ruoff, Phys. Rev. Ser. B, 42, 8651-8654 (1990).

[8] W. J. Nellis, J. A. Moriarty, A. C. Mitchell, M. Ross, R. G. Dandrea, N. W. Ashcroft, N. C. Holmes, G. R. Gathers, Phys. Rev. Lett., 60, 1414-1417 (1988).

[9] P. W. Mirwald, G. C. Kennedy, J. Phys. Chem. Solids, 37, 795-797 (1976).

[10] G. E. Duvall, R. A. Graham, Rev.Mod.Phys., 49, 523-579 (1977).

[11] H. Bernier, P. Lalle, in: *High Pressure in Research and Industry* (Proceed. 8 th AIRAPT Conference); Eds. C.-M.Backman, T.Johannisson and L.Tegner. - Uppsala, Arkitektopia, 1, 194-197 (1981).

[12] T. J. Neal, J. Phys. Chem. Solids, 38, 225 (1977).

[13] L. V. Al'tshuler, B. S. Chekin, In: Proceed. 1-st All-union symposium of pulse pressures, Moscow: VNIIFTRI, V. 1, 5 (1974).

[14] LASL Shock Hugoniot Data / Ed. S.P.Marsh. - Berkeley: Univ. of California Press, 1980.

[15] A. C. Mitchell, W. J. Nellis, J. A. Moriarty, R. A. Heinle, N. C. Holmes, R. E. Tipton, G. W. Repp, J.Appl.Phys., 69, 2981-2986 (1991).

[16] R. F. Trunin, G. V. Simakov, Yu. N. Sutulov, A. B. Medvedev, B. D. Rogozkin, Yu. E. Fedorov, Zh. Eksp. Teor. Fiz. 96(9), 1024-1038 (1989) [in Russian] (Sov. Phys. - JETP 69(3), 580-588 (1989)).

[17] L. V. Al'tshuler, S. B. Kormer, M. I. Brazhnik, L. A. Vladimirov, M. P. Speranskaya, A. I. Funtikov, Zh. Eksp. Teor. Fiz. 38(4), 1061-1073 (1960) [in Russian] (Sov. Phys. - JETP 11(4), 766-775 (1960)).

[18] D. A. Boness, J. M. Brown, J. W. Shaner, In: Shock Waves in Condensed Matter - 87 / Eds. S.C.Schmidt, N.C.Holmes - Amsterdam: North Holland, 115-118 (1988).

[19] C. E. Ragan, Phys. Rev. Ser.A, 25, 3360-3375 (1982).

[20] L. V. Al'tshuler, N. N. Kalitkin, L. V. Kuz'mina, B. S. Chekin, Zh. Teor. Fiz. 72(1), 317-325 (1977) [in Russian] (Sov. Phys. - JETP 45(1), 167-171 (1977)).

[21] L. V. Al'tshuler, A. V. Bushman, M. V. Zhernokletov, V. N. Zubarev, A. A. Leont'ev, V. E. Fortov, Sov. Phys. - JETP, 51, 373 (1980).

[22] E. N. Avrorin, B. K. Vodolaga, V. A. Simonenko, V. E. Fortov, *Powerful Shock Waves and Extreme States of Matter,* Moscow: Inst. High. Temp., 1990 [in Russian].

[23] L. V. Al'tshuler, A. A. Bakanova, A. V. Bushman, I. P. Dudoladov, V. N. Zubarev, Zh. Eksp. Teor. Fiz. 73(11), 1866-1872 (1977) [in Russian] (Sov. Phys. - JETP 46(5), 980-983 (1977)).

[24] D. A. Young, B. J. Alder, Phys. Rev. A, 1971, 3, 364-371 (1971).

[25] K. Hornung, J. Appl. Phys., 46, 2548 (1975).

[26] D. A. Young, UCRL-52352 (Lawrence Livermore Laboratory, 1977)

[27] V. E. Fortov, I. T. Yakubov, *Physics of Non-Ideal Plasmas,* Chernogolovka: Inst. Chem. Phys., 1983 [in Russian].

[28] G. Pottlacher, H. Jager, Int. J. Thermophys., 11(4), 719-729 (1990).

[29] R. S. Hixson, M. A. Winkler, J. W. Shaner, High Temp. - High Press., 17, 267-270 (1985).

[30] G. R. Gathers, Rep. Progr. Phys., 49, 341-396 (1986).

[31] E. Yu. Tonkov, *Phase Diagrams of Elements at High Pressure,* Moscow: Nauka, 1977 [in Russian].

[32] H. K. Mao, P. M. Bell, J. Geophys. Res. Ser.B, 84, 4533-4536 (1979).

[33] J. M. Brown, R. G. McQueen, Geophys. Res. Ser.B, 91, 7485-7494 (1986).

[34] L. V. Al'tshuler, A. A. Bakanova, I. P. Dudoladov, E. A. Dynin, R. F. Trunin, B. S. Chekin, Sov. J. Appl. Mech. Tech. Phys., 22, 145 (1981).

[35] R. G. McQueen, S. P. Marsh, J. W. Taylor, J. N. Fritz, W. J. Carter, - In: High Velocity Impact Phenomena (1970)/ Ed. R.Kinslow. - New-York: Academic Press, p.293-417; appendies on pp. 515-568.

[36] R. F. Trunin, G. V. Simakov, Yu. N. Sutulov, A. B. Medvedev, B. D. Rogozkin, Yu. E. Fedorov, Zh. Eksp. Teor. Fiz. 96(9), 1024-1038 (1989) [in Russian] (Sov. Phys. - JETP 69(3), 580-588 (1989)).

[37] R. F. Trunin, A. B. Medvedev, A. I. Funtikov, M. A. Podurets, G. V. Simakov, A. G. Sevast'yanov, Zh. Eksp. Teor. Fiz. 95, 631-641 (1989) [in Russian] (Sov. Phys. - JETP 68(2), 356-361 (1989)).

[38] R. F. Trunin, M. A. Podurets, L. V. Popov, V. N. Zubarev, A. A. Bakanova,V. M. Ktitorov, A. G. Sevast'yanov, G. V. Simakov, I. P. Dudoladov, Zh. Eksp. Teor. Fiz. 102(9), 1433-1438 (1992) [in Russian] (Sov. Phys. - JETP 75(4), 777-780 (1992)).

[39] L. V. Al'tshuler, B. N. Moiseev, L. V. Popov, G. V. Simakov, R. F. Trunin, Zh. Eksp. Teor. Fiz. 54, 785-789 (1968) [in Russian] (Sov. Phys. - JETP 27(3), 420-422 (1968)).

[40] R. F. Trunin, M. A. Podurets, G. V. Simakov, L. V. Popov, B. N. Moiseev, Zh. Eksp. Teor. Fiz. 62(3), 1043-1048 (1972) [in Russian] (Sov. Phys. - JETP 35(3), 550-552 (1972)).

[41] C. E. Ragan, Phys. Rev. Ser.A, 29, 1391-1402 (1984).

[42] C. S. Yoo, N. C. Holmes, M. Ross, D. J. Webb, C. Pike, Phys. Rev. Lett., 70(25), 3931-3934 (1993).

[43] R. S. Hixson, M. A. Winkler, M. L. Hodgson, Phys. Rev. Ser. B, 32(10), 6485-6491 (1990).

[44] R. Hultgren, P. D. Desai, D. T. Hawkins, M. Gleiser, K. K. Kelley, D. D. Wagman, *Selected Values of the Thermodynamic Properties of the Elements.* - Metals Park, Ohio: ASME, 1973.

[45] L. C. Ming, M. H. Manghnani, J. Appl. Phys., 48, 208-212 (1978).

[46] L. F. Vereshchagin, N. S. Fateeva, High Temp. - High Press., 9, 619-628 (1977).

[47] J. W. Shaner, G. R. Gathers, C. A. Minichino, High Temp. - High Press., 8, 425-429 (1976).

[48] K. K. Krupnikov, M. I. Brazhnik, V. P. Krupnikova, Zh. Eksp. Teor. Fiz. 42, 675-685 (1962) [in Russian] (Sov. Phys. - JETP 15(3), 470-476 (1962)).

[49] A. H. Jones, W.H. Isbell, C. J. Maiden, J. Appl. Phys., 37, 3493-3499 (1966).

[50] A. A. Bakanova, I. P. Dudoladov, Yu. N. Sutulov, Zh. Prikl. Mekh. Tekhn. Fiz. 2, 117-122 (1974) [in Russian](J. Appl. Mech. Techn. Phys. 15, 241 (1974)).

[51] R. R. Boade, J. Appl. Phys., 40, 3781-3792 (1969).

[52] U. Seydel, W. Kitzel, J. Phys. F: Metal Phys., 9(9), L153-L160 (1979).

[53] A. Berthault, L. Arles, J. Matrinson, Intern. J. of Thermophys., 7(1), 167-179 (1986).

[54] R. S. Hixson, M. A. Winkler, Intern. J. of Thermophys., 11(4), 709-718 (1990).

[55] W. Fucke, U. Seydel, High Temper. - High Pressures, 12(4), 419-432 (1980).

[56] V. V. Ivanov, S. V. Lebedev, A. I. Savvatimskii, J. Phys. F: Met. Phys., 14, 1641-1650 (1984).

Appendix: Pictures to Report

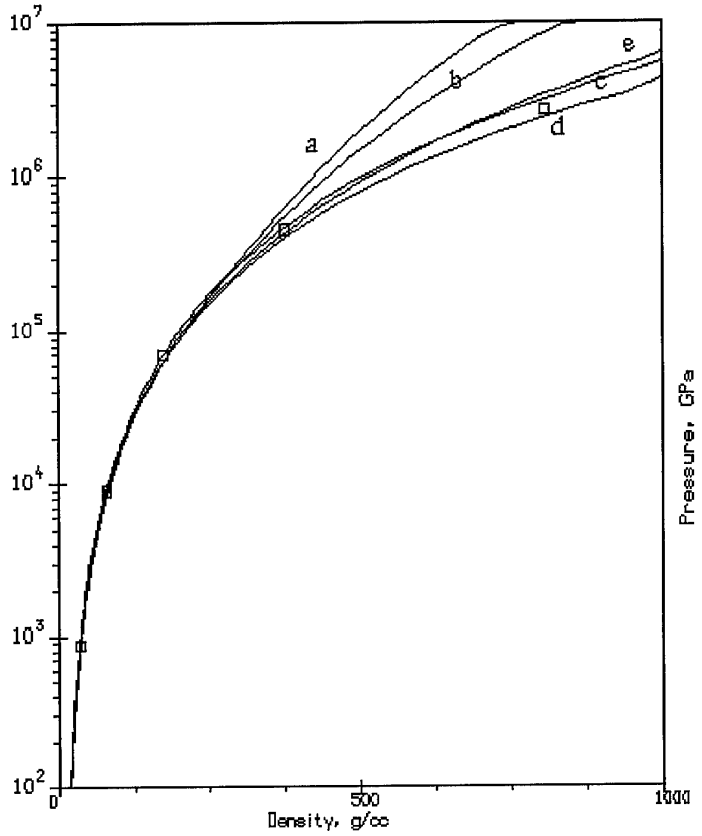

Fig. 1. Cold pressure (p(T=0 K)) in lead. Curves: a - [1], b - [2], c - [3], d - [4], e - this work; points - Thomas-Fermi calculations [5].

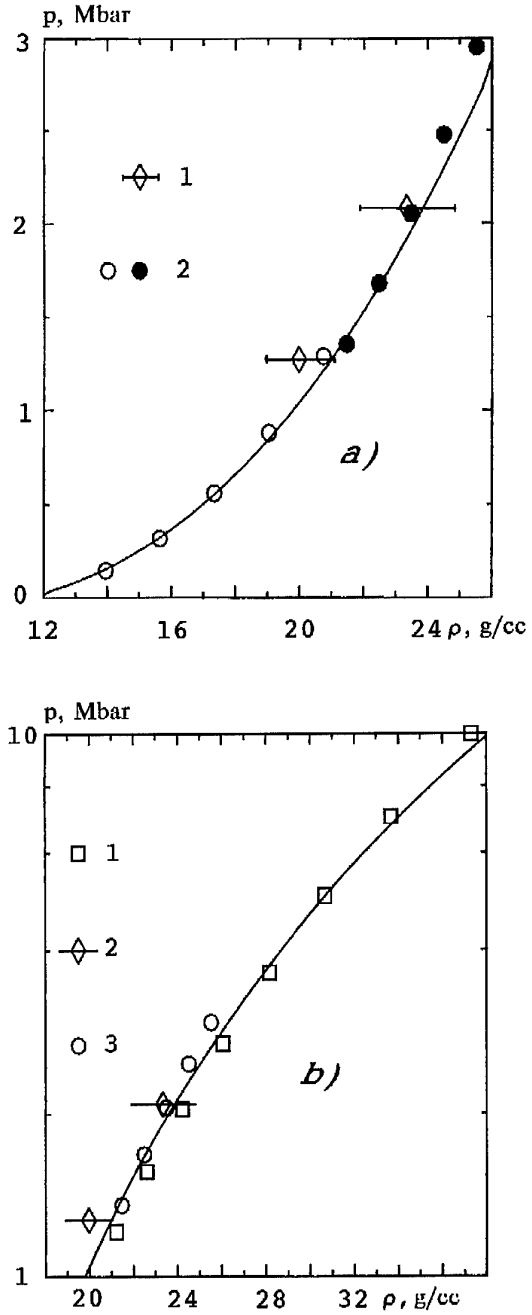

Fig. 2. Lead compressibility at T=298 K.
a) experimental data: 1 - [6], 2 - [7] (open circles - hcp phase, closed - bcc)
b) theoretical calculations: 1 - [8]; experimental data: 2 - [6], 3 - [7] (bcc phase)

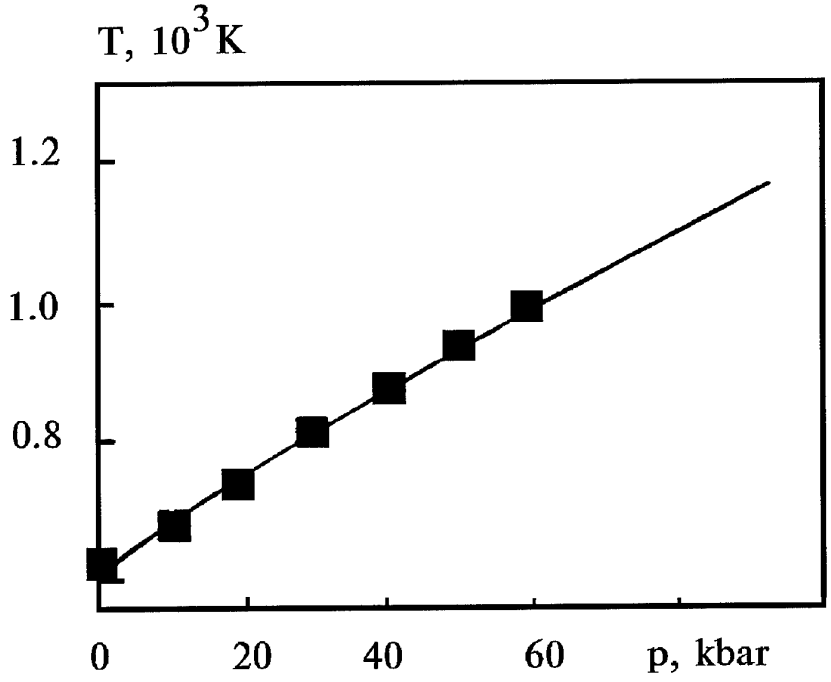

Fig. 3. Melting curve of lead. Points - experimental data [9].

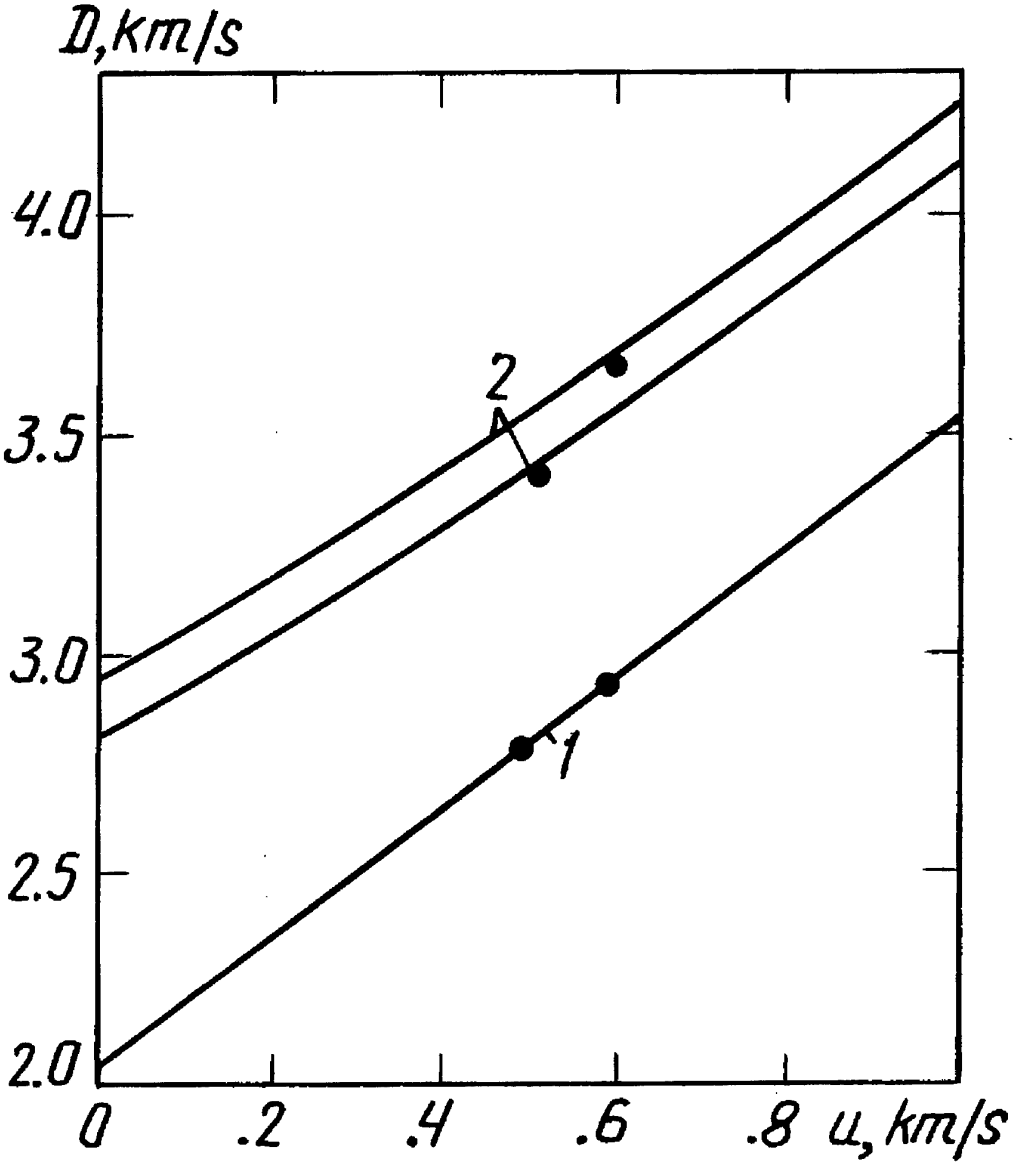

Fig. 4. Single- and double-shock Hugoniot data for lead. Shown are principal Hugoniot (1) and reflected (2) shock waves; points - experimental data [12].

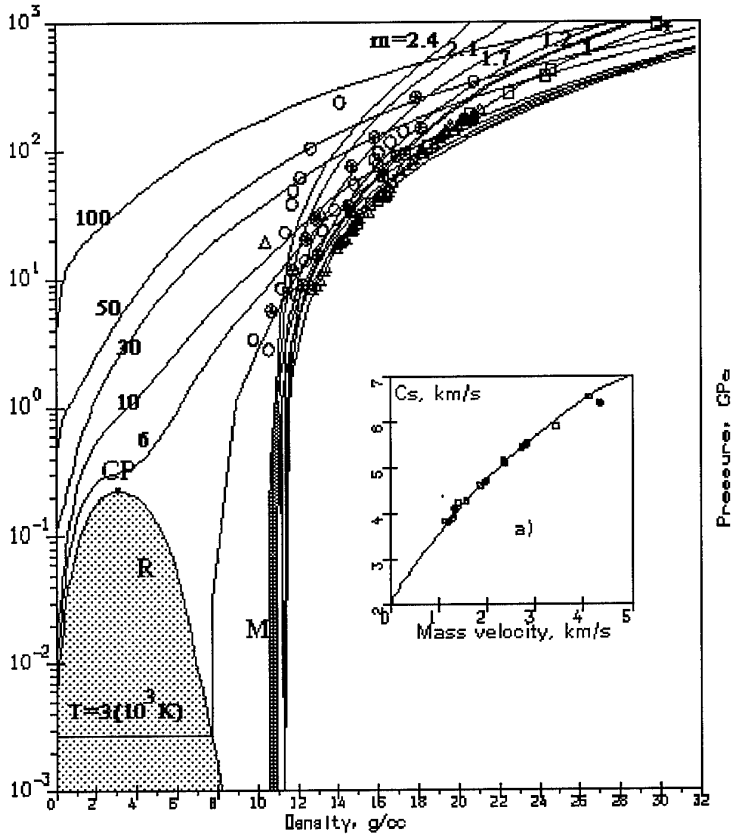

Fig. 5. Phase diagram for lead. T, isotherms; m, porous Hugoniots; M, melting region; R, liquid-vapor equilibrium curve with the critical point CP. Experimental data: □ - [13], Δ - [14], * - [15], ❍,⊗ - [16].
a) Sound velocity in shocked lead. Experimental data: □ - [17], ❍ - [18].

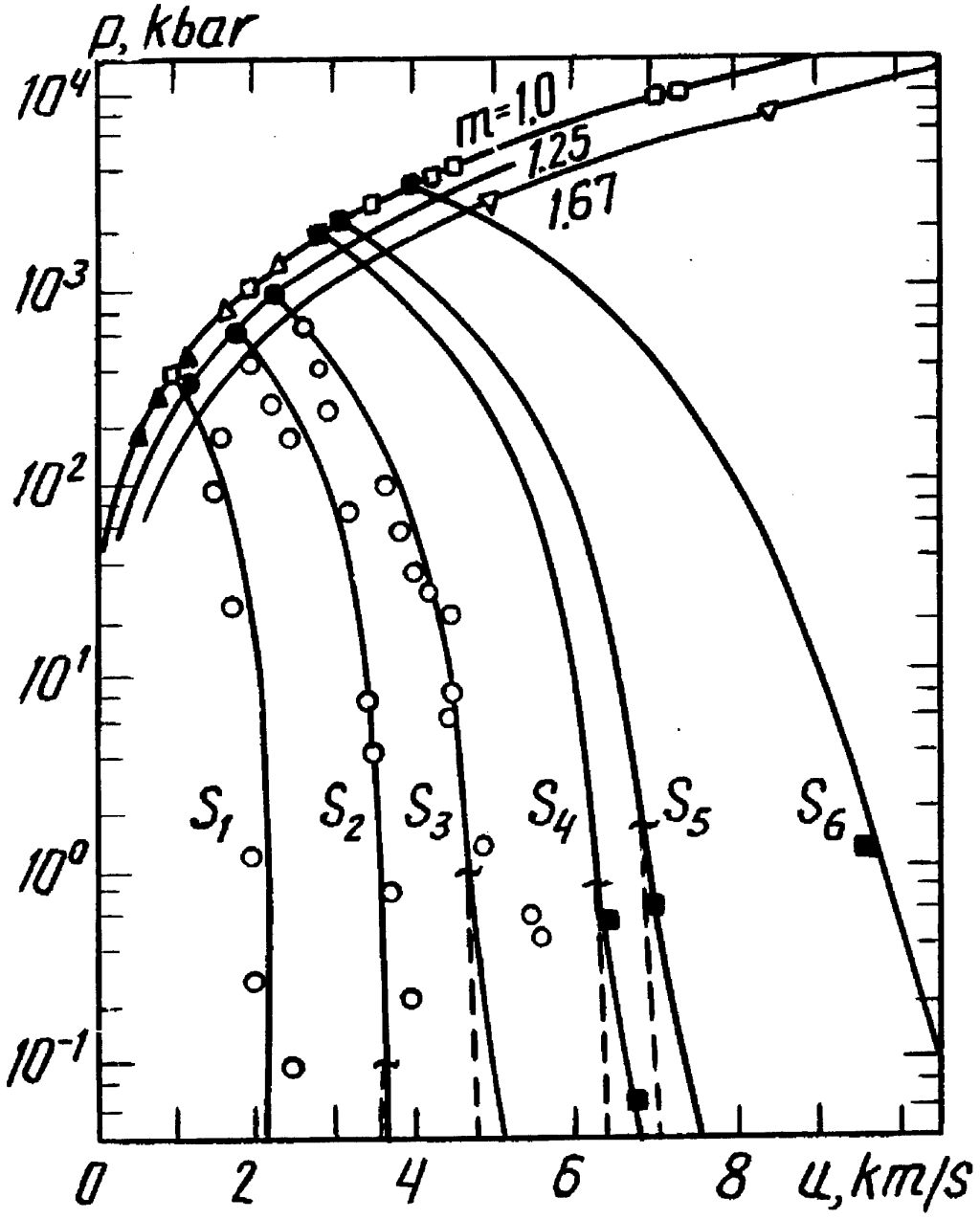

Fig. 6. Shock adiabats (m) and release isentropes (S) for lead. Calculations: solid lines, equilibrium states; dashed lines, metastable states, wavy lines mean the entry into liquid-gas region. Experimental data: □ - [13], Δ - [14], ○- [21], ■ - [23].

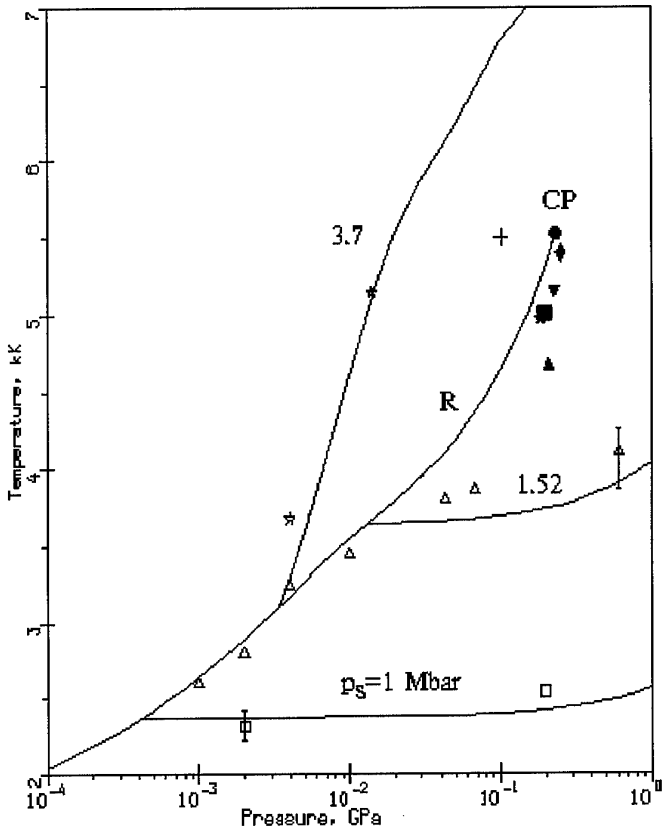

Fig. 7. Pressure-temperature diagram for lead in evaporation region. Shown are: R - boiling curve with critical point CP, p_S - release isentropes (1, 1.52, 3.7 Mbar are pressures on shock Hugoniot). Points - experimental data with error bars: □ - for isentrope 1 Mbar, Δ - 1.52 Mbar, ★ - 3.7 Mbar; predictions of critical point for lead: Δ - [24], + - [25], ∇ - [26], ■ - [27], ♦ - [28], • - this work.

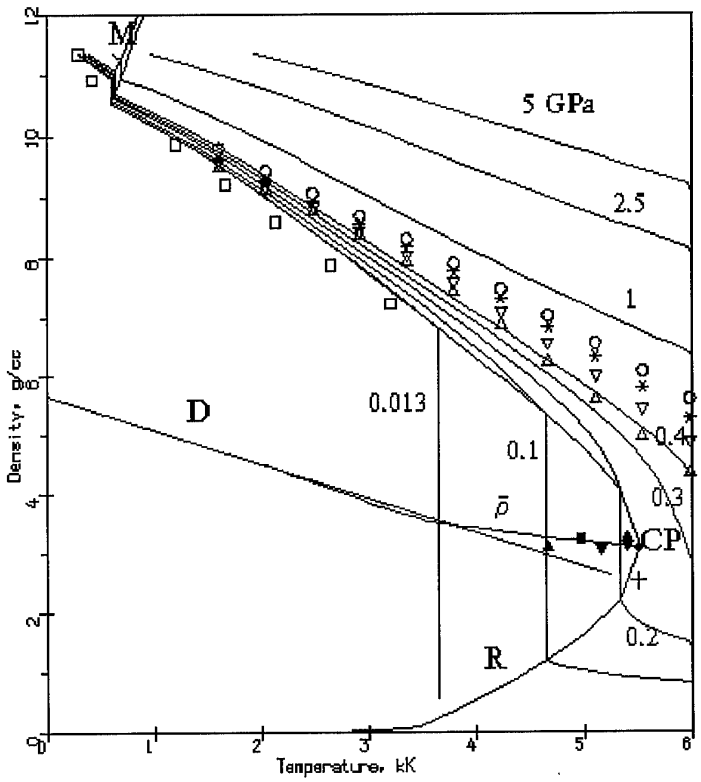

Fig. 8. Phase diagram for lead in the region of lower temperatures. P, isobars; M, melting region; R, liquid-vapor equilibrium curve; D, rectilinear diameter; $\bar{\rho}$, half-sum of liquid and vapor densities. Isobaric expansion data: □ - 0.013 GPa [29], Δ,∇,✱,○ - 0.1, 0.2, 0.3, 0.4 GPa [30]; evaluations of the critical-point parameters: Δ - [24], + - [25], ∇ - [26], ■ - [27], ♦ - [28], • - this work.

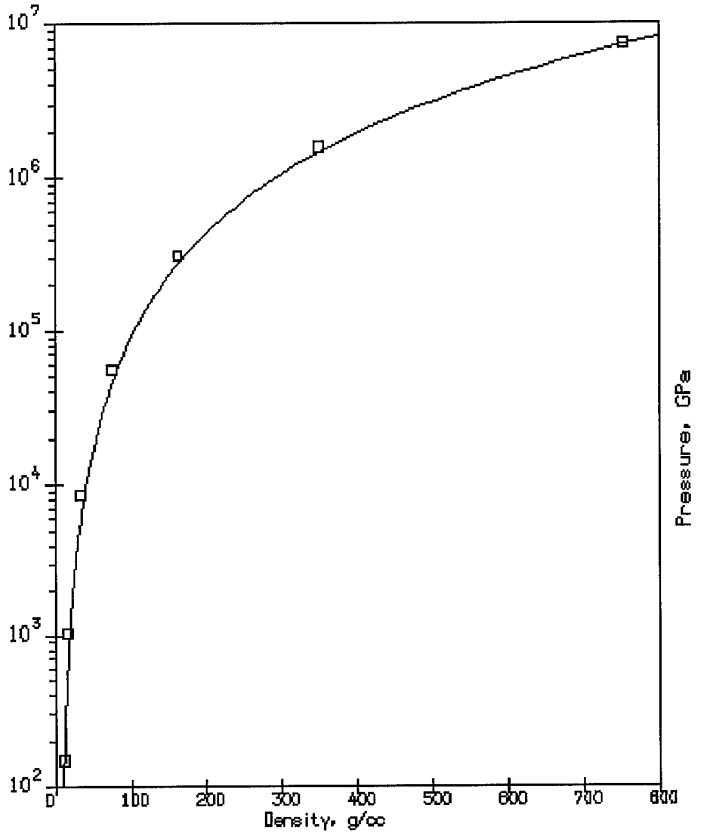

Fig. 9. Cold pressure (p(T=0 K)) in iron. Curve - this work; points - Thomas-Fermi calculations [5].

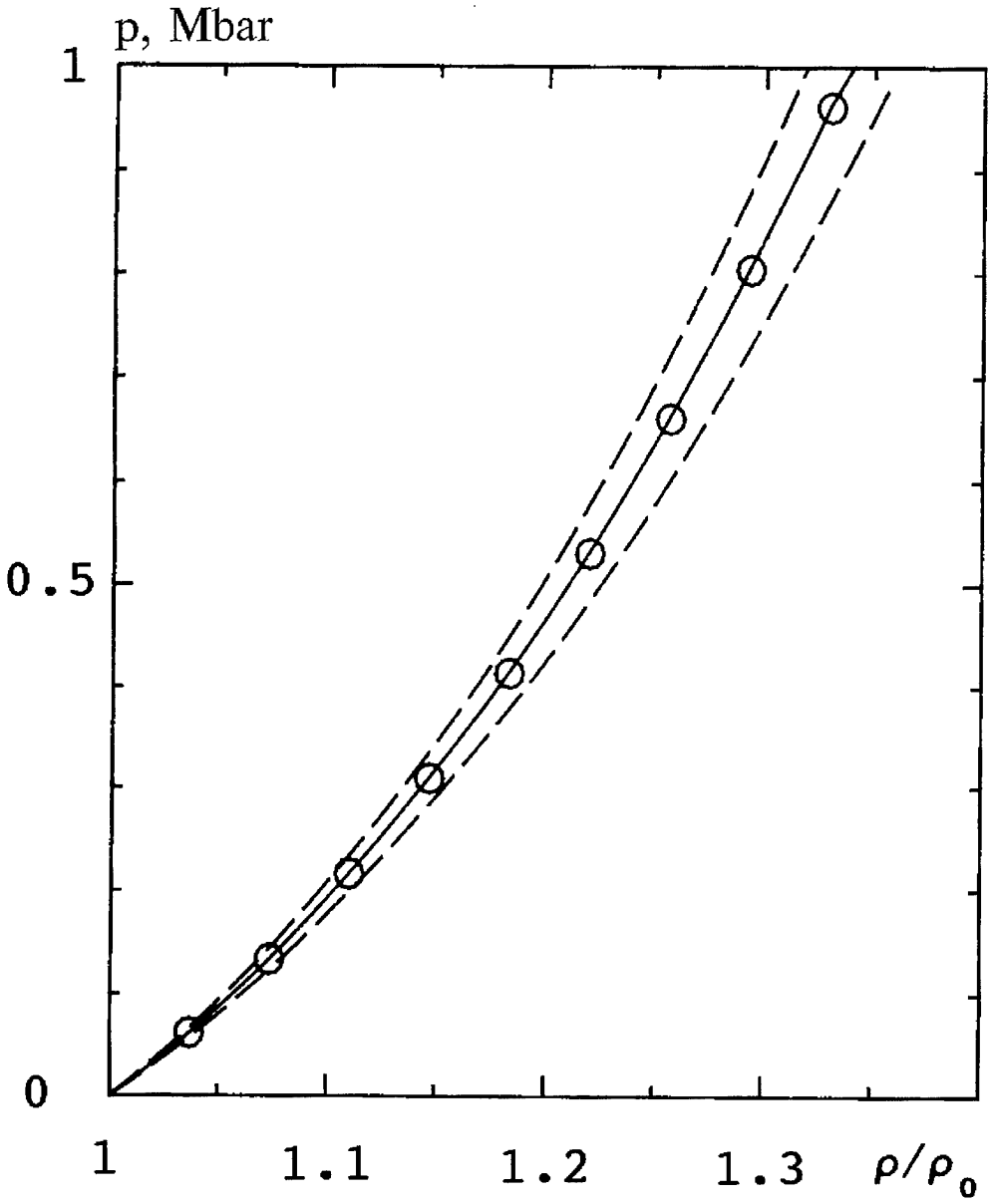

Fig. 10. Iron compressibility at T=298 K.
Solid line - EOS calculation, dashed line - region of experimental error, points - experimental data [32].

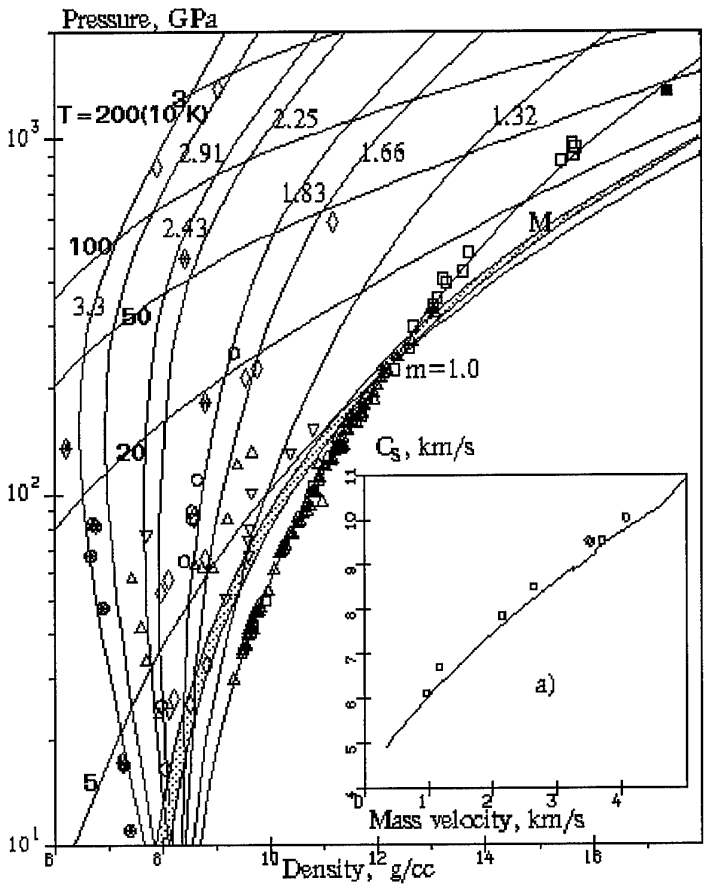

Fig. 11. Phase diagram for iron. T, isotherms; m, porous Hugoniots; M, melting region. Experimental data: □ - [13], Δ,∇ - [14], ◊,♦ - [37], ❍,⊗ - [36], ■ - [34].
a) Sound velocity in shocked iron. Experimental data: □ - [17], ❍ - [33].

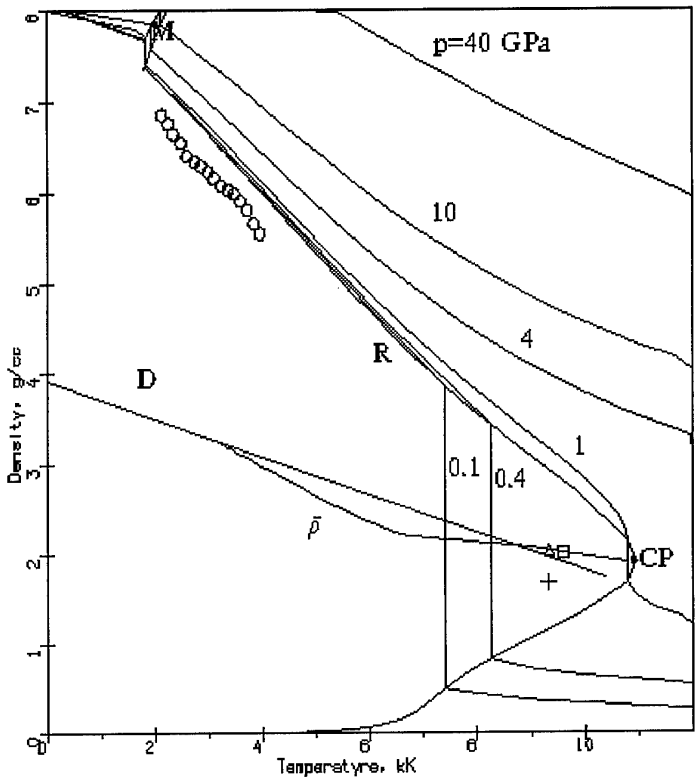

Fig. 12. Phase diagram for iron in the region of lower temperatures. P, isobars; M, melting region; R, liquid-vapor equilibrium curve; D, rectilinear diameter; $\bar{\rho}$, half-sum of liquid and vapor densities. Points: isobaric expansion measurements O - [42]; evaluations of the critical-point parameters: Δ - [24], + - [25], □ - [27], • - this work.

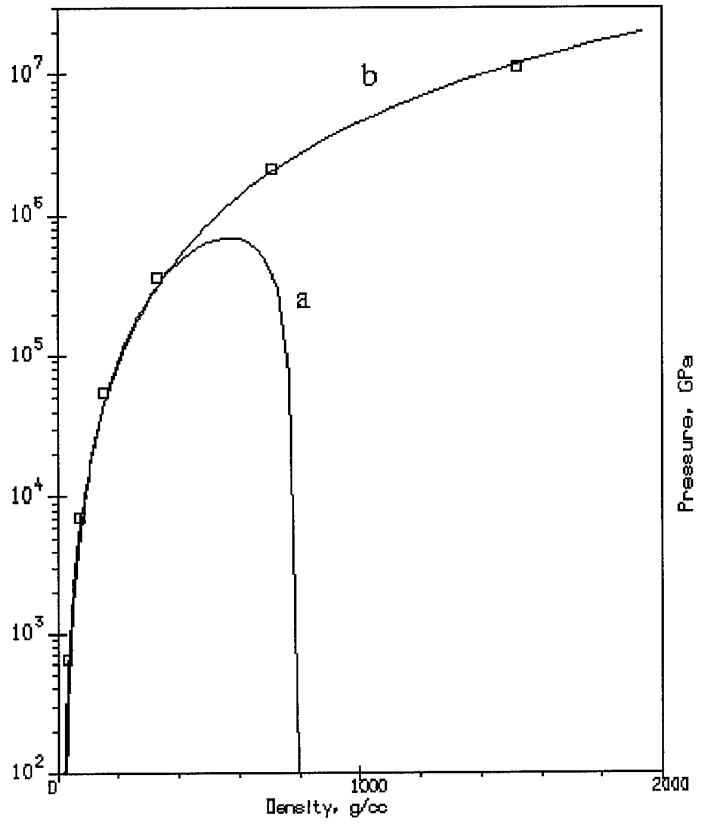

Fig. 13. Cold pressure (p(T=0 K)) in tungsten. Curves: a - [2], b - this work; points - Thomas-Fermi calculations [5].

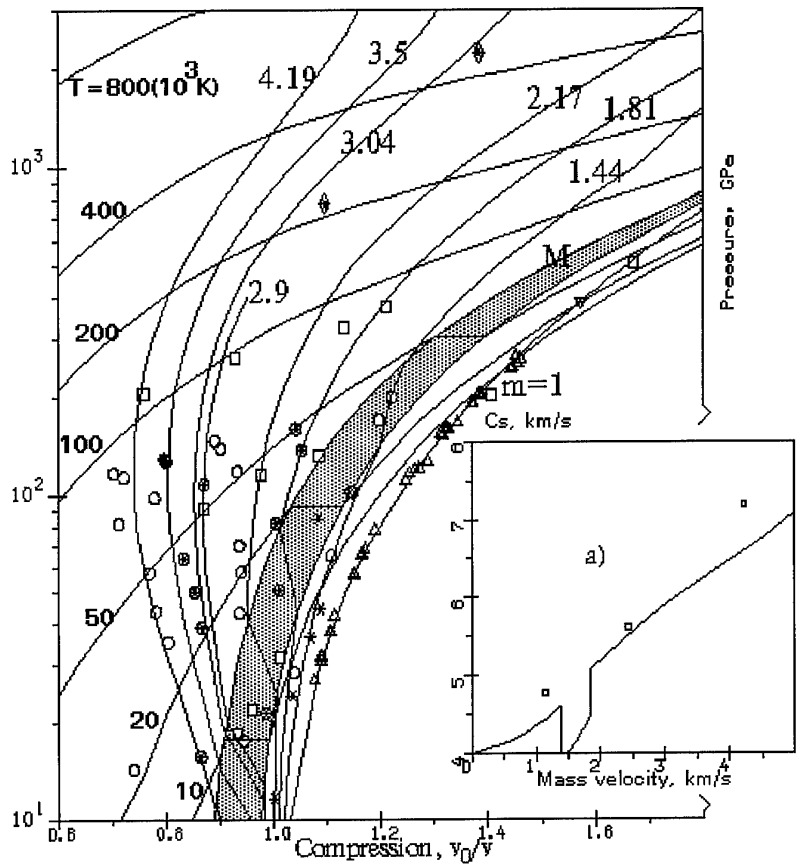

Fig. 14. Phase diagram for tungsten. T, isotherms; m, porous Hugoniots; M, melting region. Experimental data: □ - [48], Δ - [14], ∇ - [49], ♦ - [37], ○,⊗ - [36], ✶ - [50].
a) Sound velocity in shocked porous (m=1.8) tungsten. Experimental data: □ - [48].

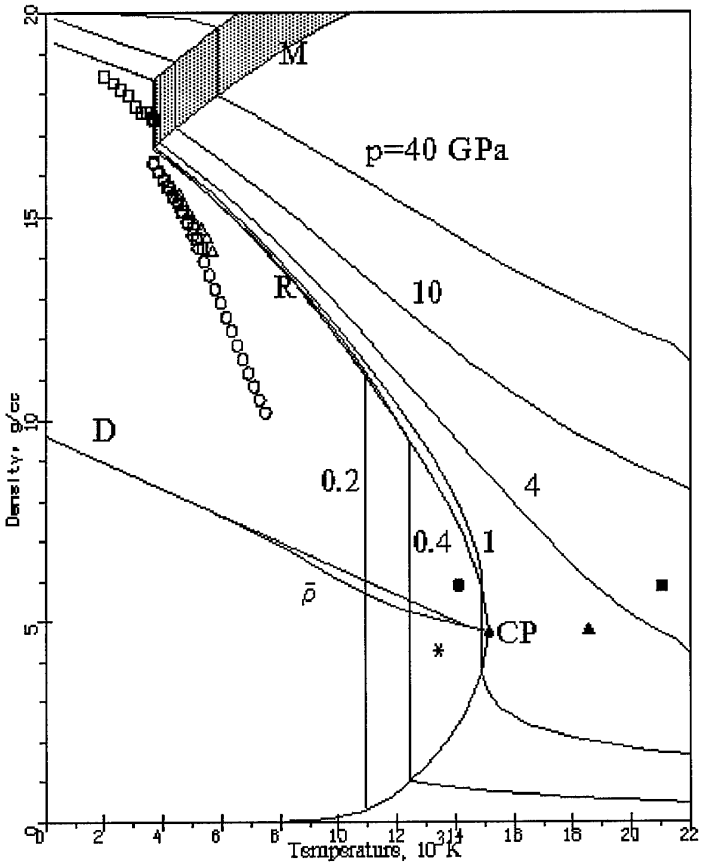

Fig. 15. Phase diagram for tungsten in the region of lower temperatures. P, isobars; M, melting region; R, liquid-vapor equilibrium curve; D, rectilinear diameter; $\bar{\rho}$, half-sum of liquid and vapor densities. Points: isobaric expansion measurements ○ - [52], □ - [53], Δ - [54]; evaluations of the critical-point parameters: Δ - [24], ● - [52], ✶ - [55], ■ - [27], • - this work.

HEDRC REPORT

Printed December 1993

WIDE-RANGE EQUATION OF STATE FOR LARGE COMPUTER CODES

I. V. Lomonosov, V. E. Fortov, and K. V. Khishchenko

Prepared by
High Energy Density Research Center
Russian Academy of Sciences
Izhorskaya Str. 14/19, Moscow 127412, Russia
for USAF
by contract SPC-93-4074

WIDE-RANGE EQUATION OF STATE FOR LARGE COMPUTER CODES

I. V. Lomonosov, V. E. Fortov, and K. V. Khishchenko

High Energy Density Research Center
Russian Academy of Sciences
Izhorskaya Str. 14/19, Moscow 127412, Russia

Abstract

The report is devoted to equation-of-state (EOS) problem. It describes wide-range four-phase (solid, liquid, gas and plasma) semiempirical EOS model. The EOS is given by free-energy thermodynamical potential and is complete in thrmodynamical sense. The EOS model, its structure, procedure of determination EOS coefficients are described. Results of construction EOS for aluminum, copper and lithium are reported. The comparison of thermodynamical properties of these metals calculated by EOS with available high-pressure theoretical and experimental data is given.

1. Introduction

Equation of state is the fundamental characteristic of matter determining its thermodynamic properties over a wide range of the phase diagram. Semiempirical EOS use with great efficiency results obtained by first-principle theories and experimental data. For more details see, for example, review [1] and references therein. Presented in the paper are semiempirical EOS model that was developed to describe metals in solid, liquid and plasma states and results of EOS construction for aluminum, copper, and lithium.

2. EOS Model

A thermodynamically complete temperature EOS is defined by the free energy, F, written as,

$$F(V,T)=F_c(V)+F_a(V,T)+F_e(V,T) \tag{1}$$

describing the elastic contribution at T=0 K (F_c), and the heat contribution by atoms (F_a) and electrons (F_e), respectively.

2.1. Cold Curve

The elastic energy for the solid phase is given in form

$$F_c^{(s)}(V) = 3V_{0c} \sum_{i=1,5} \frac{a_i}{i}\left(\sigma_c^{i/3} - 1\right), \tag{2}$$

(where $\sigma_c = V_{0c} / V$, V_{0c} - specific volume at p=0) providing for conditions $F_c^{(s)}(V_{0c}) = 0$, $p_c(V_{0c}) = 0$, correct tabular values (with heat component) of bulk compression modulus and its pressure derivative at ambient conditions, as well as the accordance with first-principle theories up to 100-fold compressions [2].

The cold energy for the liquid phase in compression region ($\sigma_c \geq 1$) is given by Formula (2), while in the rarefaction region ($\sigma_c < 1$) it is represented by a polynomial of the form

$$F_c^{(l)} = V_{0c}\left[A\left(\frac{\sigma_c^m}{m} - \frac{\sigma_c^n}{n}\right) + B\left(\frac{\sigma_c^l}{l} - \frac{\sigma_c^n}{n}\right)\right] + E_{sub}, \quad (3)$$

which leads to the tabular values [3] of the cohesion energy $E_c(V \to \infty) = E_{sub}$ and satisfies the condition $p_c(V_{0c}) = 0$. The equality of the cold-energy derivatives $p_c = -\frac{dE_c}{dV}, B_c = -\frac{1}{V}\frac{dp_c}{dV}, B_{pc} = \frac{dB_c}{dp}$ at $\sigma_c = 1$ remains in (3) two free parameters, *n* and *l*. They are determined by the experimental temperature dependence of density and sound velocity for liquid metals.

2.2. Thermal Contribution of the Atoms

2.2.1. Solid phase

The lattice contribution to the free energy of the solid phase is defined by the expression

$$F_a^{(s)}(V,T) = 3RT \ln \frac{\theta_c^{(s)}(V)}{T}, \quad (4)$$

where R is the gas constant. The characteristic temperature is given by empirical expression

$$\theta_c^{(s)}(V) = \theta_0^s \sigma^{2/3} \exp\left\{\frac{(\gamma_{0s} - 2/3)\left(B_s^2 + D_s^2\right)}{B_s} \operatorname{arctg}\left[\frac{xB_s}{B_s^2 + D_s(x + D_s)}\right]\right\}, \quad (5)$$

where $x = \ln\sigma$. Constants B_s and D_s are determined by the experimental dependence of Gruneisen gamma $\gamma = \frac{d\ln\theta}{d\ln\sigma}$ on compression σ. This dependence

is obtained on the base of shock-wave data. The value of γ_{0s} corresponds to tabular one of Gruneisen gamma at ambient conditions [3]. Note that at high compressions Eq. (5) provides for the correct ideal-gas asymptote $\cong \sigma^{2/3}$. The value of θ_0^s is given by condition $s(V_0)=0$.

2.2.2. Liquid phase

The atomic contribution to the free energy of the liquid phase is represented as a sum

$$F_a^{(l)}(V,T) = F_t(V,T) + F_m(V,T), \tag{6}$$

the first term accounts for anharmonicity effects and the second provides for a proper behavior of melting curve.

In the liquid phase the phonon contribution has a form similar to Eq. (4) but with a volume- and temperature-dependent heat capacity c_a and a characteristic temperature $\theta^{(l)}$

$$F_t^{(l)}(V,T) = c_a(V,T)T\ln\frac{\theta^{(l)}(V,T)}{T}. \tag{7}$$

The heat capacity in the liquid phase is given by the expression

$$c_a(V,T) = \frac{3R}{2}\left[1+\frac{\sigma T_a}{(\sigma+\sigma_a)(T+T_a)}\right], \tag{8}$$

describing a smooth variation from the value 3R close to the lattice heat capacity to that one of an ideal atomic gas, 3R/2. Coefficients σ_a and T_a define the characteristic density and temperature of this transition.

The vibrational spectrum defined by the variation of the characteristic temperature reflects the gradual change of the Gruneisen coefficientof the liquid phase from values $\gamma^{(l)} \approx \gamma^{(s)}$ corresponding to condensed states to the ideal-gas value of 2/3 in the limit of high temperatures and very low densities. Under these assumptions, the characteristic temperature is given by the approximating formula

$$\theta^{(l)}(V,T) = T_{sa}\frac{\left(T_{ca}\theta_c^{(l)} + T\right)\sigma_c^{2/3}}{T_{ca} + T}, \qquad (9)$$

where characteristic temperature is liquid phase is presented in form analogoqus to Eq. (5)

$$\theta_c^{(l)}(V) = \theta_0^1 \exp\left\{\frac{(\gamma_{01} - 2/3)\left(B_l^2 + D_l^2\right)}{B_l}\operatorname{arctg}\left[\frac{xB_l}{B_l^2 + D_l(x + D_l)}\right]\right\}. \qquad (10)$$

The parameters in Eq. (10) B_l and D_l are found from shock-wave experimentson solid and porous samples, the constant θ_0^1 is determined by equation $\theta_a(0) = T_{ca}$.

The potential term $F_m(V,T)$ provides for a correct value of the entropy $\Delta s = \Delta s_{m0}$ and volume $\Delta V = \Delta V_{m0}$ changes on melting at ambient pressure and disappears in the gas phase. The contribution of F_m should also decrease upom compression due to decresing differences between the properties of the solid and liquid phases. These requirements are satisfied by the relation

$$F_m(V,T) = 3R\left\{\frac{2\sigma_m^2 T_{m0}}{1+\sigma_m^3}\left[C_m + \frac{2A_m}{5}\left(\sigma_m^{5/3} - 1\right)\right] + (B_m - C_m)T\right\}, \qquad (11)$$

where $\sigma_m = \sigma / \sigma_{m0}$ is the relative density of the liquid phase on the melting curve. The constants A_m, B_m, C_m are uniquely determined by the equilibrium conditions along the melting curve at $T = T_m$.

2.3. Electron Contribution

The thermal electrons contribution has the same form for solid and liquid phases. It is given by following relationship

$$F_e(V,T) = -c_e(V,T)T \times \ln\left[1 + \frac{B_e(T)T}{2c_{ei}}\exp(-\gamma_e(V,T))\right] \quad (12)$$

This formula contains generalized analog of the coefficient of electron heat capacity B

$$B_e(T) = \frac{2}{T^2}\int\left(\int_0^T \beta(\tau)d\tau\right)dT, \quad (13)$$

$$c_{ei} = \frac{3RZ}{2}, \quad (14)$$

the heat capacity of the electron gas

$$c_{ei}(V,T) = \frac{3R}{2}\left[Z + \frac{\sigma_z T_z^2(1-Z)}{(\sigma+\sigma_z)\left(T^2+T_z^2\right)}\right]\exp\left[-\frac{\tau_i}{T}\right], \quad (15)$$

the analogs of the electronic Gruneisen coefficient

$$\gamma_e(V,T) = \gamma_{ei} + \left(\gamma_{e0} - \gamma_{ei} + \gamma_m\frac{T}{T_g}\right)\exp\left[-\frac{T}{T_g} - \frac{(\sigma-\sigma_e)^2}{\sigma\sigma_d}\right], \quad (16)$$

and of the coefficient of the electronic heat capacity

$$\beta(T) = \beta_i + \left(\beta_0 - \beta_i + \beta_m\frac{T}{T_b}\right)\exp\left[-\frac{T}{T_b}\right]. \quad (17)$$

Approximating dependences are selected such to satisfy primarily the asymptotic relations for the electron gas free energy, namely expressions for degenerate electron gas at moderate ($T<<T_{Fermi}$) temperatures

$$F_e(V,T) = -\frac{\beta_0 T^2}{2}\sigma^{-\gamma_0},$$

and expressions for an ideal electron gas at $T \to \infty$ range

$$F_e(V,T) = \frac{3RZ}{2}\ln\left(\sigma^{2/3}T\right).$$

Here Z is the atomic number and R is the gas constant. The specific form of writing down separate expressions of the potential (12) depends upon the satisfaction of these requirements.

The Eqs. (12)-(17) are written in a form which represents correctly the primary ionization effects in the plasma region and the behaviour of the partially ionized metal. The expression $\tau_i = T_i \exp(-\sigma_i / \sigma)$ describes a decrease of the ionization potential as the plasma density increases, and the constants σ_z and T_z define, respectively, the characteristic density of the 'metal-insulator' transition and the temperature dependence of the transition from a singly ionized gas to a plasma with the ion-charge mean value Z.

3. Procedure for constructing EOS

The set of equations (1)-(17) fully assigns the thermodynamic potential for metals over entire phase diagram region of practical interest. Some coefficients in the equation of state, included in the analytical expressions, are constants characteristic for each metal and are found from tabular data, while the rest serve as fitting parameters and their values are found from the optimum description fo the available experimental and theoretical data. It should be emphasized that, even though the number of coefficients in Eqs. (1)-(17) is large, most of them are rigidly defined constants whose values are assigned explicitly or implicitly from the fulfilment of various thermodynamic conditions at specific points on the phase diagram. A few coefficients (about ten) serve to characterize the densities and temperatures on transition from one typical phase-plane region to another and are found empirically.

In determining the numerical values of coefficients in the EOS, use was made of the numerous experimental and theoretical data characterizing the thermodynamic properties of metals under study for a wide range of parameters.

This procedure was carried out with the aid of a specially developed computer program using the Eqs. (1)-(17) for thermodynamic calculations. At the preliminary satge of calculations, some thermodynamic constants known for each substance (such as normal density; changes in density and entropy at the melting point under normal pressure; cohesion energy; and the like) were used by the program automatically find a number of other uniquely defined coefficients (parameters of the cold curve, melting curve, and so on).

This further enables one, by way of calculating algebraic or integral relations valid for self-simular hydrodynamic flows to perform calculations of kinematic characteristics measured experimentally at high and ultrahigh pressures, namely, the incident and reflected wave velocities and velocities in adiabatic expansion waves (release isentropes), as well as to allow for melting and evaporation effects in the results obtained. The range of action of each fitting coefficient that remains free is very localized, as a result of which its value may be selected independently from a comparioson of the calculations with available experimental data.

4. Thermodynamic properties of metals

The performance of specific hydrodynamic calculations calls for the assignment of thermodynamic characteristics of metals over a large area of thre phase diagram with correct asymptotic behavior in the high-temperature/high-pressure limit. This part of the report deals with the description of the thermodynamics of aluminum, copper and lithium over a wide range of pressures and temperatures, based on the above-discussed semiempirical EOS.

The most significant experiments for constructing EOS are described for each metals investigated; experimental data are compared with calculations. Also presented are new results obtained by calculations of regions for which no experimental data are presently available and for which theoretical models only yield general estimations. This applies primarily to the position of the high-temperature evaporation curve and of the critical point, which are important for the calculation of most high-energy processes. No less essential is a correct thermodynamic description of the metallic liquid and dense plasma, as well as the

shape of the melting curves with respect to which only isolated, often thermodynamically incomplete experimental data are available. Finally, the most important result obtained would appear to be the consistent description, within a unified EOS, of numerous diverse experimental data, many of which are not directly related to the EOS but reflect rather the integral or differential thermodynamic characteristics of substances.

4.1. Aluminum

Aluminum and its alloys are used extensively as basic structural materials of experimental end production facilities operating under conditions of intensive pulsed-energy release. In addition, aluminum serves as a standard material for investigations in the high-pressure region and, consequently, the equation of state for this metal needs to be especially exact and reliable.

In the case of aluminum in the region of low pressures and relatively low temperatures ($T<2500$ K), numerous steady-state thermophysical data are available including the results of measuring the density, heat capacity and velocity of sound for the solid and liquid phases, and of determining the shape of the melting curve. Without dwelling on details, we shall note that all of these characteristics are described by the equation of state obtained to an accuracy of 1-3% or better, as illustrated by Fig. 1 which presents a comparison of the theoretical and experimental data on the pressure dependence of temperature on the melting curve.

The reliability of the equation of state for aluminum in the region of high pressures and reduced (relative to the standard shock adiabat) temperatures is illustrated by Fig. 2 which presents calculations and experimental data on double-shock compression of samples [6,7]. The characteristics of increased (as compared with the principal shock adiabat) temperatures are found from experiments in shock compression of samples with different initial porosities. Shown in Fig. 3 is a comparison of data from such experiments with theoretical data obtained from the semiempirical equation of state. Also plotted in this figure are experimental [8] and theoretical data on isentropic expansion of shock-compressed porous samples. In spite of the heterogeneous nature of source experimental data obtained by independent researchers and assigned usually as the simplest approximations, all

the data could effectively be combined and described within a unified wide-range equation of state. In addition to the shock adiabats for porous samples, the point of intersection of the melting curve and the adiabat with m=1.69, which coincided with the experimentally registered point, has also been determined for aluminum in the region of moderate pressures; this was registered by a sharp velocity decrease in the isentropic release wave following the disappearance of the transverse component of the velocity of sound upon melting [11].

The phase diagram for aluminum is shown in Fig. 4 in which are plotted the experimental points for shock compression of solid and porous samples in the high-pressure region, and calculated shock adiabats for different porosities and isotherms; the melting and evaporation regions are also mapped out. As follows from this figure, the traditional region of shock-wave studies restricted to a pressure of ca. 5 Mbar is described to a high accuracy by the equation of state obtained. An adequate description of experiments is observed both in the case of velocity-of-sound measurements in shock compressed samples (Fig. 4a). A good theoretical description is available for the experimentally obtained dependence of the Gruneisen coefficient upon volume on the shock adiabat [7].

According to calculations, the melting region on the shock adiabat of aluminum corresponds to pressures of 1.13 to 1.84 Mbar. The lower limit is in excellent agreement with the experimentally obtained value for the onset of melting, p>1 Mbar, found from measurements of the viscosity behind the shock front [18].

Special attention was given to the problem of correct description of the few experimental data in the region of ultrahigh pressures which play a decisive role in the construction of semiempirical equations of state for the high-energy range of parameters. In the case of aluminum, the situation is aggravated by the fact that band-theory calculations [19] at a pressure of p=2 Mbar led to the prediction of an electron phase transition which had earlier appeared to have some experimental support [20]. In view of this, a shock adiabat allowing for this transition [21] was employed in calculations in the region of ultrahigh pressures. New experimental data which made their appearance in recent years [14,22-24] failed, however, to point to any anomalies that could be attributed to the effects of rearrangement of the electronic structure. Fig. 5 presents a comparison of the available experimental points with calculations from various equations of state. It

can be seen from the figure that, as distinct from the Thomas-Fermi model with corrections [25], the semiempirical equation of state obtained by the present authors makes it possible to accurately reproduce the entire set of data on absolute measurements of compressibility at high and ultrahigh pressures. It is worthy of note that the results obtained turned out to be close to recent theoretical calculations from modified Hartree-Fock-Slater models [26,27] which also fail to show any phase transition.

The characteristics of the dense highly heated liquid phase of aluminum and the parameters of the liquid-vapor equilibrium line have not been investigated since the high temperatures required considerably exceed the heat resistance limits of stationary facilities. Apart from the evaporation-temperature data at standard pressure, information on the critical parameters is only available in the form of semiempirical evaluations [30-33]. Plotted in Fig. 6 for aluminum are the calculated values of the temperature dependence of density on the isobars and on the liquid-vapor equilibrium line. Also shown in the drawing is the deviation of the calculated temperature dependence of the half-sum of liquid and vapor densities from the law of rectilinear diameter. Calculations have yielded the exact experimental value of the evaporation temperature, T =2772 K, and the critical-point parameters, p_c=5.71 kbar, T_c=7222 K, V_c=1.24 cc/g and s_c=4.66 J/g·K, which are in good agreement with current evaluations, also plotted in the figure. Practically coinciding with the experimental data are the calculated temperature dependencies of density and velocity of sound in the liquid phase.

The foregoing drawings fully cover the experimental information on the thermodynamic properties of aluminum in the region of high pressures and temperatures. It is evident that the entire set of experimental data is described to a high accuracy by the equation of state obtained. The equation of state further provides an accurate description of primary ionization and displays the requisite asymptotic behavior in the limit of high temperatures and large volumes. As a result, the equation of state obtained can be used efficiently in hydrodynamic calculations under conditions of intensive energy release.

4.2. Copper

Like aluminum, copper finds extensive application as a structural material and, consequently, the thermodynamic properties of this metal must be calculated reliably. In order to avoid a repetition of the contents of the preceding section will only contain (as following sections on lead and lithium) a summary of the principal results accompanied by a minimum comment.

The data in the region of moderate pressures and temperatures obtained for copper from stationary thermophysical experiments have, analogously to the case of aluminum, an accuracy of description of the order of 1% or more. The most accurate data determining the course of the melting curve [4] are presented in Fig. 1, together with the results of calculation which practically coincide with experiment.

The thermodynamical properties for a wide region of the phase diagram at moderate pressures ($p<1$ Mbar) are determined from numerous shock-compression experiments on porous samples. Figure 7 shows a complete set of those data with the corresponding calculated shock adiabats. This figure suggests that the calculated curves agree with experiment over a wide range of porosity values, overlapping the area of the phase diagram from the principal shock adiabat to volumes of $V<1.2V_0$.

A large area of the phase plane of copper ranging from states on the shock adiabats to the near-critical region of parameters was studied using the isentropic expansion method [36]. This method involves a continuous study of a pressure range of four orders of magnitude and a density range of two orders of magnitude, i.e., from a highly compressed metallic liquid to a quasi-nonideal Boltzmann plasma and metallic vapor. Plotted in Fig. 8 are metastable and equilibrium isentropes of expansion and shock adiabats calculated for different porosities. A comparison of the calculated isentropes with the experimental data shows that, at an above-critical pressure, the maximum divergence in the expansion rate is about 3% which is just within the experimental error. Upon entry into the two-phase region, an increasing deviation of the calculated curves from the experimental results is observed which is probably due to a nonuniform energy distribution in the heated metal particles. Note should be made, however, of the correspondence

between kinks in the calculated curves at the onset of evaporation and the experimentally observed additional increase of the expansion rate within the two-phase liquid-vapor region.

The phase diagram for copper shown in Fig. 9 presents a consistent description of shock-wave data in a pressure range of hundreds of kilobars to tens of megabars. The semiempirical equation of state obtained for copper further describes, with similar accuracy, experimental measurements of the velocity of sound on the shock adiabat (Fig. 9a).

Of special interest are the experiments in shock compression of highly porous copper in the 10-20-Mbar pressure range [37]. As distinct from the case of compression of solid samples, the attendant states correspond to a weakly generate electron gas with extremely high heat energy-density of about $3*10^3$ kJ/cc. Corresponding to such conditions in the TFC model [39], which is widely used for describing this region of parameters, are the characteristic values of the Gruneisen coefficient of about 0.45 which lead to high compression ratios upon shock-loading (shown by the dashed line in Fig. 9). This result is clearly in conflict with the experimental results of Ref. [37] and points to the inapplicability of TFC-based calculations in the region in question. As distinct from this model, the equation of state developed describes correctly all the data on shock compression at ultrahigh pressures [37,40].

The adequacy of calculations on the shape of the melting curve for copper in the high-pressure region can be verified by experiments on the residual temperature in the isentropic release wave (Fig. 9b). According to the calculations, the melting region on the shock adiabat corresponds to the 1.9-2.7-Mbar range; the values of temperatures in the release wave are in good agreement with experiment. Calculations in which melting is ignored yield, as can be seen from Fig. 9b, residual temperature values over estimated by 500 K.

The liquid-phase parameters and the position of the evaporation curve for copper have been determined quite reliably by experiments on the isentropic expansion [36]. In constructing an equation of state, the expansion isentropes serve as a closing link in that they link together the parameters of the equilibrium curve upon entry into the two-phase liquid-vapor region.

The coefficients of the equation of state for copper obtained from the above-mentioned experiments in isentropic expansion made possible highly reliable and complete calculations of the characteristics of the highly heated liquid and dense plasma.

Presented in Fig. 10 are the results of calculating the isobars and the equilibrium curve; also plotted are estimated values of the critical-point parameters obtained from methods of thermodynamic similarity. The calculated value of the evaporation temperature, T_c =2841 K, practically coincides with the experimental value, with critical-point parameters equal to, p_c=9.04 kbar, T_c=7830 K, V_c=0.44 cc/g and s_c=1.97 J/gK which, as can be seen from the figure, are close to most estimates.

All of the figures in this section are indicative of the adequate and self-consistent description of the available set of experimental data over the entire phase plane. Consequently, the results obtained may be used widely in calculations of the thermodynamic characteristics of copper when solving applied problems.

4.3. Lithium

The extensive utilization of lithium as the working medium of many modern power-generating plants adds to the importance of reliable temperature range covering the entire spectrum of working states. For lithium, with its relatively low melting and evaporation temperatures, many highly experiment data are available in the traditional region of stationary thermophysical experiment. The bulk of those data, covering relatively low static pressures and temperatures of T<2000 K, were treated simultaneously in a monograph [44] containing detailed tables of thermodynamic properties of lithium in this range of parameters. In the region of high temperatures and pressures, however, the available data from static and dynamic experimental measurements are very limited and often thermodynamically incomplete, which prevents one from employing a statistical treatment of the data for the interest in constructing an equation of state. These facts account for the interest in constructing a semiempirical equation of state for lithium from a small number of precise experimental data in the high-pressure and high-temperature region.

A comparison of the calculations with temperature and volume measurement data on the melting curve is given in Fig. 11. As distinct from the melting curves for aluminum, copper and lead which are monotonic (cf. Fig. 1), Figure 11a reveals the presence for lithium of a temperature maximum at $p \approx 90$ kbar. This points to a phase transition to a more close-packed structure in the high-pressure region, the completion of this phase transition leading to the restoration of the normal shape of the melting curve. The results of calculations and of precision experimental measurements of the density of the solid and liquid phases along the melting curve presented in Fig. 11b demonstrate that the theory fully describes this high-accuracy ($\Delta V/V \approx 0.01\%$) experiment.

Figure 12 shows the phase diagram of lithium on which are plotted experimental data on the compressibility of lithium upon dynamic loading to pressures of 700 kbar and temperatures of about 8000 K, and the calculated shock adiabat, isotherms and solid-liquid and liquid-vapor phase equilibrium curves.

The liquid-phase region of lithium has been studied best of all at high temperatures in static experiments. Figure 12a shows a comparison of the calculated and experimental data on the velocity of sound in liquid lithium against the evaporation temperature, and Fig. 13 presents experimental data on the liquid density up to T=2000 K. The calculations of the liquid-vapor phase equilibrium curve yielded an accurate value of the evaporation temperature, T_c=1612 K, and critical-point parameters, p_c=954 bar, T_c=3940 K, V_c=10.3 cc/g, s_c=12.9 J/gK, which are in good agreement with estimates made on the basis of principles of thermodynamic similarity. This is indicative of the high degree of reliability of the equation of state obtained for lithium in the region of the liquid phase and near-critical states which is important from the standpoint of practical applications.

Conclusion

As revealed by the report wide-range EOS for aluminum, copper and lithium have been developed on the base of semiempirical model and available high pressure data. These EOS are suitable for a continuous (global) description of the thermodynamic properties of selected metals in solid, liquid and plasma states as well as in solid-liquid and liquid-vapor two-phase regions.

References

[1] A. V. Bushman and V. E. Fortov, Sov. Phys. Usp., 26, 465 (1983).

[2] *Equations of State for Metals at High Energy Densities,* A. V. Bushman, I. V. Lomonosov, V. E. Fortov, Chernogolovka: Institute of Chemical Physics RAS, 1992, 196 pp. [in Russian].

[3] M. W. Guinan, D. J. Steinberg, J. Phys. Chem. Solids, 35, 1501 (1974).

[4] J. Lees, B. H. Williamson, Nature, 208, 278 (1965).

[5] P. W. Mirwald, G. C. Kennedy, J. Geophys. Res. Ser. B, 84, 6750 (1979).

[6] L. V. Al'tshuler, A. P. Petrunin, Sov. Phys. - Tech. Phys., 6, 516 (1961).

[7] T. Neal, Phys. Rev. Ser. B, 14, 5172 (1976).

[8] J. R. Asay, J. Appl. Phys., 46, 197 (1975).

[9] R. G. McQueen, S. P. Marsh, J. W. Taylor, J. N. Fritz, W. J. Carter, - In: High Velocity Impact Phenomena (1970)/ Ed. R.Kinslow. - New-York: Academic Press, p.293-417; appendies on pp. 515-568.

[10] A. A. Bakanova, I. P. Dudoladov, Yu. N. Sutulov, Zh. Prikl. Mekh. Tekhn. Fiz. 2, 117 (1974) [in Russian] (J. Appl. Mech. Techn. Phys. 15, 241 (1974)).

[11] J. R. Asay, D. B. Hayes, J. Appl. Phys., 46, 4789 (1975).

[12] L. V. Al'tshuler, A. A. Bakanova, R. F. Trunin, Zh. Eksp. Teor. Fiz. 42, 91-104 (1962) [in Russian] (Sov. Phys. - JETP 15, 65-74 (1962)).

[13] L. V. Al'tshuler, B. S. Chekin, Metrology of high pulse pressures, In: Proceed. 1-st All-Union symposium of pulse pressures, Moscow: VNIIFTRI, V. 1, 5 (1974) [in Russian].

[14] A. C Mitchell, W. J. Nellis, J. Appl. Phys., 52, 3363 (1981).

[15] S. B. Kormer, A. I. Funtikov, V. D. Ulrin, A. N. Kolesnikova, Zh. Eksp. Teor. Fiz. 42, 686-701 (1962) [in Russian] (Sov. Phys. - JETP 15, 477-478 (1962)).

[16] L. V. Al'tshuler, S. B. Kormer, M. I. Brazhnik, L. A. Vladimirov, M. P. Speranskaya, A. I. Funtikov, Zh. Eksp. Teor. Fiz. 38(4), 1061-1073 (1960) [in Russian] (Sov. Phys. - JETP 11(4), 766-775 (1960)).

[17] T. Neal, J. Appl. Phys., 46, 2521 (1975).

[18] A. D. Sakharov, R. M. Zaidel', V. N. Mineev, A. G. Oleinik, Dokl. Akad. Nauk SSSR, 159, 1019 (1965).

[19] G. M. Gandel'man, Zh. Eksp. Teor. Fiz., 51, 147 (1966) [in Russian] (Sov. Phys. JETP 24, 99 (1967)).

[20] L. V. Al'tshuler, A. A. Bakanova, Usp. Fiz. Nauk, 96, 163 (1968) [in Russian] (Sov. Phys. - Usp., 11, 678 (1969)).

[21] R. F. Trunin, G. V. Simakov, M. A. Podurets, B. N. Moiseev, L. V. Popov, Izv. Akad. Nauk SSSR, Ser. Fizika Zemli, 1, 13 (1971) [in Russian] (Bull. Acad. Sci. USSR, Phys. Solid Earth, 1, 8 (1971)).

[22] B. L. Glushak, A. P. Zharkov, M. V. Zhernokletov, V. Ya. Ternovoi, A. S. Filimonov, V. E. Fortov, Sov. Phys. - JETP, 69, 739 (1989).

[23] C. E. Ragan C.E. Phys. Rev. Ser. A, 25, 3360 (1982).

[24] C. E. Ragan C.E. Phys. Rev. Ser. A, 29, 1391-1402 (1984).

[25] L. V. Al'tshuler, N. N. Kalitkin, L. V. Kuz'mina, B. S. Chekin, Zh. Eksp. Teor. Fiz. 72(1), 317-325 (1977) [in Russian] (Sov. Phys. - JETP 45(1), 167-171 (1977)).

[26] G. V. Sin'ko, Teprofiz. Vis. Temp., 21, 1041 (1983).

[27] A. F. Nikiforov, V. G. Novikov, V. B. Uvarov, Dokl. Akad. Nauk SSSR, 267, 615 (1982) [in Russian] (Sov. Phys. - Dokl. 27).

[28] S. B. Kormer, A. I. Funtikov, V. D. Ulrin, A. N. Kolesnikova, Zh. Eksp. Teor. Fiz. 42, 686-701 (1962) [in Russian] (Sov. Phys. - JETP 15, 477-478 (1962)).

[29] V. A. Simonenko, N. P. Voloshin, A. S. Vladimirov, A. P. Nagibin, V. N. Nogin, V. A. Popov, V. A. Sal'nikov, Yu. A. Shoidin, Sov. Phys. - JETP, 61, 869 (1985).

[30] V. E. Fortov, A. N. Dremin, A. A. Leont'ev, Teplofiz. Visok. Temper., 13, 1072 (1975) [in Russian].

[31] D. A. Young, B. A. Alder, Phys. Rev. Ser. A, 3, 1439 (1971).

[32] D. A. Young, Report UCRL-52352, Univ. of California, Livermore (1977).

[33] E. Morris, AWRE Report 067/64, UKAEA, London (1964).

[34] E. I. Gol'tsova, Teplofiz. Visok. Temper., 3, 483 (1965) [in Russian].

[35] R. R. Boade, J. Appl. Phys., 39, 5693-5702 (1968).

[36] L. V. Al'tshuler, A. V. Bushman, M. V. Zhernokletov, V. N. Zubarev, A. A. Leont'ev, V. E. Fortov, Zh. Eksp. Teor. Fiz. 78, 741-760 (1980) [in Russian] (Sov. Phys. - JETP 51(2), 373-383 (1980)).

[37] R. F. Trunin, A. B. Medvedev, A. I. Funtikov, M. A. Podurets, G. V. Simakov, A. G. Sevast'yanov, Zh. Eksp. Teor. Fiz. 95, 631-641 (1989) [in Russian] (Sov. Phys. - JETP 68(2), 356-361 (1989)).

[38] Ph. de Beaumont, J. Leygonie, In: Fifth Symp. on Detonation. - Washington: U.S.Government Printing Office, 430-439 (1970).

[39] N. N. Kalitkin, L. V. Kuz'mina, Preprint No. 35, Inst. of Applied Mathem. of USSR Acad. Sci., Moscow (1975) [in Russian].

[40] R. F. Trunin, M. A. Podurets, G. V. Simakov, L. V. Popov, B. N. Moiseev, Zh. Eksp. Teor. Fiz., 62(3), 1043-1048 (1972) [in Russian] (Sov. Phys. - JETP 35(3), 550-552 (1972)).

[41] L. V. Al'tshuler, A. A. Bakanova, A. V. Bushman, I. P. Dudoladov, V. N. Zubarev, Zh. Eksp. Teor. Fiz., 73(11), 1866-1872 (1977) [in Russian] (Sov. Phys. - JETP 46(5), 980-983 (1977)).

[42] A. D. Kirshenbaum, J. A. Cahill, A. V. Grosse, J. Inorg. Nucl. Chem., 22, 33 (1961).

[43] E. E. Spil'rain, K. A. Yakimovich, E. E. Totoskii, D. L. Timrot, V. A. Fomin, *Teplofizicheskie svoistva shelochikh metallov (Thermphysical Properties of Alkali Metals),* ed. by V. A. Kirillin, Moscow: Izdatel'stvo Standartov, 1970 [in Russian].

[44] H. D. Luedemann, G. C. Kennedy, J. Geophys. Res., 73, 2795 (1968).

[45] I. N. Makarenko, A. M. Nikolaenko, S. M. Stishov, Zh. Eksp. Teor. Fiz., 74, 2175 (1978) [in Russian] (Sov. Phys. - JETP, 47, 1132 (1978)).

[46] A. A. Bakanova, I. P. Dudoladov, R. F. Trunin, Fizika Tverd. Tela, 7(6), 1615-1622 (1965) [in Russian] (Sov. Phys. - Solid State, 7, 1307 (1965)).

[47] *LASL Shock Hugoniot Data* / Ed. S.P.Marsh. - Berkeley: Univ. of California Press, 1980.

[48] I. I. Novikov, Yu. S. Trelin, T. A. Tsyganova, Teplofiz. Visok. Temper., 7, 1220 (1969).

[49] E. I. Gol'tsova, Teplofiz. Visok. Temper., 4, 360 (1966).

[50] V. V. Gogoleva, L. R. Fokin, Preprint No. IVTAN 1-061, Moscow: IVT AN SSSR, 1981 [in Russian] (Report Inst. of High Temper., USSR Acad. Sci.).

Appendix: Pictures to Report

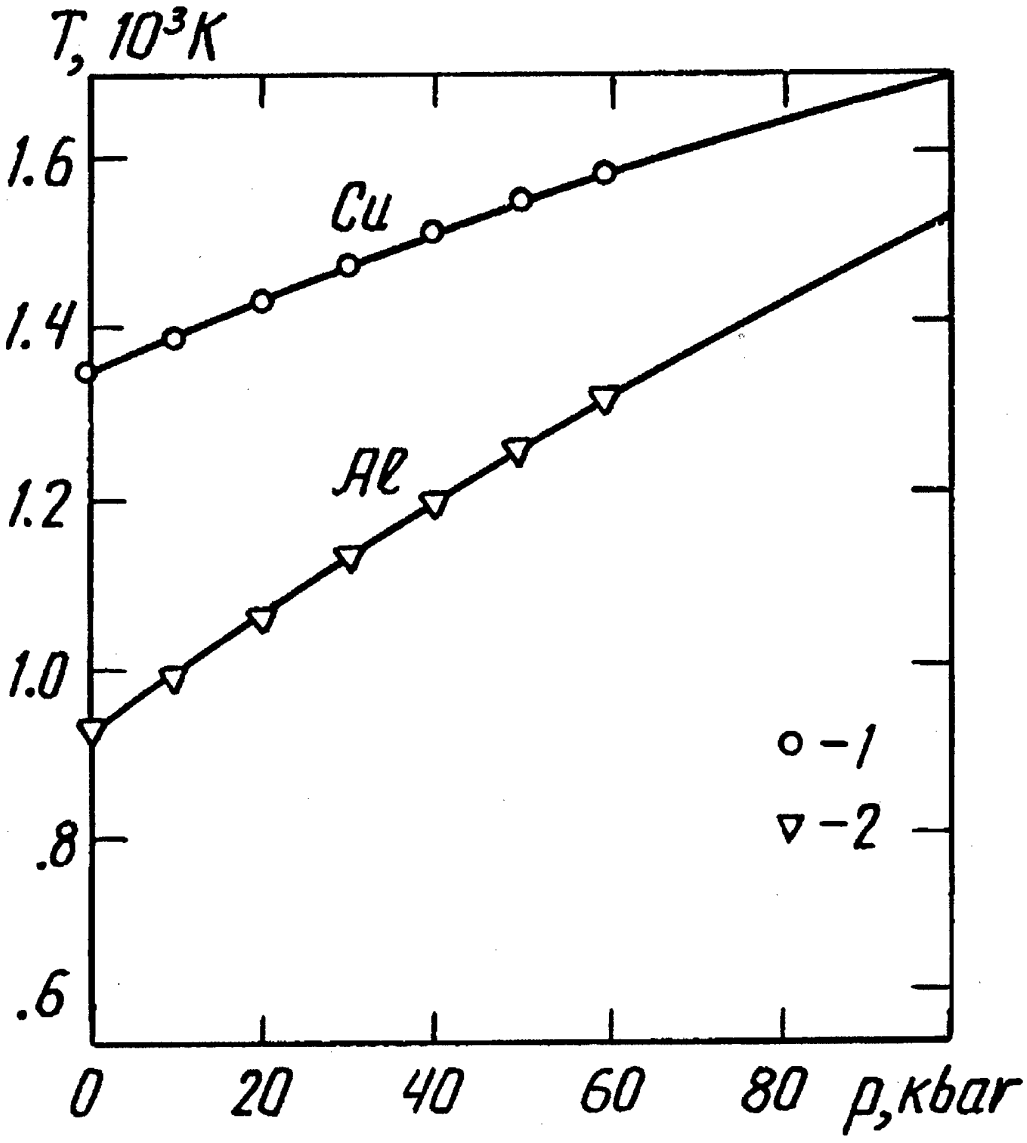

Fig. 1. Melting curves for aluminum and copper. Experimental data: 1 - [4], 2- [5].

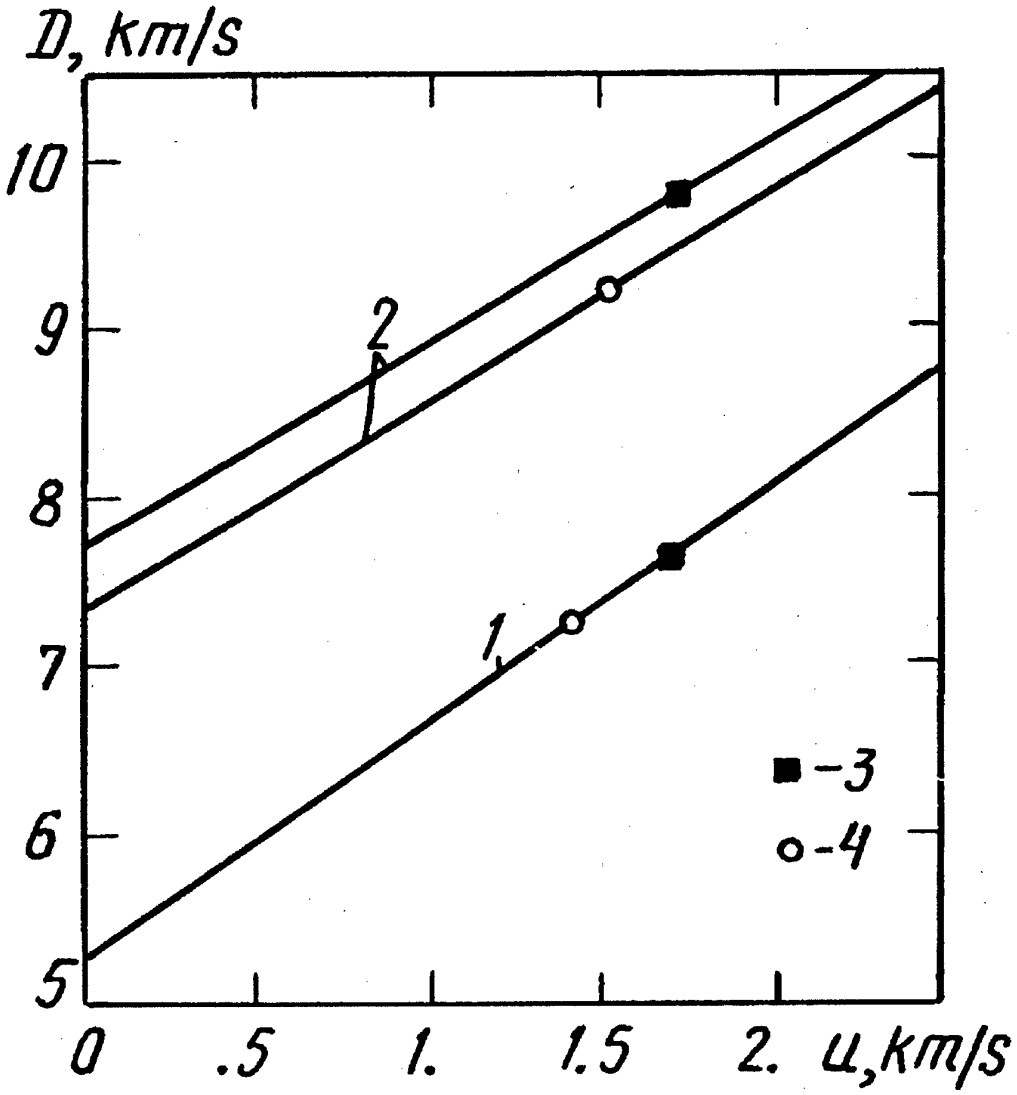

Fig. 2. Velocity of incident shock wave (1) and reflected shock waves (2) in aluminum. Experimental data: 3 - [6], 4 - [7].

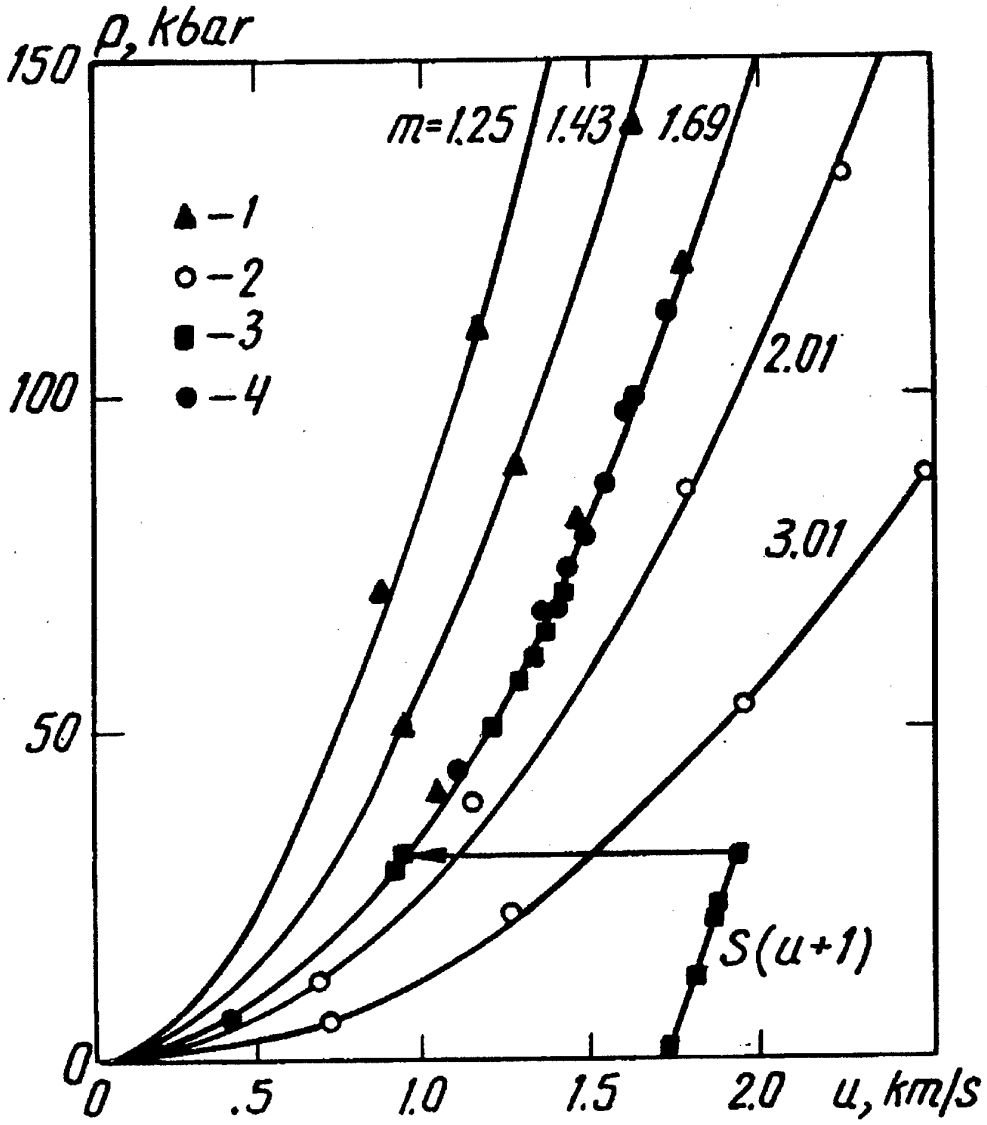

Fig. 3. Porous Hugoniots (m) and release isentrope (S) for aluminum. Experimental data: 1 - [9], 2 - [10], 3 - [8], 4 - [11].

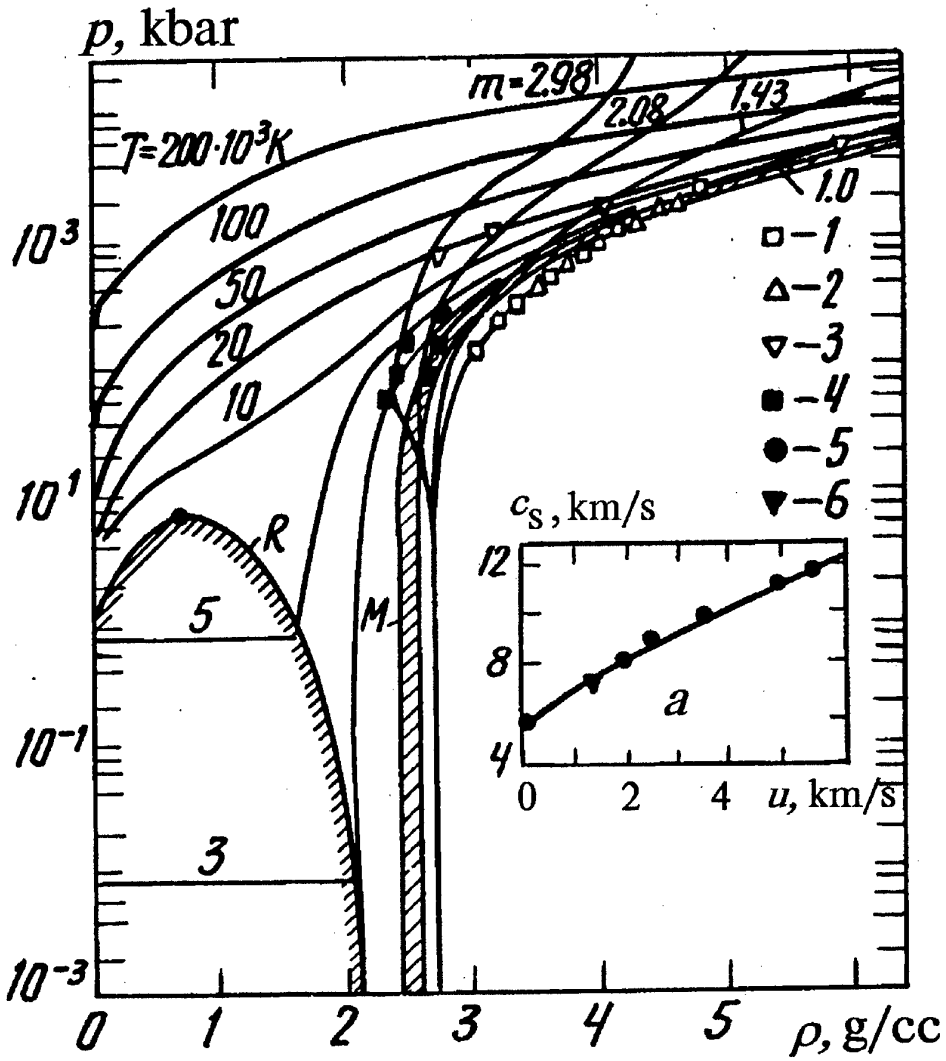

Fig. 4. Phase diagram for aluminum. T, isotherms; m, porous Hugoniots; M, melting region; R, liquid-vapor equilibrium curve. (a) The sound velocity in shocked aluminum. Experimental data: 1 - [12,13], 2 - [14], 3 - [15], 4 - [10], 5 - [16], 6 - [17].

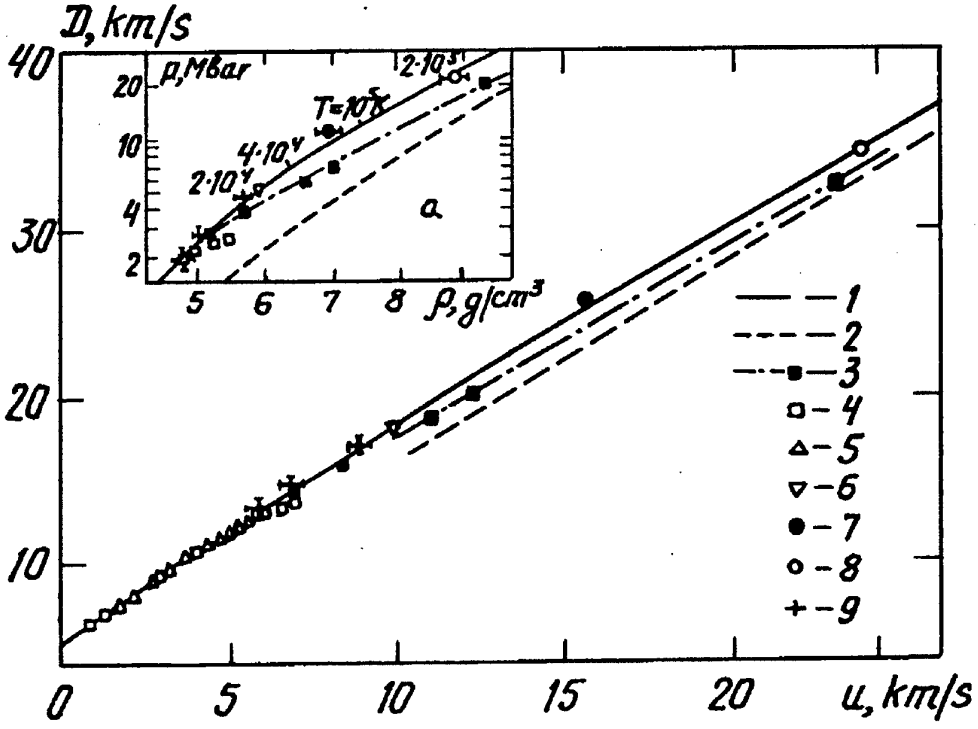

Fig. 5. Shock adiabat for aluminum at ultrahigh pressures. Calculations: 1 - this EOS, 2 - from Thomas - Fermi model with corrections [25], 3 - interpretation of nuclear-explosion data with quartzite standard, calculated by Thomas - Fermi model [25]. Experimental data: 4 - [12,13], 5 - [14], 6 - [28], 7 - [29], 8 - [23], 9 - [22].

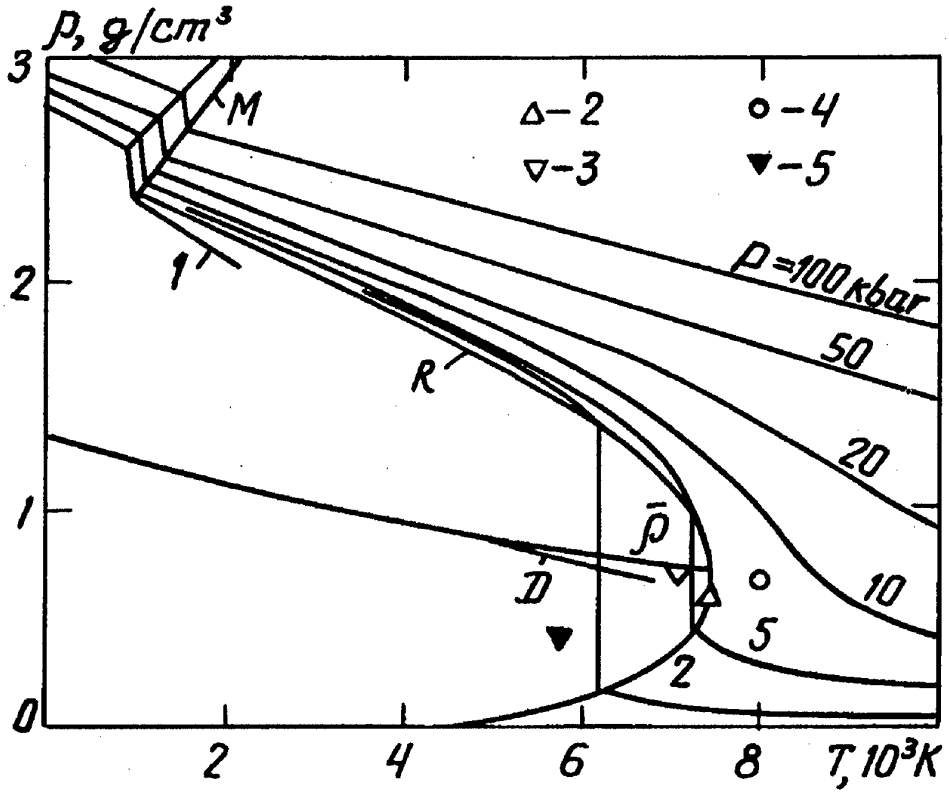

Fig. 6. Phase diagram for aluminum in the region of lower temperatures. P, isobars; M, melting region; R, liquid-vapor equilibrium curve; D, rectilinear diameter; $\bar{\rho}$, half-sum of liquid and vapor densities. 1 - data from measuring the liquid-metal density at p=1 bar [34]; evaluations of the critical-point parameters: 2 - [33], 3 - [31], 4 - [30], 5 - [32].

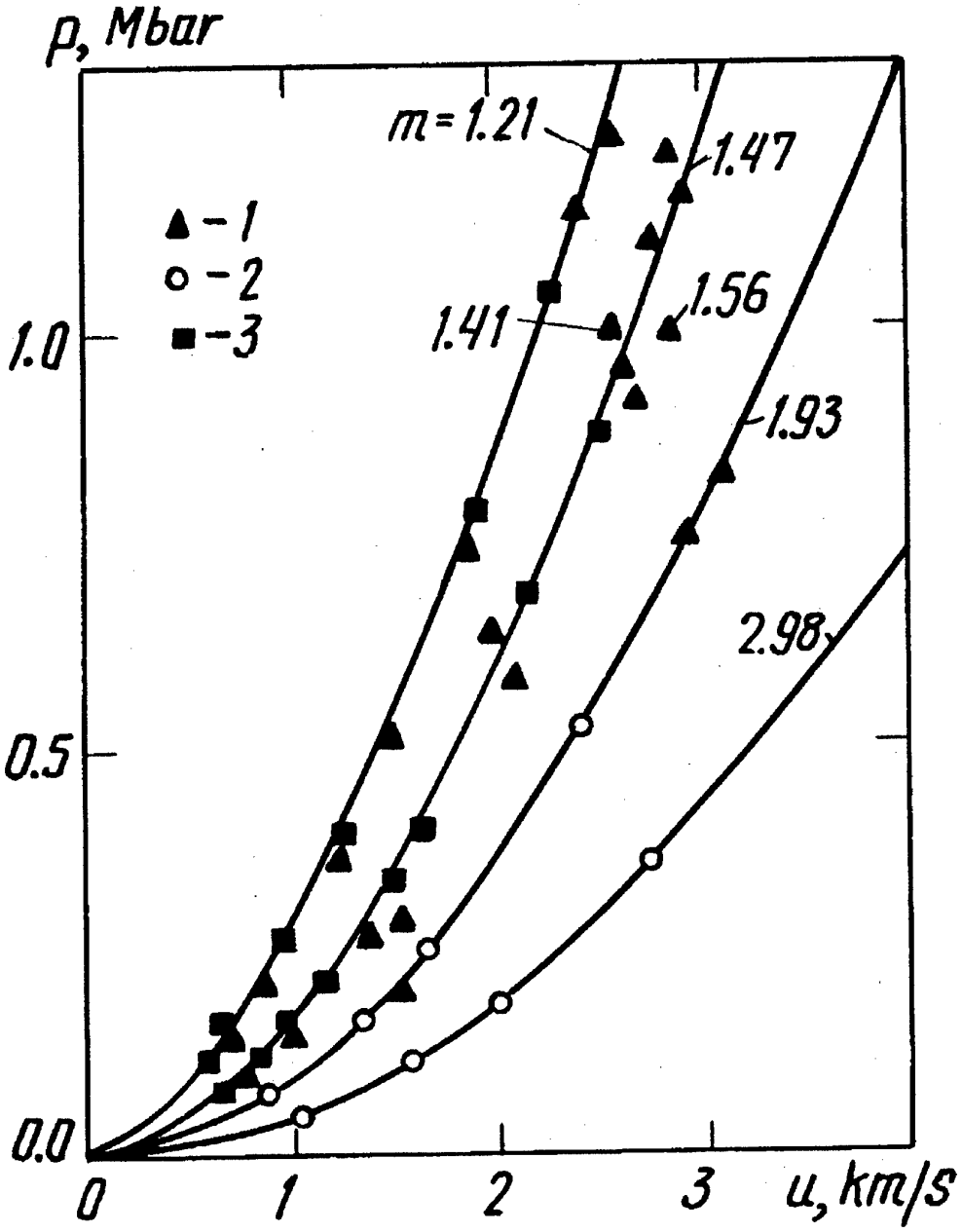

Fig. 7. Shock adiabats for porous copper. Designations are the same as in Fig. 3, exept that the experiemntal data shown as 3 come from Ref. [35].

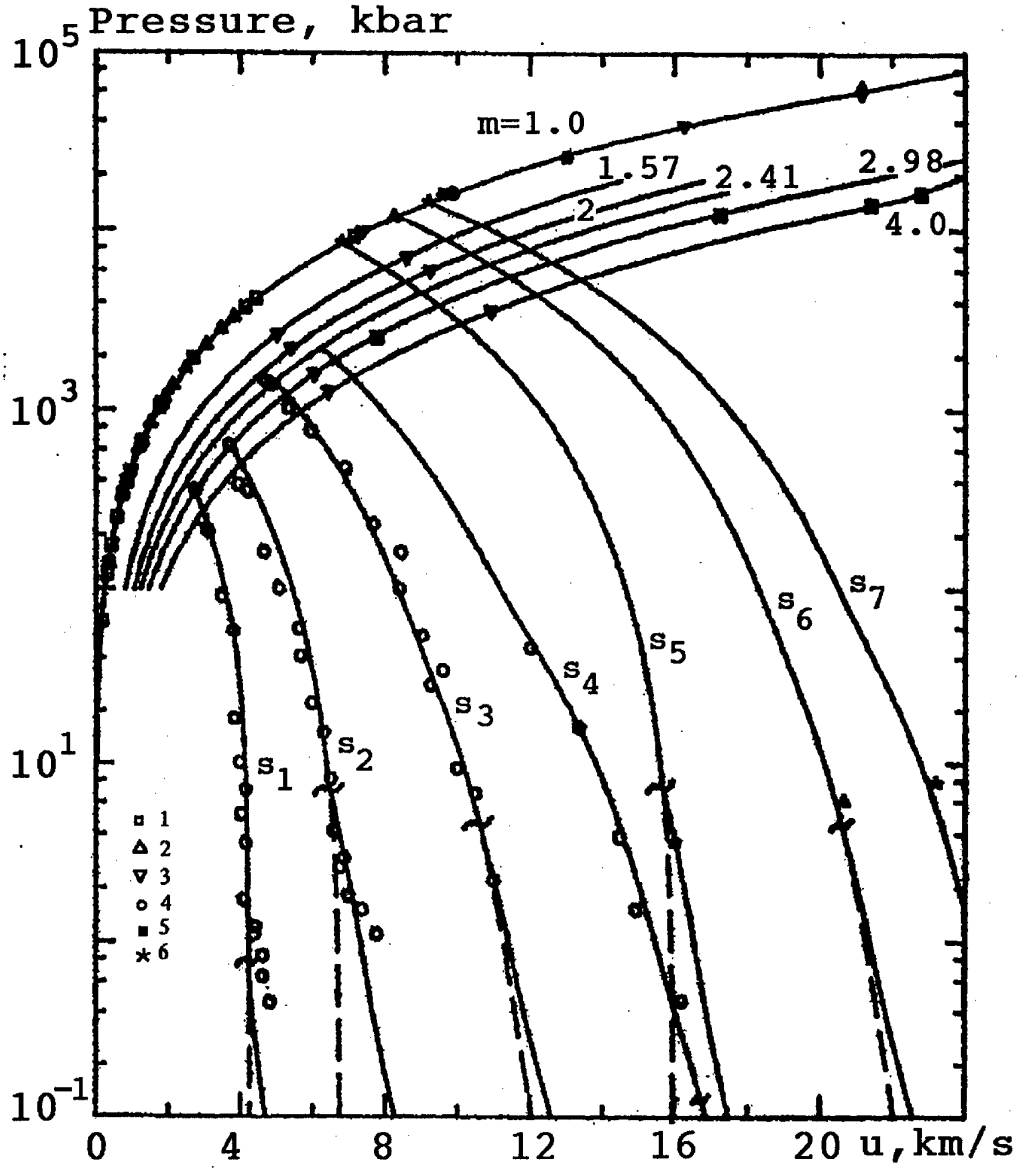

Fig. 8. Shock adiabats (m) and release isentropes (S) for copper. Calculations: solid lines, equilibrium states; dashed kines, metastable states. Experimental data: 1 - [12,13], 2 - [14], 3 - [15], 4 - [36], 5 - [37], 6 - [38].

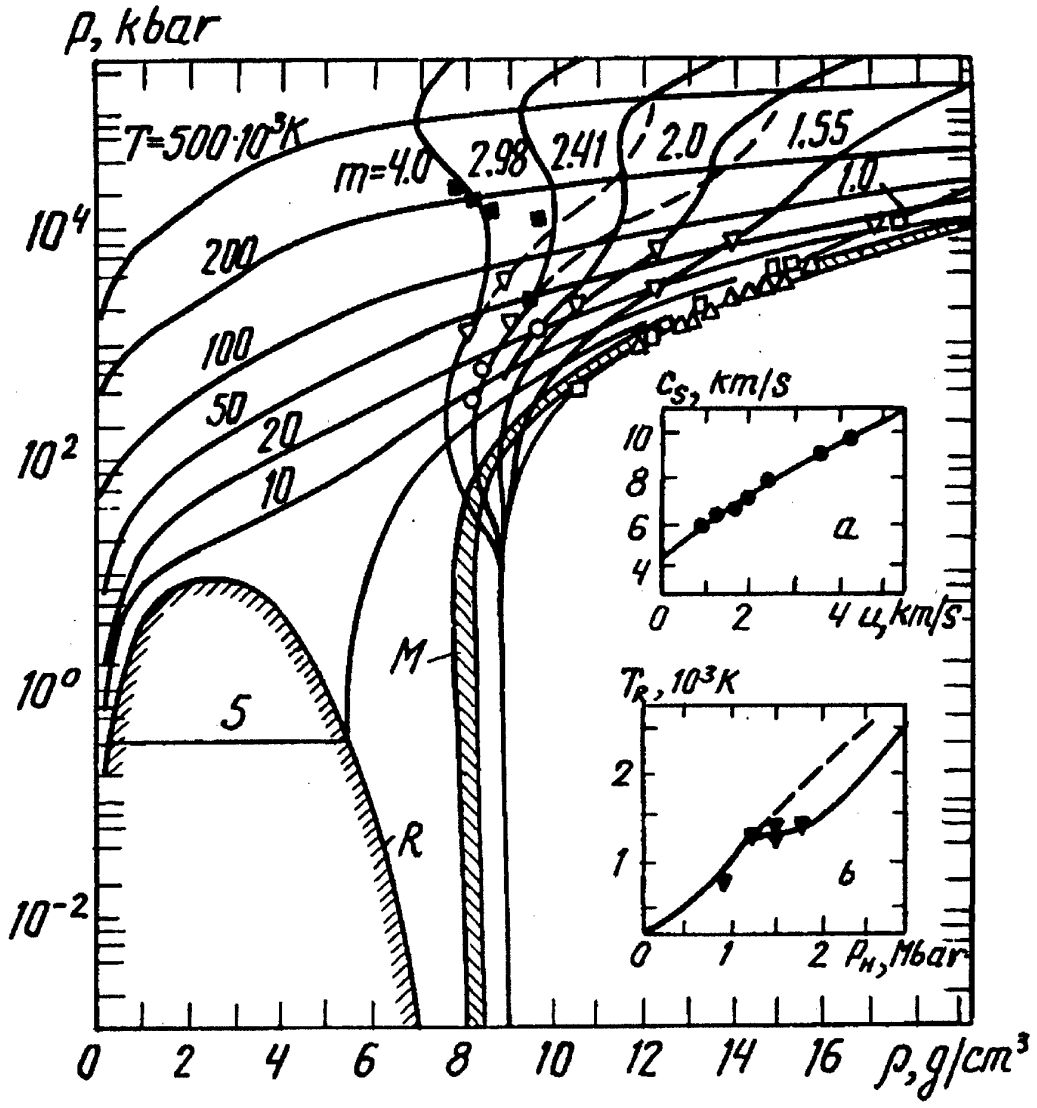

Fig. 9. Phase diagram for copper. Designations are the same as in Fig. 4, exept that the experimental data shon: 4 - [37], 6 - [41]. The dashed lines represent the interpretation of shock adiabats from the corrected Thomas-Fermi model [39]. (a) Velocity of sound in shocked copper; (b) residual temperature in the isentropic release wave, the dashed lin representing the calculation of Ref. [9] in which melting is ignored.

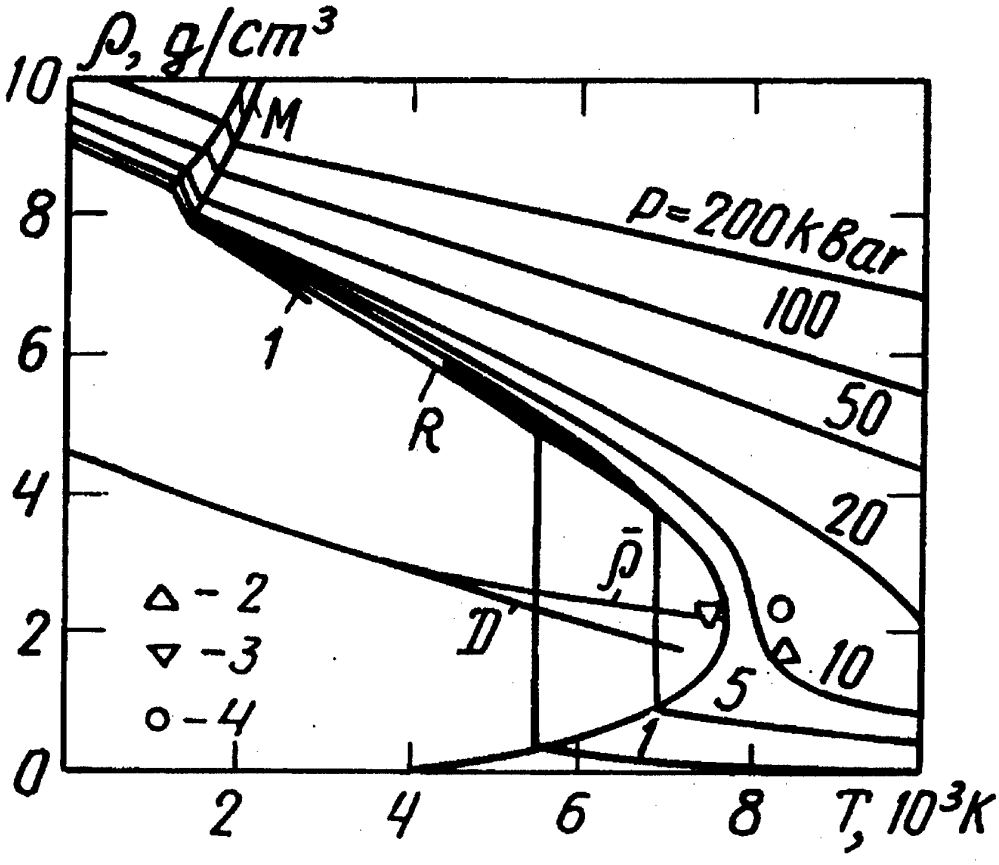

Fig. 10. Phase diagram for copper in the region of lower temperatures. Designations are the same as in in Fig. 6, exept that the data shown at 1 come from Ref. [42].

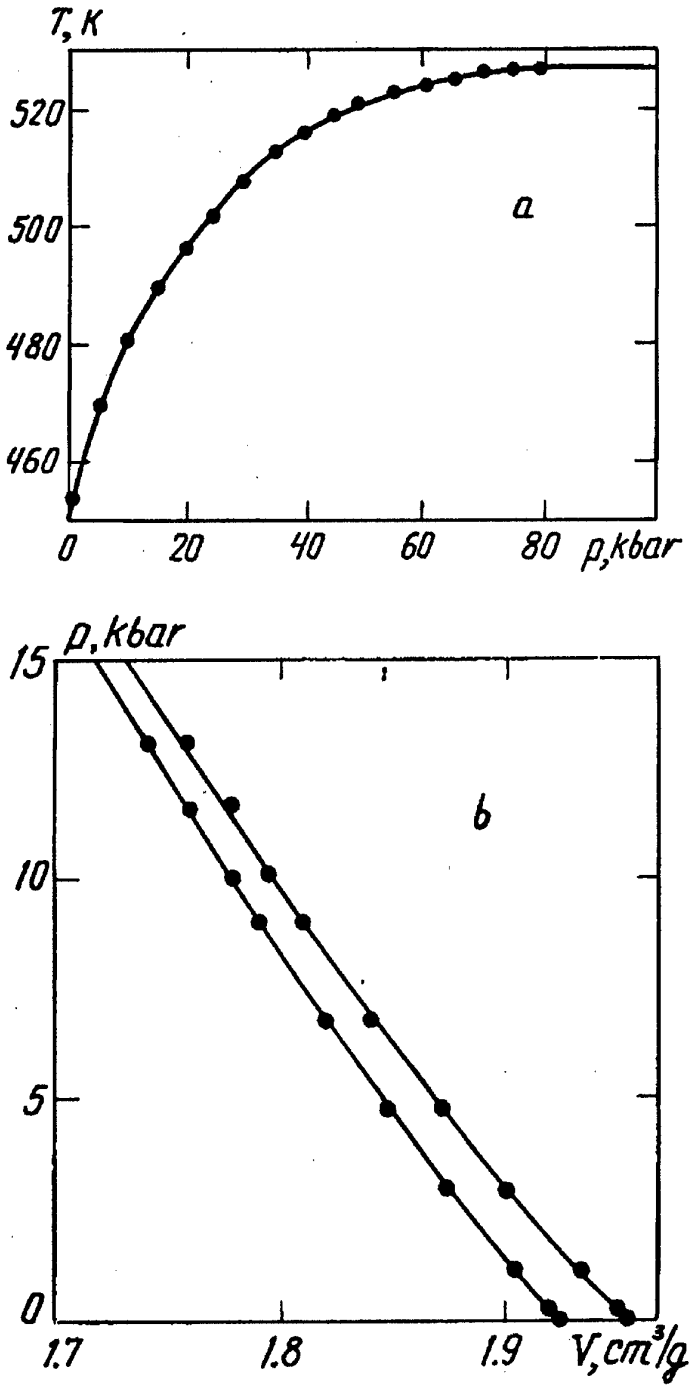

Fig. 11. Temperature (a) and density (b) on the lithium melting curve. Points represent the experimental data: (a) from Ref. [44], (b) from Ref. [45].

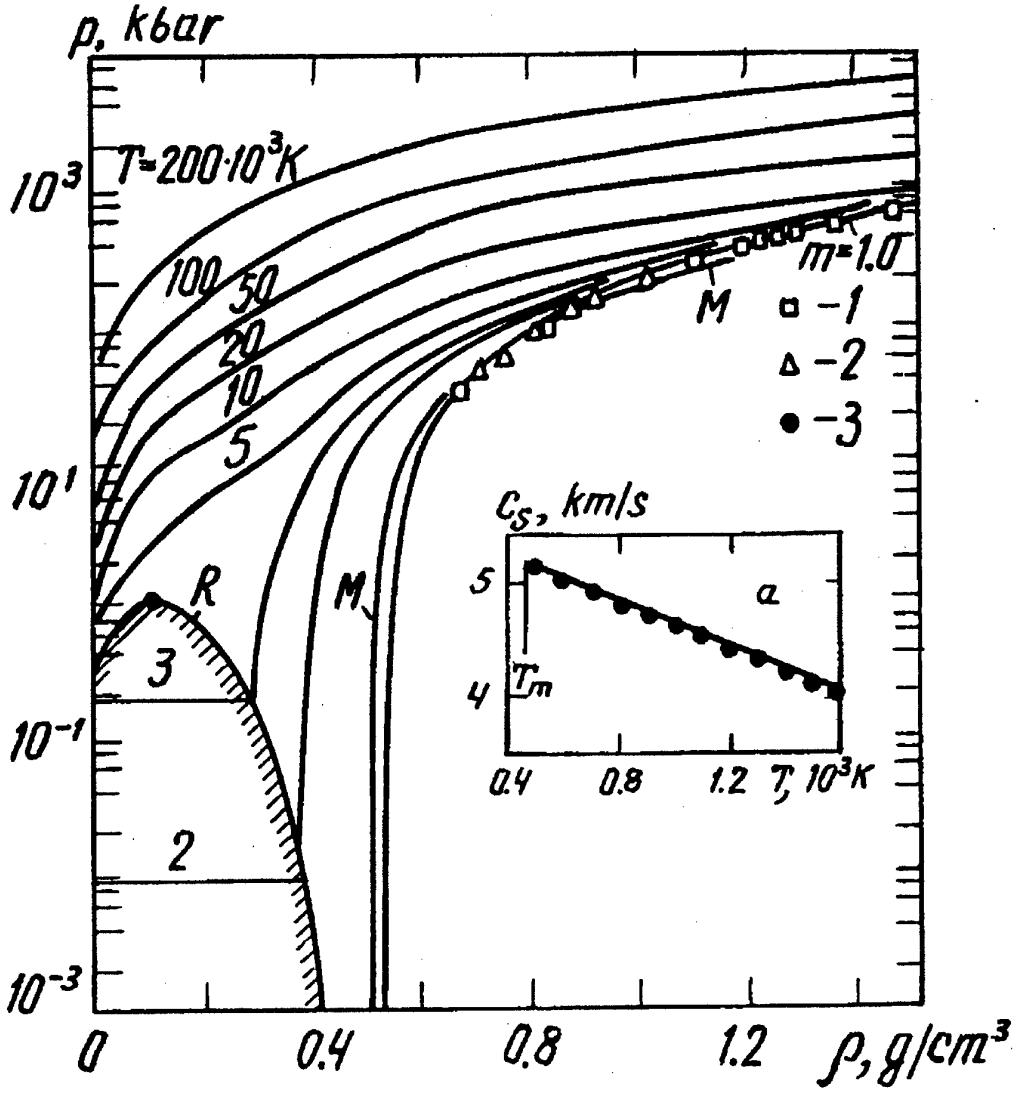

Fig. 12. Phase diagram for lithium. Designations are the same as in Fig. 4, exept that the data: 1 - [46], 2 - [47], 3 - [48]. (a) velocity of sound in liquid lithium.

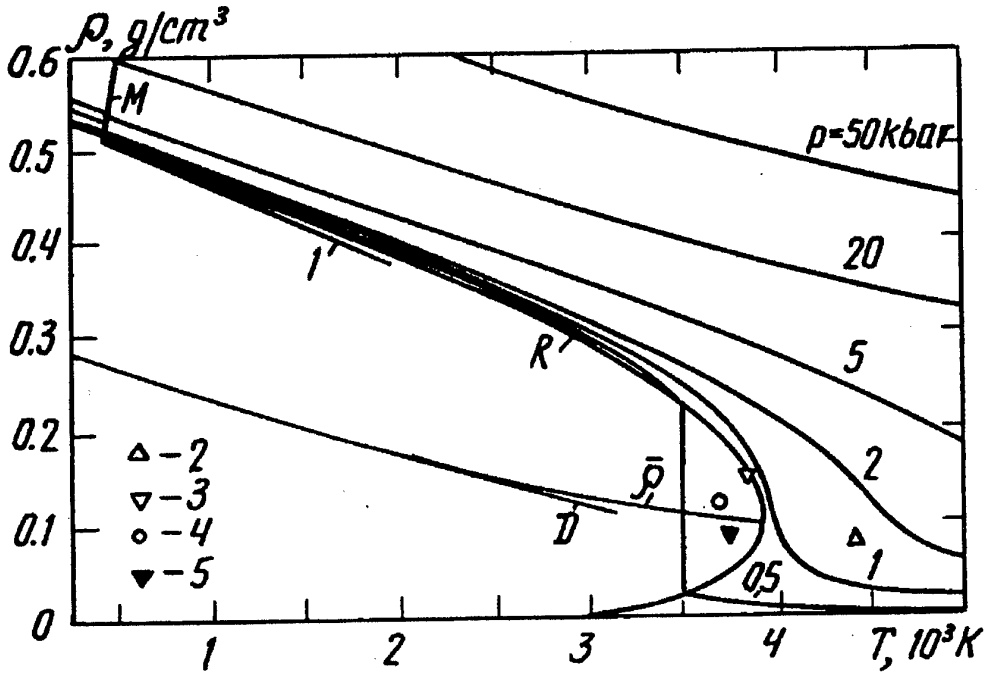

Fig. 13. Phase diagram for lithium in the region of lower temperatures. Designations are the same as in Fig. 6, exept: 1 - [49], 4 - [50].

HEDRC REPORT

Printed November 1994

WIDE-RANGE EQUATION OF STATE FOR LARGE COMPUTER CODES: USER GUIDE

I. V. Lomonosov, V. E. Fortov, and K. V. Khishchenko

Prepared by
High Energy Density Research Center
Russian Academy of Sciences
Izhorskaya Str. 14/19, Moscow 127412, Russia
for USAF
by contract SPC-93-4074

WIDE-RANGE EQUATION OF STATE FOR LARGE COMPUTER CODES: USER GUIDE

I. V. Lomonosov, V. E. Fortov, and K. V. Khishchenko

High Energy Density Research Center
Russian Academy of Sciences
Izhorskaya Str. 14/19, Moscow 127412, Russia

Abstract

This is fourth (12-month) report performed for USAF by contract SPC-93-4074. Described are the generation of output tables, prepared by the multi-phase equation-of-state (EOS) code, their internal structure and utilization. Regimes of calculations for different cases are discussed with typical examples. Possible code problems, errors are also given. Appendix contents useful thermodynamical calculations for all metals.

1. Introduction

The goal of the report is description of work of the EOS code. It requires minimum knowledges in hydrodynamics, thermodynamics and programming. The manual is devoted to typical hydrocode user with an experience in numerical modeling of such processes, as high-velocity impact, for example.

The code is oriented to users which utilize different numerical schemes and methods. The output tables can be obtained in dependence of 3 pairs of input data, viz. *(volume, temperature), (volume, internal energy)* and *(volume, pressure).*

Discussed are also such necessary things, as normilizing conditions, structure of tables, possible problems, mistakes and code errors.

2. About the EOS code

The multi-phase EOS (file **tabeos.exe**) is computer code which has been developed to use real thermodynamical data of metals in solid, liquid, gas, plasma states, solid-liquid and liquid-gas regions in hydrocodes.

2.1. Region of applicability

The EOS provides for an accurate calculation of all equilibrium thermodynamical functions in following range of the phase diagram:

1. to 100-fold compressions at T=0 K;

2. at high temperature the limits are:

up to about 100 Mbar point on the principal Hugoniot and all states which lie down the release isentrope, originating in the 100 Mbar point, i.e $0.001<V_0 / V<3\text{-}4$.

2.2. Phase boundaries

The EOS code can not be used directly in hydrocodes as it calculates correctly by solving numerically the equation for Gibb's energy in different phase states. It is possible to use only output tabular data. Each point in these tables has its own phase identificator.

The nomencalture of the identificators is given in Table 1 (file **physid.tab**).

Table 1. Nomenclature of the phase identificatores.

Identificator value	Physical state
0	unphysical region
1	solid
2	solid + liquid, melting
3	liquid
4	liquid + gas, evaporation
5	plasma

2.3. Input and output

The code calculates tables of thermodynamical functions with maximum dimension 256*256 in linear, logarithm ore arbitrary grid.

Users dealing with hydrocodes need different dependencies, such as *pressure(volume, temperature), pressure(volume, internal energy)* or *internal energy(volume,pressure).* The code provides for calculations in the three regimes, i.e. when input pairs are *(volume, temperature)*, *(volume, internal energy)*, and *(volume,pressure).*

The scale of the input greed (let's suppose, *volume*, for instance) can be linear, logarithm or arbitrary. Details are described below.

As output, generated are following tables: *pressure, entropy, enthalpy, internal energy, isentropical and isothermal sound velocities, temperature, heat capacities at constant volume and pressure, phase identificators.*

3. How it works?

This section contents the details of organizing calculations, structure of input and output data.

3.1. Load

All manipulations with regime of calculations, dimension of grid, and others, are made by editing managing file **data.man**. So if you need to calculate new tables, you should correct the file.

data.man must be placed in the same directory, as **tabeos.exe** (the EOS code) and **tt50.dat** (coefficients for EOS code). The output files with thermodynamic tables will be placed also in this work directory.

So, you work directory will contain following files:

tabeos.exe - the EOS code;
tt50.dat - internal data for EOS code;
data.man - managing file;
volume.in - file containing data for arbitrary-volume grid;
temper.in - file containing data for arbitrary-temperature grid;
pressu.in - file containing data for arbitrary-pressure grid;
energy.in - file containing data for arbitrary-internal_energy grid.

You may calculate tables of different dimension in different grids for any one of available ten metals: ***Li, Al, Fe, Ni, Cu, Mo, Ta, W, Au, Pb***.

At first you should clearly understand, what region of the phase diagram is of the most interst and significance for your calculations and introduce the limits and dimension of input grid into managing file **data.man**. After completing the edition of file **data.man** you may run the calculations.

3.2. Structure of managing file data.man

The typical contents of the file **data.man** is following:

Parameter	Unit	Comment
01	[-]	number of material used
0.300E-03	10**3 [K]	initial temperature
0.100E+03	10**3 [K]	final temperature
0.200E-00	[cc/g]	initial volume
0.100E+02	[cc/g]	final volume
256	[-]	number of points in temperature grid
256	[-]	number of points in volume grid
+0	[-]	scale identificator (linear grid)
+0	[-]	scale identificator (linear grid)
+0	[-]	output identificator
+0	[-]	regime identificator

In this file only 1-st column is used; the others contain only comments.

Let's clarify each value in the column:

- number of material used (note, that only **I2** format ***must be used***):

Number	01	02	03	04	05	06	07	08	09	10
Metal	Li	Al	Fe	Ni	Cu	Mo	Ta	W	Au	Pb

- values of initial temperature, final temperature (*temperature* grid) or initial and final energy (*energy* grid) or initial and final pressure (*pressure* grid) are introduced by format **E9.3**;

- dimension of grid is limited to 256*256 and is introduced by format **I3**;

- scale identificator allows to calculate linear (+0), logarithm (+1) or arbitrary (-1) grid. The first scale identificator manages *energy, temperature, pressure* grids, while second always manages the *volume* grid. If scale identificator equals -1, the data are read from file and in this case the previously read data are not significant;

- output identificator manages the format of output tables, they can be written in fixed (+0) or binary (+1) format;
- regime identificator (ri) forces the code to calculate output tables using as input pairs *volume-temperature* (ri = +0), *volume-internal_energy* (ri = +1) or *volume-pressure* (ri = -1).

3.3. Structure of input and output data

As it has been written in Section 3.1, you should have in your work directory special files for calculation tables in arbitrary grids. It is possible to have such arbitrary data for both X (volume) and Y (temperature, pressure, internal_energy) grids.

Note, that units for input data are following: pressure [GPa], temperature [10^3 K], internal energy [kJ/g], volume [cc/g]; all thermodynamical functions are given per 1 g of metal.

See in Appendies a simple FORTRAN file **make$tab.f** (it is also included in EOS Kit) created especially for producing files ***.in.**

Also given in Appendies is file **read.f**, which allows to load tables and find any desired point.

Correspondence between output files and thermodynamical functions is following:

Filename	Function	Unit
temper.tab	temperature	10^3 K
pressu.tab	pressure	GPa
energy.tab	internal energy	kJ/g
entropy.tab	entropy	J/(gK)
sndvls.tab	isentropic sound velocity	km/s
sndvlt.tab	isothermal sound velocity	km/s
hcapap.tab	heat capacity at constant pressure	J/(gK)
hcapav.tab	heat capacity at constant volume	J/(gK)

physid.tab	physical-state (solid, liquid,...) identificator	dimensionless

3.4 Normilizing conditions

Obviously, the knowledge of normilizing conditions is of importance in hydrocalculations. In the EOS they are following:

ar room temperature (293 K), normal volume ($V=V_0$) pressure p=1 bar (± 0.001%), internal energy E=0 kJ/(gK) ($\pm 10^{-8}$, computer zero), entropy s=0 J/(gK) ($\pm 10^{-8}$, computer zero).

4. Running calculations

A model test of calculation thermodynamical tables for a typical problem is given in this section.

4.1. Problem setup

Let's suppose that we should generate correct tables for calculation high-velocity (22 km/s) impact with aluminum as impactor (1 cm thickness) and target (also 1 cm) material. Our goal is to match the velocity, form and mass of debris clouds. Our code needs *volume-temperature* calcualtions.

I choose 22 km/s to have a large amount of evaporated metal and all physical states during the process - solid, liquid, gas and plasma.

4.2. Determination of grid limits

At first, we should to determine the maximum value of pressure and entropy. Given in Appendies shock Hugoniot and saturation curve for aluminum indicate, that under conditions of our impact realized will be following states:

- in shocked material: p<5.78 Mbar, s<4.57 J/(gK), V>0.161 cc/g, T<33500 K;

- aluminum will be evaporated on release isentrope with s=4.57 J(gK), so final value of volume will be V=8.69E+03 cc/g, of temperature T=300 K.

4.3. Choosing of grids

It is reasonable to make a detailed logarithm grid for volume, i.e. to have about 150-200 points; as for temperature, 100 points in logarithm grid is enough.

Execution **make$tab.exe** will make any desired grid. For instance, we may pay more attention to evaporation and divide the volume grid into 3 regions:

- 0.161<V<0.369 - 30 points from shocked metal to normal volume;
- 0.369<V<1.188 - 100 points from normal volume to critical one;
- 1.88<V<8.69E+03 - 70 points from critical volume to full evaporation.

4.4. Managing file

Finally, file **data.man** is following:

Parameter	Unit	Comment
02	[-]	number of material used
0.300E-00	10**3 [K]	initial temperature
0.350E+03	10**3 [K]	final temperature
0.160E-00	[cc/g]	initial volume
0.100E+05	[cc/g]	final volume
100	[-]	number of points in temperature grid
200	[-]	number of points in volume grid
+1	[-]	scale identificator (linear grid)
+1	[-]	scale identificator (linear grid)
+0	[-]	output identificator
+0	[-]	regime identificator

5. Possible errors

The code can stop calculations in 2 following sitiations:

- p=const, T=const functions are near critical point. In this case sometimes (when T or P are less then critical-point parameters in 0.1-0.5%) the code can

not find numerical soluion in 2-phase liquid-gas region, as the liquid-gas equilibrium curve is approximately horizontal.

Recommendation: match the values of T and P and avoid this sutuation.

- the logical scheme of the code requires to begin calculations from condensed phase; they must begin from $V_{initial} \leq V_0$, otherwise the code can not find correctly the phase boundaries.

Recommendation: introduce initial volume less or of the order of V_0 then increase volume on the volume grid. Never start calculations inside liquid-gas mixture.

6. References

Utilizing the code, refer to [1] for EOS of Al, Cu, Pb, Li and to [2] for Fe, Ni, Mo, Ta, W metals:

[1] A. V. Bushman, G. I. Kanel', A. L. Ni, and V. E. Fortov, *Intense Dynamic Loading of Condensed Matter,* New York: Taylor&Francis, 1993.

[2] V. E. Fortov and I. V. Lomonosov, High Pressure Research (1995) [in press].

7. Servise office

Call for help Igor Lomonosov:

Address	Fax/Phone	E-mail
Institute of Chemical Physics in Chernogolovka RAS P.O. 142432 Chernogolovka Moscow region Russia	(7-095)485-7988 (7-096)517-1870	*ivl@ficp.ac.ru* *ivl@hedric.msk.su*

(e-mail is preferred).

Send briff description of your problem with file **data.man.**

Appendixes

Placed in appendixes are results of phase-diagram calcualtions for metals and few useful FORTRAN programs for preparing, reading and manipulating the input and output data.

Appendix A. Phase diagrams of metals

Given in the Appenidxes A1-A10 are calculations of phase diagrams for Li, Al, Fe, Ni, Cu, Mo, Ta, W, Au, Pb.

Nomenclature:

Symbol	Name	Unit
P	pressure	GPa
T	temperature	10^3 K
VS	volume of solid phase	cc/g
VL	volume of liquid phase	cc/g
VG	volume of gas phase	cc/g
SS	entropy of solid phase	J/(gK)
SL	entropy of liquid phase	J/(gK)
SG	entropy of gase phase	J/(gK)
ES	energy of solid phase	kJ/g
EL	energy of liquid phase	kJ/g
EG	energy of gas phase	kJ/g
E	internal energy	kJ/g
S	entropy	J/(gK)
V	volume	cc/g
D	shock velocity	km/s
U	mass velocity	km/s
CS	sound velocity	km/s
CV	heat capacity	J/(gK)

Empty lines in the shock adiabat tables mark the position of melting.

Appendix A1

Lithium

MELTING CURVE

P	T	VS/VS0	VS	VL	ES	EL	DV/VS	DS/R
1.000-4	4.540-1	1.000 0	1.909 0	1.948 0	6.184-1	1.052 0	2.041-2	7.901-1
1.000 0	4.849-1	9.242-1	1.765 0	1.786 0	6.785-1	1.110 0	1.211-2	7.711-1
1.500 0	4.948-1	8.937-1	1.707 0	1.723 0	7.346-1	1.171 0	9.436-3	7.687-1
2.000 0	5.024-1	8.668-1	1.655 0	1.667 0	8.035-1	1.247 0	7.326-3	7.686-1
2.500 0	5.080-1	8.427-1	1.609 0	1.618 0	8.828-1	1.334 0	5.628-3	7.702-1
3.000 0	5.122-1	8.210-1	1.568 0	1.574 0	9.705-1	1.430 0	4.240-3	7.728-1
4.000 0	5.174-1	7.832-1	1.495 0	1.499 0	1.166 0	1.641 0	2.123-3	7.801-1
5.000 0	5.194-1	7.513-1	1.434 0	1.435 0	1.381 0	1.873 0	6.007-4	7.888-1
6.000 0	5.194-1	7.237-1	1.382 0	1.381 0	1.611 0	2.117 0	-5.368-4	7.982-1
8.000 0	5.156-1	6.782-1	1.295 0	1.292 0	2.102 0	2.634 0	-2.106-3	8.176-1
1.000 1	5.090-1	6.417-1	1.225 0	1.221 0	2.618 0	3.172 0	-3.130-3	8.373-1
1.500 1	4.872-1	5.743-1	1.097 0	1.091 0	3.963 0	4.561 0	-4.605-3	8.863-1
2.000 1	4.632-1	5.267-1	1.006 0	1.000 0	5.333 0	5.967 0	-5.415-3	9.357-1
2.500 1	4.395-1	4.906-1	9.367-1	9.312-1	6.700 0	7.364 0	-5.935-3	9.866-1
3.000 1	4.168-1	4.618-1	8.817-1	8.762-1	8.053 0	8.743 0	-6.282-3	1.039 0
4.000 1	3.758-1	4.179-1	7.980-1	7.927-1	1.070 1	1.143 1	-6.587-3	1.149 0
5.000 1	3.413-1	3.856-1	7.362-1	7.314-1	1.326 1	1.402 1	-6.454-3	1.261 0
6.000 1	3.134-1	3.603-1	6.879-1	6.838-1	1.574 1	1.651 1	-5.985-3	1.369 0
8.000 1	2.741-1	3.227-1	6.161-1	6.133-1	2.049 1	2.124 1	-4.609-3	1.556 0
1.000 2	2.504-1	2.955-1	5.641-1	5.623-1	2.500 1	2.570 1	-3.318-3	1.695 0
1.500 2	2.233-1	2.504-1	4.781-1	4.774-1	3.537 1	3.598 1	-1.441-3	1.892 0
2.000 2	2.138-1	2.217-1	4.234-1	4.231-1	4.475 1	4.532 1	-6.438-4	1.983 0
2.500 2	2.102-1	2.014-1	3.845-1	3.844-1	5.340 1	5.394 1	-2.462-4	2.030 0
3.000 2	2.093-1	1.858-1	3.548-1	3.548-1	6.147 1	6.199 1	-1.655-5	2.059 0
4.000 2	2.109-1	1.634-1	3.119-1	3.120-1	7.629 1	7.679 1	2.298-4	2.089 0
5.000 2	2.143-1	1.475-1	2.817-1	2.818-1	8.977 1	9.027 1	3.561-4	2.105 0

SATURATION CURVE

P	T	T/TC	VL	VG	SL	SG	EL	EG
1.058-1	3.942 0	1.000 0	9.760 0	9.760 0	1.297 1	1.297 1	2.132 1	2.132 1
1.000-1	3.907 0	9.911-1	7.399 0	1.360 1	1.247 1	1.347 1	1.961 1	2.289 1
8.000-2	3.770 0	9.564-1	5.600 0	2.242 1	1.187 1	1.410 1	1.745 1	2.452 1
6.000-2	3.600 0	9.132-1	4.695 0	3.554 1	1.140 1	1.460 1	1.580 1	2.544 1
5.000-2	3.496 0	8.868-1	4.345 0	4.583 1	1.117 1	1.485 1	1.498 1	2.577 1
4.000-2	3.373 0	8.555-1	4.029 0	6.108 1	1.091 1	1.512 1	1.411 1	2.603 1
3.000-2	3.221 0	8.170-1	3.731 0	8.608 1	1.062 1	1.544 1	1.315 1	2.620 1
2.500-2	3.129 0	7.938-1	3.584 0	1.057 2	1.044 1	1.562 1	1.261 1	2.625 1
2.000-2	3.022 0	7.665-1	3.434 0	1.347 2	1.025 1	1.584 1	1.200 1	2.627 1
1.500-2	2.891 0	7.334-1	3.275 0	1.819 2	1.001 1	1.610 1	1.130 1	2.625 1
1.000-2	2.721 0	6.903-1	3.101 0	2.733 2	9.695 0	1.647 1	1.042 1	2.615 1
8.000-3	2.634 0	6.683-1	3.022 0	3.398 2	9.534 0	1.666 1	9.996 0	2.608 1
6.000-3	2.529 0	6.416-1	2.934 0	4.479 2	9.337 0	1.691 1	9.488 0	2.598 1
5.000-3	2.467 0	6.257-1	2.885 0	5.323 2	9.218 0	1.707 1	9.189 0	2.592 1
4.000-3	2.393 0	6.071-1	2.831 0	6.564 2	9.076 0	1.727 1	8.847 0	2.583 1
3.000-3	2.305 0	5.846-1	2.769 0	8.580 2	8.902 0	1.751 1	8.438 0	2.572 1
2.500-3	2.252 0	5.711-1	2.734 0	1.016 3	8.796 0	1.767 1	8.196 0	2.565 1
2.000-3	2.190 0	5.554-1	2.694 0	1.247 3	8.670 0	1.787 1	7.916 0	2.556 1
1.500-3	2.114 0	5.363-1	2.648 0	1.624 3	8.514 0	1.812 1	7.581 0	2.545 1
1.000-3	2.016 0	5.114-1	2.591 0	2.351 3	8.306 0	1.847 1	7.151 0	2.530 1
8.000-4	1.966 0	4.987-1	2.562 0	2.881 3	8.197 0	1.867 1	6.933 0	2.522 1
6.000-4	1.905 0	4.831-1	2.529 0	3.743 3	8.060 0	1.893 1	6.669 0	2.513 1
5.000-4	1.868 0	4.738-1	2.510 0	4.419 3	7.977 0	1.909 1	6.512 0	2.506 1
4.000-4	1.824 0	4.628-1	2.487 0	5.413 3	7.877 0	1.929 1	6.328 0	2.499 1
3.000-4	1.771 0	4.493-1	2.461 0	7.033 3	7.753 0	1.956 1	6.105 0	2.490 1
2.500-4	1.739 0	4.412-1	2.445 0	8.303 3	7.677 0	1.972 1	5.971 0	2.485 1
2.000-4	1.702 0	4.317-1	2.427 0	1.018 4	7.586 0	1.993 1	5.814 0	2.478 1
1.500-4	1.656 0	4.200-1	2.405 0	1.323 4	7.472 0	2.020 1	5.623 0	2.470 1
1.000-4	1.595 0	4.045-1	2.377 0	1.916 4	7.318 0	2.057 1	5.373 0	2.460 1

Lithium

SHOCK ADIABAT M= 1.000

P	T	V	S	E	D	U	CS	CV
1.000-4	2.930-1	1.860 0	-9.537-7	-8.382-8	.000 0	.000 0	4.662 0	3.633 0
5.000 0	4.291-1	1.424 0	5.397-1	1.091 0	6.297 0	1.477 0	6.146 0	3.683 0
6.000 0	4.688-1	1.376 0	7.639-1	1.451 0	6.552 0	1.703 0	6.347 0	3.692 0
7.103 0	5.178-1	1.331 0	1.032 0	1.878 0	6.818 0	1.938 0	6.551 0	3.701 0
7.103 0	5.178-1	1.331 0	1.031 0	1.878 0	6.818 0	1.938 0	6.423 0	5.401 3
8.000 0	5.157-1	1.294 0	1.235 0	2.264 0	6.993 0	2.128 0	6.545 0	2.652 3
9.898 0	5.094-1	1.225 0	1.744 0	3.144 0	7.342 0	2.508 0	6.783 0	1.183 3
9.898 0	5.094-1	1.225 0	1.744 0	3.144 0	7.342 0	2.508 0	6.913 0	3.463 0
1.000 1	5.160-1	1.222 0	1.783 0	3.192 0	7.363 0	2.526 0	6.927 0	3.465 0
1.500 1	8.586-1	1.108 0	3.334 0	5.638 0	8.309 0	3.358 0	7.529 0	3.547 0
2.000 1	1.265 0	1.028 0	4.557 0	8.324 0	9.118 0	4.080 0	7.975 0	3.615 0
2.500 1	1.718 0	9.651-1	5.544 0	1.119 1	9.831 0	4.730 0	8.315 0	3.669 0
3.000 1	2.205 0	9.140-1	6.364 0	1.419 1	1.047 1	5.327 0	8.582 0	3.710 0
4.000 1	3.264 0	8.334-1	7.674 0	2.053 1	1.161 1	6.408 0	8.985 0	3.757 0
5.000 1	4.420 0	7.716-1	8.700 0	2.721 1	1.261 1	7.377 0	9.366 0	3.765 0
6.000 1	5.671 0	7.238-1	9.548 0	3.409 1	1.352 1	8.257 0	9.869 0	3.747 0
8.000 1	8.474 0	6.598-1	1.091 1	4.801 1	1.519 1	9.799 0	1.122 1	3.675 0
1.000 2	1.162 1	6.224-1	1.197 1	6.189 1	1.672 1	1.113 1	1.255 1	3.601 0
1.500 2	2.039 1	5.759-1	1.382 1	9.631 1	2.010 1	1.388 1	1.499 1	3.492 0
2.000 2	2.974 1	5.539-1	1.505 1	1.306 2	2.302 1	1.616 1	1.670 1	3.473 0
2.500 2	3.926 1	5.407-1	1.596 1	1.649 2	2.561 1	1.816 1	1.809 1	3.512 0
3.000 2	4.872 1	5.317-1	1.669 1	1.992 2	2.795 1	1.996 1	1.930 1	3.589 0
4.000 2	6.710 1	5.196-1	1.781 1	2.681 2	3.213 1	2.316 1	2.142 1	3.813 0
5.000 2	8.449 1	5.113-1	1.868 1	3.372 2	3.581 1	2.597 1	2.329 1	4.074 0
6.000 2	1.009 2	5.049-1	1.939 1	4.065 2	3.914 1	2.851 1	2.499 1	4.331 0
8.000 2	1.315 2	4.956-1	2.054 1	5.458 2	4.504 1	3.304 1	2.806 1	4.776 0
1.000 3	1.597 2	4.893-1	2.146 1	6.854 2	5.024 1	3.702 1	3.084 1	5.117 0

Appendix A2

Aluminum

MELTING CURVE

P	T	VS/VS0	VS	VL	SS	SL	ES	EL
1.000-4	9.330-1	1.000 0	3.904-1	4.230-1	1.201 0	1.629 0	6.740-1	1.073 0
5.000 0	1.259 0	9.487-1	3.704-1	3.967-1	1.378 0	1.842 0	9.139-1	1.367 0
6.000 0	1.314 0	9.395-1	3.668-1	3.924-1	1.400 0	1.872 0	9.619-1	1.428 0
8.000 0	1.418 0	9.220-1	3.600-1	3.843-1	1.437 0	1.923 0	1.059 0	1.554 0
1.000 1	1.515 0	9.057-1	3.536-1	3.770-1	1.466 0	1.966 0	1.159 0	1.684 0
1.500 1	1.733 0	8.694-1	3.394-1	3.611-1	1.519 0	2.051 0	1.422 0	2.019 0
2.000 1	1.925 0	8.385-1	3.274-1	3.477-1	1.557 0	2.115 0	1.702 0	2.369 0
2.500 1	2.099 0	8.117-1	3.169-1	3.362-1	1.585 0	2.166 0	1.993 0	2.730 0
3.000 1	2.259 0	7.882-1	3.077-1	3.261-1	1.607 0	2.207 0	2.293 0	3.097 0
4.000 1	2.544 0	7.485-1	2.922-1	3.090-1	1.640 0	2.271 0	2.912 0	3.844 0
5.000 1	2.795 0	7.160-1	2.795-1	2.950-1	1.664 0	2.318 0	3.544 0	4.598 0
6.000 1	3.020 0	6.886-1	2.688-1	2.832-1	1.682 0	2.356 0	4.183 0	5.353 0
8.000 1	3.411 0	6.444-1	2.516-1	2.642-1	1.707 0	2.410 0	5.465 0	6.851 0
1.000 2	3.746 0	6.097-1	2.380-1	2.493-1	1.724 0	2.449 0	6.740 0	8.326 0
1.500 2	4.418 0	5.470-1	2.136-1	2.225-1	1.749 0	2.510 0	9.855 0	1.188 1
2.000 2	4.942 0	5.036-1	1.966-1	2.040-1	1.761 0	2.546 0	1.285 1	1.526 1
2.500 2	5.372 0	4.709-1	1.839-1	1.902-1	1.766 0	2.570 0	1.574 1	1.848 1
3.000 2	5.738 0	4.449-1	1.737-1	1.793-1	1.769 0	2.587 0	1.854 1	2.156 1
4.000 2	6.339 0	4.056-1	1.583-1	1.628-1	1.769 0	2.609 0	2.387 1	2.741 1
5.000 2	6.822 0	3.765-1	1.470-1	1.508-1	1.765 0	2.623 0	2.893 1	3.289 1
6.000 2	7.227 0	3.538-1	1.381-1	1.414-1	1.760 0	2.633 0	3.375 1	3.810 1
8.000 2	7.883 0	3.199-1	1.249-1	1.275-1	1.748 0	2.644 0	4.286 1	4.785 1
1.000 3	8.405 0	2.952-1	1.152-1	1.174-1	1.736 0	2.650 0	5.139 1	5.691 1

SATURATION CURVE

P	T	T/TC	VL	VG	SL	SG	EL	EG
4.452-1	6.388 0	1.000 0	1.169 0	1.169 0	4.525 0	4.525 0	1.072 1	1.072 1
4.000-1	6.299 0	9.861-1	9.711-1	1.481 0	4.394 0	4.648 0	9.968 0	1.137 1
3.000-1	6.089 0	9.532-1	8.493-1	1.949 0	4.267 0	4.761 0	9.226 0	1.190 1
2.500-1	5.974 0	9.351-1	8.088-1	2.247 0	4.212 0	4.811 0	8.903 0	1.213 1
2.000-1	5.848 0	9.155-1	7.734-1	2.645 0	4.156 0	4.864 0	8.582 0	1.235 1
1.500-1	5.707 0	8.934-1	7.405-1	3.251 0	4.097 0	4.924 0	8.245 0	1.259 1
1.000-1	5.538 0	8.670-1	7.075-1	4.423 0	4.028 0	5.002 0	7.866 0	1.289 1
8.000-2	5.456 0	8.541-1	6.932-1	5.383 0	3.996 0	5.046 0	7.688 0	1.304 1
6.000-2	5.355 0	8.383-1	6.769-1	7.464 0	3.956 0	5.113 0	7.474 0	1.326 1
5.000-2	5.289 0	8.280-1	6.668-1	1.004 1	3.930 0	5.169 0	7.336 0	1.342 1
4.000-2	5.197 0	8.135-1	6.536-1	1.608 1	3.894 0	5.256 0	7.147 0	1.361 1
3.000-2	5.053 0	7.911-1	6.348-1	2.782 1	3.838 0	5.360 0	6.863 0	1.374 1
2.500-2	4.953 0	7.754-1	6.230-1	3.692 1	3.800 0	5.415 0	6.671 0	1.377 1
2.000-2	4.826 0	7.555-1	6.094-1	5.006 1	3.752 0	5.477 0	6.436 0	1.377 1
1.500-2	4.661 0	7.297-1	5.935-1	7.115 1	3.690 0	5.552 0	6.142 0	1.376 1
1.000-2	4.436 0	6.944-1	5.744-1	1.116 2	3.605 0	5.651 0	5.756 0	1.372 1
8.000-3	4.317 0	6.758-1	5.653-1	1.409 2	3.560 0	5.704 0	5.559 0	1.369 1
6.000-3	4.170 0	6.528-1	5.549-1	1.887 2	3.504 0	5.773 0	5.321 0	1.365 1
5.000-3	4.081 0	6.388-1	5.489-1	2.260 2	3.469 0	5.816 0	5.179 0	1.363 1
4.000-3	3.976 0	6.224-1	5.422-1	2.809 2	3.429 0	5.868 0	5.015 0	1.359 1
3.000-3	3.847 0	6.023-1	5.345-1	3.704 2	3.378 0	5.936 0	4.818 0	1.355 1
2.500-3	3.770 0	5.901-1	5.300-1	4.404 2	3.347 0	5.980 0	4.700 0	1.352 1
2.000-3	3.679 0	5.759-1	5.249-1	5.436 2	3.310 0	6.033 0	4.563 0	1.349 1
1.500-3	3.567 0	5.584-1	5.189-1	7.118 2	3.265 0	6.101 0	4.398 0	1.345 1
1.000-3	3.421 0	5.355-1	5.114-1	1.038 3	3.204 0	6.199 0	4.185 0	1.339 1
8.000-4	3.345 0	5.237-1	5.077-1	1.276 3	3.172 0	6.253 0	4.077 0	1.336 1
6.000-4	3.252 0	5.092-1	5.033-1	1.665 3	3.132 0	6.323 0	3.945 0	1.332 1
5.000-4	3.196 0	5.004-1	5.007-1	1.970 3	3.107 0	6.367 0	3.866 0	1.330 1
4.000-4	3.130 0	4.900-1	4.977-1	2.420 3	3.078 0	6.422 0	3.774 0	1.327 1
3.000-4	3.049 0	4.774-1	4.941-1	3.155 3	3.042 0	6.493 0	3.661 0	1.324 1
2.500-4	3.000 0	4.697-1	4.920-1	3.732 3	3.019 0	6.538 0	3.594 0	1.322 1
2.000-4	2.942 0	4.606-1	4.895-1	4.584 3	2.993 0	6.594 0	3.514 0	1.319 1
1.500-4	2.871 0	4.494-1	4.865-1	5.976 3	2.959 0	6.665 0	3.417 0	1.316 1
1.000-4	2.776 0	4.346-1	4.826-1	8.687 3	2.914 0	6.767 0	3.290 0	1.312 1

Aluminum

SHOCK ADIABAT M= 1.000

P	T	V	S	E	D	U	CS	CV
1.000-4	2.930-1	3.690-1	-3.576-7	-1.281-7	.000 0	.000 0	5.266 0	9.305-1
1.000 1	3.832-1	3.322-1	4.785-2	1.841-1	6.083 0	6.067-1	6.186 0	9.339-1
1.500 1	4.454-1	3.195-1	1.196-1	3.711-1	6.426 0	8.614-1	6.533 0	9.368-1
2.000 1	5.235-1	3.091-1	2.145-1	5.994-1	6.741 0	1.095 0	6.836 0	9.400-1
2.500 1	6.179-1	3.002-1	3.228-1	8.601-1	7.034 0	1.312 0	7.107 0	9.433-1
3.000 1	7.282-1	2.925-1	4.368-1	1.147 0	7.309 0	1.515 0	7.353 0	9.465-1
4.000 1	9.941-1	2.798-1	6.639-1	1.784 0	7.815 0	1.889 0	7.789 0	9.529-1
5.000 1	1.315 0	2.696-1	8.758-1	2.485 0	8.276 0	2.229 0	8.169 0	9.596-1
6.000 1	1.683 0	2.611-1	1.068 0	3.237 0	8.702 0	2.544 0	8.507 0	9.664-1
8.000 1	2.541 0	2.476-1	1.394 0	4.855 0	9.474 0	3.116 0	9.093 0	9.808-1
1.000 2	3.530 0	2.372-1	1.661 0	6.589 0	1.017 1	3.630 0	9.595 0	9.953-1
1.057 2	3.833 0	2.347-1	1.728 0	7.102 0	1.035 1	3.769 0	9.727 0	9.994-1
1.057 2	3.833 0	2.347-1	1.728 0	7.102 0	1.035 1	3.769 0	9.714 0	9.953 0
1.500 2	4.418 0	2.195-1	2.258 0	1.121 1	1.169 1	4.735 0	1.057 1	1.389 1
1.726 2	4.668 0	2.134-1	2.528 0	1.342 1	1.229 1	5.181 0	1.095 1	1.595 1
1.726 2	4.668 0	2.134-1	2.528 0	1.342 1	1.229 1	5.181 0	1.097 1	1.236 0
2.000 2	6.050 0	2.061-1	2.811 0	1.629 1	1.293 1	5.707 0	1.140 1	1.258 0
2.500 2	8.770 0	1.954-1	3.222 0	2.170 1	1.400 1	6.589 0	1.209 1	1.268 0
3.000 2	1.175 1	1.869-1	3.544 0	2.732 1	1.498 1	7.392 0	1.269 1	1.253 0
4.000 2	1.849 1	1.742-1	4.032 0	3.896 1	1.672 1	8.827 0	1.372 1	1.201 0
5.000 2	2.613 1	1.651-1	4.392 0	5.098 1	1.827 1	1.010 1	1.460 1	1.168 0
6.000 2	3.436 1	1.581-1	4.673 0	6.327 1	1.968 1	1.125 1	1.537 1	1.175 0
8.000 2	5.118 1	1.476-1	5.098 0	8.858 1	2.218 1	1.331 1	1.667 1	1.285 0
1.000 3	6.720 1	1.396-1	5.421 0	1.147 2	2.436 1	1.515 1	1.775 1	1.456 0
1.500 3	1.025 2	1.256-1	6.021 0	1.825 2	2.897 1	1.911 1	1.996 1	1.888 0
2.000 3	1.333 2	1.165-1	6.481 0	2.525 2	3.284 1	2.247 1	2.180 1	2.214 0
2.500 3	1.618 2	1.101-1	6.867 0	3.236 2	3.626 1	2.544 1	2.343 1	2.428 0
3.000 3	1.891 2	1.057-1	7.205 0	3.950 2	3.939 1	2.811 1	2.498 1	2.554 0
4.000 3	2.426 2	1.003-1	7.781 0	5.375 2	4.502 1	3.279 1	2.803 1	2.633 0
5.000 3	2.958 2	9.791-2	8.264 0	6.777 2	5.011 1	3.682 1	3.119 1	2.614 0
6.000 3	3.486 2	9.733-2	8.682 0	8.150 2	5.484 1	4.037 1	3.447 1	2.603 0
8.000 3	4.488 2	9.832-2	9.373 0	1.083 3	6.344 1	4.653 1	4.055 1	2.749 0
1.000 4	5.391 2	9.959-2	9.932 0	1.347 3	7.109 1	5.191 1	4.535 1	3.060 0

Appendix A3

Iron

MELTING CURVE

P	T	VS/VS0	VS	VL	SS	SL	ES	EL
1.000-4	1.810 0	1.000 0	1.306-1	1.359-1	9.474-1	1.105 0	8.194-1	1.105 0
1.000 1	2.116 0	9.441-1	1.233-1	1.273-1	9.794-1	1.122 0	9.165-1	1.178 0
1.500 1	2.252 0	9.222-1	1.205-1	1.241-1	9.919-1	1.129 0	9.793-1	1.233 0
2.000 1	2.381 0	9.030-1	1.179-1	1.213-1	1.003 0	1.135 0	1.048 0	1.297 0
2.500 1	2.505 0	8.858-1	1.157-1	1.188-1	1.013 0	1.141 0	1.123 0	1.368 0
3.000 1	2.624 0	8.704-1	1.137-1	1.166-1	1.022 0	1.147 0	1.201 0	1.443 0
4.000 1	2.850 0	8.433-1	1.101-1	1.128-1	1.037 0	1.158 0	1.368 0	1.605 0
5.000 1	3.065 0	8.202-1	1.071-1	1.096-1	1.052 0	1.168 0	1.545 0	1.779 0
6.000 1	3.271 0	8.000-1	1.045-1	1.068-1	1.064 0	1.177 0	1.730 0	1.963 0
8.000 1	3.660 0	7.660-1	1.001-1	1.021-1	1.086 0	1.194 0	2.116 0	2.348 0
1.000 2	4.028 0	7.381-1	9.640-2	9.827-2	1.106 0	1.210 0	2.517 0	2.751 0
1.500 2	4.873 0	6.845-1	8.941-2	9.101-2	1.145 0	1.244 0	3.554 0	3.799 0
2.000 2	5.639 0	6.450-1	8.425-2	8.567-2	1.175 0	1.272 0	4.609 0	4.874 0
2.500 2	6.339 0	6.138-1	8.017-2	8.147-2	1.198 0	1.295 0	5.665 0	5.955 0
3.000 2	6.982 0	5.881-1	7.681-2	7.801-2	1.217 0	1.314 0	6.712 0	7.031 0
4.000 2	8.120 0	5.475-1	7.151-2	7.255-2	1.245 0	1.344 0	8.764 0	9.151 0
5.000 2	9.099 0	5.161-1	6.742-2	6.833-2	1.263 0	1.364 0	1.075 1	1.122 1
6.000 2	9.948 0	4.908-1	6.411-2	6.493-2	1.275 0	1.379 0	1.268 1	1.322 1
8.000 2	1.135 1	4.517-1	5.900-2	5.968-2	1.289 0	1.397 0	1.638 1	1.706 1
1.000 3	1.248 1	4.223-1	5.516-2	5.573-2	1.295 0	1.407 0	1.988 1	2.072 1

SATURATION CURVE

P	T	T/TC	VL	VG	SL	SG	EL	EG
1.025 0	1.095 1	1.000 0	5.223-1	5.223-1	2.815 0	2.815 0	1.011 1	1.011 1
1.000 0	1.082 1	9.875-1	4.647-1	5.879-1	2.795 0	2.818 0	9.945 0	1.007 1
8.000-1	9.849 0	8.991-1	3.691-1	7.616-1	2.700 0	2.788 0	9.045 0	9.605 0
6.000-1	9.018 0	8.232-1	3.240-1	9.295-1	2.612 0	2.765 0	8.250 0	9.270 0
5.000-1	8.629 0	7.877-1	3.064-1	1.042 0	2.567 0	2.758 0	7.865 0	9.146 0
4.000-1	8.244 0	7.526-1	2.904-1	1.200 0	2.520 0	2.755 0	7.476 0	9.048 0
3.000-1	7.848 0	7.164-1	2.751-1	1.454 0	2.469 0	2.757 0	7.066 0	8.975 0
2.500-1	7.638 0	6.972-1	2.673-1	1.663 0	2.440 0	2.761 0	6.844 0	8.946 0
2.000-1	7.410 0	6.764-1	2.591-1	2.000 0	2.407 0	2.767 0	6.600 0	8.923 0
1.500-1	7.146 0	6.523-1	2.499-1	2.676 0	2.367 0	2.780 0	6.314 0	8.898 0
1.000-1	6.790 0	6.199-1	2.379-1	4.681 0	2.311 0	2.808 0	5.922 0	8.850 0
8.000-2	6.586 0	6.013-1	2.314-1	6.618 0	2.277 0	2.827 0	5.695 0	8.809 0
6.000-2	6.317 0	5.766-1	2.230-1	9.987 0	2.230 0	2.854 0	5.393 0	8.746 0
5.000-2	6.146 0	5.611-1	2.179-1	1.264 1	2.199 0	2.870 0	5.202 0	8.705 0
4.000-2	5.943 0	5.425-1	2.121-1	1.652 1	2.162 0	2.891 0	4.975 0	8.656 0
3.000-2	5.693 0	5.197-1	2.053-1	2.276 1	2.114 0	2.918 0	4.697 0	8.597 0
2.500-2	5.543 0	5.060-1	2.013-1	2.760 1	2.084 0	2.935 0	4.531 0	8.562 0
2.000-2	5.368 0	4.901-1	1.968-1	3.469 1	2.049 0	2.957 0	4.339 0	8.521 0
1.500-2	5.158 0	4.709-1	1.917-1	4.616 1	2.005 0	2.985 0	4.110 0	8.472 0
1.000-2	4.888 0	4.462-1	1.853-1	6.821 1	1.948 0	3.026 0	3.819 0	8.410 0
8.000-3	4.751 0	4.337-1	1.823-1	8.423 1	1.918 0	3.049 0	3.674 0	8.379 0
6.000-3	4.586 0	4.187-1	1.787-1	1.102 2	1.881 0	3.080 0	3.502 0	8.341 0
5.000-3	4.488 0	4.097-1	1.766-1	1.305 2	1.858 0	3.099 0	3.401 0	8.319 0
4.000-3	4.374 0	3.993-1	1.743-1	1.604 2	1.832 0	3.124 0	3.284 0	8.293 0
3.000-3	4.237 0	3.867-1	1.715-1	2.090 2	1.800 0	3.155 0	3.145 0	8.262 0
2.500-3	4.154 0	3.792-1	1.699-1	2.470 2	1.780 0	3.176 0	3.063 0	8.243 0
2.000-3	4.058 0	3.704-1	1.681-1	3.030 2	1.757 0	3.201 0	2.968 0	8.221 0
1.500-3	3.941 0	3.598-1	1.659-1	3.942 2	1.728 0	3.234 0	2.854 0	8.195 0
1.000-3	3.789 0	3.459-1	1.632-1	5.711 2	1.691 0	3.280 0	2.708 0	8.160 0
8.000-4	3.711 0	3.387-1	1.618-1	7.005 2	1.671 0	3.306 0	2.634 0	8.142 0
6.000-4	3.615 0	3.300-1	1.602-1	9.115 2	1.647 0	3.340 0	2.544 0	8.121 0
5.000-4	3.557 0	3.247-1	1.592-1	1.077 3	1.632 0	3.362 0	2.491 0	8.107 0
4.000-4	3.489 0	3.185-1	1.581-1	1.322 3	1.614 0	3.389 0	2.429 0	8.092 0
3.000-4	3.406 0	3.109-1	1.568-1	1.721 3	1.592 0	3.423 0	2.354 0	8.073 0
2.500-4	3.355 0	3.063-1	1.560-1	2.035 3	1.579 0	3.445 0	2.309 0	8.062 0
2.000-4	3.296 0	3.009-1	1.550-1	2.499 3	1.563 0	3.472 0	2.256 0	8.048 0
1.500-4	3.222 0	2.942-1	1.539-1	3.258 3	1.543 0	3.507 0	2.191 0	8.031 0
1.000-4	3.125 0	2.853-1	1.524-1	4.738 3	1.517 0	3.557 0	2.107 0	8.009 0

Iron

SHOCK ADIABAT M= 1.050

P	T	V	S	E	D	U	CS	CV
1.000-4	2.930-1	1.210-1	-7.153-7	-2.331-7	.000 0	.000 0	4.436 0	4.597-1
1.000 1	3.944-1	1.150-1	9.322-2	6.019-2	3.662 0	3.470-1	4.950 0	4.653-1
1.500 1	4.503-1	1.126-1	1.368-1	1.081-1	4.098 0	4.650-1	5.163 0	4.678-1
2.000 1	5.105-1	1.105-1	1.793-1	1.651-1	4.422 0	5.747-1	5.357 0	4.703-1
2.500 1	5.758-1	1.087-1	2.211-1	2.298-1	4.686 0	6.779-1	5.534 0	4.730-1
3.000 1	6.461-1	1.070-1	2.619-1	3.010-1	4.912 0	7.759-1	5.697 0	4.756-1
4.000 1	8.017-1	1.040-1	3.406-1	4.601-1	5.298 0	9.592-1	5.993 0	4.813-1
5.000 1	9.760-1	1.016-1	4.145-1	6.372-1	5.627 0	1.129 0	6.255 0	4.873-1
6.000 1	1.168 0	9.940-2	4.835-1	8.294-1	5.919 0	1.288 0	6.492 0	4.935-1
8.000 1	1.597 0	9.582-2	6.076-1	1.249 0	6.430 0	1.581 0	6.907 0	5.063-1
1.000 2	2.079 0	9.291-2	7.154-1	1.707 0	6.877 0	1.848 0	7.266 0	5.190-1
1.500 2	3.455 0	8.746-2	9.324-1	2.969 0	7.821 0	2.437 0	8.005 0	5.474-1
2.000 2	5.013 0	8.354-2	1.100 0	4.351 0	8.614 0	2.950 0	8.602 0	5.694-1
2.326 2	6.103 0	8.150-2	1.191 0	5.298 0	9.078 0	3.255 0	8.941 0	5.804-1
2.326 2	6.103 0	8.150-2	1.191 0	5.298 0	9.078 0	3.255 0	8.837 0	2.723 0
2.500 2	6.339 0	8.073-2	1.240 0	5.790 0	9.334 0	3.403 0	9.021 0	2.828 0
2.731 2	6.643 0	7.979-2	1.305 0	6.453 0	9.659 0	3.593 0	9.248 0	2.979 0
2.731 2	6.643 0	7.979-2	1.305 0	6.453 0	9.659 0	3.593 0	9.332 0	6.565-1
3.000 2	7.514 0	7.854-2	1.370 0	7.278 0	9.991 0	3.815 0	9.557 0	6.700-1
4.000 2	1.086 1	7.467-2	1.574 0	1.048 1	1.110 1	4.578 0	1.029 1	7.080-1
5.000 2	1.436 1	7.167-2	1.735 0	1.385 1	1.207 1	5.262 0	1.090 1	7.338-1
6.000 2	1.797 1	6.922-2	1.870 0	1.735 1	1.294 1	5.890 0	1.142 1	7.534-1
8.000 2	2.543 1	6.537-2	2.086 0	2.467 1	1.447 1	7.025 0	1.229 1	7.859-1
1.000 3	3.309 1	6.236-2	2.257 0	3.235 1	1.580 1	8.043 0	1.300 1	8.154-1
1.500 3	5.259 1	5.686-2	2.577 0	5.264 1	1.857 1	1.026 1	1.444 1	8.768-1
2.000 3	7.241 1	5.304-2	2.814 0	7.402 1	2.089 1	1.217 1	1.565 1	9.161-1
2.500 3	9.262 1	5.023-2	3.005 0	9.603 1	2.292 1	1.386 1	1.674 1	9.401-1
3.000 3	1.132 2	4.813-2	3.167 0	1.184 2	2.477 1	1.539 1	1.778 1	9.597-1
4.000 3	1.548 2	4.527-2	3.432 0	1.636 2	2.810 1	1.809 1	1.973 1	1.020 0
5.000 3	1.948 2	4.343-2	3.646 0	2.091 2	3.107 1	2.045 1	2.148 1	1.126 0
6.000 3	2.318 2	4.209-2	3.826 0	2.549 2	3.376 1	2.258 1	2.301 1	1.265 0
8.000 3	2.966 2	4.009-2	4.126 0	3.478 2	3.854 1	2.638 1	2.555 1	1.559 0
1.000 4	3.525 2	3.861-2	4.376 0	4.422 2	4.272 1	2.974 1	2.767 1	1.818 0

Appendix A4
Nickel

MELTING CURVE

P	T	VS/VS0	VS	VL	SS	SL	ES	EL
1.000-4	1.730 0	1.000 0	1.201-1	1.276-1	8.263-1	9.983-1	6.874-1	9.849-1
5.000 0	1.941 0	9.733-1	1.169-1	1.239-1	8.549-1	1.026 0	7.475-1	1.045 0
6.000 0	1.982 0	9.685-1	1.163-1	1.232-1	8.601-1	1.031 0	7.608-1	1.059 0
8.000 0	2.062 0	9.594-1	1.152-1	1.220-1	8.699-1	1.041 0	7.883-1	1.088 0
1.000 1	2.140 0	9.508-1	1.142-1	1.208-1	8.791-1	1.051 0	8.170-1	1.118 0
1.500 1	2.328 0	9.313-1	1.119-1	1.182-1	9.002-1	1.072 0	8.931-1	1.198 0
2.000 1	2.508 0	9.140-1	1.098-1	1.159-1	9.187-1	1.091 0	9.741-1	1.285 0
2.500 1	2.681 0	8.985-1	1.079-1	1.138-1	9.353-1	1.109 0	1.059 0	1.377 0
3.000 1	2.848 0	8.843-1	1.062-1	1.120-1	9.503-1	1.125 0	1.147 0	1.472 0
4.000 1	3.168 0	8.594-1	1.032-1	1.087-1	9.766-1	1.153 0	1.331 0	1.671 0
5.000 1	3.469 0	8.378-1	1.006-1	1.059-1	9.989-1	1.178 0	1.521 0	1.879 0
6.000 1	3.755 0	8.189-1	9.835-2	1.034-1	1.018 0	1.199 0	1.715 0	2.092 0
8.000 1	4.284 0	7.866-1	9.448-2	9.912-2	1.050 0	1.234 0	2.111 0	2.529 0
1.000 2	4.765 0	7.598-1	9.126-2	9.556-2	1.074 0	1.262 0	2.511 0	2.974 0
1.500 2	5.795 0	7.078-1	8.501-2	8.860-2	1.116 0	1.311 0	3.505 0	4.093 0
2.000 2	6.632 0	6.688-1	8.033-2	8.337-2	1.142 0	1.342 0	4.478 0	5.197 0
2.500 2	7.326 0	6.379-1	7.661-2	7.921-2	1.158 0	1.363 0	5.425 0	6.275 0
3.000 2	7.911 0	6.123-1	7.354-2	7.579-2	1.169 0	1.377 0	6.347 0	7.323 0
4.000 2	8.841 0	5.719-1	6.869-2	7.042-2	1.180 0	1.395 0	8.125 0	9.335 0
5.000 2	9.550 0	5.408-1	6.495-2	6.633-2	1.183 0	1.404 0	9.830 0	1.125 1
6.000 2	1.011 1	5.157-1	6.194-2	6.307-2	1.183 0	1.408 0	1.148 1	1.308 1
8.000 2	1.095 1	4.771-1	5.730-2	5.811-2	1.176 0	1.410 0	1.463 1	1.654 1
1.000 3	1.155 1	4.481-1	5.382-2	5.444-2	1.167 0	1.407 0	1.765 1	1.980 1

SATURATION CURVE

P	T	T/TC	VL	VG	SL	SG	EL	EG
1.049 0	7.585 0	1.000 0	4.785-1	4.785-1	2.526 0	2.526 0	7.734 0	7.734 0
1.000 0	7.504 0	9.893-1	3.950-1	5.955-1	2.461 0	2.581 0	7.329 0	8.034 0
8.000-1	7.156 0	9.435-1	3.160-1	8.449-1	2.356 0	2.646 0	6.634 0	8.287 0
6.000-1	6.769 0	8.924-1	2.749-1	1.144 0	2.268 0	2.689 0	6.052 0	8.376 0
5.000-1	6.554 0	8.641-1	2.585-1	1.349 0	2.223 0	2.709 0	5.758 0	8.396 0
4.000-1	6.318 0	8.330-1	2.436-1	1.625 0	2.174 0	2.729 0	5.450 0	8.403 0
3.000-1	6.052 0	7.979-1	2.293-1	2.035 0	2.119 0	2.751 0	5.116 0	8.397 0
2.500-1	5.903 0	7.782-1	2.222-1	2.333 0	2.088 0	2.763 0	4.933 0	8.387 0
2.000-1	5.737 0	7.564-1	2.150-1	2.746 0	2.054 0	2.776 0	4.734 0	8.372 0
1.500-1	5.549 0	7.316-1	2.074-1	3.380 0	2.014 0	2.792 0	4.511 0	8.350 0
1.000-1	5.322 0	7.016-1	1.990-1	4.540 0	1.965 0	2.811 0	4.248 0	8.314 0
8.000-2	5.212 0	6.872-1	1.952-1	5.373 0	1.942 0	2.821 0	4.123 0	8.294 0
6.000-2	5.083 0	6.702-1	1.910-1	6.757 0	1.913 0	2.835 0	3.977 0	8.267 0
5.000-2	5.007 0	6.602-1	1.886-1	7.896 0	1.896 0	2.844 0	3.892 0	8.250 0
4.000-2	4.919 0	6.485-1	1.859-1	9.695 0	1.877 0	2.856 0	3.794 0	8.229 0
3.000-2	4.809 0	6.340-1	1.826-1	1.300 1	1.852 0	2.873 0	3.674 0	8.202 0
2.500-2	4.740 0	6.250-1	1.807-1	1.592 1	1.836 0	2.887 0	3.599 0	8.184 0
2.000-2	4.657 0	6.139-1	1.783-1	2.068 1	1.817 0	2.905 0	3.509 0	8.163 0
1.500-2	4.547 0	5.995-1	1.754-1	2.920 1	1.792 0	2.931 0	3.392 0	8.137 0
1.000-2	4.392 0	5.790-1	1.714-1	4.699 1	1.755 0	2.971 0	3.229 0	8.101 0
8.000-3	4.306 0	5.677-1	1.693-1	6.042 1	1.735 0	2.994 0	3.140 0	8.081 0
6.000-3	4.197 0	5.533-1	1.667-1	8.260 1	1.708 0	3.024 0	3.029 0	8.057 0
5.000-3	4.129 0	5.443-1	1.651-1	1.002 2	1.692 0	3.044 0	2.960 0	8.042 0
4.000-3	4.047 0	5.336-1	1.633-1	1.262 2	1.672 0	3.068 0	2.879 0	8.024 0
3.000-3	3.945 0	5.201-1	1.610-1	1.688 2	1.647 0	3.099 0	2.779 0	8.001 0
2.500-3	3.882 0	5.118-1	1.597-1	2.024 2	1.631 0	3.119 0	2.717 0	7.987 0
2.000-3	3.808 0	5.020-1	1.582-1	2.521 2	1.613 0	3.144 0	2.646 0	7.971 0
1.500-3	3.715 0	4.898-1	1.563-1	3.334 2	1.589 0	3.175 0	2.558 0	7.950 0
1.000-3	3.591 0	4.735-1	1.539-1	4.920 2	1.558 0	3.221 0	2.442 0	7.922 0
8.000-4	3.526 0	4.649-1	1.527-1	6.085 2	1.541 0	3.246 0	2.382 0	7.908 0
6.000-4	3.446 0	4.543-1	1.512-1	7.991 2	1.520 0	3.279 0	2.309 0	7.890 0
5.000-4	3.397 0	4.479-1	1.503-1	9.492 2	1.507 0	3.299 0	2.265 0	7.879 0
4.000-4	3.339 0	4.402-1	1.493-1	1.171 3	1.492 0	3.325 0	2.213 0	7.866 0
3.000-4	3.267 0	4.307-1	1.481-1	1.535 3	1.473 0	3.358 0	2.150 0	7.850 0
2.500-4	3.223 0	4.250-1	1.473-1	1.821 3	1.461 0	3.379 0	2.112 0	7.840 0
2.000-4	3.171 0	4.181-1	1.465-1	2.245 3	1.447 0	3.405 0	2.067 0	7.829 0
1.500-4	3.107 0	4.096-1	1.454-1	2.940 3	1.429 0	3.439 0	2.012 0	7.814 0
1.000-4	3.020 0	3.982-1	1.441-1	4.298 3	1.405 0	3.487 0	1.939 0	7.795 0

Nickel

SHOCK ADIABAT M= 1.000

P	T	V	S	E	D	U	CS	CV
1.000-4	2.930-1	1.120-1	-7.749-7	-2.346-7	.000 0	.000 0	4.556 0	4.264-1
1.000 1	3.235-1	1.068-1	4.165-3	2.579-2	4.931 0	2.272-1	5.055 0	4.268-1
1.500 1	3.415-1	1.048-1	1.190-2	5.431-2	5.097 0	3.296-1	5.264 0	4.271-1
2.000 1	3.631-1	1.029-1	2.422-2	9.089-2	5.253 0	4.264-1	5.454 0	4.275-1
2.500 1	3.885-1	1.012-1	4.073-2	1.344-1	5.401 0	5.184-1	5.629 0	4.279-1
3.000 1	4.180-1	9.975-2	6.086-2	1.838-1	5.542 0	6.063-1	5.791 0	4.284-1
4.000 1	4.904-1	9.711-2	1.095-1	2.979-1	5.804 0	7.719-1	6.085 0	4.295-1
5.000 1	5.802-1	9.485-2	1.647-1	4.289-1	6.047 0	9.261-1	6.347 0	4.308-1
6.000 1	6.871-1	9.287-2	2.228-1	5.738-1	6.273 0	1.071 0	6.584 0	4.322-1
8.000 1	9.493-1	8.957-2	3.376-1	8.973-1	6.689 0	1.340 0	7.004 0	4.351-1
1.000 2	1.271 0	8.687-2	4.440-1	1.257 0	7.065 0	1.585 0	7.369 0	4.381-1
1.500 2	2.288 0	8.176-2	6.637-1	2.268 0	7.888 0	2.130 0	8.126 0	4.465-1
2.000 2	3.549 0	7.805-2	8.315-1	3.395 0	8.597 0	2.606 0	8.739 0	4.557-1
2.500 2	4.994 0	7.517-2	9.646-1	4.603 0	9.228 0	3.034 0	9.262 0	4.654-1
3.000 2	6.579 0	7.283-2	1.074 0	5.875 0	9.802 0	3.428 0	9.721 0	4.755-1
3.553 2	8.458 0	7.068-2	1.176 0	7.341 0	1.039 1	3.832 0	1.017 1	4.871-1
3.553 2	8.458 0	7.068-2	1.176 0	7.341 0	1.039 1	3.832 0	1.016 1	4.934 0
4.000 2	8.841 0	6.928-2	1.254 0	8.543 0	1.084 1	4.134 0	1.042 1	6.040 0
4.870 2	9.468 0	6.681-2	1.403 0	1.100 1	1.163 1	4.691 0	1.088 1	8.567 0
4.870 2	9.468 0	6.681-2	1.403 0	1.100 1	1.163 1	4.691 0	1.089 1	7.084-1
5.000 2	9.812 0	6.644-2	1.424 0	1.139 1	1.173 1	4.773 0	1.096 1	7.125-1
6.000 2	1.251 1	6.393-2	1.573 0	1.442 1	1.251 1	5.371 0	1.151 1	7.374-1
8.000 2	1.822 1	5.999-2	1.813 0	2.081 1	1.389 1	6.451 0	1.244 1	7.648-1
1.000 3	2.431 1	5.700-2	2.003 0	2.750 1	1.510 1	7.417 0	1.323 1	7.763-1
1.500 3	4.094 1	5.184-2	2.356 0	4.512 1	1.769 1	9.500 0	1.486 1	7.941-1
2.000 3	5.870 1	4.844-2	2.610 0	6.356 1	1.987 1	1.128 1	1.617 1	8.351-1
2.500 3	7.652 1	4.595-2	2.809 0	8.257 1	2.179 1	1.285 1	1.729 1	9.012-1
3.000 3	9.379 1	4.399-2	2.975 0	1.020 2	2.352 1	1.428 1	1.828 1	9.803-1
4.000 3	1.261 2	4.106-2	3.246 0	1.419 2	2.659 1	1.685 1	1.999 1	1.146 0
5.000 3	1.558 2	3.892-2	3.468 0	1.827 2	2.930 1	1.912 1	2.146 1	1.300 0
6.000 3	1.833 2	3.730-2	3.660 0	2.241 2	3.174 1	2.117 1	2.278 1	1.437 0
8.000 3	2.340 2	3.498-2	3.986 0	3.081 2	3.610 1	2.482 1	2.511 1	1.668 0
1.000 4	2.803 2	3.342-2	4.262 0	3.929 2	3.996 1	2.803 1	2.716 1	1.856 0

Appendix A5

Copper

MELTING CURVE

P	T	VS/VS0	VS	VL	SS	SL	ES	EL
1.000-4	1.360 0	1.000 0	1.205-1	1.271-1	6.599-1	8.089-1	4.701-1	6.727-1
5.000 0	1.547 0	9.564-1	1.153-1	1.202-1	6.781-1	8.325-1	5.088-1	7.230-1
6.000 0	1.578 0	9.494-1	1.144-1	1.191-1	6.806-1	8.359-1	5.173-1	7.342-1
8.000 0	1.635 0	9.366-1	1.129-1	1.172-1	6.850-1	8.419-1	5.350-1	7.574-1
1.000 1	1.687 0	9.253-1	1.115-1	1.155-1	6.886-1	8.471-1	5.533-1	7.813-1
1.500 1	1.801 0	9.009-1	1.086-1	1.120-1	6.951-1	8.575-1	6.013-1	8.425-1
2.000 1	1.901 0	8.793-1	1.060-1	1.093-1	6.994-1	8.666-1	6.548-1	9.072-1
2.500 1	1.997 0	8.599-1	1.036-1	1.068-1	7.031-1	8.748-1	7.144-1	9.771-1
3.000 1	2.089 0	8.424-1	1.015-1	1.047-1	7.065-1	8.821-1	7.792-1	1.052 0
4.000 1	2.262 0	8.118-1	9.784-2	1.009-1	7.125-1	8.946-1	9.207-1	1.211 0
5.000 1	2.426 0	7.858-1	9.471-2	9.769-2	7.181-1	9.053-1	1.074 0	1.379 0
6.000 1	2.581 0	7.633-1	9.200-2	9.492-2	7.232-1	9.145-1	1.236 0	1.555 0
8.000 1	2.876 0	7.259-1	8.748-2	9.032-2	7.333-1	9.308-1	1.578 0	1.919 0
1.000 2	3.157 0	6.956-1	8.384-2	8.661-2	7.434-1	9.450-1	1.935 0	2.295 0
1.500 2	3.820 0	6.392-1	7.704-2	7.971-2	7.684-1	9.758-1	2.862 0	3.253 0
2.000 2	4.452 0	5.989-1	7.219-2	7.480-2	7.931-1	1.003 0	3.807 0	4.220 0
2.500 2	5.066 0	5.680-1	6.846-2	7.102-2	8.170-1	1.028 0	4.756 0	5.187 0
3.000 2	5.664 0	5.431-1	6.546-2	6.797-2	8.397-1	1.052 0	5.701 0	6.149 0
4.000 2	6.819 0	5.047-1	6.083-2	6.323-2	8.807-1	1.094 0	7.564 0	8.057 0
5.000 2	7.916 0	4.758-1	5.734-2	5.963-2	9.159-1	1.130 0	9.383 0	9.937 0
6.000 2	8.951 0	4.528-1	5.457-2	5.673-2	9.456-1	1.161 0	1.115 1	1.178 1
8.000 2	1.083 1	4.177-1	5.035-2	5.225-2	9.914-1	1.209 0	1.454 1	1.537 1
1.000 3	1.245 1	3.915-1	4.719-2	4.885-2	1.023 0	1.243 0	1.774 1	1.882 1

SATURATION CURVE

P	T	T/TC	VL	VG	SL	SG	EL	EG
9.375-1	7.946 0	1.000 0	4.353-1	4.353-1	1.979 0	1.979 0	5.554 0	5.554 0
8.000-1	7.664 0	9.645-1	3.229-1	6.485-1	1.896 0	2.050 0	5.002 0	5.919 0
6.000-1	7.215 0	9.080-1	2.752-1	9.122-1	1.830 0	2.096 0	4.542 0	6.080 0
5.000-1	6.966 0	8.767-1	2.581-1	1.090 0	1.797 0	2.117 0	4.319 0	6.134 0
4.000-1	6.693 0	8.423-1	2.428-1	1.330 0	1.762 0	2.139 0	4.088 0	6.175 0
3.000-1	6.384 0	8.034-1	2.285-1	1.685 0	1.723 0	2.162 0	3.838 0	6.203 0
2.500-1	6.211 0	7.816-1	2.214-1	1.943 0	1.701 0	2.175 0	3.702 0	6.211 0
2.000-1	6.019 0	7.574-1	2.143-1	2.300 0	1.677 0	2.188 0	3.554 0	6.214 0
1.500-1	5.799 0	7.298-1	2.067-1	2.845 0	1.648 0	2.203 0	3.388 0	6.209 0
1.000-1	5.534 0	6.965-1	1.985-1	3.834 0	1.614 0	2.221 0	3.192 0	6.192 0
8.000-2	5.406 0	6.804-1	1.947-1	4.538 0	1.597 0	2.231 0	3.099 0	6.179 0
6.000-2	5.256 0	6.615-1	1.906-1	5.702 0	1.576 0	2.242 0	2.991 0	6.159 0
5.000-2	5.168 0	6.504-1	1.882-1	6.656 0	1.564 0	2.249 0	2.928 0	6.145 0
4.000-2	5.065 0	6.375-1	1.855-1	8.167 0	1.550 0	2.259 0	2.855 0	6.127 0
3.000-2	4.938 0	6.215-1	1.823-1	1.098 1	1.532 0	2.273 0	2.766 0	6.101 0
2.500-2	4.859 0	6.114-1	1.804-1	1.352 1	1.521 0	2.283 0	2.711 0	6.083 0
2.000-2	4.760 0	5.991-1	1.780-1	1.774 1	1.507 0	2.298 0	2.643 0	6.060 0
1.500-2	4.631 0	5.828-1	1.751-1	2.546 1	1.488 0	2.320 0	2.554 0	6.030 0
1.000-2	4.444 0	5.593-1	1.710-1	4.168 1	1.460 0	2.354 0	2.428 0	5.988 0
8.000-3	4.341 0	5.463-1	1.688-1	5.387 1	1.444 0	2.374 0	2.360 0	5.966 0
6.000-3	4.209 0	5.297-1	1.662-1	7.390 1	1.424 0	2.400 0	2.273 0	5.939 0
5.000-3	4.127 0	5.194-1	1.645-1	8.967 1	1.411 0	2.417 0	2.220 0	5.922 0
4.000-3	4.029 0	5.070-1	1.627-1	1.129 2	1.396 0	2.438 0	2.156 0	5.903 0
3.000-3	3.907 0	4.917-1	1.604-1	1.509 2	1.376 0	2.465 0	2.079 0	5.878 0
2.500-3	3.832 0	4.823-1	1.591-1	1.807 2	1.364 0	2.482 0	2.031 0	5.864 0
2.000-3	3.744 0	4.711-1	1.575-1	2.246 2	1.349 0	2.503 0	1.976 0	5.846 0
1.500-3	3.635 0	4.574-1	1.557-1	2.961 2	1.331 0	2.531 0	1.908 0	5.825 0
1.000-3	3.490 0	4.392-1	1.533-1	4.349 2	1.306 0	2.570 0	1.820 0	5.797 0
8.000-4	3.415 0	4.297-1	1.521-1	5.364 2	1.293 0	2.592 0	1.774 0	5.782 0
6.000-4	3.322 0	4.181-1	1.506-1	7.020 2	1.276 0	2.621 0	1.718 0	5.764 0
5.000-4	3.266 0	4.110-1	1.498-1	8.319 2	1.266 0	2.639 0	1.685 0	5.753 0
4.000-4	3.200 0	4.027-1	1.488-1	1.024 3	1.254 0	2.662 0	1.646 0	5.740 0
3.000-4	3.118 0	3.924-1	1.476-1	1.337 3	1.239 0	2.691 0	1.598 0	5.724 0
2.500-4	3.069 0	3.862-1	1.469-1	1.583 3	1.230 0	2.709 0	1.569 0	5.715 0
2.000-4	3.010 0	3.788-1	1.460-1	1.946 3	1.219 0	2.732 0	1.535 0	5.703 0
1.500-4	2.938 0	3.697-1	1.450-1	2.539 3	1.205 0	2.762 0	1.494 0	5.689 0
1.000-4	2.842 0	3.577-1	1.437-1	3.695 3	1.186 0	2.804 0	1.439 0	5.670 0

Copper

SHOCK ADIABAT M= 1.000

P	T	V	S	E	D	U	CS	CV
1.000-4	2.930-1	1.120-1	3.368-6	9.800-7	.000 0	.000 0	3.867 0	3.903-1
1.000 1	3.354-1	1.054-1	6.367-3	3.323-2	4.347 0	2.577-1	4.423 0	3.907-1
1.500 1	3.614-1	1.027-1	1.658-2	6.952-2	4.507 0	3.728-1	4.595 0	3.911-1
2.000 1	3.929-1	1.004-1	3.230-2	1.157-1	4.656 0	4.811-1	4.754 0	3.915-1
2.500 1	4.307-1	9.838-2	5.295-2	1.703-1	4.798 0	5.836-1	4.901 0	3.919-1
3.000 1	4.751-1	9.654-2	7.759-2	2.320-1	4.933 0	6.811-1	5.040 0	3.925-1
4.000 1	5.846-1	9.336-2	1.347-1	3.728-1	5.189 0	8.634-1	5.295 0	3.938-1
5.000 1	7.211-1	9.070-2	1.967-1	5.325-1	5.427 0	1.032 0	5.526 0	3.953-1
6.000 1	8.836-1	8.843-2	2.591-1	7.073-1	5.650 0	1.189 0	5.737 0	3.972-1
8.000 1	1.279 0	8.471-2	3.765-1	1.092 0	6.064 0	1.478 0	6.114 0	4.022-1
1.000 2	1.755 0	8.175-2	4.802-1	1.512 0	6.440 0	1.739 0	6.445 0	4.088-1
1.500 2	3.201 0	7.636-2	6.855-1	2.673 0	7.266 0	2.312 0	7.133 0	4.308-1
1.805 2	4.209 0	7.391-2	7.836-1	3.438 0	7.711 0	2.622 0	7.485 0	4.459-1
1.805 2	4.209 0	7.391-2	7.836-1	3.438 0	7.711 0	2.622 0	7.405 0	2.647 0
2.000 2	4.452 0	7.286-2	8.474-1	3.914 0	8.006 0	2.798 0	7.660 0	2.606 0
2.500 2	5.065 0	7.080-2	1.010 0	5.150 0	8.725 0	3.209 0	8.279 0	2.526 0
2.566 2	5.144 0	7.058-2	1.031 0	5.313 0	8.815 0	3.260 0	8.357 0	2.518 0
2.566 2	5.144 0	7.058-2	1.031 0	5.313 0	8.815 0	3.260 0	8.477 0	5.373-1
3.000 2	6.581 0	6.871-2	1.145 0	6.493 0	9.324 0	3.604 0	8.878 0	5.651-1
4.000 2	9.997 0	6.533-2	1.348 0	9.335 0	1.037 1	4.321 0	9.657 0	6.066-1
5.000 2	1.358 1	6.277-2	1.504 0	1.231 1	1.129 1	4.962 0	1.030 1	6.247-1
6.000 2	1.734 1	6.073-2	1.631 0	1.538 1	1.212 1	5.546 0	1.085 1	6.298-1
8.000 2	2.539 1	5.765-2	1.831 0	2.174 1	1.359 1	6.594 0	1.176 1	6.276-1
1.000 3	3.402 1	5.536-2	1.985 0	2.832 1	1.488 1	7.527 0	1.249 1	6.265-1
1.500 3	5.700 1	5.132-2	2.259 0	4.551 1	1.761 1	9.541 0	1.389 1	6.475-1
2.000 3	8.042 1	4.853-2	2.451 0	6.347 1	1.988 1	1.127 1	1.494 1	6.987-1
2.500 3	1.031 2	4.638-2	2.601 0	8.203 1	2.186 1	1.281 1	1.578 1	7.674-1
3.000 3	1.247 2	4.462-2	2.726 0	1.011 2	2.363 1	1.422 1	1.646 1	8.421-1
4.000 3	1.647 2	4.181-2	2.931 0	1.404 2	2.674 1	1.676 1	1.750 1	9.927-1
4.590 3	1.865 2	4.043-2	3.033 0	1.642 2	2.836 1	1.812 1	1.797 1	1.081 0
5.000 3	2.010 2	3.955-2	3.099 0	1.811 2	2.942 1	1.903 1	1.825 1	1.142 0
6.000 3	2.342 2	3.762-2	3.243 0	2.232 2	3.181 1	2.113 1	1.885 1	1.291 0
8.000 3	2.934 2	3.443-2	3.489 0	3.103 2	3.597 1	2.491 1	1.997 1	1.580 0
1.000 4	3.453 2	3.199-2	3.702 0	4.001 2	3.960 1	2.829 1	2.124 1	1.843 0

Appendix A6

Molibdenum

MELTING CURVE

P	T	VS/VS0	VS	VL	SS	SL	ES	EL
1.000-4	2.890 0	1.000 0	1.020-1	1.066-1	6.213-1	7.573-1	7.195-1	1.113 0
5.000 0	3.053 0	9.820-1	1.002-1	1.043-1	6.295-1	7.592-1	7.486-1	1.124 0
6.000 0	3.084 0	9.786-1	9.982-2	1.038-1	6.311-1	7.597-1	7.553-1	1.128 0
8.000 0	3.146 0	9.720-1	9.916-2	1.030-1	6.341-1	7.605-1	7.692-1	1.136 0
1.000 1	3.206 0	9.657-1	9.851-2	1.022-1	6.369-1	7.615-1	7.840-1	1.146 0
1.500 1	3.354 0	9.509-1	9.700-2	1.005-1	6.436-1	7.638-1	8.248-1	1.176 0
2.000 1	3.497 0	9.371-1	9.559-2	9.889-2	6.497-1	7.664-1	8.705-1	1.212 0
2.500 1	3.637 0	9.242-1	9.427-2	9.743-2	6.555-1	7.690-1	9.206-1	1.254 0
3.000 1	3.775 0	9.120-1	9.303-2	9.607-2	6.610-1	7.716-1	9.748-1	1.301 0
4.000 1	4.046 0	8.899-1	9.077-2	9.360-2	6.711-1	7.768-1	1.093 0	1.408 0
5.000 1	4.310 0	8.700-1	8.875-2	9.140-2	6.804-1	7.819-1	1.223 0	1.528 0
6.000 1	4.569 0	8.520-1	8.691-2	8.942-2	6.889-1	7.869-1	1.362 0	1.659 0
8.000 1	5.072 0	8.205-1	8.369-2	8.598-2	7.040-1	7.964-1	1.659 0	1.945 0
1.000 2	5.559 0	7.935-1	8.094-2	8.306-2	7.171-1	8.055-1	1.976 0	2.255 0
1.500 2	6.727 0	7.395-1	7.543-2	7.730-2	7.442-1	8.262-1	2.823 0	3.095 0
2.000 2	7.838 0	6.980-1	7.120-2	7.293-2	7.656-1	8.448-1	3.715 0	3.991 0
2.500 2	8.903 0	6.646-1	6.779-2	6.942-2	7.835-1	8.616-1	4.630 0	4.918 0
3.000 2	9.926 0	6.366-1	6.494-2	6.651-2	7.988-1	8.768-1	5.556 0	5.860 0
4.000 2	1.186 1	5.919-1	6.038-2	6.185-2	8.239-1	9.033-1	7.414 0	7.767 0
5.000 2	1.364 1	5.571-1	5.683-2	5.822-2	8.435-1	9.253-1	9.257 0	9.672 0
6.000 2	1.528 1	5.288-1	5.394-2	5.527-2	8.594-1	9.436-1	1.107 1	1.156 1
8.000 2	1.820 1	4.848-1	4.945-2	5.065-2	8.832-1	9.721-1	1.459 1	1.524 1
1.000 3	2.072 1	4.515-1	4.606-2	4.714-2	9.000-1	9.929-1	1.795 1	1.879 1

SATURATION CURVE

P	T	T/TC	VL	VG	SL	SG	EL	EG
5.878-1	1.521 1	1.000 0	6.358-1	6.358-1	1.617 0	1.617 0	8.320 0	8.320 0
5.000-1	1.442 1	9.480-1	3.738-1	1.163 0	1.559 0	1.646 0	7.607 0	8.471 0
4.000-1	1.351 1	8.878-1	2.880-1	1.689 0	1.510 0	1.660 0	6.956 0	8.422 0
3.000-1	1.254 1	8.243-1	2.326-1	2.466 0	1.453 0	1.674 0	6.243 0	8.344 0
2.500-1	1.202 1	7.900-1	2.108-1	3.052 0	1.421 0	1.683 0	5.847 0	8.297 0
2.000-1	1.145 1	7.528-1	1.915-1	3.900 0	1.384 0	1.695 0	5.419 0	8.243 0
1.500-1	1.081 1	7.109-1	1.744-1	5.256 0	1.341 0	1.710 0	4.947 0	8.178 0
1.000-1	1.005 1	6.605-1	1.587-1	7.839 0	1.289 0	1.733 0	4.412 0	8.096 0
8.000-2	9.678 0	6.362-1	1.526-1	9.701 0	1.265 0	1.745 0	4.168 0	8.054 0
6.000-2	9.244 0	6.076-1	1.465-1	1.270 1	1.236 0	1.762 0	3.896 0	8.004 0
5.000-2	8.991 0	5.910-1	1.433-1	1.504 1	1.219 0	1.772 0	3.743 0	7.974 0
4.000-2	8.701 0	5.720-1	1.400-1	1.846 1	1.200 0	1.786 0	3.575 0	7.938 0
3.000-2	8.357 0	5.493-1	1.364-1	2.399 1	1.178 0	1.803 0	3.383 0	7.896 0
2.500-2	8.154 0	5.360-1	1.345-1	2.830 1	1.164 0	1.814 0	3.273 0	7.870 0
2.000-2	7.920 0	5.206-1	1.324-1	3.463 1	1.149 0	1.828 0	3.149 0	7.840 0
1.500-2	7.640 0	5.022-1	1.301-1	4.487 1	1.130 0	1.846 0	3.005 0	7.804 0
1.000-2	7.279 0	4.785-1	1.274-1	6.462 1	1.106 0	1.872 0	2.827 0	7.756 0
8.000-3	7.096 0	4.665-1	1.261-1	7.898 1	1.094 0	1.887 0	2.740 0	7.732 0
6.000-3	6.875 0	4.519-1	1.246-1	1.023 2	1.079 0	1.906 0	2.636 0	7.703 0
5.000-3	6.743 0	4.432-1	1.237-1	1.206 2	1.071 0	1.918 0	2.575 0	7.685 0
4.000-3	6.588 0	4.331-1	1.228-1	1.474 2	1.060 0	1.932 0	2.505 0	7.664 0
3.000-3	6.400 0	4.207-1	1.216-1	1.911 2	1.047 0	1.952 0	2.421 0	7.638 0
2.500-3	6.287 0	4.133-1	1.210-1	2.253 2	1.039 0	1.964 0	2.372 0	7.623 0
2.000-3	6.154 0	4.045-1	1.203-1	2.757 2	1.030 0	1.979 0	2.314 0	7.605 0
1.500-3	5.992 0	3.939-1	1.194-1	3.579 2	1.019 0	1.999 0	2.245 0	7.583 0
1.000-3	5.779 0	3.799-1	1.183-1	5.174 2	1.003 0	2.027 0	2.156 0	7.554 0
8.000-4	5.668 0	3.726-1	1.177-1	6.341 2	9.955-1	2.043 0	2.110 0	7.538 0
6.000-4	5.533 0	3.637-1	1.170-1	8.247 2	9.856-1	2.063 0	2.055 0	7.520 0
5.000-4	5.450 0	3.583-1	1.166-1	9.744 2	9.796-1	2.076 0	2.022 0	7.509 0
4.000-4	5.353 0	3.519-1	1.162-1	1.195 3	9.724-1	2.091 0	1.983 0	7.495 0
3.000-4	5.233 0	3.440-1	1.156-1	1.557 3	9.635-1	2.112 0	1.936 0	7.479 0
2.500-4	5.160 0	3.392-1	1.153-1	1.841 3	9.580-1	2.125 0	1.907 0	7.469 0
2.000-4	5.074 0	3.335-1	1.149-1	2.261 3	9.514-1	2.141 0	1.873 0	7.457 0
1.500-4	4.967 0	3.265-1	1.144-1	2.949 3	9.432-1	2.162 0	1.832 0	7.443 0
1.000-4	4.824 0	3.171-1	1.138-1	4.291 3	9.321-1	2.191 0	1.778 0	7.423 0

Molibdenum

SHOCK ADIABAT M= 1.000

P	T	V	S	E	D	U	CS	CV
1.000-4	2.930-1	9.780-2	7.153-7	2.082-7	.000 0	.000 0	5.117 0	2.610-1
1.000 1	3.117-1	9.445-2	1.552-3	1.674-2	5.344 0	1.830-1	5.378 0	2.610-1
1.500 1	3.238-1	9.297-2	4.782-3	3.622-2	5.451 0	2.692-1	5.496 0	2.610-1
2.000 1	3.388-1	9.160-2	1.025-2	6.200-2	5.554 0	3.522-1	5.608 0	2.610-1
2.500 1	3.574-1	9.032-2	1.821-2	9.350-2	5.654 0	4.324-1	5.714 0	2.610-1
3.000 1	3.801-1	8.913-2	2.854-2	1.301-1	5.752 0	5.101-1	5.815 0	2.610-1
4.000 1	4.389-1	8.695-2	5.543-2	2.170-1	5.939 0	6.587-1	6.004 0	2.610-1
5.000 1	5.172-1	8.502-2	8.847-2	3.195-1	6.118 0	7.993-1	6.179 0	2.611-1
6.000 1	6.159-1	8.329-2	1.252-1	4.353-1	6.289 0	9.331-1	6.342 0	2.614-1
8.000 1	8.750-1	8.030-2	2.012-1	7.002-1	6.612 0	1.183 0	6.636 0	2.631-1
1.000 2	1.212 0	7.778-2	2.738-1	1.001 0	6.912 0	1.415 0	6.898 0	2.668-1
1.500 2	2.343 0	7.286-2	4.259-1	1.870 0	7.585 0	1.934 0	7.454 0	2.773-1
2.000 2	3.826 0	6.922-2	5.428-1	2.859 0	8.181 0	2.391 0	7.921 0	2.857-1
2.500 2	5.597 0	6.637-2	6.356-1	3.929 0	8.722 0	2.803 0	8.326 0	2.930-1
3.000 2	7.600 0	6.405-2	7.117-1	5.062 0	9.221 0	3.182 0	8.683 0	3.002-1
3.912 2	1.169 1	6.073-2	8.219-1	7.251 0	1.005 1	3.808 0	9.245 0	3.146-1
3.912 2	1.169 1	6.073-2	8.219-1	7.251 0	1.005 1	3.808 0	9.064 0	1.506 0
4.000 2	1.186 1	6.054-2	8.325-1	7.452 0	1.013 1	3.861 0	9.124 0	1.519 0
4.745 2	1.320 1	5.908-2	9.200-1	9.187 0	1.083 1	4.286 0	9.592 0	1.641 0
4.745 2	1.320 1	5.908-2	9.200-1	9.187 0	1.083 1	4.286 0	9.769 0	3.849-1
5.000 2	1.428 1	5.844-2	9.451-1	9.840 0	1.102 1	4.436 0	9.890 0	3.909-1
6.000 2	1.860 1	5.622-2	1.032 0	1.247 1	1.175 1	4.995 0	1.033 1	4.112-1
8.000 2	2.756 1	5.271-2	1.168 0	1.804 1	1.303 1	6.006 0	1.106 1	4.419-1
1.000 3	3.684 1	5.002-2	1.276 0	2.389 1	1.415 1	6.912 0	1.169 1	4.663-1
1.500 3	6.065 1	4.531-2	1.478 0	3.937 1	1.653 1	8.873 0	1.296 1	5.262-1
2.000 3	8.412 1	4.214-2	1.627 0	5.566 1	1.854 1	1.055 1	1.399 1	5.952-1
2.500 3	1.065 2	3.979-2	1.749 0	7.251 1	2.030 1	1.204 1	1.487 1	6.699-1
3.000 3	1.275 2	3.794-2	1.854 0	8.979 1	2.189 1	1.340 1	1.565 1	7.455-1
4.000 3	1.661 2	3.517-2	2.030 0	1.253 2	2.472 1	1.583 1	1.701 1	8.901-1
5.000 3	2.010 2	3.316-2	2.179 0	1.616 2	2.720 1	1.798 1	1.819 1	1.021 0
6.000 3	2.331 2	3.162-2	2.311 0	1.985 2	2.945 1	1.993 1	1.926 1	1.138 0
8.000 3	2.912 2	2.944-2	2.539 0	2.735 2	3.346 1	2.339 1	2.116 1	1.338 0
1.000 4	3.437 2	2.796-2	2.736 0	3.492 2	3.701 1	2.643 1	2.287 1	1.502 0

Appendix A7

Tantalum

MELTING CURVE

P	T	VS/VS0	VS	VL	SS	SL	ES	EL
1.000-4	3.290 0	1.000 0	6.423-2	6.797-2	3.624-1	4.234-1	4.730-1	6.737-1
5.000 0	3.585 0	9.740-1	6.256-2	6.589-2	3.714-1	4.302-1	5.080-1	7.020-1
6.000 0	3.641 0	9.692-1	6.225-2	6.552-2	3.731-1	4.315-1	5.158-1	7.088-1
8.000 0	3.751 0	9.600-1	6.166-2	6.481-2	3.763-1	4.341-1	5.319-1	7.234-1
1.000 1	3.859 0	9.513-1	6.110-2	6.414-2	3.794-1	4.366-1	5.487-1	7.390-1
1.500 1	4.118 0	9.311-1	5.981-2	6.263-2	3.866-1	4.427-1	5.934-1	7.820-1
2.000 1	4.364 0	9.128-1	5.863-2	6.129-2	3.930-1	4.483-1	6.413-1	8.294-1
2.500 1	4.600 0	8.960-1	5.755-2	6.008-2	3.989-1	4.536-1	6.917-1	8.802-1
3.000 1	4.827 0	8.806-1	5.656-2	5.898-2	4.042-1	4.585-1	7.440-1	9.335-1
4.000 1	5.256 0	8.530-1	5.479-2	5.701-2	4.134-1	4.671-1	8.521-1	1.045 0
5.000 1	5.655 0	8.291-1	5.325-2	5.529-2	4.210-1	4.742-1	9.629-1	1.162 0
6.000 1	6.024 0	8.078-1	5.189-2	5.378-2	4.273-1	4.801-1	1.074 0	1.279 0
8.000 1	6.692 0	7.717-1	4.957-2	5.120-2	4.368-1	4.892-1	1.296 0	1.516 0
1.000 2	7.277 0	7.416-1	4.763-2	4.907-2	4.433-1	4.955-1	1.515 0	1.752 0
1.500 2	8.470 0	6.833-1	4.389-2	4.497-2	4.519-1	5.041-1	2.045 0	2.325 0
2.000 2	9.391 0	6.399-1	4.110-2	4.195-2	4.548-1	5.072-1	2.556 0	2.877 0
2.500 2	1.012 1	6.056-1	3.890-2	3.959-2	4.549-1	5.078-1	3.051 0	3.411 0
3.000 2	1.072 1	5.775-1	3.709-2	3.767-2	4.537-1	5.070-1	3.533 0	3.930 0
4.000 2	1.165 1	5.335-1	3.427-2	3.469-2	4.494-1	5.037-1	4.466 0	4.927 0
5.000 2	1.234 1	5.001-1	3.212-2	3.246-2	4.443-1	4.996-1	5.364 0	5.880 0
6.000 2	1.288 1	4.736-1	3.042-2	3.069-2	4.391-1	4.954-1	6.232 0	6.795 0
8.000 2	1.368 1	4.335-1	2.784-2	2.804-2	4.296-1	4.877-1	7.895 0	8.535 0
1.000 3	1.425 1	4.040-1	2.595-2	2.610-2	4.213-1	4.809-1	9.477 0	1.018 1

SATURATION CURVE

P	T	T/TC	VL	VG	SL	SG	EL	EG
7.756-1	1.426 1	1.000 0	2.592-1	2.592-1	9.528-1	9.528-1	5.099 0	5.099 0
6.000-1	1.354 1	9.491-1	1.823-1	4.081-1	9.130-1	9.668-1	4.599 0	5.190 0
5.000-1	1.311 1	9.192-1	1.667-1	4.815-1	8.962-1	9.686-1	4.382 0	5.174 0
4.000-1	1.267 1	8.879-1	1.541-1	5.730-1	8.788-1	9.703-1	4.164 0	5.155 0
3.000-1	1.219 1	8.546-1	1.431-1	7.016-1	8.601-1	9.723-1	3.936 0	5.136 0
2.500-1	1.193 1	8.366-1	1.379-1	7.923-1	8.498-1	9.736-1	3.813 0	5.126 0
2.000-1	1.166 1	8.173-1	1.327-1	9.163-1	8.386-1	9.750-1	3.682 0	5.116 0
1.500-1	1.135 1	7.960-1	1.274-1	1.105 0	8.260-1	9.769-1	3.538 0	5.105 0
1.000-1	1.100 1	7.711-1	1.217-1	1.462 0	8.109-1	9.795-1	3.370 0	5.090 0
8.000-2	1.083 1	7.592-1	1.191-1	1.744 0	8.035-1	9.810-1	3.289 0	5.082 0
6.000-2	1.062 1	7.449-1	1.161-1	2.320 0	7.945-1	9.836-1	3.193 0	5.069 0
5.000-2	1.050 1	7.358-1	1.142-1	2.994 0	7.887-1	9.860-1	3.132 0	5.059 0
4.000-2	1.032 1	7.234-1	1.118-1	4.684 0	7.807-1	9.914-1	3.049 0	5.040 0
3.000-2	1.004 1	7.037-1	1.081-1	8.378 0	7.678-1	1.001 0	2.918 0	5.008 0
2.500-2	9.838 0	6.897-1	1.057-1	1.124 1	7.585-1	1.007 0	2.826 0	4.989 0
2.000-2	9.585 0	6.720-1	1.027-1	1.532 1	7.467-1	1.014 0	2.711 0	4.966 0
1.500-2	9.259 0	6.491-1	9.924-2	2.181 1	7.313-1	1.023 0	2.566 0	4.938 0
1.000-2	8.819 0	6.183-1	9.496-2	3.416 1	7.103-1	1.035 0	2.376 0	4.903 0
8.000-3	8.591 0	6.023-1	9.293-2	4.310 1	6.994-1	1.043 0	2.281 0	4.885 0
6.000-3	8.311 0	5.826-1	9.061-2	5.759 1	6.859-1	1.052 0	2.167 0	4.863 0
5.000-3	8.142 0	5.708-1	8.929-2	6.892 1	6.778-1	1.058 0	2.100 0	4.851 0
4.000-3	7.945 0	5.570-1	8.783-2	8.559 1	6.683-1	1.065 0	2.024 0	4.836 0
3.000-3	7.705 0	5.402-1	8.615-2	1.127 2	6.567-1	1.075 0	1.933 0	4.818 0
2.500-3	7.561 0	5.301-1	8.519-2	1.340 2	6.497-1	1.081 0	1.880 0	4.808 0
2.000-3	7.392 0	5.182-1	8.412-2	1.653 2	6.415-1	1.089 0	1.818 0	4.796 0
1.500-3	7.186 0	5.038-1	8.287-2	2.163 2	6.315-1	1.099 0	1.746 0	4.781 0
1.000-3	6.916 0	4.849-1	8.134-2	3.154 2	6.184-1	1.113 0	1.653 0	4.761 0
8.000-4	6.777 0	4.751-1	8.060-2	3.880 2	6.116-1	1.121 0	1.606 0	4.751 0
6.000-4	6.607 0	4.632-1	7.972-2	5.064 2	6.032-1	1.132 0	1.551 0	4.739 0
5.000-4	6.504 0	4.560-1	7.921-2	5.995 2	5.982-1	1.138 0	1.517 0	4.732 0
4.000-4	6.383 0	4.475-1	7.862-2	7.370 2	5.922-1	1.147 0	1.479 0	4.723 0
3.000-4	6.234 0	4.371-1	7.792-2	9.617 2	5.848-1	1.157 0	1.432 0	4.713 0
2.500-4	6.144 0	4.307-1	7.751-2	1.138 3	5.803-1	1.164 0	1.405 0	4.706 0
2.000-4	6.037 0	4.233-1	7.704-2	1.400 3	5.750-1	1.172 0	1.372 0	4.699 0
1.500-4	5.906 0	4.140-1	7.648-2	1.827 3	5.684-1	1.183 0	1.333 0	4.690 0
1.000-4	5.731 0	4.018-1	7.575-2	2.662 3	5.596-1	1.199 0	1.282 0	4.677 0

Tantalum

SHOCK ADIABAT M= 1.000

P	T	V	S	E	D	U	CS	CV
1.000-4	2.930-1	6.000-2	-1.252-6	-3.731-7	.000 0	.000 0	3.410 0	1.380-1
1.000 1	3.222-1	5.724-2	1.659-3	1.378-2	3.612 0	1.661-1	3.637 0	1.380-1
1.500 1	3.420-1	5.607-2	4.959-3	2.950-2	3.706 0	2.429-1	3.739 0	1.380-1
2.000 1	3.675-1	5.501-2	1.035-2	4.994-2	3.797 0	3.161-1	3.835 0	1.380-1
2.500 1	3.995-1	5.404-2	1.770-2	7.455-2	3.885 0	3.861-1	3.925 0	1.380-1
3.000 1	4.388-1	5.315-2	2.681-2	1.028-1	3.970 0	4.535-1	4.011 0	1.380-1
4.000 1	5.411-1	5.157-2	4.879-2	1.687-1	4.132 0	5.809-1	4.172 0	1.381-1
5.000 1	6.757-1	5.020-2	7.348-2	2.451-1	4.285 0	7.001-1	4.318 0	1.386-1
6.000 1	8.419-1	4.900-2	9.879-2	3.301-1	4.431 0	8.125-1	4.453 0	1.402-1
8.000 1	1.253 0	4.696-2	1.467-1	5.215-1	4.700 0	1.021 0	4.692 0	1.464-1
1.000 2	1.747 0	4.528-2	1.895-1	7.360-1	4.946 0	1.213 0	4.907 0	1.538-1
1.500 2	3.289 0	4.210-2	2.771-1	1.342 0	5.493 0	1.638 0	5.391 0	1.660-1
2.000 2	5.239 0	3.988-2	3.447-1	2.012 0	5.982 0	2.006 0	5.810 0	1.719-1
2.500 2	7.539 0	3.823-2	3.985-1	2.722 0	6.430 0	2.333 0	6.175 0	1.751-1
3.000 2	1.012 1	3.695-2	4.425-1	3.457 0	6.845 0	2.630 0	6.498 0	1.779-1
3.137 2	1.087 1	3.665-2	4.532-1	3.663 0	6.954 0	2.707 0	6.581 0	1.787-1
3.137 2	1.087 1	3.665-2	4.532-1	3.663 0	6.954 0	2.707 0	6.573 0	3.120 0
3.830 2	1.151 1	3.514-2	5.044-1	4.761 0	7.447 0	3.086 0	6.835 0	4.403 0
3.830 2	1.151 1	3.514-2	5.044-1	4.761 0	7.447 0	3.086 0	6.844 0	2.156-1
4.000 2	1.234 1	3.483-2	5.172-1	5.034 0	7.564 0	3.173 0	6.923 0	2.177-1
5.000 2	1.735 1	3.327-2	5.817-1	6.682 0	8.207 0	3.656 0	7.341 0	2.298-1
6.000 2	2.250 1	3.202-2	6.333-1	8.395 0	8.786 0	4.098 0	7.699 0	2.421-1
8.000 2	3.291 1	3.006-2	7.142-1	1.198 1	9.807 0	4.894 0	8.305 0	2.670-1
1.000 3	4.320 1	2.855-2	7.775-1	1.572 1	1.070 1	5.608 0	8.821 0	2.919-1
1.500 3	6.766 1	2.589-2	8.973-1	2.559 1	1.258 1	7.154 0	9.883 0	3.544-1
2.000 3	9.012 1	2.407-2	9.887-1	3.593 1	1.416 1	8.477 0	1.075 1	4.141-1
2.500 3	1.109 2	2.272-2	1.065 0	4.660 1	1.554 1	9.654 0	1.151 1	4.679-1
3.000 3	1.304 2	2.167-2	1.131 0	5.749 1	1.679 1	1.072 1	1.218 1	5.151-1
4.000 3	1.666 2	2.016-2	1.246 0	7.969 1	1.901 1	1.262 1	1.339 1	5.925-1
5.000 3	2.003 2	1.912-2	1.343 0	1.022 2	2.098 1	1.430 1	1.446 1	6.542-1
6.000 3	2.322 2	1.838-2	1.429 0	1.249 2	2.278 1	1.580 1	1.544 1	7.073-1
8.000 3	2.913 2	1.741-2	1.578 0	1.704 2	2.600 1	1.846 1	1.723 1	8.028-1
1.000 4	3.451 2	1.683-2	1.705 0	2.159 2	2.888 1	2.078 1	1.882 1	8.923-1

Appendix A8

Tungsten

MELTING CURVE

P	T	VS/VS0	VS	VL	SS	SL	ES	EL
1.000-4	3.690 0	1.000 0	5.459-2	5.999-2	3.597-1	4.307-1	4.952-1	7.572-1
5.000 0	4.067 0	9.870-1	5.387-2	5.909-2	3.711-1	4.408-1	5.411-1	7.985-1
6.000 0	4.142 0	9.845-1	5.374-2	5.893-2	3.732-1	4.427-1	5.506-1	8.073-1
8.000 0	4.291 0	9.796-1	5.347-2	5.860-2	3.773-1	4.465-1	5.699-1	8.254-1
1.000 1	4.439 0	9.749-1	5.322-2	5.829-2	3.813-1	4.501-1	5.896-1	8.441-1
1.500 1	4.805 0	9.636-1	5.260-2	5.756-2	3.907-1	4.588-1	6.404-1	8.933-1
2.000 1	5.167 0	9.530-1	5.202-2	5.688-2	3.993-1	4.669-1	6.933-1	9.454-1
2.500 1	5.524 0	9.430-1	5.148-2	5.626-2	4.072-1	4.745-1	7.478-1	1.000 0
3.000 1	5.878 0	9.335-1	5.096-2	5.567-2	4.145-1	4.816-1	8.039-1	1.057 0
4.000 1	6.572 0	9.157-1	4.999-2	5.460-2	4.277-1	4.948-1	9.199-1	1.176 0
5.000 1	7.253 0	8.995-1	4.910-2	5.363-2	4.394-1	5.067-1	1.040 0	1.302 0
6.000 1	7.919 0	8.846-1	4.829-2	5.275-2	4.498-1	5.174-1	1.164 0	1.432 0
8.000 1	9.209 0	8.578-1	4.682-2	5.114-2	4.676-1	5.361-1	1.418 0	1.703 0
1.000 2	1.044 1	8.342-1	4.554-2	4.971-2	4.822-1	5.516-1	1.677 0	1.985 0
1.500 2	1.326 1	7.853-1	4.287-2	4.662-2	5.095-1	5.806-1	2.330 0	2.710 0
2.000 2	1.573 1	7.458-1	4.071-2	4.405-2	5.281-1	6.003-1	2.974 0	3.442 0
2.500 2	1.790 1	7.127-1	3.890-2	4.185-2	5.412-1	6.140-1	3.600 0	4.166 0
3.000 2	1.979 1	6.840-1	3.734-2	3.994-2	5.506-1	6.239-1	4.206 0	4.875 0
4.000 2	2.293 1	6.365-1	3.475-2	3.679-2	5.623-1	6.362-1	5.356 0	6.235 0
5.000 2	2.539 1	5.983-1	3.266-2	3.429-2	5.681-1	6.428-1	6.432 0	7.512 0
6.000 2	2.735 1	5.668-1	3.094-2	3.226-2	5.708-1	6.461-1	7.447 0	8.712 0
8.000 2	3.026 1	5.172-1	2.823-2	2.916-2	5.710-1	6.480-1	9.332 0	1.092 1
1.000 3	3.232 1	4.798-1	2.619-2	2.688-2	5.683-1	6.469-1	1.108 1	1.292 1

SATURATION CURVE

P	T	T/TC	VL	VG	SL	SG	EL	EG
1.074 0	1.512 1	1.000 0	2.105-1	2.105-1	9.040-1	9.040-1	5.073 0	5.073 0
1.000 0	1.492 1	9.866-1	1.706-1	2.701-1	8.838-1	9.194-1	4.809 0	5.242 0
8.000-1	1.434 1	9.481-1	1.421-1	3.683-1	8.574-1	9.317-1	4.449 0	5.334 0
6.000-1	1.369 1	9.053-1	1.255-1	4.968-1	8.332-1	9.403-1	4.122 0	5.366 0
5.000-1	1.333 1	8.814-1	1.187-1	5.920-1	8.202-1	9.447-1	3.950 0	5.372 0
4.000-1	1.292 1	8.547-1	1.122-1	7.320-1	8.059-1	9.495-1	3.765 0	5.373 0
3.000-1	1.245 1	8.235-1	1.059-1	9.699-1	7.892-1	9.555-1	3.555 0	5.367 0
2.000-1	1.185 1	7.839-1	9.899-2	1.490 0	7.677-1	9.644-1	3.296 0	5.349 0
1.500-1	1.145 1	7.575-1	9.502-2	2.073 0	7.532-1	9.715-1	3.128 0	5.331 0
1.000-1	1.091 1	7.218-1	9.024-2	3.350 0	7.333-1	9.825-1	2.906 0	5.299 0
8.000-2	1.063 1	7.027-1	8.793-2	4.342 0	7.225-1	9.890-1	2.790 0	5.280 0
6.000-2	1.026 1	6.788-1	8.527-2	6.000 0	7.090-1	9.976-1	2.649 0	5.256 0
5.000-2	1.004 1	6.642-1	8.374-2	7.317 0	7.007-1	1.003 0	2.564 0	5.241 0
4.000-2	9.781 0	6.469-1	8.203-2	9.268 0	6.907-1	1.010 0	2.466 0	5.223 0
3.000-2	9.459 0	6.256-1	8.006-2	1.246 1	6.784-1	1.019 0	2.347 0	5.201 0
2.000-2	9.035 0	5.975-1	7.768-2	1.866 1	6.621-1	1.032 0	2.197 0	5.171 0
1.500-2	8.755 0	5.790-1	7.621-2	2.468 1	6.512-1	1.042 0	2.100 0	5.152 0
1.000-2	8.388 0	5.547-1	7.443-2	3.637 1	6.369-1	1.056 0	1.977 0	5.126 0
8.000-3	8.199 0	5.422-1	7.356-2	4.491 1	6.295-1	1.063 0	1.916 0	5.113 0
6.000-3	7.968 0	5.270-1	7.255-2	5.883 1	6.204-1	1.073 0	1.842 0	5.097 0
5.000-3	7.829 0	5.177-1	7.196-2	6.976 1	6.149-1	1.079 0	1.799 0	5.087 0
4.000-3	7.665 0	5.069-1	7.129-2	8.588 1	6.084-1	1.087 0	1.748 0	5.076 0
3.000-3	7.465 0	4.937-1	7.050-2	1.122 2	6.004-1	1.097 0	1.688 0	5.062 0
2.500-3	7.344 0	4.857-1	7.004-2	1.328 2	5.955-1	1.104 0	1.652 0	5.054 0
2.000-3	7.201 0	4.762-1	6.951-2	1.633 2	5.897-1	1.112 0	1.610 0	5.044 0
1.500-3	7.026 0	4.647-1	6.888-2	2.132 2	5.826-1	1.122 0	1.559 0	5.032 0
1.000-3	6.795 0	4.494-1	6.808-2	3.102 2	5.732-1	1.137 0	1.494 0	5.016 0
8.000-4	6.674 0	4.414-1	6.767-2	3.813 2	5.682-1	1.145 0	1.461 0	5.007 0
6.000-4	6.526 0	4.316-1	6.719-2	4.977 2	5.621-1	1.156 0	1.420 0	4.997 0
5.000-4	6.436 0	4.256-1	6.690-2	5.893 2	5.584-1	1.163 0	1.396 0	4.991 0
4.000-4	6.329 0	4.186-1	6.657-2	7.248 2	5.539-1	1.171 0	1.367 0	4.983 0
3.000-4	6.197 0	4.098-1	6.616-2	9.466 2	5.483-1	1.182 0	1.333 0	4.974 0
2.500-4	6.116 0	4.045-1	6.592-2	1.121 3	5.449-1	1.189 0	1.312 0	4.969 0
2.000-4	6.021 0	3.982-1	6.564-2	1.380 3	5.409-1	1.197 0	1.287 0	4.962 0
1.500-4	5.902 0	3.904-1	6.530-2	1.804 3	5.358-1	1.208 0	1.257 0	4.954 0
1.000-4	5.744 0	3.799-1	6.485-2	2.633 3	5.290-1	1.223 0	1.217 0	4.943 0

Tungsten

SHOCK ADIABAT M= 1.000

P	T	V	S	E	D	U	CS	CV
1.000-4	2.930-1	5.190-2	-1.416-6	-4.109-7	.000 0	.000 0	4.014 0	1.360-1
1.000 1	3.097-1	5.034-2	6.262-4	7.781-3	4.162 0	1.247-1	4.180 0	1.360-1
1.500 1	3.200-1	4.964-2	1.913-3	1.692-2	4.232 0	1.840-1	4.256 0	1.360-1
2.000 1	3.326-1	4.899-2	4.156-3	2.913-2	4.301 0	2.413-1	4.329 0	1.360-1
2.500 1	3.479-1	4.837-2	7.458-3	4.413-2	4.368 0	2.971-1	4.399 0	1.360-1
3.000 1	3.665-1	4.779-2	1.180-2	6.166-2	4.433 0	3.512-1	4.467 0	1.360-1
4.000 1	4.149-1	4.672-2	2.361-2	1.036-1	4.560 0	4.553-1	4.594 0	1.360-1
5.000 1	4.793-1	4.575-2	3.863-2	1.536-1	4.681 0	5.543-1	4.713 0	1.360-1
6.000 1	5.613-1	4.488-2	5.585-2	2.106-1	4.798 0	6.490-1	4.824 0	1.360-1
8.000 1	7.796-1	4.335-2	9.299-2	3.420-1	5.020 0	8.271-1	5.029 0	1.363-1
1.000 2	1.070 0	4.205-2	1.297-1	4.928-1	5.228 0	9.928-1	5.213 0	1.370-1
1.500 2	2.084 0	3.947-2	2.089-1	9.326-1	5.701 0	1.366 0	5.612 0	1.406-1
2.000 2	3.450 0	3.752-2	2.706-1	1.438 0	6.121 0	1.696 0	5.951 0	1.444-1
2.500 2	5.107 0	3.599-2	3.196-1	1.989 0	6.506 0	1.995 0	6.250 0	1.485-1
3.000 2	6.997 0	3.473-2	3.599-1	2.575 0	6.861 0	2.269 0	6.518 0	1.529-1
4.000 2	1.128 1	3.278-2	4.234-1	3.824 0	7.507 0	2.765 0	6.983 0	1.628-1
5.000 2	1.600 1	3.130-2	4.724-1	5.149 0	8.086 0	3.209 0	7.382 0	1.739-1
6.000 2	2.093 1	3.012-2	5.125-1	6.534 0	8.615 0	3.615 0	7.731 0	1.862-1
7.818 2	3.004 1	2.845-2	5.712-1	9.167 0	9.476 0	4.282 0	8.276 0	2.102-1
7.818 2	3.004 1	2.845-2	5.712-1	9.167 0	9.476 0	4.282 0	8.273 0	2.291 0
8.000 2	3.026 1	2.830-2	5.763-1	9.441 0	9.555 0	4.345 0	8.302 0	2.416 0
1.000 3	3.232 1	2.675-2	6.321-1	1.257 1	1.035 1	5.015 0	8.616 0	4.012 0
1.052 3	3.276 1	2.639-2	6.464-1	1.342 1	1.054 1	5.180 0	8.698 0	4.489 0
1.052 3	3.276 1	2.639-2	6.464-1	1.342 1	1.054 1	5.180 0	8.703 0	2.684-1
1.500 3	5.136 1	2.401-2	7.548-1	2.092 1	1.204 1	6.468 0	9.554 0	3.085-1
2.000 3	7.152 1	2.219-2	8.469-1	2.971 1	1.347 1	7.708 0	1.034 1	3.563-1
2.500 3	9.057 1	2.085-2	9.224-1	3.881 1	1.473 1	8.810 0	1.101 1	4.051-1
3.000 3	1.085 2	1.981-2	9.874-1	4.814 1	1.587 1	9.812 0	1.160 1	4.519-1
4.000 3	1.416 2	1.827-2	1.098 0	6.726 1	1.790 1	1.160 1	1.265 1	5.349-1
5.000 3	1.721 2	1.719-2	1.192 0	8.677 1	1.970 1	1.317 1	1.357 1	6.035-1
6.000 3	2.007 2	1.640-2	1.274 0	1.065 2	2.134 1	1.459 1	1.440 1	6.609-1
8.000 3	2.540 2	1.533-2	1.417 0	1.463 2	2.427 1	1.711 1	1.592 1	7.553-1
1.000 4	3.031 2	1.466-2	1.539 0	1.862 2	2.689 1	1.930 1	1.730 1	8.360-1

Appendix A9

Gold

MELTING CURVE

P	T	VS/VS0	VS	VL	SS	SL	ES	EL
1.000-4	1.340 0	1.000 0	5.444-2	5.743-2	2.118-1	2.592-1	1.486-1	2.121-1
5.000 0	1.625 0	9.789-1	5.329-2	5.575-2	2.285-1	2.760-1	1.760-1	2.408-1
6.000 0	1.676 0	9.749-1	5.307-2	5.545-2	2.309-1	2.785-1	1.812-1	2.467-1
8.000 0	1.773 0	9.670-1	5.264-2	5.489-2	2.351-1	2.830-1	1.914-1	2.584-1
1.000 1	1.864 0	9.594-1	5.223-2	5.436-2	2.387-1	2.869-1	2.016-1	2.702-1
1.500 1	2.070 0	9.414-1	5.125-2	5.316-2	2.453-1	2.947-1	2.269-1	3.004-1
2.000 1	2.253 0	9.247-1	5.034-2	5.210-2	2.500-1	3.006-1	2.528-1	3.318-1
2.500 1	2.419 0	9.092-1	4.950-2	5.114-2	2.534-1	3.054-1	2.798-1	3.643-1
3.000 1	2.571 0	8.947-1	4.871-2	5.027-2	2.560-1	3.093-1	3.079-1	3.981-1
4.000 1	2.844 0	8.686-1	4.729-2	4.871-2	2.597-1	3.156-1	3.676-1	4.693-1
5.000 1	3.086 0	8.456-1	4.603-2	4.736-2	2.622-1	3.204-1	4.313-1	5.443-1
6.000 1	3.304 0	8.251-1	4.492-2	4.617-2	2.640-1	3.243-1	4.983-1	6.222-1
8.000 1	3.688 0	7.900-1	4.301-2	4.415-2	2.663-1	3.303-1	6.394-1	7.840-1
1.000 2	4.024 0	7.609-1	4.142-2	4.248-2	2.677-1	3.348-1	7.870-1	9.507-1
1.500 2	4.730 0	7.049-1	3.837-2	3.930-2	2.690-1	3.419-1	1.169 0	1.375 0
2.000 2	5.314 0	6.638-1	3.614-2	3.697-2	2.687-1	3.456-1	1.556 0	1.799 0
2.500 2	5.818 0	6.317-1	3.439-2	3.514-2	2.676-1	3.475-1	1.942 0	2.218 0
3.000 2	6.263 0	6.054-1	3.296-2	3.365-2	2.661-1	3.482-1	2.325 0	2.632 0
4.000 2	7.021 0	5.643-1	3.072-2	3.131-2	2.625-1	3.479-1	3.079 0	3.444 0
5.000 2	7.652 0	5.329-1	2.901-2	2.952-2	2.586-1	3.464-1	3.817 0	4.235 0
6.000 2	8.188 0	5.076-1	2.763-2	2.808-2	2.547-1	3.444-1	4.540 0	5.007 0
8.000 2	9.057 0	4.688-1	2.552-2	2.588-2	2.473-1	3.400-1	5.943 0	6.500 0
1.000 3	9.740 0	4.397-1	2.394-2	2.423-2	2.405-1	3.357-1	7.298 0	7.934 0

SATURATION CURVE

P	T	T/TC	VL	VG	SL	SG	EL	EG
7.568-1	9.007 0	1.000 0	1.514-1	1.514-1	6.336-1	6.336-1	1.933 0	1.933 0
6.000-1	8.653 0	9.607-1	1.149-1	2.256-1	6.079-1	6.548-1	1.731 0	2.070 0
5.000-1	8.408 0	9.335-1	1.069-1	2.674-1	5.980-1	6.612-1	1.651 0	2.102 0
4.000-1	8.142 0	9.040-1	1.006-1	3.208-1	5.883-1	6.669-1	1.573 0	2.125 0
3.000-1	7.843 0	8.708-1	9.516-2	3.987-1	5.778-1	6.725-1	1.491 0	2.143 0
2.500-1	7.676 0	8.522-1	9.255-2	4.562-1	5.720-1	6.754-1	1.447 0	2.149 0
2.000-1	7.489 0	8.315-1	8.994-2	5.391-1	5.656-1	6.785-1	1.399 0	2.154 0
1.500-1	7.273 0	8.075-1	8.722-2	6.779-1	5.581-1	6.821-1	1.344 0	2.157 0
1.000-1	6.997 0	7.768-1	8.414-2	1.002 0	5.485-1	6.873-1	1.276 0	2.155 0
8.000-2	6.848 0	7.603-1	8.262-2	1.333 0	5.433-1	6.909-1	1.240 0	2.151 0
6.000-2	6.643 0	7.375-1	8.068-2	2.126 0	5.360-1	6.975-1	1.191 0	2.141 0
5.000-2	6.499 0	7.215-1	7.941-2	2.889 0	5.308-1	7.024-1	1.157 0	2.132 0
4.000-2	6.310 0	7.006-1	7.788-2	4.057 0	5.240-1	7.086-1	1.113 0	2.119 0
3.000-2	6.060 0	6.728-1	7.601-2	5.943 0	5.149-1	7.164-1	1.057 0	2.102 0
2.500-2	5.901 0	6.552-1	7.493-2	7.396 0	5.090-1	7.213-1	1.022 0	2.091 0
2.000-2	5.711 0	6.341-1	7.371-2	9.508 0	5.019-1	7.272-1	9.809-1	2.079 0
1.500-2	5.476 0	6.080-1	7.232-2	1.290 1	4.930-1	7.349-1	9.311-1	2.063 0
1.000-2	5.167 0	5.737-1	7.063-2	1.937 1	4.810-1	7.459-1	8.671-1	2.043 0
8.000-3	5.009 0	5.561-1	6.983-2	2.405 1	4.747-1	7.521-1	8.350-1	2.033 0
6.000-3	4.817 0	5.348-1	6.890-2	3.160 1	4.669-1	7.602-1	7.967-1	2.020 0
5.000-3	4.702 0	5.220-1	6.837-2	3.749 1	4.622-1	7.654-1	7.741-1	2.013 0
4.000-3	4.568 0	5.071-1	6.777-2	4.612 1	4.565-1	7.719-1	7.481-1	2.004 0
3.000-3	4.405 0	4.891-1	6.707-2	6.012 1	4.496-1	7.803-1	7.170-1	1.994 0
2.500-3	4.308 0	4.783-1	6.667-2	7.104 1	4.454-1	7.857-1	6.986-1	1.987 0
2.000-3	4.195 0	4.657-1	6.621-2	8.708 1	4.404-1	7.925-1	6.773-1	1.980 0
1.500-3	4.057 0	4.505-1	6.567-2	1.131 2	4.342-1	8.012-1	6.518-1	1.971 0
1.000-3	3.878 0	4.306-1	6.498-2	1.635 2	4.259-1	8.138-1	6.191-1	1.960 0
8.000-4	3.787 0	4.204-1	6.464-2	2.001 2	4.216-1	8.208-1	6.026-1	1.954 0
6.000-4	3.675 0	4.080-1	6.424-2	2.598 2	4.163-1	8.299-1	5.826-1	1.947 0
5.000-4	3.607 0	4.005-1	6.400-2	3.065 2	4.130-1	8.357-1	5.706-1	1.942 0
4.000-4	3.528 0	3.917-1	6.372-2	3.754 2	4.091-1	8.429-1	5.567-1	1.937 0
3.000-4	3.432 0	3.810-1	6.339-2	4.875 2	4.042-1	8.523-1	5.399-1	1.931 0
2.500-4	3.373 0	3.745-1	6.319-2	5.755 2	4.013-1	8.582-1	5.298-1	1.927 0
2.000-4	3.305 0	3.669-1	6.296-2	7.053 2	3.977-1	8.656-1	5.179-1	1.923 0
1.500-4	3.220 0	3.575-1	6.268-2	9.170 2	3.933-1	8.751-1	5.035-1	1.917 0
1.000-4	3.109 0	3.451-1	6.232-2	1.329 3	3.874-1	8.887-1	4.847-1	1.910 0

Gold

SHOCK ADIABAT M= 1.000

P	T	V	S	E	D	U	CS	CV
1.000-4	2.930-1	5.180-2	-2.846-6	-8.327-7	.000 0	.000 0	3.019 0	1.270-1
1.000 1	3.454-1	4.930-2	2.013-3	1.250-2	3.277 0	1.581-1	3.353 0	1.270-1
1.500 1	3.780-1	4.830-2	5.600-3	2.625-2	3.392 0	2.291-1	3.492 0	1.270-1
2.000 1	4.173-1	4.742-2	1.109-2	4.380-2	3.500 0	2.960-1	3.619 0	1.270-1
2.500 1	4.642-1	4.664-2	1.822-2	6.456-2	3.604 0	3.593-1	3.736 0	1.270-1
3.000 1	5.193-1	4.593-2	2.659-2	8.805-2	3.703 0	4.197-1	3.845 0	1.270-1
4.000 1	6.551-1	4.471-2	4.577-2	1.418-1	3.891 0	5.326-1	4.044 0	1.270-1
5.000 1	8.250-1	4.368-2	6.620-2	2.029-1	4.066 0	6.371-1	4.223 0	1.272-1
6.000 1	1.028 0	4.280-2	8.647-2	2.699-1	4.230 0	7.347-1	4.384 0	1.280-1
8.000 1	1.511 0	4.135-2	1.238-1	4.181-1	4.532 0	9.144-1	4.658 0	1.331-1
1.000 2	2.061 0	4.015-2	1.559-1	5.824-1	4.800 0	1.079 0	4.882 0	1.416-1
1.500 2	3.603 0	3.784-2	2.203-1	1.047 0	5.369 0	1.447 0	5.359 0	1.588-1
1.974 2	5.286 0	3.624-2	2.687-1	1.536 0	5.835 0	1.753 0	5.769 0	1.657-1
1.974 2	5.286 0	3.624-2	2.687-1	1.536 0	5.835 0	1.753 0	5.769 0	1.767 0
2.000 2	5.314 0	3.617-2	2.711-1	1.564 0	5.859 0	1.768 0	5.788 0	1.784 0
2.500 2	5.818 0	3.487-2	3.181-1	2.117 0	6.294 0	2.058 0	6.132 0	2.115 0
2.812 2	6.101 0	3.418-2	3.480-1	2.477 0	6.543 0	2.226 0	6.320 0	2.326 0
2.812 2	6.101 0	3.418-2	3.480-1	2.477 0	6.543 0	2.226 0	6.321 0	1.812-1
3.000 2	6.836 0	3.380-2	3.654-1	2.701 0	6.687 0	2.324 0	6.443 0	1.820-1
4.000 2	1.118 1	3.217-2	4.403-1	3.926 0	7.394 0	2.802 0	7.017 0	1.798-1
5.000 2	1.623 1	3.101-2	4.959-1	5.198 0	8.033 0	3.224 0	7.490 0	1.747-1
6.000 2	2.185 1	3.011-2	5.391-1	6.508 0	8.615 0	3.608 0	7.884 0	1.718-1
8.000 2	3.407 1	2.873-2	6.031-1	9.230 0	9.645 0	4.296 0	8.509 0	1.744-1
1.000 3	4.675 1	2.763-2	6.498-1	1.209 1	1.054 1	4.917 0	9.001 0	1.845-1
1.500 3	7.737 1	2.550-2	7.316-1	1.972 1	1.237 1	6.281 0	9.958 0	2.242-1
2.000 3	1.051 2	2.390-2	7.908-1	2.790 1	1.387 1	7.470 0	1.073 1	2.703-1
2.500 3	1.302 2	2.264-2	8.395-1	3.646 1	1.517 1	8.539 0	1.142 1	3.162-1
3.000 3	1.531 2	2.162-2	8.821-1	4.527 1	1.633 1	9.516 0	1.204 1	3.602-1
4.000 3	1.942 2	2.008-2	9.560-1	6.345 1	1.839 1	1.126 1	1.315 1	4.409-1
5.000 3	2.308 2	1.896-2	1.020 0	8.210 1	2.021 1	1.281 1	1.413 1	5.120-1
6.000 3	2.641 2	1.811-2	1.078 0	1.011 2	2.186 1	1.422 1	1.500 1	5.746-1
8.000 3	3.240 2	1.691-2	1.181 0	1.396 2	2.481 1	1.671 1	1.655 1	6.790-1
1.000 4	3.780 2	1.610-2	1.271 0	1.785 2	2.742 1	1.889 1	1.791 1	7.621-1

Appendix A10

Lead

MELTING CURVE

P	T	VS/VS0	VS	VL	SS	SL	ES	EL
1.000-4	6.020-1	1.000 0	9.152-2	9.494-2	1.003-1	1.385-1	4.343-2	6.643-2
1.000 1	1.009 0	8.526-1	7.803-2	7.966-2	1.156-1	1.731-1	1.106-1	1.524-1
2.000 1	1.263 0	7.771-1	7.112-2	7.266-2	1.188-1	1.851-1	2.153-1	2.683-1
3.000 1	1.481 0	7.261-1	6.645-2	6.792-2	1.223-1	1.932-1	3.354-1	3.965-1
4.000 1	1.678 0	6.880-1	6.297-2	6.436-2	1.260-1	1.993-1	4.626-1	5.300-1
5.000 1	1.861 0	6.578-1	6.020-2	6.152-2	1.297-1	2.043-1	5.931-1	6.661-1
6.000 1	2.033 0	6.328-1	5.791-2	5.917-2	1.331-1	2.086-1	7.252-1	8.031-1
7.000 1	2.195 0	6.116-1	5.597-2	5.718-2	1.364-1	2.124-1	8.578-1	9.404-1
8.000 1	2.350 0	5.933-1	5.430-2	5.545-2	1.394-1	2.157-1	9.905-1	1.077 0
9.000 1	2.498 0	5.771-1	5.282-2	5.392-2	1.423-1	2.186-1	1.123 0	1.214 0
1.000 2	2.640 0	5.628-1	5.150-2	5.256-2	1.449-1	2.213-1	1.254 0	1.350 0
1.100 2	2.776 0	5.498-1	5.032-2	5.134-2	1.474-1	2.238-1	1.385 0	1.485 0
1.200 2	2.907 0	5.381-1	4.924-2	5.023-2	1.497-1	2.261-1	1.516 0	1.620 0
1.300 2	3.034 0	5.273-1	4.826-2	4.921-2	1.519-1	2.282-1	1.645 0	1.753 0
1.400 2	3.156 0	5.174-1	4.736-2	4.827-2	1.539-1	2.301-1	1.773 0	1.885 0
1.500 2	3.274 0	5.083-1	4.652-2	4.740-2	1.558-1	2.319-1	1.901 0	2.017 0
1.600 2	3.389 0	4.998-1	4.574-2	4.660-2	1.576-1	2.336-1	2.027 0	2.148 0
1.700 2	3.500 0	4.919-1	4.501-2	4.584-2	1.593-1	2.352-1	2.153 0	2.277 0
1.800 2	3.608 0	4.844-1	4.433-2	4.514-2	1.609-1	2.367-1	2.278 0	2.406 0
1.900 2	3.712 0	4.774-1	4.369-2	4.447-2	1.624-1	2.381-1	2.401 0	2.534 0
2.000 2	3.814 0	4.708-1	4.309-2	4.385-2	1.638-1	2.394-1	2.524 0	2.661 0
2.100 2	3.912 0	4.646-1	4.252-2	4.326-2	1.651-1	2.407-1	2.646 0	2.787 0
2.200 2	4.008 0	4.587-1	4.198-2	4.269-2	1.663-1	2.418-1	2.767 0	2.913 0
2.300 2	4.102 0	4.531-1	4.147-2	4.216-2	1.675-1	2.430-1	2.888 0	3.037 0
2.400 2	4.193 0	4.478-1	4.098-2	4.165-2	1.686-1	2.440-1	3.007 0	3.161 0
2.500 2	4.281 0	4.427-1	4.051-2	4.117-2	1.697-1	2.450-1	3.126 0	3.283 0
2.600 2	4.368 0	4.378-1	4.007-2	4.071-2	1.707-1	2.460-1	3.243 0	3.405 0
2.700 2	4.452 0	4.331-1	3.964-2	4.027-2	1.716-1	2.469-1	3.361 0	3.526 0
2.800 2	4.535 0	4.287-1	3.923-2	3.984-2	1.725-1	2.477-1	3.477 0	3.647 0
2.900 2	4.615 0	4.244-1	3.884-2	3.944-2	1.734-1	2.486-1	3.592 0	3.766 0
3.000 2	4.693 0	4.203-1	3.846-2	3.905-2	1.742-1	2.493-1	3.707 0	3.885 0
3.100 2	4.770 0	4.163-1	3.810-2	3.867-2	1.749-1	2.501-1	3.821 0	4.003 0
3.200 2	4.845 0	4.125-1	3.775-2	3.831-2	1.757-1	2.508-1	3.935 0	4.121 0
3.300 2	4.918 0	4.088-1	3.742-2	3.796-2	1.764-1	2.515-1	4.048 0	4.237 0
3.400 2	4.990 0	4.053-1	3.709-2	3.762-2	1.770-1	2.521-1	4.160 0	4.354 0
3.500 2	5.060 0	4.018-1	3.678-2	3.730-2	1.777-1	2.528-1	4.271 0	4.469 0
3.600 2	5.129 0	3.985-1	3.647-2	3.698-2	1.783-1	2.534-1	4.382 0	4.584 0
3.700 2	5.196 0	3.953-1	3.618-2	3.668-2	1.788-1	2.539-1	4.492 0	4.698 0
3.800 2	5.262 0	3.922-1	3.589-2	3.638-2	1.794-1	2.545-1	4.602 0	4.811 0
3.900 2	5.326 0	3.892-1	3.562-2	3.610-2	1.799-1	2.550-1	4.711 0	4.924 0
4.000 2	5.389 0	3.863-1	3.535-2	3.582-2	1.804-1	2.555-1	4.820 0	5.036 0
4.100 2	5.451 0	3.834-1	3.509-2	3.555-2	1.809-1	2.560-1	4.927 0	5.148 0
4.200 2	5.512 0	3.807-1	3.484-2	3.529-2	1.813-1	2.565-1	5.035 0	5.259 0
4.300 2	5.572 0	3.780-1	3.459-2	3.504-2	1.818-1	2.569-1	5.142 0	5.370 0
4.400 2	5.630 0	3.754-1	3.435-2	3.479-2	1.822-1	2.574-1	5.248 0	5.480 0
4.500 2	5.688 0	3.728-1	3.412-2	3.455-2	1.826-1	2.578-1	5.354 0	5.589 0
4.600 2	5.744 0	3.703-1	3.389-2	3.431-2	1.829-1	2.582-1	5.459 0	5.698 0
4.700 2	5.800 0	3.679-1	3.367-2	3.408-2	1.833-1	2.586-1	5.564 0	5.806 0
4.800 2	5.854 0	3.656-1	3.346-2	3.386-2	1.837-1	2.590-1	5.668 0	5.914 0
4.900 2	5.907 0	3.633-1	3.325-2	3.365-2	1.840-1	2.593-1	5.772 0	6.021 0
5.000 2	5.960 0	3.610-1	3.304-2	3.343-2	1.843-1	2.597-1	5.875 0	6.128 0

Lead

SATURATION CURVE

P	T	T/TC	VL	VG	SL	SG	EL	EG
2.316-1	5.524 0	1.000 0	3.228-1	3.228-1	5.513-1	5.513-1	1.110 0	1.110 0
2.000-1	5.329 0	9.647-1	2.463-1	4.531-1	5.311-1	5.640-1	1.017 0	1.151 0
1.000-1	4.639 0	8.398-1	1.867-1	8.419-1	4.927-1	5.760-1	8.349-1	1.156 0
8.000-2	4.475 0	8.100-1	1.783-1	9.904-1	4.840-1	5.785-1	7.960-1	1.154 0
6.000-2	4.293 0	7.771-1	1.701-1	1.213 0	4.742-1	5.814-1	7.537-1	1.151 0
5.000-2	4.191 0	7.587-1	1.659-1	1.377 0	4.687-1	5.830-1	7.306-1	1.149 0
4.000-2	4.079 0	7.385-1	1.616-1	1.611 0	4.625-1	5.849-1	7.053-1	1.147 0
3.000-2	3.952 0	7.154-1	1.570-1	1.988 0	4.554-1	5.872-1	6.766-1	1.143 0
2.000-2	3.795 0	6.869-1	1.516-1	2.771 0	4.464-1	5.906-1	6.419-1	1.137 0
1.500-2	3.693 0	6.685-1	1.484-1	3.695 0	4.404-1	5.935-1	6.196-1	1.132 0
1.000-2	3.550 0	6.426-1	1.440-1	6.328 0	4.318-1	5.996-1	5.884-1	1.122 0
8.000-3	3.465 0	6.272-1	1.415-1	8.932 0	4.265-1	6.044-1	5.701-1	1.116 0
6.000-3	3.347 0	6.058-1	1.383-1	1.362 1	4.192-1	6.114-1	5.450-1	1.107 0
5.000-3	3.269 0	5.918-1	1.362-1	1.736 1	4.142-1	6.159-1	5.287-1	1.102 0
4.000-3	3.174 0	5.746-1	1.338-1	2.286 1	4.081-1	6.215-1	5.089-1	1.095 0
3.000-3	3.053 0	5.526-1	1.308-1	3.173 1	4.001-1	6.288-1	4.840-1	1.087 0
2.000-3	2.890 0	5.231-1	1.271-1	4.873 1	3.890-1	6.392-1	4.511-1	1.077 0
1.000-3	2.639 0	4.776-1	1.218-1	9.643 1	3.711-1	6.575-1	4.016-1	1.061 0
8.000-4	2.565 0	4.644-1	1.204-1	1.192 2	3.657-1	6.636-1	3.875-1	1.057 0
6.000-4	2.476 0	4.483-1	1.187-1	1.562 2	3.589-1	6.716-1	3.706-1	1.051 0
5.000-4	2.423 0	4.386-1	1.177-1	1.850 2	3.548-1	6.767-1	3.605-1	1.048 0
4.000-4	2.360 0	4.273-1	1.166-1	2.275 2	3.499-1	6.830-1	3.488-1	1.044 0
3.000-4	2.284 0	4.135-1	1.153-1	2.964 2	3.439-1	6.913-1	3.347-1	1.039 0
2.000-4	2.185 0	3.955-1	1.136-1	4.298 2	3.357-1	7.031-1	3.165-1	1.033 0
1.500-4	2.120 0	3.837-1	1.125-1	5.590 2	3.303-1	7.116-1	3.047-1	1.029 0
1.000-4	2.034 0	3.683-1	1.112-1	8.093 2	3.229-1	7.238-1	2.895-1	1.024 0

SHOCK ADIABAT M= 1.000

P	T	V	S	E	D	U	CS	CV
1.000-4	2.930-1	8.820-2	4.470-7	1.300-7	.000 0	.000 0	1.882 0	1.213-1
1.000 1	5.026-1	7.629-2	2.186-2	5.954-2	2.556 0	3.451-1	2.652 0	1.236-1
1.500 1	6.674-1	7.292-2	4.463-2	1.146-1	2.763 0	4.788-1	2.857 0	1.248-1
2.000 1	8.750-1	7.028-2	6.896-2	1.792-1	2.947 0	5.986-1	3.030 0	1.262-1
2.500 1	1.121 0	6.814-2	9.258-2	2.508-1	3.113 0	7.082-1	3.180 0	1.278-1
3.000 1	1.400 0	6.633-2	1.146-1	3.281-1	3.267 0	8.100-1	3.314 0	1.295-1
3.204 1	1.523 0	6.567-2	1.231-1	3.610-1	3.326 0	8.497-1	3.364 0	1.302-1
3.204 1	1.523 0	6.567-2	1.231-1	3.610-1	3.326 0	8.497-1	3.358 0	1.421 0
4.000 1	1.679 0	6.358-2	1.584-1	4.924-1	3.555 0	9.924-1	3.558 0	1.493 0
4.984 1	1.858 0	6.156-2	2.043-1	6.639-1	3.815 0	1.152 0	3.780 0	1.572 0
4.984 1	1.858 0	6.156-2	2.043-1	6.639-1	3.815 0	1.152 0	3.799 0	1.432-1
5.000 1	1.870 0	6.153-2	2.051-1	6.670-1	3.819 0	1.155 0	3.803 0	1.433-1
6.000 1	2.558 0	5.962-2	2.441-1	8.575-1	4.041 0	1.310 0	3.992 0	1.493-1
8.000 1	4.070 0	5.663-2	3.046-1	1.263 0	4.440 0	1.589 0	4.314 0	1.592-1
1.000 2	5.707 0	5.433-2	3.510-1	1.693 0	4.793 0	1.840 0	4.585 0	1.669-1
1.500 2	1.016 1	5.026-2	4.350-1	2.846 0	5.546 0	2.386 0	5.126 0	1.802-1
2.000 2	1.492 1	4.745-2	4.948-1	4.075 0	6.179 0	2.855 0	5.553 0	1.909-1
2.500 2	1.984 1	4.533-2	5.415-1	5.359 0	6.736 0	3.274 0	5.912 0	2.025-1
3.000 2	2.475 1	4.363-2	5.802-1	6.686 0	7.236 0	3.657 0	6.222 0	2.161-1
4.000 2	3.427 1	4.097-2	6.428-1	9.446 0	8.117 0	4.347 0	6.741 0	2.488-1
5.000 2	4.312 1	3.891-2	6.934-1	1.232 1	8.884 0	4.964 0	7.166 0	2.856-1
6.000 2	5.128 1	3.723-2	7.367-1	1.529 1	9.569 0	5.530 0	7.529 0	3.237-1
8.000 2	6.589 1	3.456-2	8.104-1	2.145 1	1.077 1	6.551 0	8.135 0	3.976-1
1.000 3	7.879 1	3.252-2	8.734-1	2.784 1	1.182 1	7.462 0	8.643 0	4.647-1
1.500 3	1.066 2	2.899-2	1.005 0	4.441 1	1.404 1	9.424 0	9.699 0	5.966-1
2.000 3	1.312 2	2.676-2	1.116 0	6.144 1	1.591 1	1.109 1	1.062 1	6.838-1
2.500 3	1.542 2	2.529-2	1.214 0	7.864 1	1.758 1	1.254 1	1.150 1	7.387-1
3.000 3	1.764 2	2.431-2	1.302 0	9.584 1	1.911 1	1.384 1	1.237 1	7.737-1
4.000 3	2.190 2	2.328-2	1.456 0	1.298 2	2.189 1	1.611 1	1.415 1	8.237-1
5.000 3	2.586 2	2.292-2	1.589 0	1.632 2	2.441 1	1.807 1	1.588 1	8.815-1
6.000 3	2.946 2	2.284-2	1.707 0	1.961 2	2.672 1	1.980 1	1.745 1	9.555-1
8.000 3	3.572 2	2.290-2	1.908 0	2.612 2	3.087 1	2.286 1	2.001 1	1.125 0
1.000 4	4.108 2	2.296-2	2.079 0	3.262 2	3.453 1	2.554 1	2.202 1	1.290 0

Appendix B

Reference volumes of metals

Metal	Li	Al	Fe	Ni	Cu	Mo	Ta	W	Au	Pb
Volume [cc/g]	1.86	0.369	0.121	0.112	0.112	0.0978	0.0600	0.0519	0.0518	0.0882

Appendix C

make$tab.f program - source text

```
      PROGRAM MAKE$TAB
      DIMENSION V(256)
      OPEN(99, FILE='OUT.IN', STATUS='UNKNOWN',
     *FORM='FORMATTED')
      WRITE(*,*)'Input data:initial, intermediate and final'
      WRITE(*,*)' VI           V1           V2           VF'
      READ(*,*) VI,V1,V2,VF
      WRITE(*,*)'Number of points in regions and scale(IL-0lin,1log)'
      WRITE(*,*)'in VI-V1(I1,IL1)  V1-V2(I2,IL2)   V2-VF(I3,IL3)'
      READ(*,*)I1,IL1,I2,IL2,I3,IL3
C     --- Tabular data output
C     - Region Vm<Vh for I1 points:
      DO 13 I=1,I1
      IF(IL1) 12,11,12
   11 X=VH+(V1-VH*(I-1.)/I1)
      GO TO 13
   12 X=VH*((V1/VH)**((I-1.)/I1))
   13 V(I)=X
C     - Region V1<V2 for I2 points:
      DO 23 I=1,I2
      IF(IL2) 22,21,22
   21 X=V1+(V2-V1*FLOAT(I-1)/I2)
      GO TO 23
   22 X=V1*((V2/V1)**(FLOAT(I-1)/I2))
   23 V(I1+I)=X
C     - Region V2<VK for I3 points:
      DO 33 I=1,I3
      IF(IL3) 32,31,32
   31 X=V2+(VK-V2*FLOAT(I-1)/I3)
      GO TO 33
   32 X=V2*((VK/V2)**(FLOAT(I-1)/I3))
   33 V(I2+I1+I)=X
C     --- Print output
      WRITE(*,*)(V(J),J=1,I1+I2+I3)
      WRITE(99,*)(V(J),J=1,I1+I2+I3)
      CLOSE(99)
      STOP
      END
```

Appendix D

read.f program - sorce text

```
      PROGRAM READ$TAB
      COMMON /RT/V(256),T(256),P(256,256),E(256,256),S(256,256),
     ,H(256,256),F(256,256),CS(256,256),CT(256,256),
     ,CP(256,256),CV(256,256),IPS(256,256)
      CALL RE$TAB
      STOP
      END
      SUBROUTINE RE$TAB
C-----------------------------------------------------------------------
C (C) I.V.Lomonosov, 1993
C Purpose: RE$TAB is small subroutine to read and manage EOS data
C          generated by TABEOS program. Parameters for TABEOS are
C          placed in file DATA.MAN
C Used:
C       files: DATA.MAN - TABEOS managing file
C              VOLUME.IN - data for volume scale (L2=-1)
C              TEMPER.IN - data for temperature scale (L1=-1)
C
C       parameters: NV - dimension of volume scale (256 max)
C                   NT - dimension of temperature scale (256 max)
C                 V(NV) - volume array, calculated or in file  VOLUME.IN
C                 T(NT) - temper. array, calculated or in file TEMPER.IN
C               P(NT,NV) - pressure table in file              PRESSU.TAB
C               E(NT,NV) - energy table in file                ENERGY.TAB
C               S(NT,NV) - entropy table in file               ENTROP.TAB
C               H(NT,NV) - enthalpy table in file              ENTHAL.TAB
C              CP(NT,NV) - heat capacity p=const table in file HCAPAP.TAB
C              CT(NT,NV) - heat capacity v=const table in file HCAPAV.TAB
C              CS(NT,NV) - sound velocity s=const table in file SNDVLS.TAB
C              CT(NT,NV) - sound velocity T=const table in file SNDVLT.TAB
C             IPS(NT,NV) - identifier of phase state in file   PHYSID.TAB
C                     L1 - identifier of V-scale (log or linear)
C                     L2 - identifier of T-scale (log or linear)
C                     L3 - identifier of table (fixed or binary)
C-----------------------------------------------------------------------
      COMMON /RT/V(256),T(256),P(256,256),E(256,256),S(256,256),
     ,H(256,256),F(256,256),CS(256,256),CT(256,256),
     ,CP(256,256),CV(256,256),IPS(256,256)
C
C +-- Open managing file and read scaling parameters from it
      OPEN(50,NAME='DATA.MAN',STATUS='OLD',FORM='FORMATTED',READONLY)
      READ(50,1001) TI,TF,VI,VF,NT,NV,L1,L2,L3
 1001 FORMAT(//E9.3/E9.3/E9.3/E9.3/I3/I3/I2/I2/I2)
      CLOSE(50)
C
C +-- Determination of volume- and temperature arrays
      IF(L1) 10,11,13
   10 OPEN(51,NAME='TEMPER.IN',STATUS='OLD',FORM='FORMATTED',READONLY)
      READ(51,*) (T(I),I=1,NT)
      CLOSE(51)
      GO TO 15
   11 DO 12 I=1,NT
      T(I)=TI+(TF-TI)*(I-1.)/(NT-1.)
   12 CONTINUE
      GO TO 15
   13 DO 14 I=1,NT
      T(I)=TI*EXP(ALOG(TF/TI)*(I-1.)/(NT-1.))
   14 CONTINUE
   15 CONTINUE
```

```
C      --- end of filling T-array
       IF(L1) 20,21,23
   20 OPEN(52,NAME='VOLUME.IN',STATUS='OLD',FORM='FORMATTED',READONLY)
       READ(52,*) (V(I),I=1,NV)
       CLOSE(52)
       GO TO 25
   21 DO 22 I=1,NV
       V(I)=VI+(VF-VI)*(I-1.)/(NV-1.)
   22 CONTINUE
       GO TO 25
   23 DO 24 I=1,NV
       V(I)=VI*EXP(ALOG(VF/VI)*(I-1.)/(NV-1.))
   24 CONTINUE
   25 CONTINUE
C      --- End of V(olume) array
C +--- Arrays V and T have been determinated
C
C +-- Reading data and phase ident-s arrays
       IF(L3) 31,31,33
   31 OPEN(99,FILE='PRESSU.TAB',STATUS='UNKNOWN',FORM='FORMATTED')
       OPEN(98,FILE='ENERGY.TAB',STATUS='UNKNOWN',FORM='FORMATTED')
       OPEN(97,FILE='SNDVLS.TAB',STATUS='UNKNOWN',FORM='FORMATTED')
       OPEN(96,FILE='SNDVLT.TAB',STATUS='UNKNOWN',FORM='FORMATTED')
       OPEN(95,FILE='ENTROP.TAB',STATUS='UNKNOWN',FORM='FORMATTED')
       OPEN(94,FILE='HCAPAP.TAB',STATUS='UNKNOWN',FORM='FORMATTED')
       OPEN(93,FILE='HCAPAV.TAB',STATUS='UNKNOWN',FORM='FORMATTED')
       OPEN(92,FILE='ENTHAL.TAB',STATUS='UNKNOWN',FORM='FORMATTED')
       OPEN(91,FILE='FRENER.TAB',STATUS='UNKNOWN',FORM='FORMATTED')
       OPEN(90,FILE='PHYSID.TAB',STATUS='UNKNOWN',FORM='FORMATTED')
       DO 32 I=1,NT
C      --- Thermodynamical data:
       READ(99,1002) (P(I,J), J=1,NV)
       READ(98,1002) (E(I,J), J=1,NV)
       READ(97,1002) (CS(I,J), J=1,NV)
       READ(96,1002) (CT(I,J), J=1,NV)
       READ(95,1002) (S(I,J), J=1,NV)
       READ(94,1002) (CP(I,J), J=1,NV)
       READ(93,1002) (CV(I,J), J=1,NV)
       READ(92,1002) (H(I,J), J=1,NV)
       READ(91,1002) (F(I,J), J=1,NV)
 1002 FORMAT(6E10.3)
C      --- Phase ident-s
       READ(90,1003) (IPS(I,J),J=1,NV)
 1003 FORMAT(60I1)
   32 CONTINUE
       WRITE(*,*)P(1,1),IPS(1,1),E(1,1),CS(1,1)
       GO TO 35
   33 OPEN(99,FILE='PRESSU.TAB',STATUS='UNKNOWN',FORM='UNFORMATTED')
       OPEN(98,FILE='ENERGY.TAB',STATUS='UNKNOWN',FORM='UNFORMATTED')
       OPEN(97,FILE='SNDVLS.TAB',STATUS='UNKNOWN',FORM='UNFORMATTED')
       OPEN(96,FILE='SNDVLT.TAB',STATUS='UNKNOWN',FORM='UNFORMATTED')
       OPEN(95,FILE='ENTROP.TAB',STATUS='UNKNOWN',FORM='UNFORMATTED')
       OPEN(94,FILE='HCAPAP.TAB',STATUS='UNKNOWN',FORM='UNFORMATTED')
       OPEN(93,FILE='HCAPAV.TAB',STATUS='UNKNOWN',FORM='UNFORMATTED')
       OPEN(92,FILE='ENTHAL.TAB',STATUS='UNKNOWN',FORM='UNFORMATTED')
       OPEN(91,FILE='FRENER.TAB',STATUS='UNKNOWN',FORM='UNFORMATTED')
       OPEN(90,FILE='PHYSID.TAB',STATUS='UNKNOWN',FORM='UNFORMATTED')
       DO 34 I=1,NT
C      --- Thermodynamical data:
       READ(99) (P(I,J), J=1,NV)
       READ(98) (E(I,J), J=1,NV)
       READ(97) (CS(I,J), J=1,NV)
       READ(96) (CT(I,J), J=1,NV)
       READ(95) (S(I,J), J=1,NV)
```

```
      READ(94) (CP(I,J), J=1,NV)
      READ(93) (CV(I,J), J=1,NV)
      READ(92) (H(I,J), J=1,NV)
      READ(91) (F(I,J), J=1,NV)
C     --- Phase ident-s
      READ(90) (IPS(I,J),J=1,NV)
      WRITE(*,*)P(1,1),IPS(1,1),E(1,1),CS(1,1)
   34 CONTINUE
   35 WRITE(*,*)'Data are loaded in arrays. Test is for (I,J) point:'
      WRITE(*,*)'Enter I, J (I OR J =0 --> EXIT'
      READ(*,*) I,J
      IF(I.LE.0.OR.J.LE.0) GO TO 36
      WRITE(*,*)'P=',P(I,J),' E=',E(I,J),' Cs=',CS(I,J),' I=',IPS(I,J)
      GO TO 35
   36 CLOSE(99)
      CLOSE(98)
      CLOSE(97)
      CLOSE(96)
      CLOSE(95)
      CLOSE(94)
      CLOSE(93)
      CLOSE(92)
      CLOSE(91)
      CLOSE(90)
      RETURN
      END
```

HEDRC REPORT

Printed October 1994

WIDE-RANGE EQUATION OF STATE FOR LARGE COMPUTER CODES: EQUATIONS OF STATE OF MOLYBDENUM, TANTALUM, NICKEL AND GOLD

I. V. Lomonosov, V. E. Fortov, and K. V. Khishchenko

Prepared by
High Energy Density Research Center
Russian Academy of Sciences
Izhorskaya Str. 14/19, Moscow 127412, Russia
for USAF
by contract SPC-93-4074

WIDE-RANGE EQUATION OF STATE FOR LARGE COMPUTER CODES: EQUATIONS OF STATE OF MOLYBDENUM, TANTALUM, NICKEL AND GOLD

I. V. Lomonosov, V. E. Fortov, and K. V. Khishchenko

High Energy Density Research Center
Russian Academy of Sciences
Izhorskaya Str. 14/19, Moscow 127412, Russia

Abstract

This is third (9-months) report performed for USAF by contract SPC-93-4074. Described is comparison between calculated by multi-phase equation of state (EOS) thermodynamical properties for molybdenum, tantalum, nickel and gold metals and available experimental data. For each metal we carried out a construction of EOS on the base of the model and procedure given in previous report and, after it, a calculation of metal's phase diagram. The comparison was made for: principal and porous Hugoniots, release isentropes, static compression data, phase-diagram data, and isobaric expansion data. The comparison and discussion with predictions of critical points are also done.

1. Introduction

Each section of the report is devoted to a selected metal. Discussed are measurements under static conditions, such diamond-anvil-cells (DAC) data, measurements of melting curve with use of high-pressure vessels, isobaric expansion investigations along with predictions of critical point and, finally, dynamic studies. They are explorations of shock Hugoniots and release isentropes. We supply the discussion by correspondent figures, shown on which are both our calculated characteristics and experimental data with theoretical predictions.

2. Molybdenum

Molybdenum is characterized by large values of melting and evaporation temperature. This fact explains a wide use of the metal in modern nuclear, aviation and space technologies. Along with aluminum and iron, molybdenum also serves as an etalon material on carrying out shock-wave measurements at extreme pressures.

2.1. Cold curve

Calculated cold curve for molybdenum is compared with theoretical calculations and the semiempirical cold curve [1] on Fig. 1.

As it was shown previously for large number of metals [3], the developed procedure of determination of the cold curve allows to describe thermodynamical properties of metals at T=0 K in a broad range of densities up to 100-fold compression. Fig. 1 confirms the fact for such metal, as molybdenum.

2.2. Static compression and melting curve

Molybdenum is bcc at ambient conditions. Diamond-Anvil-Cell (DAC) data [4,5] show no phase transition in Mo at room temperature up to 2.8 Mbar. Carried out comparison between calculated with the use of EOS T=298 K isotherm and results of DAC experiment [4] proved their excellent agreement.

The initial slope of molybdenum melting curve dT/dp=0.8 K/kbar [6] measured with the use of an optical technique to 90 kbar differs significantly from those one 3.4±0.6 K/kbar measured on isobaric-expansion (IEX) experiment [7]. Note, that the value dT/dp=3.5±0.2 K/kbar obtained on the base of reduction of static data for solid and liquid molybdenum [8] is also more realistic then the one given in [6]. The developed EOS for molybdenum gives the value for dT/dp=3.34 K/kbar, which should be considered in very good agreement with results [7,8].

Note, that the calculated melting region in the high-pressure range corresponds to an intersection with the shock adiabat in the 3.91-4.75 Mbar pressure range. The result of determination of sound velocity in shocked molybdenum, obtained with the use of optical-analyzer technique, shows a disappearing of transverse component, which corresponds to melting, at p=3.9 Mbar [9]. This very good agreement proves the reliability of calculation of molybdenum melting curve at high pressure.

2.3. Shock-wave data

The shock compressibility of molybdenum have been studied thoroughly in megabar-pressure range with the use of different traditional shock-wave generators [10,11,12,13]. Experiments on light-gas gun increased the investigated range of pressure to 5 Mbar [14], higher pressures to 10 Mbar have been explored with the use of special powerful systems [15,16]. The region of high pressures and reduced (with respect to normal) densities for molybdenum has been subjected to intensive studies using the method of shock compression of porous samples [17,18].

The use of nuclear explosives made it possible to determine the shock compressibility of molybdenum at extreme high pressures. Absolute measurement of the principle Hugoniot at p≈20 Mbar [19] and impedance-match data [14,20,21] determined from aluminum standard at tens of megabars are available.

Sound velocity in shocked molybdenum has measured with use of overctacken technique, while bromoform serves as an optical etalon material [9]. These results [9] revealed a solid-solid phase transition at p≈2.1 Mbar and melting in shocked metal at p≈3.9 Mbar. Taken into account shock-wave data at pressure higher then 2.1 Mbar and static data [5], it can be concluded that the solid-solid phase transition is corresponded by small change of density and leads to no breaks

in principal Hugoniot. Therefore, it is possible for molybdenum to describe the complete set of high-pressure data by one solid phase.

A comparison of shock-wave data on the compression of solid and porous samples with calculated shock adiabats is presented on Fig. 2; also plotted in the figure are the results of isotherm calculations and the boundary of the high-temperature melting region. It is worth to note, that for molybdenum is a full correspondence between numerous shock-wave data, obtained with the use of high-explosive systems [10-13,15,16], light-gas gun [14] and nuclear explosions [14,19,20,21]. As it is seen from Fig. 2, the developed EOS describes with high accuracy all principle-Hugoniot data and measurements of porous Hugoniots, including high-porous (m=8) data [18] to pressures of the order of 10 Mbar. The carried out comparison for extreme-high-pressure data [14,19,20,21] also proved the fact.

Fig. 2,a demonstrates an agreement between calculated and measured isentropic sound velocity in shocked molybdenum.

2.4. High-pressure, low-density data

The region of high pressure and reduced (with respect to normal conditions) density has been studied with the use of IEX technique. Available are density-temperature data on the isobar p=0.2 GPa to 4450 K [22], 7000 K [23] and 4100 K [24]. Calculated isobars are compared with IEX data on Fig. 3.

The developed EOS for molybdenum describes with very good accuracy the melting on the isobars; calculated values are, as it is seen from Fig. 3, in agreement with measurements [22]. The calculated value of the evaporation temperature at p=1 bar T_v=4824 K is in agreement with the tabular [30] one 4910 K. Note, that for molybdenum the value of evaporation temperature differs in ca. 10% from different references.

Obtained from this EOS critical point parameters are following: p_c =5.878 kbar, T_c=15210 K, V_c=0.636 cc/g and s_c=1.617 J/gK. The analysis of evaluations of critical point from [25-29] shows, that the data are in range 5.46 [29] - 12.6 kbar [27], 8000 [26] - 16140 K [27], 0.97 [26] - 3.18 [27] g/cc. This discrepancy is relatively large; the slope of the experimental $\rho(T)$ curves [22,23,24] does not

coincide with calculated one. Nevertheless, for IEX measurements [22,23,24] calculated isobar to 5000 K is within experimental errors , which are typically of the order of ±0.3 g/cc for density and ±250 K for temperature.

The slope of experimental isobars indicates to larger value of Gruneisen coefficient or less value of isothermal sound velocity in liquid molybdenum, then those values calculated by EOS. It is well seen from formula $\left(\partial p/\partial T\right)_\rho = \left(\partial p/\partial T\right)_V/V^2\left(\partial p/\partial V\right)_T$. It is doubtful that molybdenum has very large value of Gruneisen coefficient in liquid state (to describe IEX data, it must be ca. 3.5) - it will contradict to shock-wave data for porous specimens. Note, that IEX data [22] leads to a very large value for the specific heat c_p=8.5R near melting point. It also indicates to dramatic decrease of sound velocity in liquid molybdenum.

Finally, it is possible to conclude that developed EOS for molybdenum provides for a reasonable description of available experimental and theoretical data in liquid state. It should be revised, nevertheless, that more accurate conclusions for liquid molybdenum properties can be made only having sound velocity measurements.

2.5. Discussion

The developed EOS for molybdenum, as it is shown by Figs. 1-3, provides for an accurate and reliable description of thermodynamical properties of the metal at high pressures and temperatures. The calculated Hugoniots agree with all available shock-wave data, as well as p(T=298 K) isotherm with static data; in region of low densities the EOS provides for a reasonable description of IEX data and evaluations of critical point parameters.

3. Tantalum

Tantalum is a component of alloys which are of wide use in modern air- and spacecraft technique, as well as in nuclear reactors. Tantalum is also used as a suitable material for impactors on shock-wave experiments.

3.1. Cold curve

Theoretical calculations of tantalum cold curve have been done in work [2]; available are also results for semiempirical cold curves [1,31]. The comparison between obtained for tantalum cold curve and results [1,2,31] are plotted to 100-fold compressions on Fig. 4. The analysis of the picture proves the fact, that obtained in the work cold curve agrees with semiempirical ones [1,31] at moderate pressures and with Thomas-Fermi calculations [2] at extreme high pressure, while the other semiempirical curves [1,31] have unphysical oscillations at high pressure and density $\rho \approx 20\rho_0$.

3.2. Static compression and melting curve

Tantalum is bcc at ambient conditions. Results of isothermal compressibility measurements at T=298 K in DAC with the ruby etalon to 100 kbar [4] and to 800 kbar [32] found no phase transitions. Data [32] are of the most interest as they have been obtained at hydrostatic conditions with use of argon as pressure-transmitting medium. Calculated isotherm is compared with the data [32] on Fig. 5, which demonstrates their good agreement.

The calculated value of the initial slope of molybdenum melting curve dT/dp=6.12 K/kbar agrees with those one 5.4 K/kbar determined by optical method to 90 kbar [6], and 5.8±1 K/kbar obtained from IEX measurements [22].

The calculated melting region at high pressure corresponds to an intersection with the principal Hugoniot in the 3.14-3.83 Mbar pressure range. The result of determination of sound velocity in shocked tantalum, obtained with the use of optical-analyzer technique, shows a disappearing of transverse component, which corresponds to melting, at p=2.95 Mbar [33]. Our result is in

agreement (within experimental error) with [33]. It proves the reliability of calculation of tantalum melting curve at high pressure.

3.3. Shock-wave data

The principle Hugoniot of tantalum has been investigated with the use of different explosive systems to fee megabars in works [10,12,13]. The usage of light-gas guns increased the region of studied pressure to 4.3 Mbar [34,35]. Higher pressure to 10 Mbar has been explored with use of powerful explosive systems [15,16]. These drivers have also been used on investigation of states of liquid tantalum by method of shock compression of porous samples [18]. The sound velocity in shocked tantalum has been measured, as it mentioned previously, in work [33].

To begin with, no discontinuities have been observed on tantalum principle Hugoniot and all available data obtained with the use of different experimental methods are self-consistent. As it is seen from Fig. 6, the developed EOS describes solid and liquid states of tantalum on the principal shock adiabat with high accuracy and reliability. The region of decreased, with respect to the principal Hugoniot, densities corresponding to porous Hugoniots, is also described by the EOS (see Fig. 6).

The developed EOS for tantalum describes also measurements of sound velocity in shocked metals, which is proved by Fig. 6,a.

Therefore, tantalum EOS is in very good agreement with all available shock-wave data for this metal.

3.4. High-pressure, low-density data

IEX data at p=2 kbar to 6200 K [36] and to 7400 K [37] are available for tantalum. Sound velocity measurements have been done in liquid tantalum under condition of the fast isobaric expansion from 14.49 g/cc to 11.49 g/cc in work [38]. Shown on Fig. 7 are calculated the liquid-gas coexistence curve with critical point and selected isobars in comparison with IEX data and evaluations of critical point for this metal.

The developed EOS provides for a good agreement with experimental data on melting along the isobar and with the experimental $\rho(T)$ dependence [36] in the neighborhood of evaporation region (see Fig. 7). Note, that the slope $\rho(T)$ for data [37] does not agree with the one from [36], measurements of sound velocity [38] and evaluations of the critical point [25,26].

Calculated sound velocity in liquid tantalum is compared with experimental data on Fig. 7,a. There is a good (within experimental error) agreement between calculated and measured values.

The EOS gives following parameters of tantalum critical point: p_c =7.756 kbar, T_c=14260 K, V_c=0.259 cc/g and s_c=0.953 J/gK. These values are in reasonable agreement with analogous evaluations [25,26,27]. The value of evaporation temperature at normal pressure, T_v=5731 K coincides with the tabular one [30].

Finally, the tantalum EOS provides for very agreement with all liquid-state data at moderate pressure.

3.5. Discussion

The developed EOS for tantalum, as it is seen from Figs. 4-7, describes with very high accuracy and reliability thermodynamical properties of the metal in solid, liquid and gas states. The calculated thermodynamical characteristics are in agreement with all available experimental data. It is worth to notice very good agreement of the EOS with theoretical and experimental data in the region of the liquid state both at moderate (IEX) and high-pressure (shock-wave) data, which is usually of the most difficulty for theoretical calculations.

So the EOS for tantalum can be used in hydrocodes in the most difficult situations, when the reliability and accuracy of modeling results are defining namely by EOS.

4. Nickel

Nickel due to its anti-oxidizing properties is of use in large amount of technological alloys. This fact helped to carry out very interesting experiments on shock compression of ultra-low-density nickel specimens [39].

4.1. Cold curve

Thermodynamical properties of nickel at T=0 K have been calculated with the use Thomas-Fermi model with quantum adjustments [2] and method of augmented plane waves [40]. Approximating semiempirical cold curves for this metal have been published in works [1,31,41,42]. The comparison between obtained in the work cold curve, results of theoretical calculation [2,40] and other semiempirical cold curves is given on Fig. 8.

The obtained in the work cold curve of nickel, as it is seen from Fig. 8, agrees with theoretical calculations [2,40] overall range of pressure, while the other semiempirical cold curves have unphysical oscillations at pressure higher then 400 Mbar. Note, that all these curves coincide with each other to $p<400$ Mbar.

4.2. Static compression and melting

According to [43], nickel is fcc at ambient conditions and the structure is stable at room temperature to 650 kbar.

The calculated value of the initial slope of the melting curve $dT/dp=4.38$ K/kbar is in satisfactory agreement with the one 3.3 K/kbar given in compendium [44], which has been determined to 60 kbar.

4.3. Shock-wave data

The principal Hugoniot of nickel has been studied by virtue of traditional shock-wave generators to 1.5 Mbar in works [10,11,13] and light-gas gun to 5 Mbar [45]. Usage of special powerful high-explosive systems increased the limit of investigated pressure to ca. 10 Mbar [16,41,46]. Data on shock compression of

porous [18,41] and ultra porous [39] nickel samples in a megabar-pressure range significantly expanded the region of the investigated phase diagram. Results of work [39] are of especial interest as they occupy region of strongly heated liquid metal and, for the most porous shock Hugoniot $\rho_0 / \rho_{00}=20$ correspond to the state of weakly-ionized non-ideal plasma.

The calculated phase diagram of nickel is shown on Fig. 9 in comparison with available shock-wave data. Note, that results [41] for porosity m=1.73 does not agree with those one from recent work [18], while for m=3.0 their position on the phase diagram corresponds to the position of porous shock Hugoniots m=4.58, 2.72, 2.32 from [18]. The analysis of experimental data on shock compression of porous specimens shows, that the position of porous and ultra porous Hugoniots is reasonable (see Fig. 9). The principle Hugoniot data for nickel, obtained with the use of different shock-wave generators, are also in a good agreement with each other.

This unique set of data embraces the region of density $0.2<\rho / \rho_0<2$ to pressure ca. 10 Mbar and gives an opportunity to account for precisely thermal contribution of electrons and ions in EOS. Calculated shock adiabats of different initial densities describe with very high accuracy all available for nickel shock-wave data.

4.4. High-pressure, low-density data

Density-temperature measurements have been done for liquid nickel at p=2 kbar to 4300 K [47] along with determination of sound velocity. Evaluations of critical point for nickel are given in works [25,27].

Shown on Fig. 10 are calculated phase boundary liquid-gas with critical point CP, rectilinear diameter D and selected isobars in comparison with these data. Additionally given on Fig. 10,a are experimental and calculated sound velocity in liquid nickel.

Analogous to shock-wave data, there is a good correspondence for nickel between all available experimental data and theoretical predictions in the region of lower densities and moderate temperatures. The nickel EOS describes with very good accuracy results of experimental work [47]. Calculated parameters of the

critical point p_c =10.49 kbar, T_c=7585 K, V_c=0.479 cc/g and s_c=2.526 J/gK are in agreement with available evaluations [25,27]. Note, that given by the nickel EOS value of critical temperature is less, then the one from [25,27]. It is reasonable as for tantalum, for instance, the value of critical temperature has been changed from 17330 K [25] to 9284 K [26], when the hard-spheres model was substituted for soft-spheres one. The value of evaporation temperature at normal pressure, T_v=3020 K agrees with the tabular one 3190 K from [30] (note, that it can differ from other references in ±10%).

4.5. Discussion

Nickel is one of the most investigated metals. Both theoretical and experimental high-pressure data agree for nickel in a broad range of density and pressure. It made it possible to construct very reliable precise EOS for this metal.

The analysis of Figs. 7-10 proves the fact.

5. Gold

Gold is well-compressed metal with no phase transitions at high pressure. By this reason it is using very often as standard material for DAC measurements. Due to high density and large nuclear charge it is also used in producing targets for controlled-inertial-fusion experiments.

5.1. Cold curve

Theoretical calculations of themodynamical properties of gold at T=0 K have been done by Thomas-Fermi model with quantum corrections [2]. Semiempirical cold curves for gold have been obtained in works [1,31]. Results of these calculations are comparing with obtained in this work cold curve on Fig. 11. This picture shows a good agreement between our cold curve and [2] at high pressure. At moderate pressure obtained cold curve agrees with both semiempirical cold curves from [1,31].

5.2. Static compression and melting

Gold is fcc at ambient conditions. According to DAC measurements to 3 Mbar [48,49,50] it remains fcc on room-temperature isotherm. Calculated T=298 K isotherm agrees with DAC data.

The calculated value of the initial slope of the melting curve dT/dp=6.3 K/kbar agrees the one 6 K/kbar given in compendium [44], which has been determined to 60 kbar.

5.3. Shock-wave data

The principal Hugoniot of gold has been studied by virtue of traditional shock-wave generators to 1.9 Mbar in works [10,11,13] and light-gas gun to 5.8 Mbar [51]. Data, obtained with the usage of special powerful high-explosive systems, also are in the pressure range to 5.1 Mbar [16,52].

The calculated phase diagram for gold is shown on Fig. 12. All available shock-wave data are in agreement with each other and described by developed EOS for gold with high accuracy, as it is seen from Fig. 12.

5.4. High-pressure, low-density data

Presented on Fig. 13 are calculated phase boundary liquid-gas with critical point, rectilinear diameter, selected isobars in comparison with IEX data, calculated by approximating relationships from review [24] and evaluations of critical point [25,27]. The IEX data for Au-5Cu alloy [24] are the only available; they are put on the figure only for estimations.

Calculated parameters of the critical point p_c =7.568 kbar, T_c=9007 K, V_c=0.151 cc/g and s_c=0.636 J/gK are in agreement with available evaluations [25,27]. The value of evaporation temperature at normal pressure, T_v=3110 K agrees with the tabular one 3150 K from [30].

5.5. Discussion

The developed EOS for gold provides for accurate and reliable description all non-numerous high-pressure data.

It will be possible to revise the EOS when new interesting results, especially in liquid state, appear.

6. Conclusion

Described in the report results of construction multi-phase EOS for molybdenum, tantalum and gold demonstrate the efficiency of the approach. Developed EOS for these metals provides for reliable and accurate calculation of thermodynamical properties in solid, liquid and gas states.

Figs. 1-13 prove the fact, so these EOS can be used in hydrocodes for numerical modeling high-energy-density processes.

References

[1] S. B. Kormer, V. D. Urlin, L. T. Popova, Fizika tverd. tela, **3,** 2131-2140 (1961) [in Russian].

[2] N. N. Kalitkin, L. V. Kuz'mina, Preprint Inst. Prikl. Matem. Akad. Nauk SSSR N35: Moskva, 1975 [in Russian].

[3] A. V. Bushman, I. V. Lomonosov, V. E. Fortov, *Equation of State for Metals at High Energy Densities,* Chernogolovka: Inst. Chem. Phys., 1992 [in Russian].

[4] L. C. Ming, M. H. Manghnani, J. Appl. Phys., **48,** 208-212 (1978).

[5] Y. K. Vohra, A. L. Ruoff, Phys. Rev. Ser. B, **42,** 8651-8654 (1990).

[6] L. F. Vereshchagin, N. S. Fateeva, High Temp. - High Press., **9,** 619-628 (1977).

[7] G. R. Gathers, J. W. Shaner, W. M. Hodgson, High Temp. - High Press., **11,** 529-538 (1979).

[8] A. F. Guillermet, Int. J. Thermophys., **6,** 367-393 (1985).

[9] R. S. Hixson, D. A. Boness, J. W. Shaner, Phys. Rev. Lett., **62,** 637-640 (1989).

[10] J. M. Walsh, M. H. Rice, R. G. McQueen, F. L. Yarger, Phys.Rev., **108,** 196-216 (1957).

[11] R. G. McQueen, S. P. Marsh, J. Appl. Phys., 1960, **31,** 1253-1269 (1960).

[12] R. G. McQueen, S. P. Marsh, J. W. Taylor, J. N. Fritz, W. J. Carter, - In: *High Velocity Impact Phenomena* / Ed. R. Kinslow. - New-York: Academic Press, p.293-417; appendies on pp. 515-568 (1970).

[13] LASL Shock Hugoniot Data / Ed. S. P. Marsh. - Berkeley: Univ. of California Press, 1980.

[14] A. C. Mitchell, W. J. Nellis, J. A. Moriarty, R. A. Heinle, N. C. Holmes, R. E. Tipton, G. W. Repp, J. Appl. Phys., **69,** 2981-2986 (1991).

[15] K. K. Krupnikov, A. A. Bakanova, M. I. Brazhnik, R. F. Trunin, Dokl. Akad. Nauk SSSR, **148,** 1302-1305 (1963) [in Russian] (Sov. Phys. - Dokl. **8,** 205 (1963)).

[16] L. V. Al'tshuler, A. A. Bakanova, I. P. Dudoladov, E. A. Dynin, R. F. Trunin, B. S. Chekin, Sov. J. Appl. Mech. Tech. Phys., **22,** 145 (1981).

[17] A. A. Bakanova, I. P. Dudoladov, Yu. N. Sutulov, Zh. Prikl. Mekh. Tekhn. Fiz. **2,** 117-122 (1974) [in Russian] (J. Appl. Mech. Techn. Phys. **15,** 241 (1974)).

[18] R. F. Trunin, G. V. Simakov, Yu. N. Sutulov, A. B. Medvedev, B. D. Rogozkin, Yu. E. Fedorov, Zh. Eksp. Teor. Fiz. **96(9),** 1024-1038 (1989) [in Russian] (Sov. Phys. - JETP **69(3),** 580-588 (1989)).

[19] C. E. Ragan, M. G. Silbert, B. C. Diven, J. Appl. Phys., **48,** 2860-2870 (1977).

[20] C. E. Ragan, Phys. Rev. Ser.A, **25,** 3360-3375 (1982).

[21] A. C. Mitchell, W. J. Nellis, R. A. Heinle, G. W. Repp, J. A. Moriarty, M. Ross, N. C. Holmes, Physica Ser. B., **139&140,** 591-594 (1986).

[22] J. W. Shaner, G. R. Gathers, C. A. Minichino, High Temp. - High Press., **8,** 425-429 (1976).

[23] U. Seydel, W. Kitzel, J. Phys. F: Metal Phys., **9(9),** L153-L160 (1979).

[24] G. R. Gathers, Rep. Progr. Phys., **49,** 341-396 (1986).

[25] D. A. Young, B. J. Alder, Phys. Rev. A, 1971, **3,** 364-371 (1971).

[26] D. A. Young, UCRL-52352 (Lawrence Livermore Laboratory, 1977)

[27] V. E. Fortov, I. T. Yakubov, *Physics of Non-Ideal Plasmas,* Chernogolovka: Inst. Chem. Phys., 1983 [in Russian].

[28] U. Seydel, H. Bauhof, W. Fucke, H. Wadle, High Temper. - High Pressures, **9,** 635-642 (1979).

[29] U. Seydel, W. Fucke, J. Phys. F: Metal Phys., **8(7),** L157-L151 (1978).

[30] R. Hultgren, P. D. Desai, D. T. Hawkins, M. Gleiser, K. K. Kelley, D. D. Wagman, *Selected Values of the Thermodynamic Properties of the Elements.* - Metals Park, Ohio: ASME, 1973.

[31] S. B. Kormer, V. D. Urlin, Dokl. Akad. Nauk SSSR, **131,** 542-545 (1960) [in Russian].

[32] J. Xu, H. K. Mao, P. M. Bell, High Temp. - High Press., **16,** 495-499 (1984).

[33] J. M. Brown, J. W. Shaner, - In: *Shock Waves in Condensed Matter - 83 /* Eds. J. R. Asay, R. A. Graham, G. K. Straub - Amsterdam: North Holland, 91-94 (1984).

[34] A. C. Mitchell, W. J. Nellis, J. Appl. Phys., **52,** 3363-3374 (1981).

[35] N. C. Holmes, J. A. Moriarty, G. R. Gathers, W. J. Nellis, J. Appl. Phys., **66,** 2962-2967 (1989).

[36] J. W. Shaner, G. R. Gathers, C. Minichino, High Temp. - High Press., **9,** 331-343 (1977).

[37] A. Berthault, L. Arles, J. Matricon, Intern. J. of Thermophys., **7(1),** 167-179 (1986).

[38] R. S. Hixson, M. A. Winkler, J. W. Shaner, High Temp. - High Press., **18,** 635-638 (1986).

[39] R. F. Trunin, G. V. Simakov, Zh. Eksp. Teor. Fiz. **103(6),** 2180-2188 (1993) [in Russian] (Sov. Phys. - JETP **76(6),** 1090-1094 (1993)).

[40] A. K. McMahan, R. C. Albers, Phys. Rev. Lett., **49,** 1198-1201 (1982).

[41] S. B. Kormer, A. I. Funtikov, V. D. Urlin, A. N. Kolesnikova, Zh. Eksper. Teor. Fiz., **42,** 686-701 (1962) [in Russian].

[42] V. D. Urlin, Zh. Eksper. Teor. Fiz., **49,** 485-492 (1962) [in Russian].

[43] D. A. Young, *Phase Diagrams of the Elements,* Berkeley: Univ. of California Press, 1991.

[44] E. Yu. Tonkov, *Phase Diagrams of Elements at High Pressure,* Moscow: Nauka, 1977 [in Russian].

[45] W. H. Isbell, F. H. Shipman, A. H. Jones, General Motors Corp.: Mat. Sci. Lab. Report MSL-68-13, 1968.

[46] L. V. Al'tshuler, A. A. Bakanova, R. F. Trunin, Zh. Eksp. Teor. Fiz. **42,** 91-104 (1962) [in Russian] (Sov. Phys. - JETP **15,** 65-74 (1962)).

[47] R. S. Hixson, M. A. Winkler, M. L. Hodgson, Phys. Rev. Ser. B, **32(10),** 6485-6491 (1990).

[48] D. L. Heinz, R. Jeanloz, J. Appl. Phys., **55,** 885-893 (1984).

[49] L. C. Ming, D. Xiong, M. H. Manghnani, Physica Ser. B, **139&140,** 174-176 (1986).

[50] H. K. Mao, Y. Wu, R. J. Hemley, L. C. Chen, L. C. Shu, L. Finger, Science, **246,** 649 (1989).

[51] A. H. Jones, W. H. Isbell, C. J. Maiden, J. Appl. Phys., **37,** 3493-3499 (1966).

[52] L. V. Al'tshuler, K. K. Krupnikov, M. I. Brazhnik, Zh. Eksp. Teor. Fiz. **34,** 886-893 (1958) [in Russian] (Sov. Phys. - JETP **7,** 614-618 (1958)).

Appendix: Pictures to Report

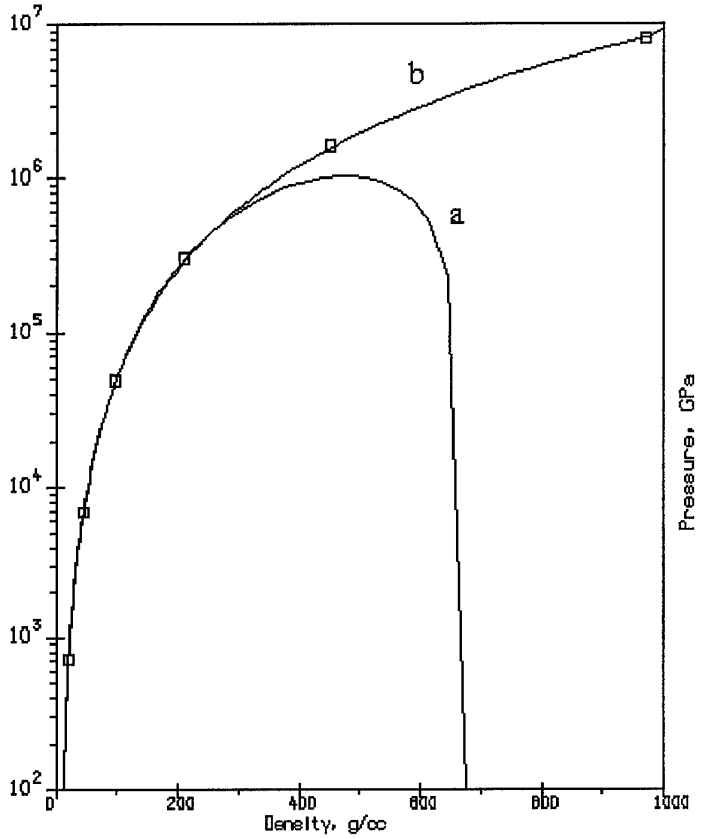

Fig. 1. Cold pressure (p(T=0 K)) in molibdenum. Curves: a - [1], b - this work; points - Thomas-Fermi calculations [2].

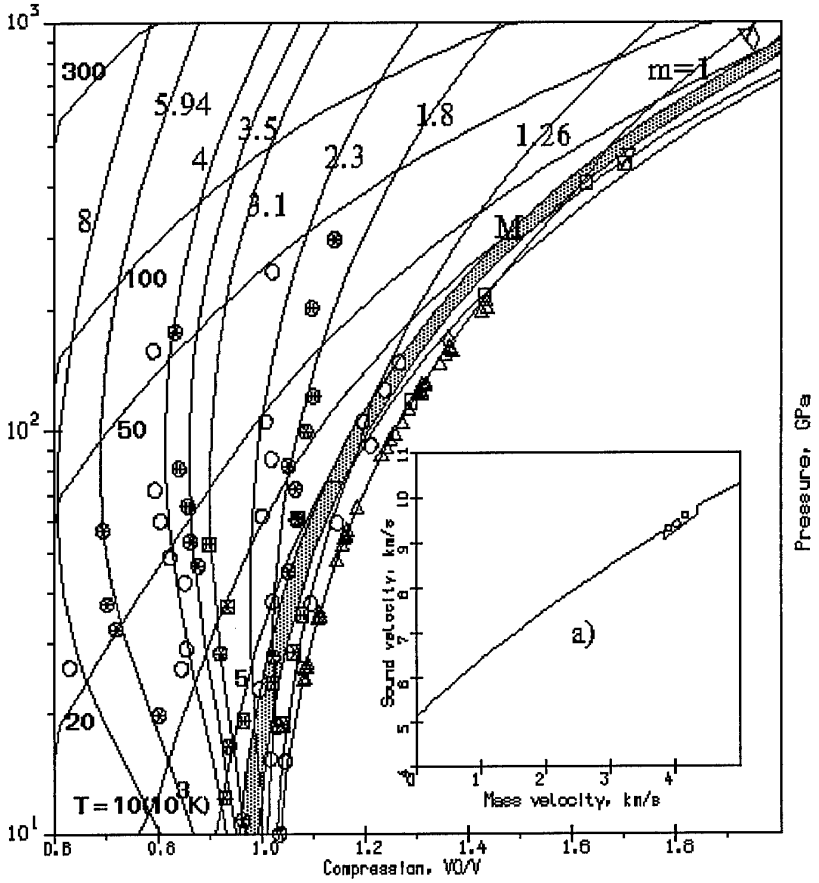

Fig. 2. Phase diagram for molybdenum. T, isotherms; m, porous Hugoniots; M, melting region. Experimental data: □ - [15], Δ - [10-13], ∇ - [14], ■ - [17], ○,⊗ - [18], ◊ - [16]. a) Sound velocity in shocked molybdenum. Points - experimental data [9].

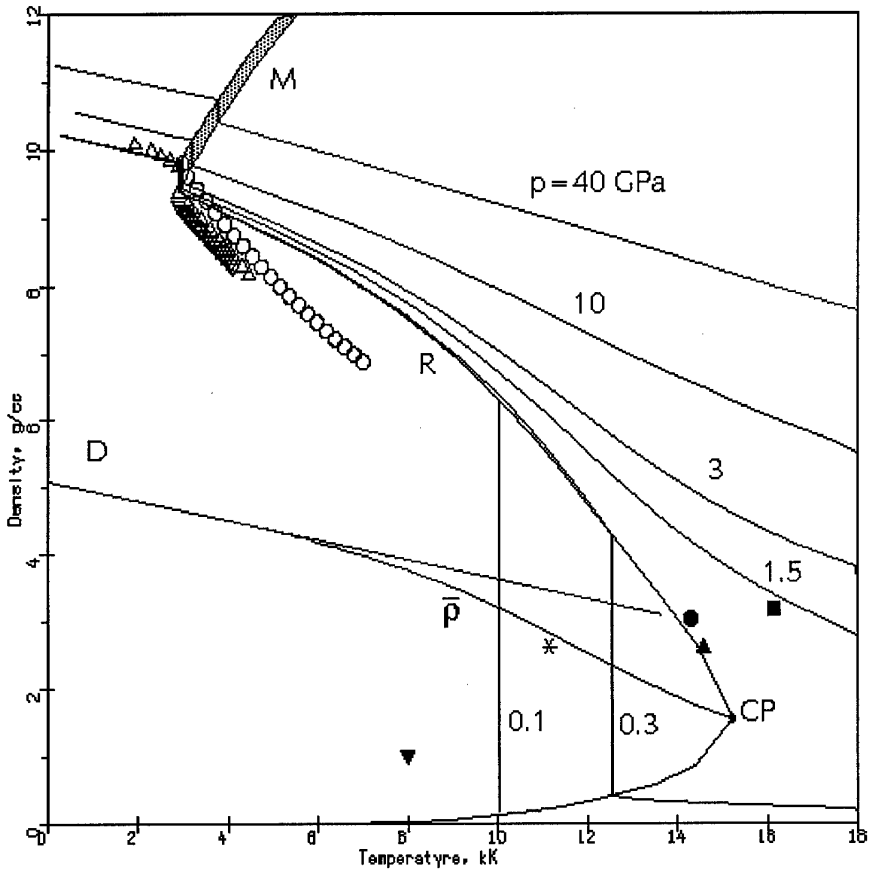

Fig. 3. Phase diagram for molybdenum in the region of lower temperatures. P, isobars; M, melting region; R, liquid-vapor equilibrium curve; D, rectilinear diameter; $\bar{\rho}$, half-sum of liquid and vapor densities. Isobaric expansion data: Δ - [22], O - [23], ∇ - [24]; evaluations of the critical-point parameters: Δ - [25], ∇ - [26], ■ - [27], ● - [28], * - [29], • - this work.

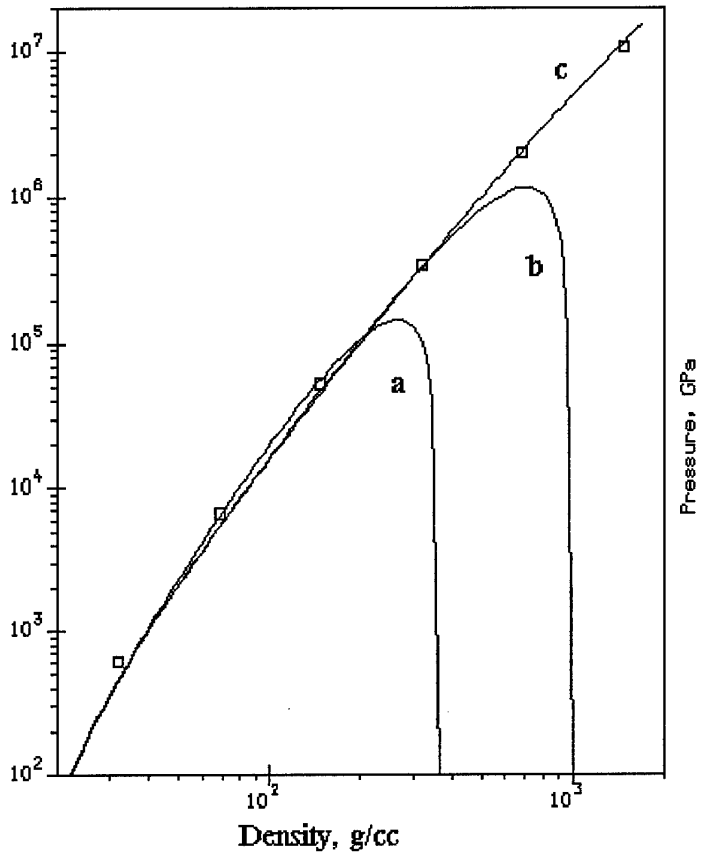

Fig. 4. Cold pressure (p(T=0 K)) in tantalum. Curves: a - [31], b - [1], c - this work; points - Thomas-Fermi calculations [2].

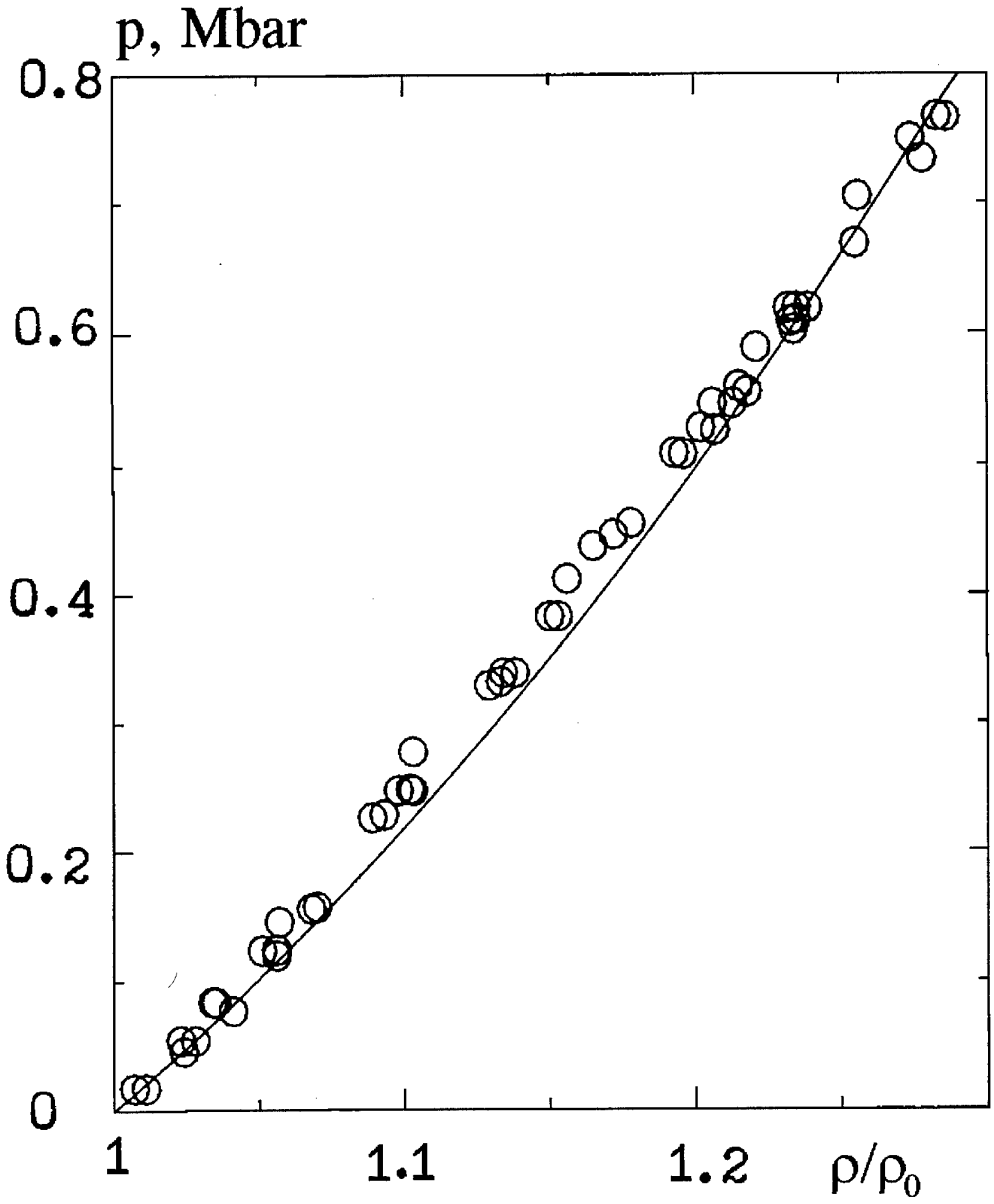

Fig. 5. Tantalum compressibility at T=298 K.
Solid line - EOS calculation, points - experimental data [32].

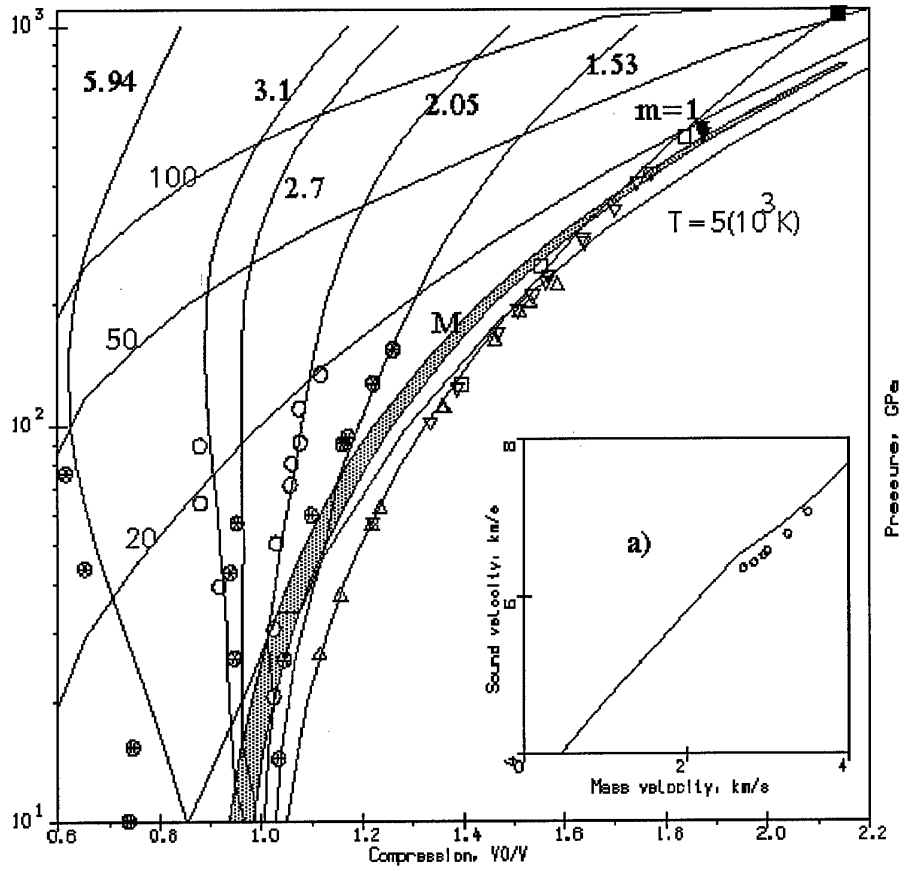

Fig. 6. Phase diagram for tantalum. T, isotherms; m, porous Hugoniots; M, melting region. Experimental data: □ - [15], ■ - [16], Δ - [34], ∇ - [11,12,13], ∇ - [35], ❍,⊗ - [18].
a) Sound velocity in shocked tantalum. Points - experimental data [33].

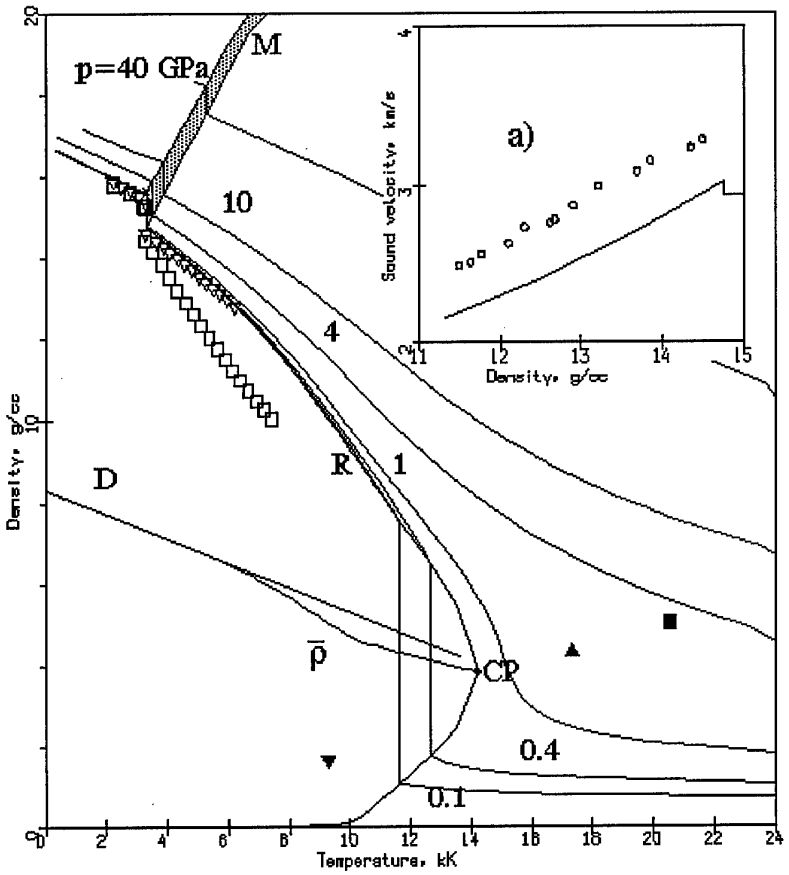

Fig. 7. Phase diagram for tantalum in the region of lower temperatures. P, isobars; M, melting region; R, liquid-vapor equilibrium curve; D, rectilinear diameter; $\bar{\rho}$, half-sum of liquid and vapor densities. Points: isobaric expansion measurements: ∇ - [36], □ - [37]; evaluations of the critical-point parameters: Δ - [25], ∇ - [26], ■ - [27], • - this work.
a) sound velocity in liquid tantalum; points - experimental data [38].

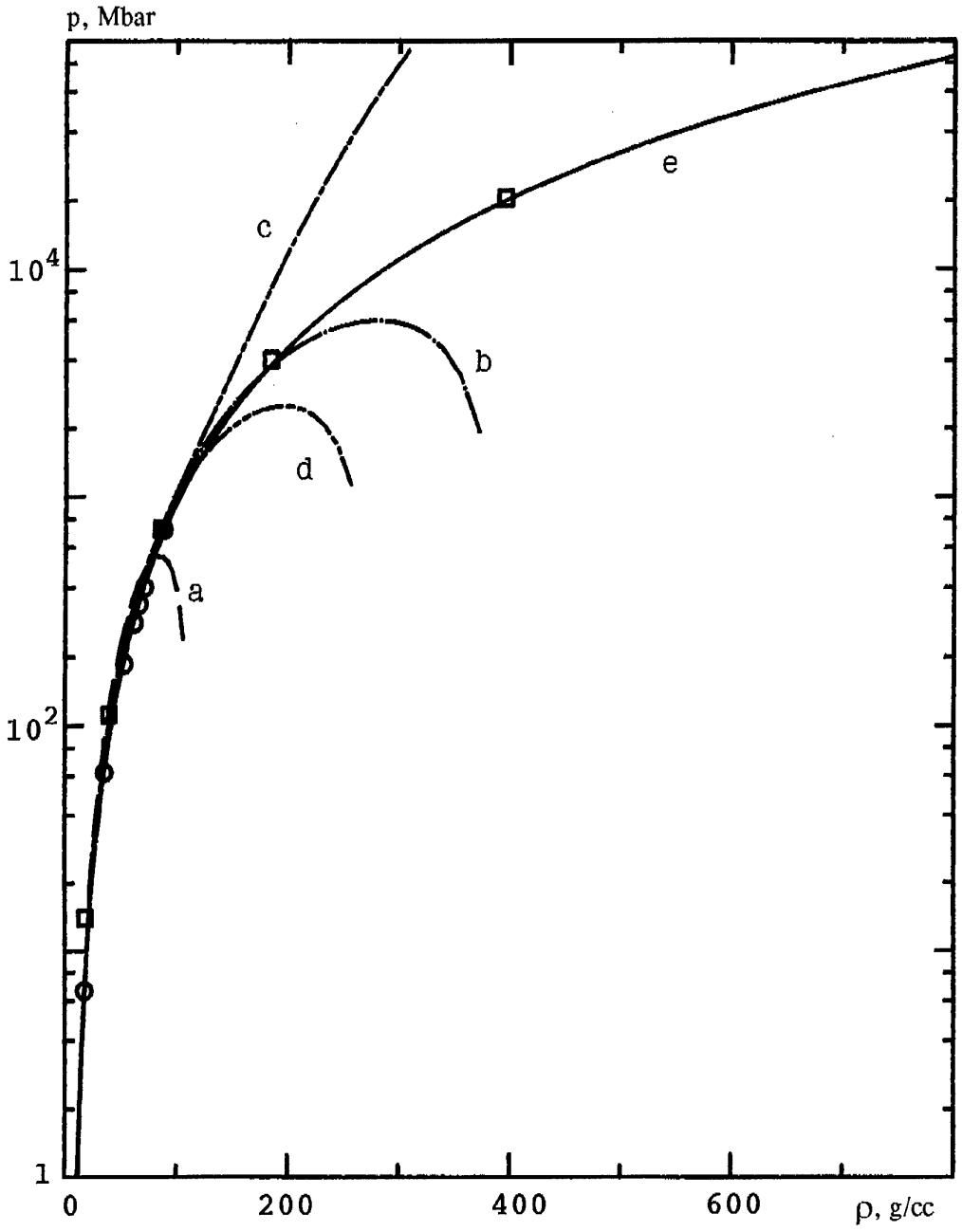

Fig. 8. Cold pressure in nickel. Theory: □ - [2], ○ - [40]; semiempirical cold curves: a - [31], b - [1], c - [41], d - [42], e - this work.

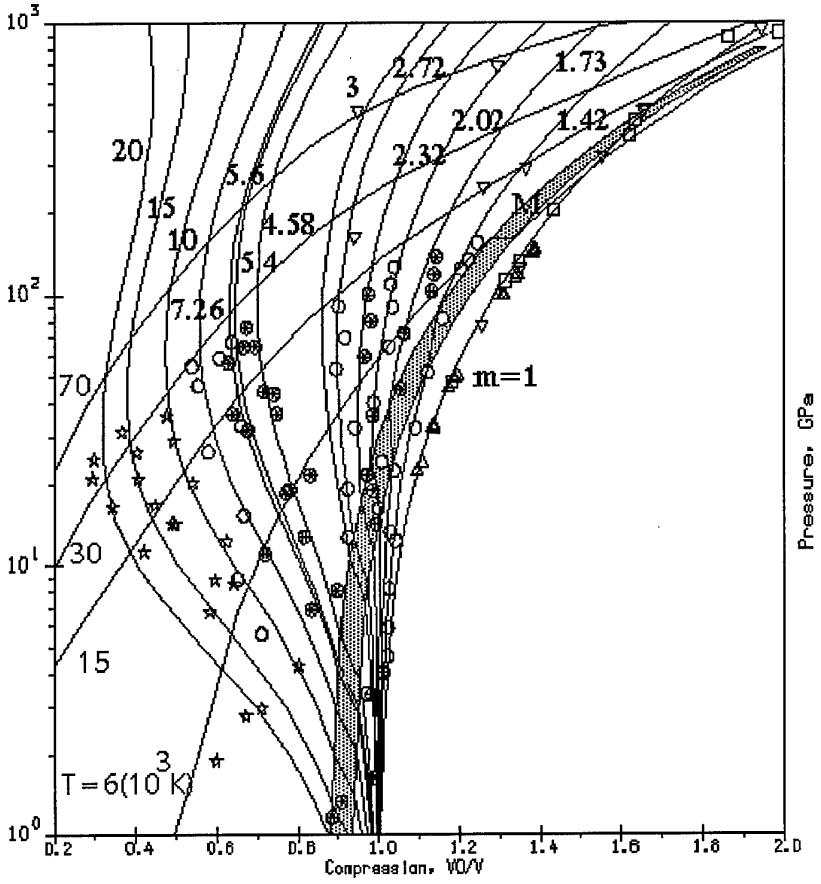

Fig. 9. Phase diagram for nickel. T, isotherms; m, porous Hugoniots; M, melting region. Experimental data: □ - [16,41,46], Δ - [10,11,13], ∇ - [45], ∇ - [41], ❍,⊗ - [18], ★ - [39].

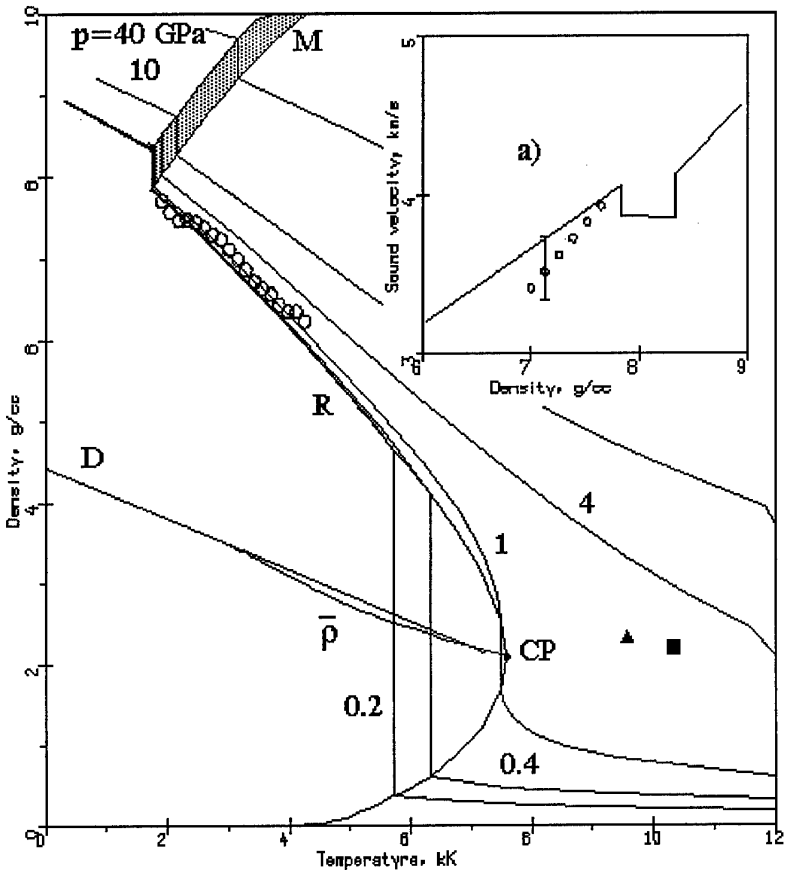

Fig. 10. Phase diagram for tungsten in the region of lower temperatures. P, isobars; M, melting region; R, liquid-vapor equilibrium curve; D, rectilinear diameter; $\bar{\rho}$, half-sum of liquid and vapor densities. Points: isobaric expansion measurements O - [47]; evaluations of the critical-point parameters: Δ - [25], ■ - [27], • - this work. a) sound velocity in liquid nickel; points - experimental data [47].

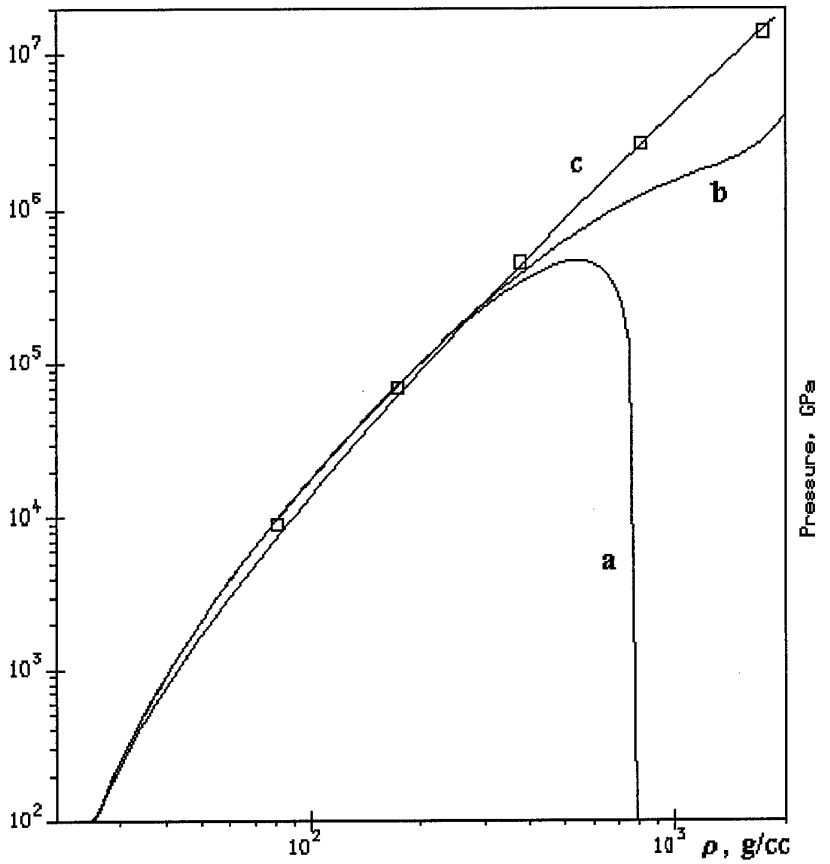

Fig. 11. Cold pressure in gold. Points - Thomas-Fermi calculations [2]; semiempirical curves: a - [31], b - [1], c - this work.

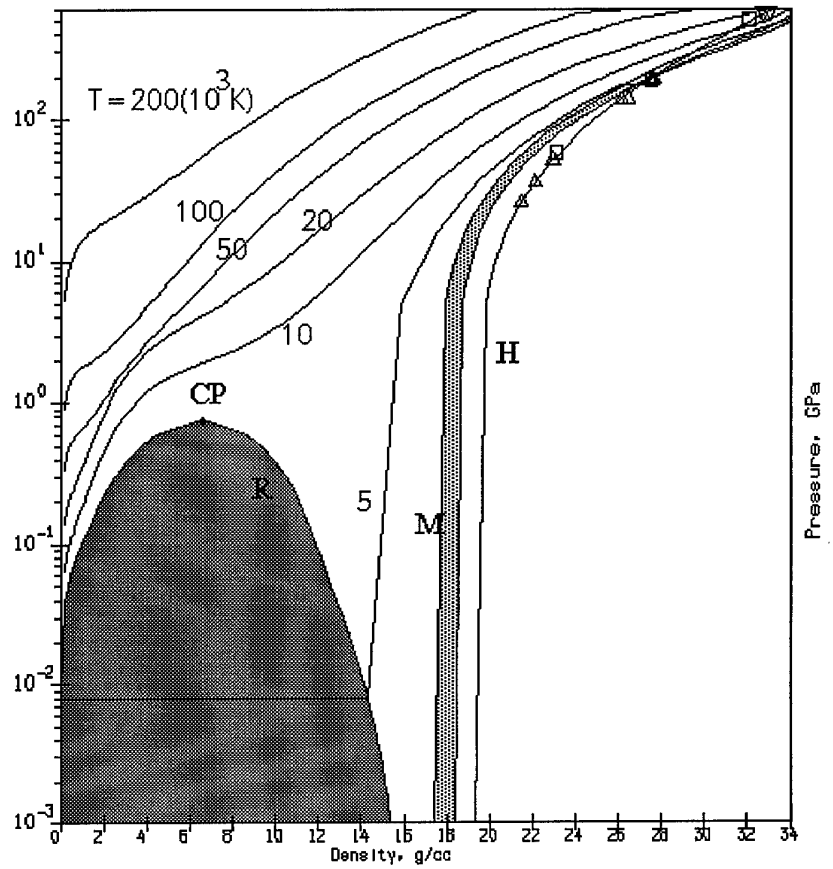

Fig. 12. Phase diagram of gold. M, melting region; R, liquid-vapor equilibrium curve with critical point CP; H - principal Hugoniot. Experimental data: □ - [16,52], Δ - [10,11,13], ∇ - [51].

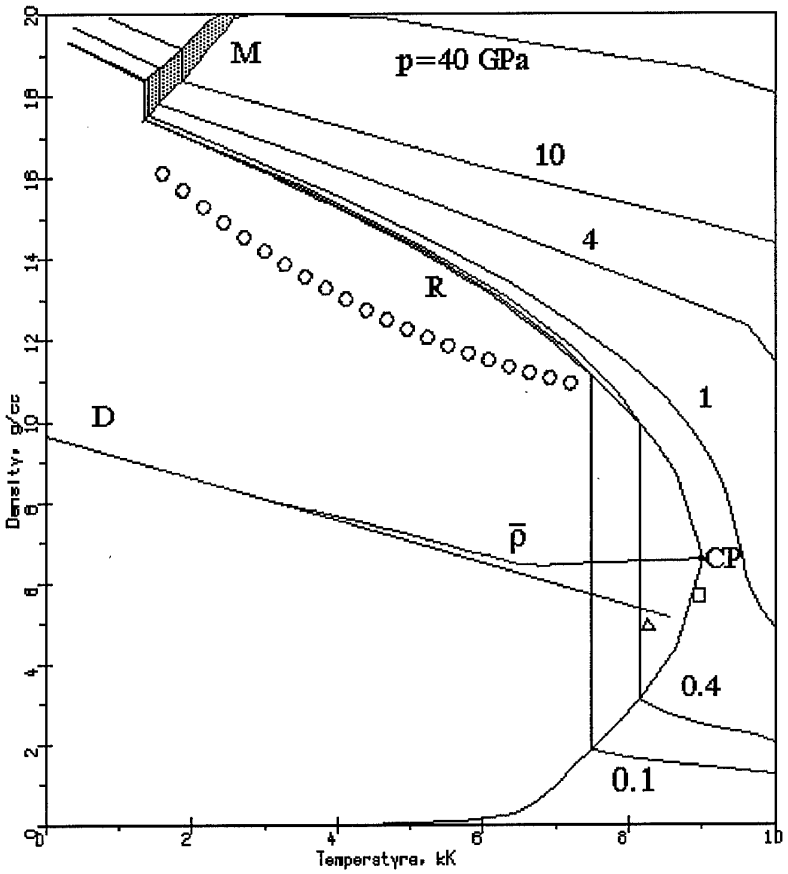

Fig. 13. Phase diagram for gold in the region of lower temperatures. P, isobars; M, melting region; R, liquid-vapor equilibrium curve; D, rectilinear diameter; $\bar{\rho}$, half-sum of liquid and vapor densities. Points: isobaric expansion measurements O - [24]; evaluations of the critical-point parameters: Δ - [25], □ - [27], • - this work.

WIDE-RANGE EQUATION OF STATE FOR LARGE COMPUTER CODES: EQUATIONS OF STATE OF LEAD, IRON AND TUNGSTEN

I. V. Lomonosov, V. E. Fortov, and K. V. Khishchenko

High Energy Density Research Center
Russian Academy of Sciences
Izhorskaya Str. 14/19, Moscow 127412, Russia

Abstract

This is second (6-months) report performed for USAF by contract SPC-93-4074. Described is comparison between calculated by multi-phase equation of state (EOS) thermodynamical properties for lead, iron and tungsten metals and available experimental data. For each metal we carried out a construction of EOS on the base of the model and procedure given in previous report and, after it, a calculation of metal's phase diagram. The comparison was made for: principal and porous Hugoniots, release isentropes, static compression data, phase-diagram data, and isobaric expansion data. The comparison and discussion with predictions of critical points are also done.

1. Introduction

Each section of the report is devoted to a selected metal. Discussed are measurements under static conditions, such diamond-anvil-cells (DAC) data, measurements of melting curve with use of high-pressure vessels, isobaric expansion investigations along with predictions of critical point and, finally, dynamic studies. They are explorations of shock Hugoniots and release isentropes. We supply the discussion by correspondent figures, shown on which are both our calculated characteristics and experiment with theoretical predictions.

2. Lead

Along with aluminum and copper, lead is one of the best investigated metals. Apart from the traditional shock-wave experiments at high and ultrahigh pressures, unique measurements on the liquid-phase characteristics at supercritical pressures were perfumed for lead, in view of its relatively low critical parameters. All this lends urgesy to the problem of the applicability of the scheme developed for constructing a wide-range semiemphirical equation of state to describe such an extensive set of heterogeneous experimental data. The lead characteristics were calculated using the coefficients obtained by procedure described previously; the results and their comparison with the available experimental data are discussed in this section.

2.1. Cold curve

Calculated cold curve for lead is compared with theoretical calculations and other semiempirical cold curves on Fig. 1.

It is well seen from the picture, that developed cold curve provide a very description of Thomas-Fermi calculations up to 100-fold compressions. At moderate densities and compressions it is in good agreement with semiempirical cold curves [1-4], obtained with analogous procedure.

2.2. Static compression and melting curve

Lead is subjected to phase transitions under condition of the static compression [6,7] - from fcc phase to hcp at 130 kbar and bcc at 1.09 Mbar. The volume changes are relatively small and are expanded with respect to pressure, so it is possible to regard that the static compression isotherm has a monotonic behavior.

These effects are accounted in the lead EOS by changing of the tabular values of the bulk compression modulus and its pressure derivative. The comparison with static and shock-wave data proved the validity of the treatment.

Shown on Fig. 2,a is a calculated by lead EOS isotherm T=298 K, which demonstrates a very good agreement with experimental data [6,7] up to highest pressures (of the order of 4 Mbar) achieved on experiment. Fig. 2,b urges such agreement in 1-10 Mbar pressure range also with theoretical calculations [8], which have been done with use of MT-orbital method.

The melting curve for lead is plotted in Fig. 3 together with the static measurement data and shows good agreement with the latter. Note, that the calculated melting line in the high-pressure region corresponds to an intersection with the shock adiabat in the 320-500 kbar pressure range, which is in a good agreement with a series of estimates obtained from shock-wave experiments [10,11].

2.3. Shock-wave data

Fig. 4, which illustrates experiments in double-shock compression for determining the characteristics of lead near the cold curve, points to the agreement between the calculated adiabats and experimental data. However, as can be seen from Fig. 4, even a simple increase of the normal velocity of sound makes it possible to allow for the phase transition which affects both the experimental data on single-shock-loading and the double-shock adiabats.

The region of high pressures and reduced (with respect to normal) densities for lead has been subjected to intensive studies using the method of shock compression of porous samples. A comparison of shock-wave data on the compression of solid and porous samples with calculated shock adiabats is presented in Fig. 5; also plotted in the figure are the results of isotherm

calculations and the boundaries of the high-temperature melting and boiling regions. The complete set of experimental measurements [13-16] is described by developed EOS with an accuracy which is not much then the experimental uncertainty. Note that here is a very good correspondence between shock-wave data obtained with the use of traditional high-explosives techniques [13,14,16] and nuclear-impedance measurements (NIM) [15]. Fig. 5,a demonstrates a quality of developed EOS on description of the isentropic sound velocity in shocked lead. In the ultrahigh-pressure region of p>10 Mbar, the results of calculations of the principal shock adiabat are in good agreement with the NIM data of lead compressibility measurements with a molybdenum standard [19] and iron standard [20].

The other possibility to study thermodynamical properties of metals at high pressures and low densities is provided by the isentropic expansion technique [21-23] which enables one to determine the characteristics of metal in the states of highly heated liquid and dense plasma and to record the point of entry of the release isentropes into the two-phase liquid-vapor region. Fig. 6 illustrates the quality of shock-compressed solid [22,23] and porous [21] samples using the semiempirical equation of state developed. As for lead, a divergence between the calculated curves and experimental data due to the nonequilibrium character of the process of heating a diffuse system, which is just within the experimental error (3-5%), is observed in the low-pressure region near the evaporation curve and inside the two-phase region upon expansion of porous samples; upon expansion of solid samples of the metal, full agreement of theory with experiment is observed.

The measurements of temperature and pressure on the release isentrope [22] give an unique possibility to determine the boiling curve of lead. Note, that the achieved on the dynamic experiment values of pressure exceed in 100 times the pressure obtained with use of static high-pressure vessels. The comparison between calculated release isentropes, evaporation curve and experimental data is given on Fig. 7, shown on which are also prediction of critical points for lead. It is seen from the figure, that developed EOS describes with very high accuracy and reliability all carried out experiments [22] and agrees with estimations of critical points.

2.4. High-pressure, low-density data

The same is demonstrated (Fig. 8) by an agreement between the calculated characteristics of high-temperature expansion of lead in the slow electric explosion of wires under pressure along the p=0.013 [29], 0.1, 0.2, 0.3, 0.4 [30] GPa isobar. Note, that shown on Fig. 8 are smoothed results of isobaric expansion measurements [30], calculated by approximating relationships presented in the work. The calculated curve both reproduces the general behavior of the experimental data over a correct description of a fine effect of the elbow in the experimental $\rho(T)$ curve towards low densities near the critical point, corresponding to an anomalously high value of the coefficient of volume expansion. The agreement between the temperature dependence of density and velocity of sound of the liquid phase of lead also points to the high reliability of description of thermodynamic characteristics in the region adjoining the evaporation curve. Calculations yielded the critical-point parameters of lead p_c =2.38 kbar, T_c=5540 K, V_c=0.32 cc/g and s_c=0.56 J/gK, and the evaporation temperature at normal pressure, T_v=2031 K. This value of the temperature coincides with the experimental value, while the critical-point parameters correspond, as can be seen from the figure, to their estimated values.

2.5. Discussion

The thermodynamic calculations of lead based on the wide-range semiempirical equation of state provide an example of efficient utilization of the scheme developed for constructing and determining the coefficients of the thermodynamic potential using a large heterogeneous set of initial experimental data. Note, that the developed EOS describe the available data with accuracy which does not exceed the typical experimental errors.

3. Iron

Iron is, probably, the material of the most use in modern technique, science and numerous applications. Iron serves also as standard material in modern physics of high dynamic pressure. These facts define the role of reliable and accurate calculation of its phase diagram at high pressures and temperatures.

Unlike simple metals, iron has very complicated phase diagram which includes, at least, 5 phases (α, β, ε, γ, θ) [31]. Developed was EOS for high-pressure phase of iron, namely ε-iron. The phase transition from α to ε–iron, occurring at normal temperature and pressure 13 GPa, is the most significant for practical calculations. The next ε-γ phase transition is following with small change of density, so it is possible to describe in the same monotonic manner this high-pressure phases. The generalized high-pressure phase was considered as ε–iron with initial density ρ=8.28 g/cc, which corresponds to reduction of static [32] and dynamic [33] data.

3.1. Cold curve

Calculated cold curve for lead is compared with theoretical calculations, based on the Thomas-Fermi model [5], on Fig. 9. The good correspondence between semiempirical cold curve and theoretical data conserves in range from 3-fold to 100-fold compression. This fact for iron (good agreement of Thomas-Fermi calculations and experimental shock Hugoniot data at pressures of the order of 20 Mbar) was used previously on revision on Russian NIM data [20].

3.2. Static compression and melting curve

The calculated isotherm T=298 K for ε–iron is compared with results of measurements of iron compressibility in diamond-anvil cell [32] on Fig. 10. This picture demonstrates their full agreement which confirms the reliability of developed EOS at normal temperature.

The calculated value of the initial slope of iron melting curve dT/dp=3.35 K/kbar agrees with those one given in [31] 3.85 K/kbar, which was determined at static conditions up to 200 kbar. As these values are very similar for both γ- and

ε–phase, the agreement confirms an adequacy of description the solid-liquid phase transition.

3.3. Shock-wave data

The shock compressibility of iron was studied with the use traditional high-explosive drivers to 2.5 Mbar [14,35]. The region of more high pressures to 14 Mbar was investigated with use of special powerful explosive systems [13,34]. The region of high pressures and lower with respect to principal Hugoniot density was studied by measurement of the porous Hugoniots [14,35-37].

The extreme high pressures were generated in iron by nuclear explosions. There are absolute [38] and impedance-match principal Hugoniot data [39-41]. Results of determination of high-porous ($m=\rho_0 / \rho_{00}=3.3$) shock Hugoniots at pressure $p \approx 14$ Mbar [37] are of great interest as the state on Hugoniot corresponds to slightly-degenerated electron gas with very large value of energy concentration.

The phase diagram for iron is given on Fig. 11. As it is seen from the picture, developed EOS for iron provides very good and reliable description of principle- and porous-Hugoniot data overall range of investigated pressures. That is right for both situations of liquid (moderate temperatures) and plasma ($100<T<200$ kK [37]) states, which are occurred on shock compression of porous samples. Note, that the full set of data [13,14,34,36,37] which were obtained with use of different methods of generating and measuring of shock waves, is described in correct self-consistent manner.

Fig. 11, a demonstrates a very good agreement between calculated by the EOS and measured in works [17,33] the of sound velocity in shocked iron.

The melting in shocked iron was determined in [33] by disappearing of transverse component of isentropic sound velocity. Recent temperature measurements [42] revised the position of melting on the principle Hugoniot: p=2.4 Mbar, T=5.8 kK (estimated from the shock energy) [33]; p=2.35 Mbar, T=6.35 kK [42]. Calculated by developed iron EOS values are: p=2.33 Mbar, T=6.1 kK. The temperature calculations describe with very good accuracy (within experimental bars) results [42].

3.4. High-pressure, low-density data

Shown on Fig. 12 are results of calculation of liquid-vapor coexistence curve with the critical point, and selected isobars. They are compared with isobaric-expansion (p=0.2 GPa) data [43] and evaluations of critical points. The results of calculations by developed EOS give slightly higher values of critical point: p_c=10.25 kbar, T_c=10.95 kK, V_c=0.0522 cc/g and s_c=2.815 J/gK; the evaporation temperature at normal pressure, T_v=3.125 kK is in very good agreement with tabular one [44]. The p=0.2 GPa isobar also deviates from experimental data [43] (see Fig. 12). Note, that this deviation is of the order of the experimental error; the slope of liquid-gas equilibrium curve is the same as from [43] and calculated sound velocity on the experimental isobar is in good agreement with the one from [43]. So it is possible to conclude, that the iron EOS provides for a necessary accuracy in the region of low densities and can be used in hydrocodes.

3.5. Discussion

The developed EOS for iron does not reflect correctly the very complicated phase diagram of real metal. It accounts only for a high-pressure phase, namely ε–iron. Obviously, due to only this reason there is no absolute agreement between EOS calculations and experimental and theoretical data at low densities. Nevertheless, it should be mentioned, that this discrepancy is not very large and does not effect on correct description of sound velocity.

The analysis of Fig. 9-12 allows to make a conclusion, that this iron EOS provides for a good accuracy and reliability on calculation in solid, liquid and plasma states and can be used in hydrocodes.

4. Tungsten

Along with iron, tungsten is of great use in numerous practical applications. It has large values of melting and evaporation temperatures which explains its usage on developing new structural materials for aviation and space technique.

4.1. Cold curve

T=0 K compression curve for tungsten is shown on Fig. 13 as well as semiempirical cold curve from [2] and results of Thomas-Fermi calculations [5]. It is interesting to mention, that cold curve [2], obtained with similar procedure, does not allow to run correct calculations of thermodynamic parameters at 10-fold and larger compressions. It can be explained by the fact, that in method [2] used were requirements $p_c(V = 0.1V_{0c}) = p^{TFC}, c_c(V = 0.1V_{0c}) = c^{TFC}$, where p and c are cold pressure and sound velocity, respectively. It leads to unphysical oscillations and even negative values of pressure at $V=0.02V_{0c}$, while the cold curve obtained in the work provides for a correct description of cold pressure up to 100-fold compression and agrees with Thomas-Fermi calculations [5].

4.2. Static compression and melting

According to [31], there is no phase transitions in tungsten at room temperature up to 60 kbar. The results [45] also does not reveal anomalies for the isothermal compressibility of tungsten up to 100 kbar. The comparison between calculated and experimental [45] dependencies p(T=298 K) showed their good agreement overall investigated range of pressure.

The value of the initial slope of the melting curve dT/dp significantly differs and depends upon the experimental technique. Optical measurements [46] gives dT/dp=7.5 K/kbar, while data obtained with the use of isobaric expansion methods lead to value 4.4 K/kbar [47]. The isobaric expansion data will be discussed below, as for calculation of the melting curve parameters, the EOS agrees with the result of optical measurements [46]: tungsten is melting at p=50 kbar, T=4050±200 K.

4.3. Shock-wave data

The shock compressibility of tungsten has been investigated thoroughly in megabar-pressure range with the use of various high-explosive systems [14,35,48] and two-stage light-gas gun [49]. Porous Hugoniots up to 3 Mbar have been studied in [36,48,50,51] also with use of high-explosive drivers. Impedance-match measurements were done at 60 Mbar [19] under condition of nuclear explosion. Data on shock compressibility of porous (m=3.06) samples [31] at p<22 Mbar are analogous to those one for iron and allow to determine the thermal electrons contribution with high accuracy.

The calculated with tungsten EOS phase diagram is shown on Fig. 14 in comparison with available shock-wave data. It is interesting to note, that tungsten has a large value of melting enthalpy. This fact leads to broad, with respect to density, melting region, which significantly effects to position of porous Hugoniots (see Fig. 14). The analysis of Fig. 14 allows to conclude, that developed EOS for tungsten provides an accurate and reliable description of all available shock-wave data. Carried out comparison with NIM data [19] also proves this fact.

The isentropic sound velocity has been measured in shocked porous (m=1.8) tungsten with use of overtaken technique [48]. Fig. 14,a demonstrates a good agreement between calculated and measured in experiment [48] sound velocity.

4.4. High-pressure, low-density data

Shown on Fig. 15 are calculated phase boundary liquid-gas with critical point CP, rectilinear diameter D and isobars in comparison with isobaric-expansion measurements [52,53,54] and evaluations of the critical point [24,27,52,55].

The thermodynamical situation for tungsten looks sophisticated as critical point estimations and isobaric expansion measurements do not agree with each other. The developed EOS for tungsten, as it is seen from Fig. 15, agrees with position of melting at moderate density and temperature given by results of measurements [52,53,54]. Calculated parameter of evaporation temperature at normal pressure, T_v=5.744 kK, agrees with tabular data [44]; critical point

parameters p_c=10.74 kbar, T_c=15.12 kK, V_c=0.2105 cc/g and s_c=0.904 J/gK are in good agreement with approximation of experimental data [52,55].

The discrepancy between position of calculated liquid-gas coexistence curve, isobars and isobaric expansion data can be explained only by difficulty of correct measurement density of liquid metal. It should to mention, that reduction of experimental data gives values for heat capacity at constant pressure c_p=0.28-0.31 J/(gK) [47,52,53,54] at melting temperature T=3690 K. Near-melting point value for solid tungsten is also of the order of 0.26-0.28 J/(gK) [30]. This exceeds in 2 or more times the one c_p=0.137 J/(gK) at ambient conditions. The value for heat capacity at melting temperature from the experimental data is too large. Note also, that typical error bars are of the order of ±250 K and ±2 g/cc (from recent publication [54]). Calculated sound velocity in liquid tungsten is in agreement with the measured one [54]. The slope of expansion curve for liquid tungsten in energy-density coordinates from [56] is less then from [47,52], so finally it is possible to conclude that developed EOS for tungsten is in satisfactory agreement with experimental and theoretical data in liquid state at moderate temperatures.

4.5. Discussion

The accuracy and reliability of developed EOS is very high at high pressures and temperatures. It describes all available static-compression and shock-wave data with accuracy which does not exceed the experimental error.

Thermodynamical data for tungsten are not in full agreement with each other in the region of liquid state at moderate temperatures. So developed EOS for tungsten describes by alternative way the set of isobaric expansion measurements and evaluations of critical point.

As the EOS describes high-pressure, high temperature data, provides for tabular value of evaporation temperature at p=1 bar and is in reasonable agreement with isobaric expansion data and evaluations of critical point, it can be resumed, that the EOS can be used in hydrocodes to calculate thermodynamical properties in solid, liquid, and gas states.

5. Conclusion

It is very difficult to satisfy simultaneously the condition of the best description of numerous high-pressure data. They have their own accuracy, occupy different regions of the phase diagram. Note also, that such information, as principal, porous Hugoniots and pressure-expansion velocity measurements on release isentropes is not thermodynamically complete.

On developing EOS for lead, iron and tungsten, the most attention was paid on correct description of dynamic, i.e. shock-wave, data. The accuracy and reliability of the EOS have been proved by comparison with the most significant experimental data. Pictures given in Appendix demonstrate this fact. The liquid state of metals is region of the greatest problems both for experimental and theoretical methods. Nevertheless, developed EOS provide for a reasonable description of metals thermodynamics at high and moderate temperatures.

Calculated with use of these EOS thermodynamical functions can be used in hydrocodes with great efficiency.

References

[1] S. B. Kormer, V. D. Urlin, Dokl. Akad. Nauk SSSR, **131,** 542-545 (1960) [in Russian].

[2] S. B. Kormer, V. D. Urlin, L. T. Popova, Fizika tverd. tela, **3,** 2131-2140 (1961) [in Russian].

[3] S. B. Kormer, A. I. Funtikov, V. D. Urlin, A. N. Kolesnikova, Zh. Eksper. Teor. Fiz., **42,** 686-701 (1962) [in Russian].

[4] V. D. Urlin, Zh. Eksper. Teor. Fiz., **49,** 485-492 (1962) [in Russian].

[5] N. N. Kalitkin, L. V. Kuz'mina, Preprint Inst. Prikl. Matem. Akad. Nauk SSSR N35: Moskva, 1975 [in Russian].

[6] C. A. Vanderborgh, Y. K. Vohra, H. Xia, A. L. Ruoff, Phys. Rev. Ser. B, **41,** 7338-7340 (1990).

[7] Y. K. Vohra, A. L. Ruoff, Phys. Rev. Ser. B, **42,** 8651-8654 (1990).

[8] W. J. Nellis, J. A. Moriarty, A. C. Mitchell, M. Ross, R. G. Dandrea, N. W. Ashcroft, N. C. Holmes, G. R. Gathers, Phys. Rev. Lett., **60,** 1414-1417 (1988).

[9] P. W. Mirwald, G. C. Kennedy, J. Phys. Chem. Solids, **37,** 795-797 (1976).

[10] G. E. Duvall, R. A. Graham, Rev.Mod.Phys., **49,** 523-579 (1977).

[11] H. Bernier, P. Lalle, in: *High Pressure in Research and Industry* (Proceed. 8 th AIRAPT Conference); Eds. C.-M.Backman, T.Johannisson and L.Tegner. - Uppsala, Arkitektopia, **1,** 194-197 (1981).

[12] T. J. Neal, J. Phys. Chem. Solids, **38,** 225 (1977).

[13] L. V. Al'tshuler, B. S. Chekin, In: Proceed. 1-st All-union symposium of pulse pressures, Moscow: VNIIFTRI, V. 1, 5 (1974).

[14] LASL Shock Hugoniot Data / Ed. S.P.Marsh. - Berkeley: Univ. of California Press, 1980.

[15] A. C. Mitchell, W. J. Nellis, J. A. Moriarty, R. A. Heinle, N. C. Holmes, R. E. Tipton, G. W. Repp, J.Appl.Phys., **69,** 2981-2986 (1991).

[16] R. F. Trunin, G. V. Simakov, Yu. N. Sutulov, A. B. Medvedev, B. D. Rogozkin, Yu. E. Fedorov, Zh. Eksp. Teor. Fiz. **96(9),** 1024-1038 (1989) [in Russian] (Sov. Phys. - JETP **69(3),** 580-588 (1989)).

[17] L. V. Al'tshuler, S. B. Kormer, M. I. Brazhnik, L. A. Vladimirov, M. P. Speranskaya, A. I. Funtikov, Zh. Eksp. Teor. Fiz. **38(4),** 1061-1073 (1960) [in Russian] (Sov. Phys. - JETP **11(4),** 766-775 (1960)).

[18] D. A. Boness, J. M. Brown, J. W. Shaner, In: Shock Waves in Condensed Matter - 87 / Eds. S.C.Schmidt, N.C.Holmes - Amsterdam: North Holland, 115-118 (1988).

[19] C. E. Ragan, Phys. Rev. Ser.A, **25,** 3360-3375 (1982).

[20] L. V. Al'tshuler, N. N. Kalitkin, L. V. Kuz'mina, B. S. Chekin, Zh. Teor. Fiz. 72(1), 317-325 (1977) [in Russian] (Sov. Phys. - JETP 45(1), 167-171 (1977)).

[21] L. V. Al'tshuler, A. V. Bushman, M. V. Zhernokletov, V. N. Zubarev, A. A. Leont'ev, V. E. Fortov, Sov. Phys. - JETP, **51,** 373 (1980).

[22] E. N. Avrorin, B. K. Vodolaga, V. A. Simonenko, V. E. Fortov, *Powerful Shock Waves and Extreme States of Matter,* Moscow: Inst. High. Temp., 1990 [in Russian].

[23] L. V. Al'tshuler, A. A. Bakanova, A. V. Bushman, I. P. Dudoladov, V. N. Zubarev, Zh. Eksp. Teor. Fiz. 73(11), 1866-1872 (1977) [in Russian] (Sov. Phys. - JETP 46(5), 980-983 (1977)).

[24] D. A. Young, B. J. Alder, Phys. Rev. A, 1971, **3,** 364-371 (1971).

[25] K. Hornung, J. Appl. Phys., **46,** 2548 (1975).

[26] D. A. Young, UCRL-52352 (Lawrence Livermore Laboratory, 1977)

[27] V. E. Fortov, I. T. Yakubov, *Physics of Non-Ideal Plasmas,* Chernogolovka: Inst. Chem. Phys., 1983 [in Russian].

[28] G. Pottlacher, H. Jager, Int. J. Thermophys., **11(4),** 719-729 (1990).

[29] R. S. Hixson, M. A. Winkler, J. W. Shaner, High Temp. - High Press., **17,** 267-270 (1985).

[30] G. R. Gathers, Rep. Progr. Phys., **49,** 341-396 (1986).

[31] E. Yu. Tonkov, *Phase Diagrams of Elements at High Pressure,* Moscow: Nauka, 1977 [in Russian].

[32] H. K. Mao, P. M. Bell, J. Geophys. Res. Ser.B, **84,** 4533-4536 (1979).

[33] J. M. Brown, R. G. McQueen, Geophys. Res. Ser.B, **91,** 7485-7494 (1986).

[34] L. V. Al'tshuler, A. A. Bakanova, I. P. Dudoladov, E. A. Dynin, R. F. Trunin, B. S. Chekin, Sov. J. Appl. Mech. Tech. Phys., **22,** 145 (1981).

[35] R. G. McQueen, S. P. Marsh, J. W. Taylor, J. N. Fritz, W. J. Carter, - In: High Velocity Impact Phenomena (1970)/ Ed. R.Kinslow. - New-York: Academic Press, p.293-417; appendies on pp. 515-568.

[36] R. F. Trunin, G. V. Simakov, Yu. N. Sutulov, A. B. Medvedev, B. D. Rogozkin, Yu. E. Fedorov, Zh. Eksp. Teor. Fiz. **96(9),** 1024-1038 (1989) [in Russian] (Sov. Phys. - JETP **69(3),** 580-588 (1989)).

[37] R. F. Trunin, A. B. Medvedev, A. I. Funtikov, M. A. Podurets, G. V. Simakov, A. G. Sevast'yanov, Zh. Eksp. Teor. Fiz. **95,** 631-641 (1989) [in Russian] (Sov. Phys. - JETP **68(2),** 356-361 (1989)).

[38] R. F. Trunin, M. A. Podurets, L. V. Popov, V. N. Zubarev, A. A. Bakanova,V. M. Ktitorov, A. G. Sevast'yanov, G. V. Simakov, I. P. Dudoladov, Zh. Eksp. Teor. Fiz. **102(9),** 1433-1438 (1992) [in Russian] (Sov. Phys. - JETP **75(4),** 777-780 (1992)).

[39] L. V. Al'tshuler, B. N. Moiseev, L. V. Popov, G. V. Simakov, R. F. Trunin, Zh. Eksp. Teor. Fiz. **54,** 785-789 (1968) [in Russian] (Sov. Phys. - JETP **27(3),** 420-422 (1968)).

[40] R. F. Trunin, M. A. Podurets, G. V. Simakov, L. V. Popov, B. N. Moiseev, Zh. Eksp. Teor. Fiz. **62(3),** 1043-1048 (1972) [in Russian] (Sov. Phys. - JETP **35(3),** 550-552 (1972)).

[41] C. E. Ragan, Phys. Rev. Ser.A, **29,** 1391-1402 (1984).

[42] C. S. Yoo, N. C. Holmes, M. Ross, D. J. Webb, C. Pike, Phys. Rev. Lett., **70(25),** 3931-3934 (1993).

[43] R. S. Hixson, M. A. Winkler, M. L. Hodgson, Phys. Rev. Ser. B, **32(10),** 6485-6491 (1990).

[44] R. Hultgren, P. D. Desai, D. T. Hawkins, M. Gleiser, K. K. Kelley, D. D. Wagman, *Selected Values of the Thermodynamic Properties of the Elements.* - Metals Park, Ohio: ASME, 1973.

[45] L. C. Ming, M. H. Manghnani, J. Appl. Phys., **48,** 208-212 (1978).

[46] L. F. Vereshchagin, N. S. Fateeva, High Temp. - High Press., **9,** 619-628 (1977).

[47] J. W. Shaner, G. R. Gathers, C. A. Minichino, High Temp. - High Press., **8,** 425-429 (1976).

[48] K. K. Krupnikov, M. I. Brazhnik, V. P. Krupnikova, Zh. Eksp. Teor. Fiz. **42,** 675-685 (1962) [in Russian] (Sov. Phys. - JETP **15(3),** 470-476 (1962)).

[49] A. H. Jones, W.H. Isbell, C. J. Maiden, J. Appl. Phys., **37,** 3493-3499 (1966).

[50] A. A. Bakanova, I. P. Dudoladov, Yu. N. Sutulov, Zh. Prikl. Mekh. Tekhn. Fiz. **2,** 117-122 (1974) [in Russian](J. Appl. Mech. Techn. Phys. **15,** 241 (1974)).

[51] R. R. Boade, J. Appl. Phys., **40,** 3781-3792 (1969).

[52] U. Seydel, W. Kitzel, J. Phys. F: Metal Phys., **9(9),** L153-L160 (1979).

[53] A. Berthault, L. Arles, J. Matrinson, Intern. J. of Thermophys., **7(1),** 167-179 (1986).

[54] R. S. Hixson, M. A. Winkler, Intern. J. of Thermophys., **11(4),** 709-718 (1990).

[55] W. Fucke, U. Seydel, High Temper. - High Pressures, **12(4),** 419-432 (1980).

[56] V. V. Ivanov, S. V. Lebedev, A. I. Savvatimskii, J. Phys. F: Met. Phys., **14,** 1641-1650 (1984).

Appendix: Pictures to Report

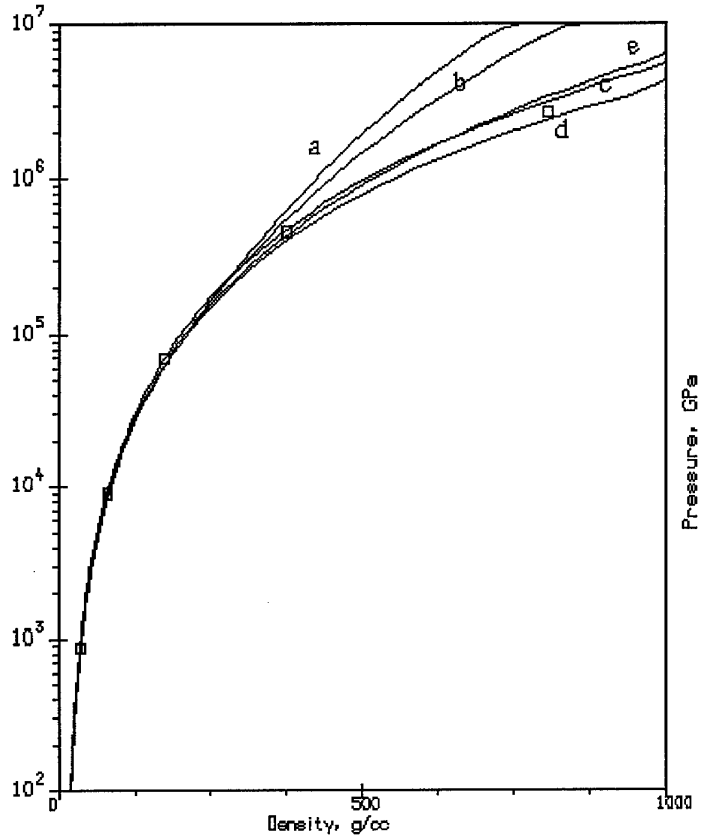

Fig. 1. Cold pressure (p(T=0 K)) in lead. Curves: a - [1], b - [2], c - [3], d - [4], e - this work; points - Thomas-Fermi calculations [5].

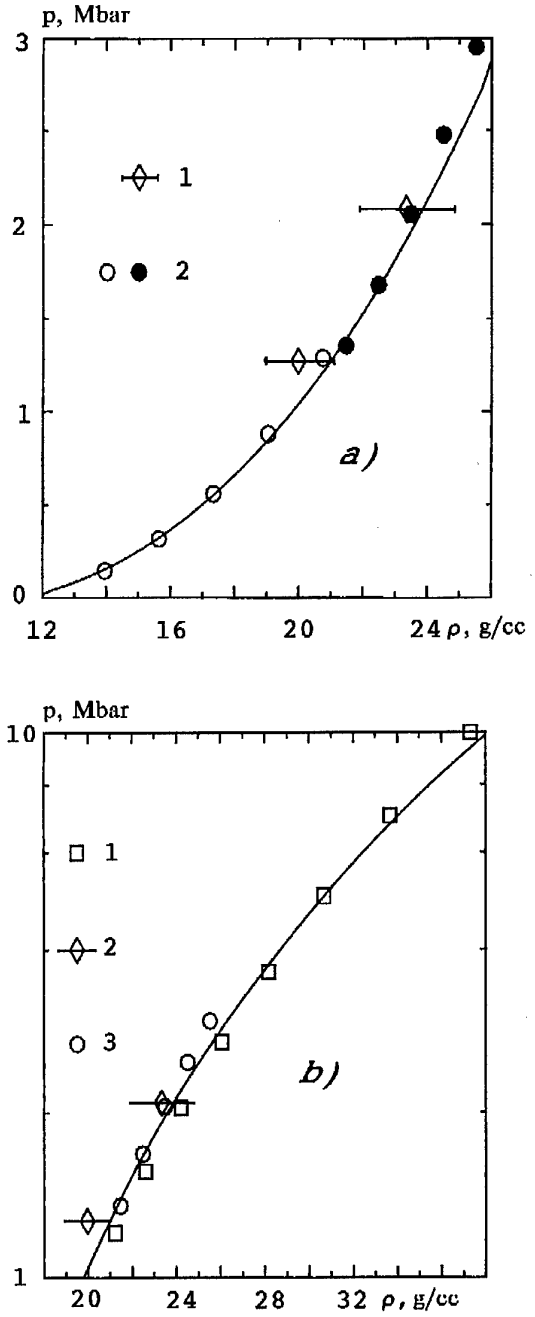

Fig. 2. Lead compressibility at T=298 K.
a) experimental data: 1 - [6], 2 - [7] (open circles - hcp phase, closed - bcc)
b) theoretical calculations: 1 - [8]; experimental data: 2 - [6], 3 - [7] (bcc phase)

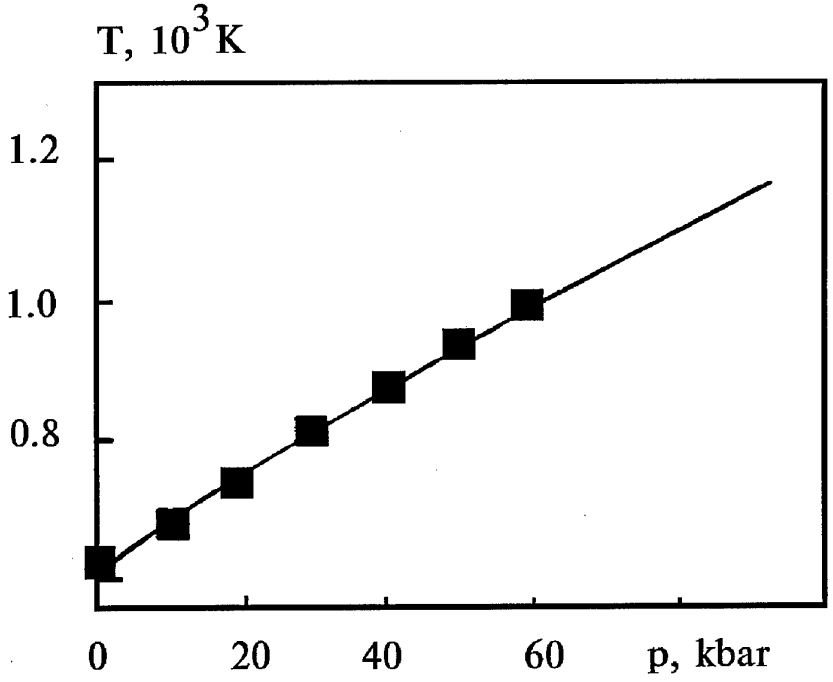

Fig. 3. Melting curve of lead. Points - experimental data [9].

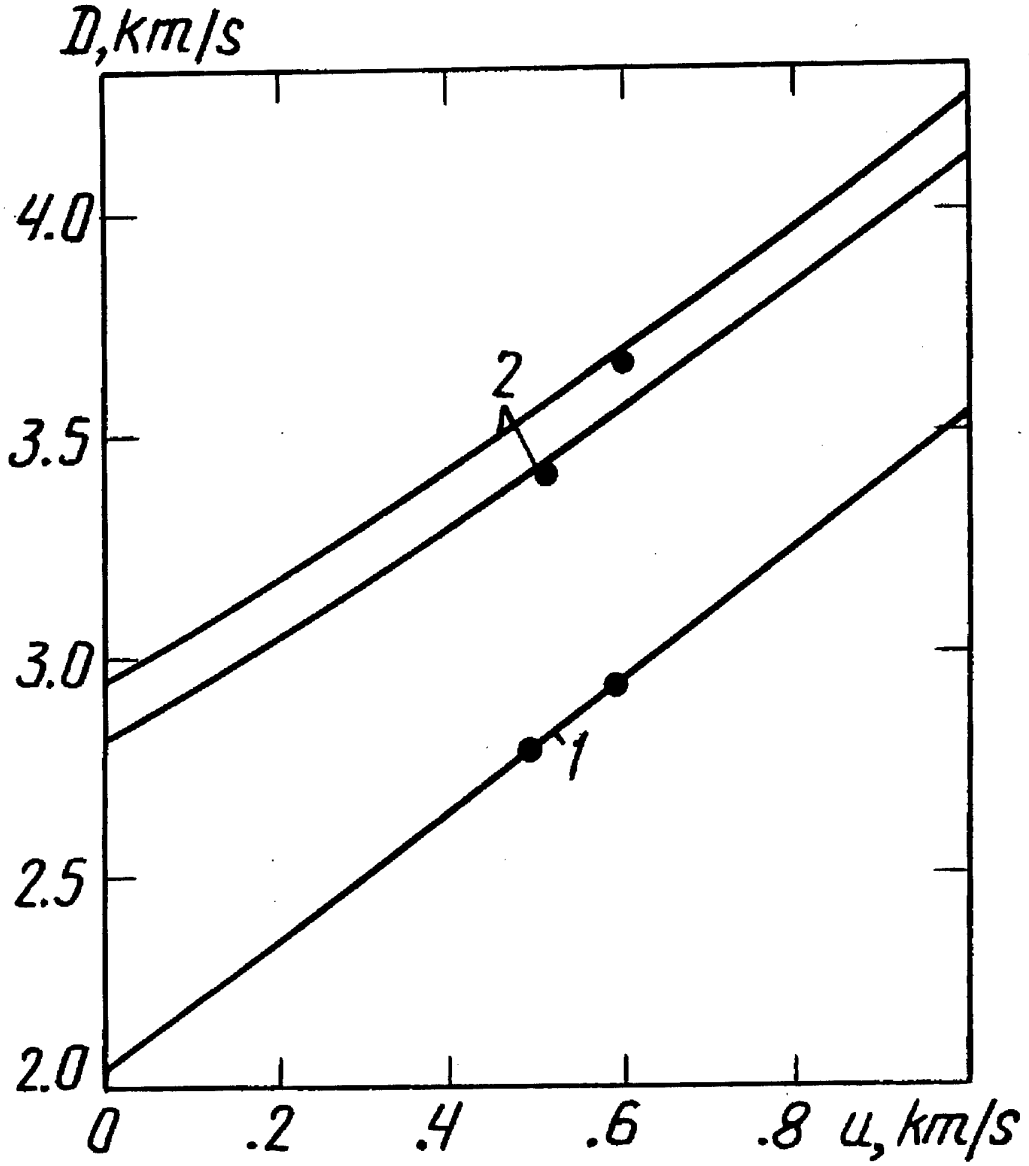

Fig. 4. Single- and double-shock Hugoniot data for lead. Shown are principal Hugoniot (1) and reflected (2) shock waves; points - experimental data [12].

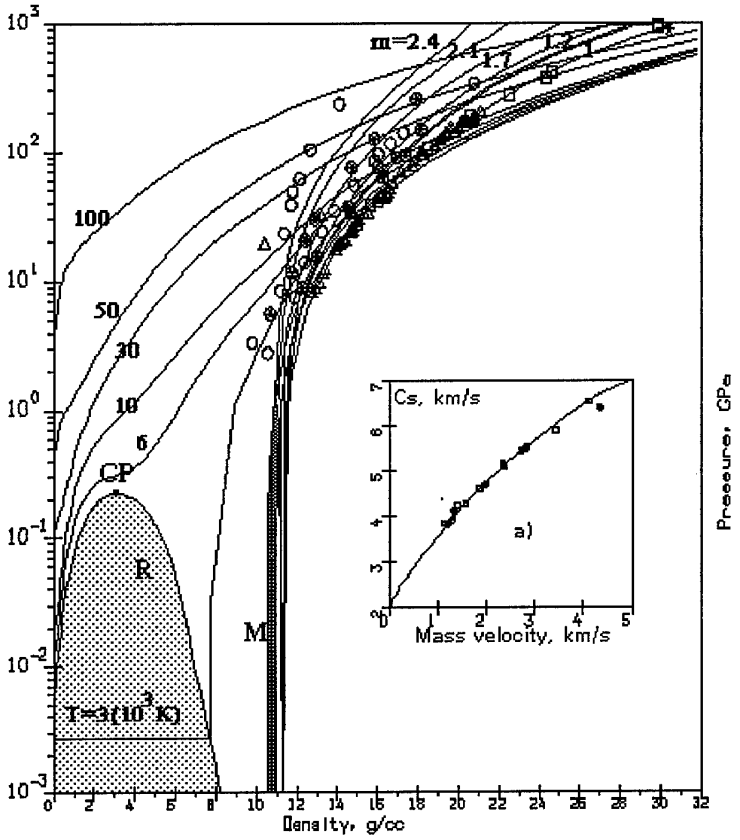

Fig. 5. Phase diagram for lead. T, isotherms; m, porous Hugoniots; M, melting region; R, liquid-vapor equilibrium curve with the critical point CP. Experimental data: □ - [13], Δ - [14], * - [15], ○,⊗ - [16].
a) Sound velocity in shocked lead. Experimental data: □ - [17], ○ - [18].

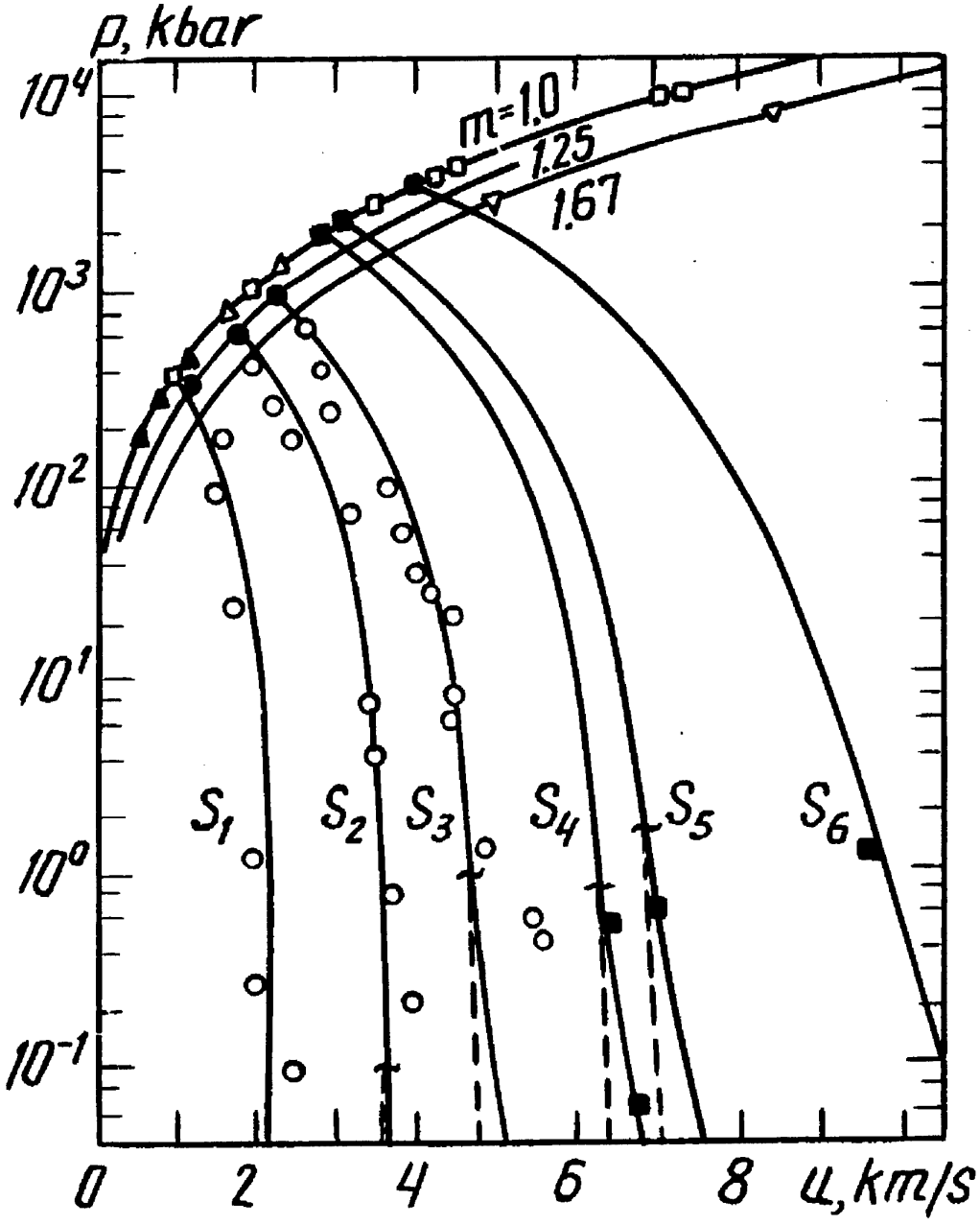

Fig. 6. Shock adiabats (m) and release isentropes (S) for lead. Calculations: solid lines, equilibrium states; dashed lines, metastable states, wavy lines mean the entry into liquid-gas region. Experimental data: □ - [13], Δ - [14], ○- [21], ■ - [23].

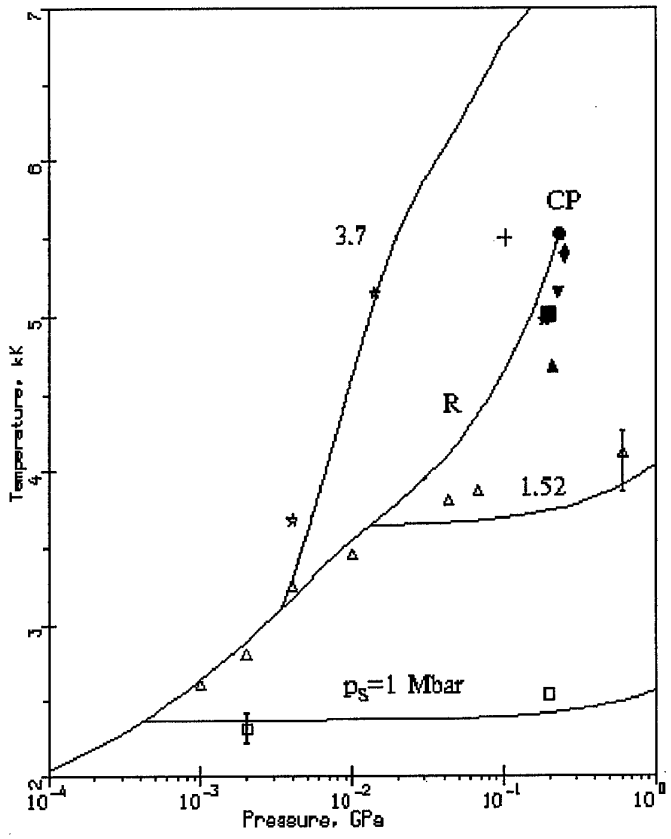

Fig. 7. Pressure-temperature diagram for lead in evaporation region. Shown are: R - boiling curve with critical point CP, ps - release isentropes (1, 1.52, 3.7 Mbar are pressures on shock Hugoniot). Points - experimental data with error bars: □ - for isentrope 1 Mbar, Δ - 1.52 Mbar, ★ - 3.7 Mbar; predictions of critical point for lead: Δ - [24], + - [25], ∇ - [26], ■ - [27], ♦ - [28], • - this work.

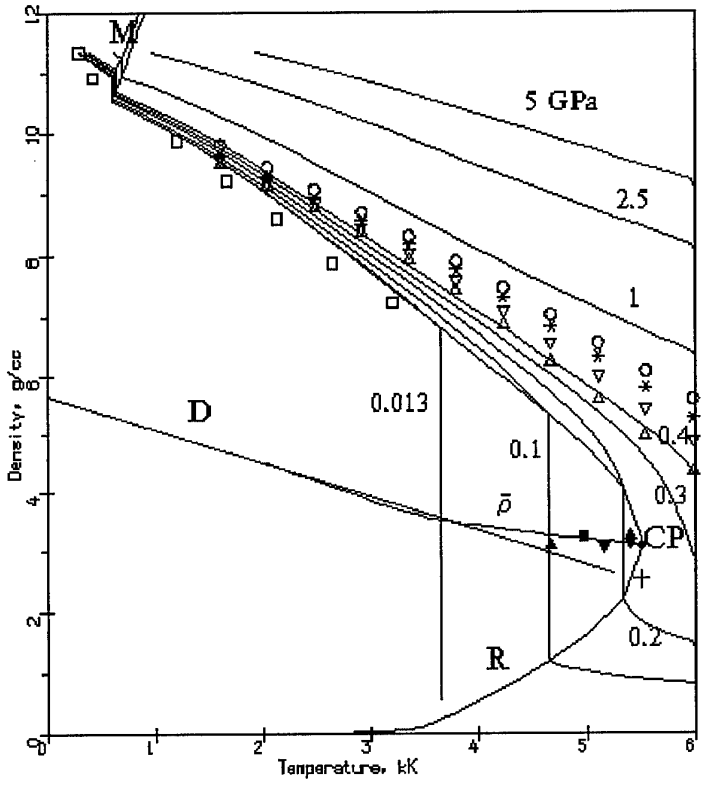

Fig. 8. Phase diagram for lead in the region of lower temperatures. P, isobars; M, melting region; R, liquid-vapor equilibrium curve; D, rectilinear diameter; $\bar{\rho}$, half-sum of liquid and vapor densities. Isobaric expansion data: □ - 0.013 GPa [29], Δ,∇,✱,○ - 0.1, 0.2, 0.3, 0.4 GPa [30]; evaluations of the critical-point parameters: Δ - [24], + - [25], ∇ - [26], ■ - [27], ♦ - [28], • - this work.

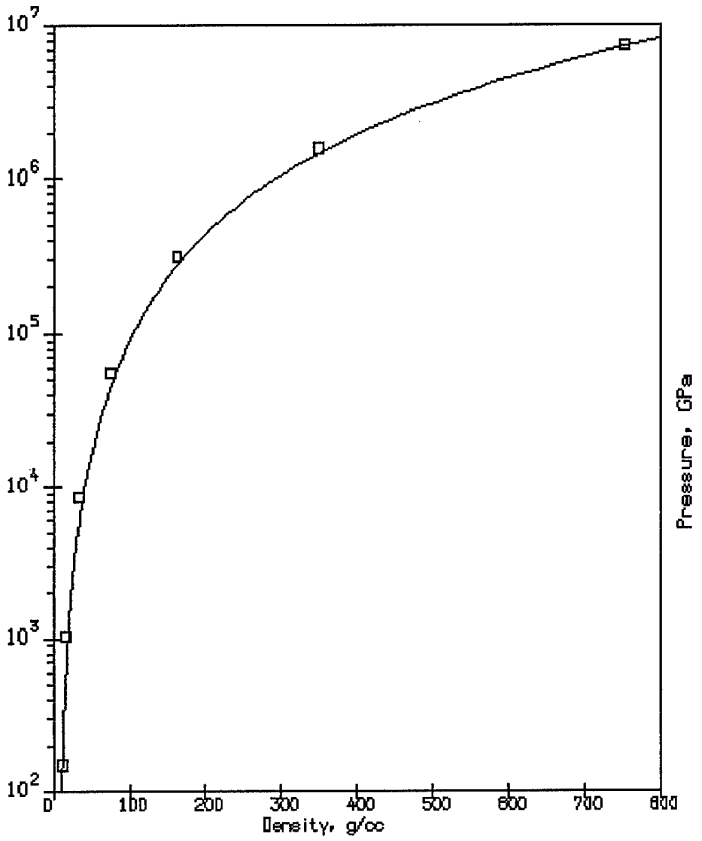

Fig. 9. Cold pressure (p(T=0 K)) in iron. Curve - this work; points - Thomas-Fermi calculations [5].

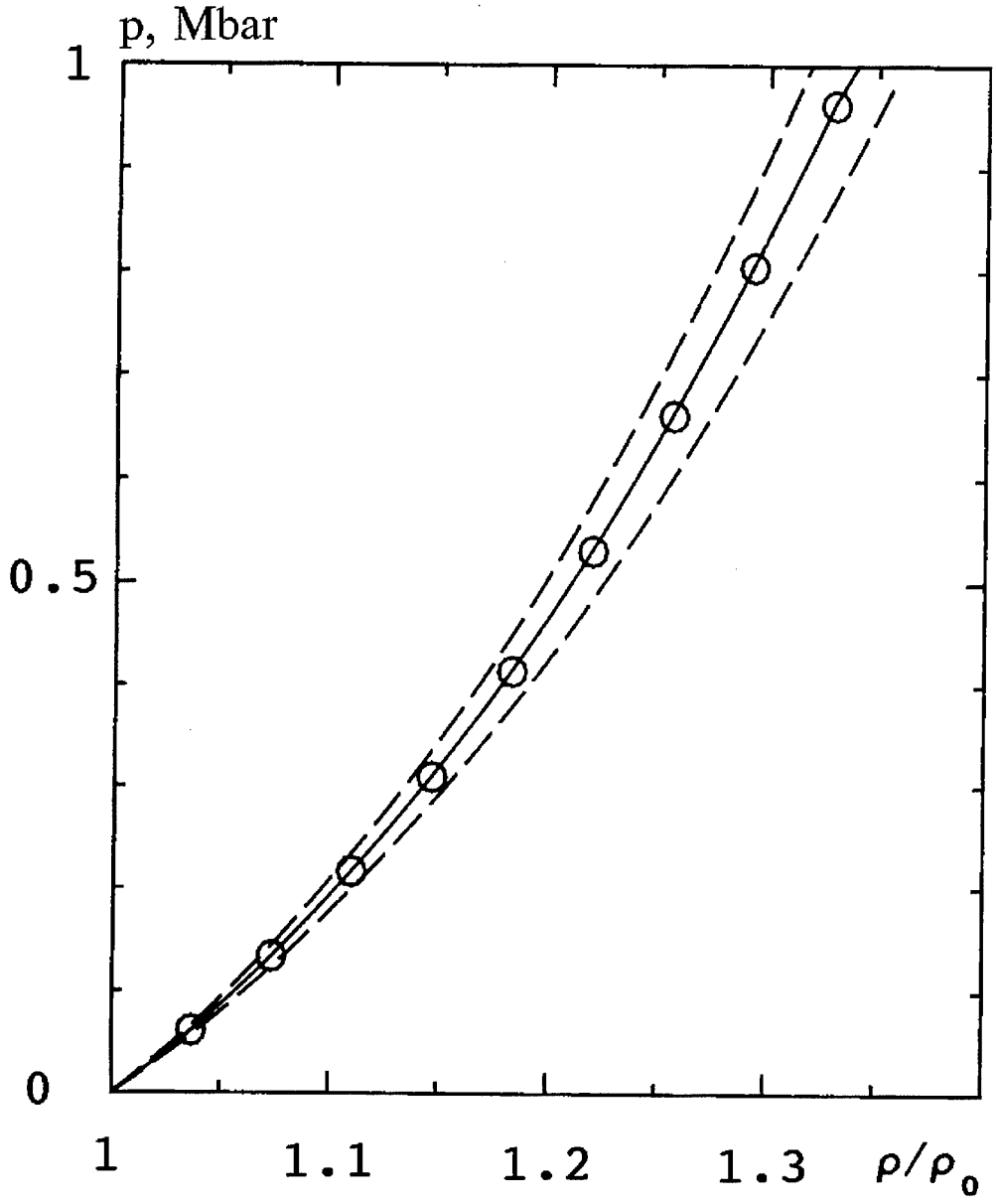

Fig. 10. Iron compressibility at T=298 K.
Solid line - EOS calculation, dashed line - region of experimental error, points - experimental data [32].

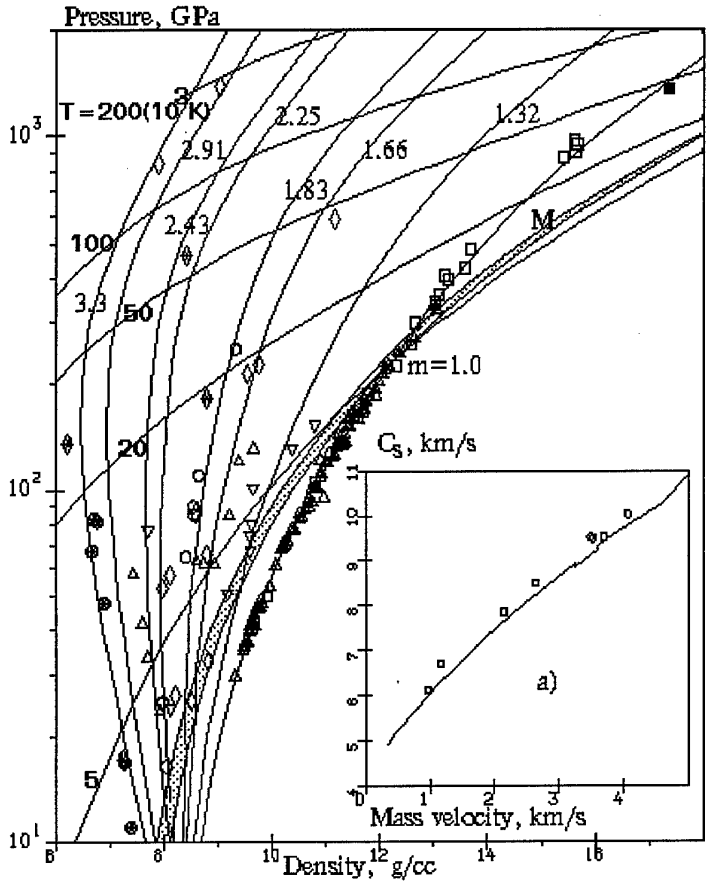

Fig. 11. Phase diagram for iron. T, isotherms; m, porous Hugoniots; M, melting region. Experimental data: □ - [13], Δ,∇ - [14], ◊, ♦ - [37], ○,⊗ - [36], ■ - [34].
a) Sound velocity in shocked iron. Experimental data: □ - [17], ○ - [33].

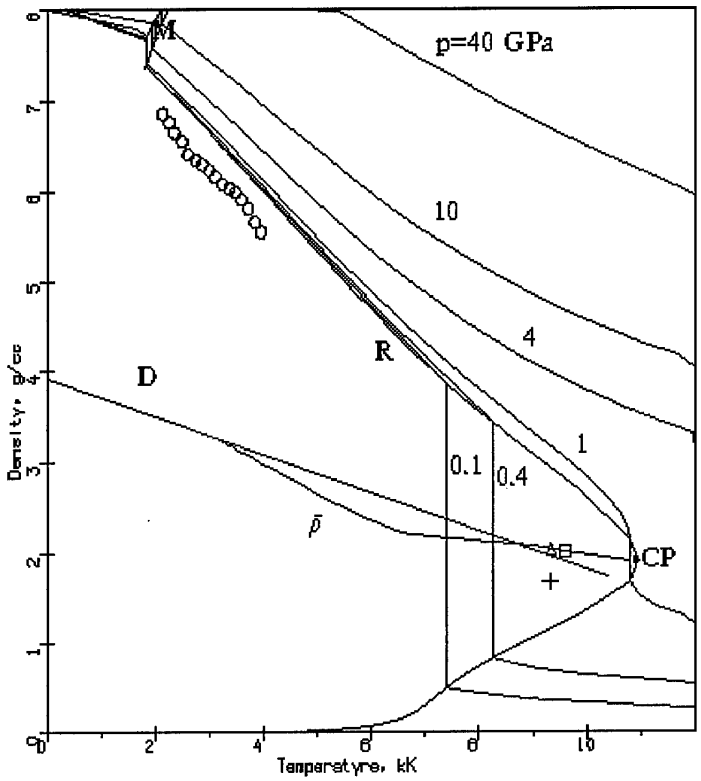

Fig. 12. Phase diagram for iron in the region of lower temperatures. P, isobars; M, melting region; R, liquid-vapor equilibrium curve; D, rectilinear diameter; $\bar{\rho}$, half-sum of liquid and vapor densities. Points: isobaric expansion measurements O - [42]; evaluations of the critical-point parameters: Δ - [24], + - [25], □ - [27], • - this work.

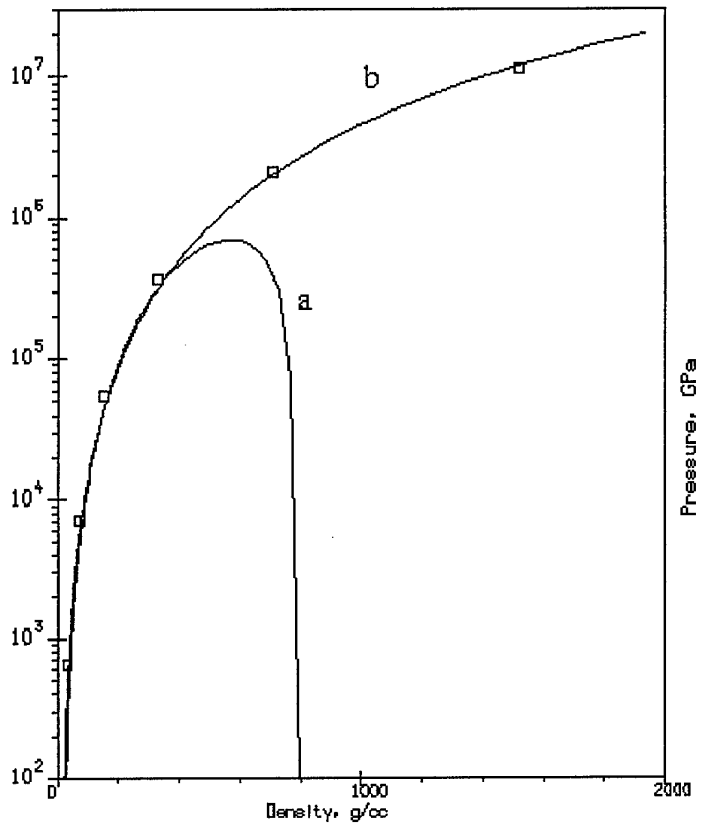

Fig. 13. Cold pressure (p(T=0 K)) in tungsten. Curves: a - [2], b - this work; points - Thomas-Fermi calculations [5].

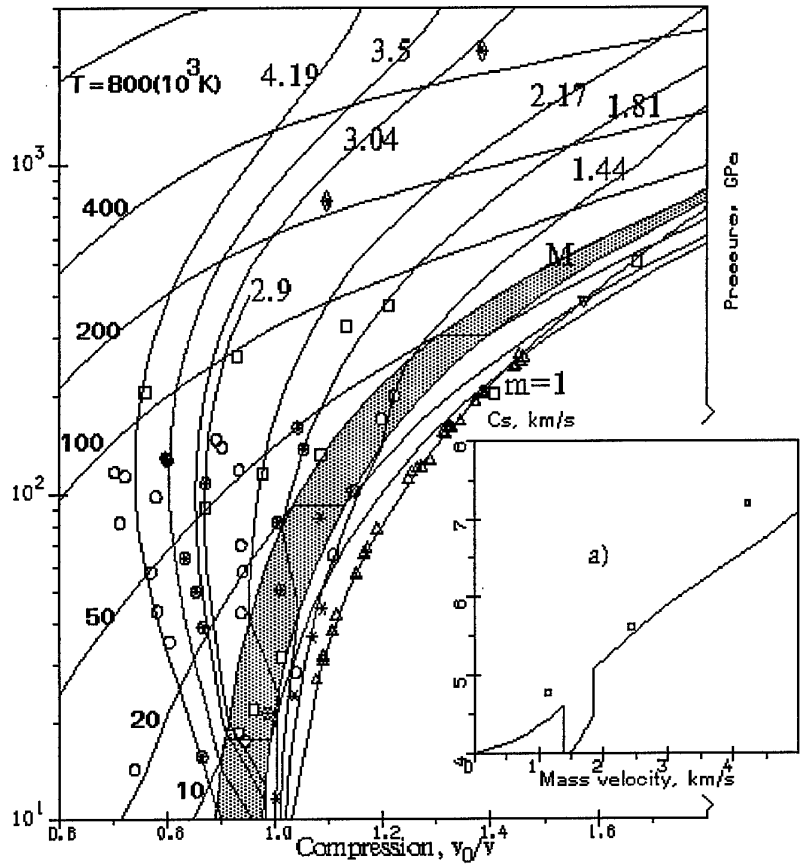

Fig. 14. Phase diagram for tungsten. T, isotherms; m, porous Hugoniots; M, melting region. Experimental data: □ - [48], Δ - [14], ∇ - [49], ♦ - [37], ○,⊗ - [36], ✶ - [50].
a) Sound velocity in shocked porous (m=1.8) tungsten. Experimental data: □ - [48].

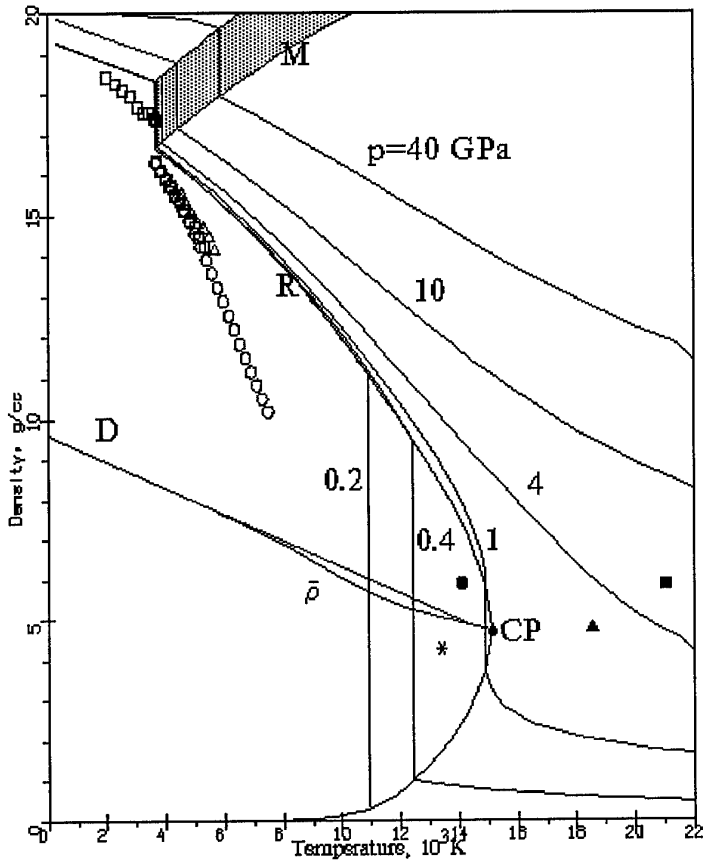

Fig. 15. Phase diagram for tungsten in the region of lower temperatures. P, isobars; M, melting region; R, liquid-vapor equilibrium curve; D, rectilinear diameter; $\bar{\rho}$, half-sum of liquid and vapor densities. Points: isobaric expansion measurements O - [52], □ - [53], Δ - [54]; evaluations of the critical-point parameters: Δ - [24], ● - [52], ✶ - [55], ■ - [27], • - this work.

HEDRC REPORT

Printed December 1993

WIDE-RANGE EQUATION OF STATE FOR LARGE COMPUTER CODES

I. V. Lomonosov, V. E. Fortov, and K. V. Khishchenko

Prepared by
High Energy Density Research Center
Russian Academy of Sciences
Izhorskaya Str. 14/19, Moscow 127412, Russia
for USAF
by contract SPC-93-4074

WIDE-RANGE EQUATION OF STATE FOR LARGE COMPUTER CODES

I. V. Lomonosov, V. E. Fortov, and K. V. Khishchenko

High Energy Density Research Center
Russian Academy of Sciences
Izhorskaya Str. 14/19, Moscow 127412, Russia

Abstract

The report is devoted to equation-of-state (EOS) problem. It describes wide-range four-phase (solid, liquid, gas and plasma) semiempirical EOS model. The EOS is given by free-energy thermodynamical potential and is complete in thrmodynamical sense. The EOS model, its structure, procedure of determination EOS coefficients are described. Results of construction EOS for aluminum, copper and lithium are reported. The comparison of thermodynamical properties of these metals calculated by EOS with available high-pressure theoretical and experimental data is given.

1. Introduction

Equation of state is the fundamental characteristic of matter determining its thermodynamic properties over a wide range of the phase diagram. Semiempirical EOS use with great efficiency results obtained by first-principle theories and experimental data. For more details see, for example, review [1] and references therein. Presented in the paper are semiempirical EOS model that was developed to describe metals in solid, liquid and plasma states and results of EOS construction for aluminum, copper, and lithium.

2. EOS Model

A thermodynamically complete temperature EOS is defined by the free energy, F, written as,

$$F(V,T)=F_c(V)+F_a(V,T)+F_e(V,T) \tag{1}$$

describing the elastic contribution at T=0 K (F_c), and the heat contribution by atoms (F_a) and electrons (F_e), respectively.

2.1. Cold Curve

The elastic energy for the solid phase is given in form

$$F_c^{(s)}(V) = 3V_{0c} \sum_{i=1,5} \frac{a_i}{i}\left(\sigma_c^{i/3} - 1\right), \tag{2}$$

(where $\sigma_c = V_{0c} / V$, V_{0c} - specific volume at p=0) providing for conditions $F_c^{(s)}(V_{0c}) = 0$, $p_c(V_{0c}) = 0$, correct tabular values (with heat component) of bulk compression modulus and its pressure derivative at ambient conditions, as well as the accordance with first-principle theories up to 100-fold compressions [2].

The cold energy for the liquid phase in compression region ($\sigma_c \geq 1$) is given by Formula (2), while in the rarefaction region ($\sigma_c < 1$) it is represented by a polynomial of the form

$$F_c^{(l)} = F_c^{(l)} = V_{0c}\left[A\left(\sigma_c^m/m - \sigma_c^n/n\right) + B\left(\sigma_c^l/l - \sigma_c^n/n\right)\right] + E_{sub}, \quad (3)$$

which leads to the tabular values [3] of the cohesion energy $E_c(V \to \infty) = E_{sub}$ and satisfies the condition $p_c(V_{0c}) = 0$. The equality of the cold-energy derivatives $p_c = -\frac{dE_c}{dV}, B_c = -\frac{1}{V}\frac{dp_c}{dV}, B_{pc} = \frac{dB_c}{dp}$ at $\sigma_c = 1$ remains in (3) two free parameters, *n* and *l*. They are determined by the experimental temperature dependence of density and sound velocity for liquid metals.

2.2. Thermal Contribution of the Atoms

2.2.1. Solid phase

The lattice contribution to the free energy of the solid phase is defined by the expression

$$F_a^{(s)}(V,T) = 3RT\ln\frac{\theta_c^{(s)}(V)}{T}, \quad (4)$$

where R is the gas constant. The characteristic temperature is given by empirical expression

$$\theta_c^{(s)}(V) = \theta_0^s \sigma^{2/3} \exp\left\{\frac{(\gamma_{0s} - 2/3)\left(B_s^2 + D_s^2\right)}{B_s} \operatorname{arctg}\left[\frac{xB_s}{B_s^2 + D_s(x + D_s)}\right]\right\}, \quad (5)$$

where $x = \ln\sigma$. Constants B_s and D_s are determined by the experimental dependence of Gruneisen gamma $\gamma = \frac{d\ln\theta}{d\ln\sigma}$ on compression σ. This dependence is obtained on the base of shock-wave data. The value of γ_{0s} corresponds to tabular one of Gruneisen gamma at ambient conditions [3]. Note that at high compressions Eq. (5) provides for the correct ideal-gas asymptote $\cong \sigma^{2/3}$. The value of θ_0^s is given by condition $s(V_0) = 0$.

2.2.2. Liquid phase

The atomic contribution to the free energy of the liquid phase is represented as a sum

$$F_a^{(l)}(V,T) = F_t(V,T) + F_m(V,T), \tag{6}$$

the first term accounts for anharmonicity effects and the second provides for a proper behavior of melting curve.

In the liquid phase the phonon contribution has a form similar to Eq. (4) but with a volume- and temperature-dependent heat capacity c_a and a characteristic temperature $\theta^{(l)}$

$$F_t^{(l)}(V,T) = c_a(V,T)T\ln\frac{\theta^{(l)}(V,T)}{T}. \tag{7}$$

The heat capacity in the liquid phase is given by the expression

$$c_a(V,T) = \frac{3R}{2}\left[1+\frac{\sigma T_a}{(\sigma+\sigma_a)(T+T_a)}\right], \tag{8}$$

describing a smooth variation from the value 3R close to the lattice heat capacity to that one of an ideal atomic gas, 3R/2. Coefficients σ_a and T_a define the characteristic density and temperature of this transition.

The vibrational spectrum defined by the variation of the characteristic temperature reflects the gradual change of the Gruneisen coefficient of the liquid phase from values $\gamma^{(l)} \approx \gamma^{(s)}$ corresponding to condensed states to the ideal-gas value of 2/3 in the limit of high temperatures and very low densities. Under these assumptions, the characteristic temperature is given by the approximating formula

$$\theta^{(l)}(V,T) = T_{sa}\frac{\left(T_{ca}\theta_c^{(l)} + T\right)\sigma_c^{2/3}}{T_{ca}+T}, \tag{9}$$

where characteristic temperature is liquid phase is presented in form analogous to Eq. (5)

$$\theta_c^{(1)}(V) = \theta_0^1 \exp\left\{\frac{\left(\gamma_{01} - 2/3\right)\left(B_1^2 + D_1^2\right)}{B_1} \operatorname{arctg}\left[\frac{xB_1}{B_1^2 + D_1(x + D_1)}\right]\right\}. \qquad (10)$$

The parameters in Eq. (10) B_1 and D_1 are found from shock-wave experiments on solid and porous samples, the constant θ_0^1 is determined by equation $\theta_a(0) = T_{ca}$.

The potential term $F_m(V,T)$ provides for a correct value of the entropy $\Delta s = \Delta s_{m0}$ and volume $\Delta V = \Delta V_{m0}$ changes on melting at ambient pressure and disappears in the gas phase. The contribution of F_m should also decrease upon compression due to decreasing differences between the properties of the solid and liquid phases. These requirements are satisfied by the relation

$$F_m(V,T) = 3R\left\{\frac{2\sigma_m^2 T_{m0}}{1+\sigma_m^3}\left[C_m + \frac{2A_m}{5}\left(\sigma_m^{5/3} - 1\right)\right] + (B_m - C_m)T\right\}, \qquad (11)$$

where $\sigma_m = \sigma / \sigma_{m0}$ is the relative density of the liquid phase on the melting curve. The constants A_m, B_m, C_m are uniquely determined by the equilibrium conditions along the melting curve at $T = T_m$.

2.3. Electron Contribution

The thermal electrons contribution has the same form for solid and liquid phases. It is given by following relationship

$$F_e(V,T) = -c_e(V,T)T \times \ln\left[1 + \frac{B_e(T)T}{2c_{ei}} \exp\left(-\gamma_e(V,T)\right)\right] \qquad (12)$$

This formula contains generalized analog of the coefficient of electron heat capacity B

$$B_e(T) = \frac{2}{T^2}\int\left(\int_0^T \beta(\tau)d\tau\right)dT, \qquad (13)$$

$$c_{ei} = \frac{3RZ}{2}, \qquad (14)$$

the heat capacity of the electron gas

$$c_e(V,T) = \frac{3R}{2}\left[Z + \frac{\sigma_z T_z^2 (1-Z)}{(\sigma+\sigma_z)\left(T^2+T_z^2\right)}\right]\exp\left[-\frac{\tau_i}{T}\right], \qquad (15)$$

the analogs of the electronic Gruneisen coefficient

$$\gamma_e(V,T) = \gamma_{ei} + \left(\gamma_{e0} - \gamma_{ei} + \gamma_m \frac{T}{T_g}\right)\exp\left[-\frac{T}{T_g} - \frac{(\sigma-\sigma_e)^2}{\sigma\sigma_d}\right], \qquad (16)$$

and of the coefficient of the electronic heat capacity

$$\beta(T) = \beta_i + \left(\beta_0 - \beta_i + \beta_m \frac{T}{T_b}\right)\exp\left[-\frac{T}{T_b}\right]. \qquad (17)$$

Approximating dependencies are selected such to satisfy primarily the asymptotic relations for the electron gas free energy, namely expressions for degenerate electron gas at moderate ($T<<T_{Fermi}$) temperatures

$$F_e(V,T) = -\frac{\beta_0 T^2}{2}\sigma^{-\gamma_0},$$

and expressions for an ideal electron gas at $T \to \infty$ range

$$F_e(V,T) = \frac{3RZ}{2}\ln\left(\sigma^{2/3}T\right).$$

Here Z is the atomic number and R is the gas constant. The specific form of writing down separate expressions of the potential (12) depends upon the satisfaction of these requirements.

The Eqs. (12)-(17) are written in a form which represents correctly the primary ionization effects in the plasma region and the behavior of the partially ionized metal. The expression $\tau_i = T_i \exp(-\sigma_i/\sigma)$ describes a decrease of the ionization potential as the plasma density increases, and the constants σ_z and T_z define, respectively, the characteristic density of the 'metal-insulator' transition and the temperature dependence of the transition from a singly ionized gas to a plasma with the ion-charge mean value Z.

3. Procedure for constructing EOS

The set of equations (1)-(17) fully assigns the thermodynamic potential for metals over entire phase diagram region of practical interest. Some coefficients in the equation of state, included in the analytical expressions, are constants characteristic for each metal and are found from tabular data, while the rest serve as fitting parameters and their values are found from the optimum description for the available experimental and theoretical data. It should be emphasized that, even though the number of coefficients in Eqs. (1)-(17) is large, most of them are rigidly defined constants whose values are assigned explicitly or implicitly from the fulfillment of various thermodynamic conditions at specific points on the phase diagram. A few coefficients (about ten) serve to characterize the densities and temperatures on transition from one typical phase-plane region to another and are found empirically.

In determining the numerical values of coefficients in the EOS, use was made of the numerous experimental and theoretical data characterizing the thermodynamic properties of metals under study for a wide range of parameters. This procedure was carried out with the aid of a specially developed computer program using the Eqs. (1)-(17) for thermodynamic calculations. At the preliminary stage of calculations, some thermodynamic constants known for each substance (such as normal density; changes in density and entropy at the melting point under normal pressure; cohesion energy; and the like) were used by the program automatically find a number of other uniquely defined coefficients (parameters of the cold curve, melting curve, and so on).

This further enables one, by way of calculating algebraic or integral relations valid for self-similar hydrodynamic flows to perform calculations of kinematic characteristics measured experimentally at high and ultrahigh pressures, namely, the incident and reflected wave velocities and velocities in adiabatic expansion waves (release isentropes), as well as to allow for melting and evaporation effects in the results obtained. The range of action of each fitting coefficient that remains free is very localized, as a result of which its value may be selected independently from a comparison of the calculations with available experimental data.

4. Thermodynamic properties of metals

The performance of specific hydrodynamic calculations calls for the assignment of thermodynamic characteristics of metals over a large area of the phase diagram with correct asymptotic behavior in the high-temperature/high-pressure limit. This part of the report deals with the description of the thermodynamics of aluminum, copper and lithium over a wide range of pressures and temperatures, based on the above-discussed semiempirical EOS.

The most significant experiments for constructing EOS are described for each metals investigated; experimental data are compared with calculations. Also presented are new results obtained by calculations of regions for which no experimental data are presently available and for which theoretical models only yield general estimations. This applies primarily to the position of the high-temperature evaporation curve and of the critical point, which are important for the calculation of most high-energy processes. No less essential is a correct thermodynamic description of the metallic liquid and dense plasma, as well as the shape of the melting curves with respect to which only isolated, often thermodynamically incomplete experimental data are available. Finally, the most important result obtained would appear to be the consistent description, within a unified EOS, of numerous diverse experimental data, many of which are not directly related to the EOS but reflect rather the integral or differential thermodynamic characteristics of substances.

4.1. Aluminum

Aluminum and its alloys are used extensively as basic structural materials of experimental end production facilities operating under conditions of intensive pulsed-energy release. In addition, aluminum serves as a standard material for investigations in the high-pressure region and, consequently, the equation of state for this metal needs to be especially exact and reliable.

In the case of aluminum in the region of low pressures and relatively low temperatures ($T<2500$ K), numerous steady-state thermophysical data are available including the results of measuring the density, heat capacity and velocity of sound for the solid and liquid phases, and of determining the shape of the

melting curve. Without dwelling on details, we shall note that all of these characteristics are described by the equation of state obtained to an accuracy of 1-3% or better, as illustrated by Fig. 1 which presents a comparison of the theoretical and experimental data on the pressure dependence of temperature on the melting curve.

The reliability of the equation of state for aluminum in the region of high pressures and reduced (relative to the standard shock adiabat) temperatures is illustrated by Fig. 2 which presents calculations and experimental data on double-shock compression of samples [6,7]. The characteristics of increased (as compared with the principal shock adiabat) temperatures are found from experiments in shock compression of samples with different initial porosities. Shown in Fig. 3 is a comparison of data from such experiments with theoretical data obtained from the semiempirical equation of state. Also plotted in this figure are experimental [8] and theoretical data on isentropic expansion of shock-compressed porous samples. In spite of the heterogeneous nature of source experimental data obtained by independent researchers and assigned usually as the simplest approximations, all the data could effectively be combined and described within a unified wide-range equation of state. In addition to the shock adiabats for porous samples, the point of intersection of the melting curve and the adiabat with m=1.69, which coincided with the experimentally registered point, has also been determined for aluminum in the region of moderate pressures; this was registered by a sharp velocity decrease in the isentropic release wave following the disappearance of the transverse component of the velocity of sound upon melting [11].

The phase diagram for aluminum is shown in Fig. 4 in which are plotted the experimental points for shock compression of solid and porous samples in the high-pressure region, and calculated shock adiabats for different porosities and isotherms; the melting and evaporation regions are also mapped out. As follows from this figure, the traditional region of shock-wave studies restricted to a pressure of ca. 5 Mbar is described to a high accuracy by the equation of state obtained. An adequate description of experiments is observed both in the case of velocity-of-sound measurements in shock compressed samples (Fig. 4a). A good theoretical description is available for the experimentally obtained dependence of the Gruneisen coefficient upon volume on the shock adiabat [7].

According to calculations, the melting region on the shock adiabat of aluminum corresponds to pressures of 1.13 to 1.84 Mbar. The lower limit is in excellent agreement with the experimentally obtained value for the onset of melting, p>1 Mbar, found from measurements of the viscosity behind the shock front [18].

Special attention was given to the problem of correct description of the few experimental data in the region of ultrahigh pressures which play a decisive role in the construction of semiempirical equations of state for the high-energy range of parameters. In the case of aluminum, the situation is aggravated by the fact that band-theory calculations [19] at a pressure of p=2 Mbar led to the prediction of an electron phase transition which had earlier appeared to have some experimental support [20]. In view of this, a shock adiabat allowing for this transition [21] was employed in calculations in the region of ultrahigh pressures. New experimental data which made their appearance in recent years [14,22-24] failed, however, to point to any anomalies that could be attributed to the effects of rearrangement of the electronic structure. Fig. 5 presents a comparison of the available experimental points with calculations from various equations of state. It can be seen from the figure that, as distinct from the Thomas-Fermi model with corrections [25], the semiempirical equation of state obtained by the present authors makes it possible to accurately reproduce the entire set of data on absolute measurements of compressibility at high and ultrahigh pressures. It is worthy of note that the results obtained turned out to be close to recent theoretical calculations from modified Hartree-Fock-Slater models [26,27] which also fail to show any phase transition.

The characteristics of the dense highly heated liquid phase of aluminum and the parameters of the liquid-vapor equilibrium line have not been investigated since the high temperatures required considerably exceed the heat resistance limits of stationary facilities. Apart from the evaporation-temperature data at standard pressure, information on the critical parameters is only available in the form of semiempirical evaluations [30-33]. Plotted in Fig. 6 for aluminum are the calculated values of the temperature dependence of density on the isobars and on the liquid-vapor equilibrium line. Also shown in the drawing is the deviation of the calculated temperature dependence of the half-sum of liquid and vapor densities from the law of rectilinear diameter. Calculations have yielded the exact

experimental value of the evaporation temperature, T =2772 K, and the critical-point parameters, p_c=5.71 kbar, T_c=7222 K, V_c=1.24 cc/g and s_c=4.66 J/g·K, which are in good agreement with current evaluations, also plotted in the figure. Practically coinciding with the experimental data are the calculated temperature dependencies of density and velocity of sound in the liquid phase.

The foregoing drawings fully cover the experimental information on the thermodynamic properties of aluminum in the region of high pressures and temperatures. It is evident that the entire set of experimental data is described to a high accuracy by the equation of state obtained. The equation of state further provides an accurate description of primary ionization and displays the requisite asymptotic behavior in the limit of high temperatures and large volumes. As a result, the equation of state obtained can be used efficiently in hydrodynamic calculations under conditions of intensive energy release.

4.2. Copper

Like aluminum, copper finds extensive application as a structural material and, consequently, the thermodynamic properties of this metal must be calculated reliably. In order to avoid a repetition of the contents of the preceding section will only contain (as following sections on lead and lithium) a summary of the principal results accompanied by a minimum comment.

The data in the region of moderate pressures and temperatures obtained for copper from stationary thermophysical experiments have, analogously to the case of aluminum, an accuracy of description of the order of 1% or more. The most accurate data determining the course of the melting curve [4] are presented in Fig. 1, together with the results of calculation which practically coincide with experiment.

The thermodynamical properties for a wide region of the phase diagram at moderate pressures ($p<1$ Mbar) are determined from numerous shock-compression experiments on porous samples. Figure 7 shows a complete set of those data with the corresponding calculated shock adiabats. This figure suggests that the calculated curves agree with experiment over a wide range of porosity

values, overlapping the area of the phase diagram from the principal shock adiabat to volumes of $V<1.2V_0$.

A large area of the phase plane of copper ranging from states on the shock adiabats to the near-critical region of parameters was studied using the isentropic expansion method [36]. This method involves a continuous study of a pressure range of four orders of magnitude and a density range of two orders of magnitude, i.e., from a highly compressed metallic liquid to a quasi-nonideal Boltzmann plasma and metallic vapor. Plotted in Fig. 8 are metastable and equilibrium isentropes of expansion and shock adiabats calculated for different porosities. A comparison of the calculated isentropes with the experimental data shows that, at an above-critical pressure, the maximum divergence in the expansion rate is about 3% which is just within the experimental error. Upon entry into the two-phase region, an increasing deviation of the calculated curves from the experimental results is observed which is probably due to a nonuniform energy distribution in the heated metal particles. Note should be made, however, of the correspondence between kinks in the calculated curves at the onset of evaporation and the experimentally observed additional increase of the expansion rate within the two-phase liquid-vapor region.

The phase diagram for copper shown in Fig. 9 presents a consistent description of shock-wave data in a pressure range of hundreds of kilobars to tens of megabars. The semiempirical equation of state obtained for copper further describes, with similar accuracy, experimental measurements of the velocity of sound on the shock adiabat (Fig. 9a).

Of special interest are the experiments in shock compression of highly porous copper in the 10-20-Mbar pressure range [37]. As distinct from the case of compression of solid samples, the attendant states correspond to a weakly generate electron gas with extremely high heat energy-density of about $3*10^3$ kJ/cc. Corresponding to such conditions in the TFC model [39], which is widely used for describing this region of parameters, are the characteristic values of the Gruneisen coefficient of about 0.45 which lead to high compression ratios upon shock-loading (shown by the dashed line in Fig. 9). This result is clearly in conflict with the experimental results of Ref. [37] and points to the inapplicability of TFC-based calculations in the region in question. As distinct from this model,

the equation of state developed describes correctly all the data on shock compression at ultrahigh pressures [37,40].

The adequacy of calculations on the shape of the melting curve for copper in the high-pressure region can be verified by experiments on the residual temperature in the isentropic release wave (Fig. 9b). According to the calculations, the melting region on the shock adiabat corresponds to the 1.9-2.7-Mbar range; the values of temperatures in the release wave are in good agreement with experiment. Calculations in which melting is ignored yield, as can be seen from Fig. 9b, residual temperature values over estimated by 500 K.

The liquid-phase parameters and the position of the evaporation curve for copper have been determined quite reliably by experiments on the isentropic expansion [36]. In constructing an equation of state, the expansion isentropes serve as a closing link in that they link together the parameters of the equilibrium curve upon entry into the two-phase liquid-vapor region.

The coefficients of the equation of state for copper obtained from the above-mentioned experiments in isentropic expansion made possible highly reliable and complete calculations of the characteristics of the highly heated liquid and dense plasma.

Presented in Fig. 10 are the results of calculating the isobars and the equilibrium curve; also plotted are estimated values of the critical-point parameters obtained from methods of thermodynamic similarity. The calculated value of the evaporation temperature, T_c =2841 K, practically coincides with the experimental value, with critical-point parameters equal to, p_c=9.04 kbar, T_c=7830 K, V_c=0.44 cc/g and s_c=1.97 J/gK which, as can be seen from the figure, are close to most estimates.

All of the figures in this section are indicative of the adequate and self-consistent description of the available set of experimental data over the entire phase plane. Consequently, the results obtained may be used widely in calculations of the thermodynamic characteristics of copper when solving applied problems.

4.3. Lithium

The extensive utilization of lithium as the working medium of many modern power-generating plants adds to the importance of reliable temperature range covering the entire spectrum of working states. For lithium, with its relatively low melting and evaporation temperatures, many highly experiment data are available in the traditional region of stationary thermophysical experiment. The bulk of those data, covering relatively low static pressures and temperatures of $T<2000$ K, were treated simultaneously in a monograph [44] containing detailed tables of thermodynamic properties of lithium in this range of parameters. In the region of high temperatures and pressures, however, the available data from static and dynamic experimental measurements are very limited and often thermodynamically incomplete, which prevents one from employing a statistical treatment of the data for the interest in constructing an equation of state. These facts account for the interest in constructing a semiempirical equation of state for lithium from a small number of precise experimental data in the high-pressure and high-temperature region.

A comparison of the calculations with temperature and volume measurement data on the melting curve is given in Fig. 11. As distinct from the melting curves for aluminum, copper and lead which are monotonic (cf. Fig. 1), Figure 11a reveals the presence for lithium of a temperature maximum at $p\approx90$ kbar. This points to a phase transition to a more close-packed structure in the high-pressure region, the completion of this phase transition leading to the restoration of the normal shape of the melting curve. The results of calculations and of precision experimental measurements of the density of the solid and liquid phases along the melting curve presented in Fig. 11b demonstrate that the theory fully describes this high-accuracy ($\Delta V/V\approx0.01\%$) experiment.

Figure 12 shows the phase diagram of lithium on which are plotted experimental data on the compressibility of lithium upon dynamic loading to pressures of 700 kbar and temperatures of about 8000 K, and the calculated shock adiabat, isotherms and solid-liquid and liquid-vapor phase equilibrium curves.

The liquid-phase region of lithium has been studied best of all at high temperatures in static experiments. Figure 12a shows a comparison of the calculated and experimental data on the velocity of sound in liquid lithium against

the evaporation temperature, and Fig. 13 presents experimental data on the liquid density up to T=2000 K. The calculations of the liquid-vapor phase equilibrium curve yielded an accurate value of the evaporation temperature, T_c=1612 K, and critical-point parameters, p_c=954 bar, T_c=3940 K, V_c=10.3 cc/g, s_c=12.9 J/gK, which are in good agreement with estimates made on the basis of principles of thermodynamic similarity. This is indicative of the high degree of reliability of the equation of state obtained for lithium in the region of the liquid phase and near-critical states which is important from the standpoint of practical applications.

Conclusion

As revealed by the report wide-range EOS for aluminum, copper and lithium have been developed on the base of semiempirical model and available high pressure data. These EOS are suitable for a continuous (global) description of the thermodynamic properties of selected metals in solid, liquid and plasma states as well as in solid-liquid and liquid-vapor two-phase regions.

References

[1] A. V. Bushman and V. E. Fortov, Sov. Phys. Usp., **26**, 465 (1983).

[2] *Equations of State for Metals at High Energy Densities,* A. V. Bushman, I. V. Lomonosov, V. E. Fortov, Chernogolovka: Institute of Chemical Physics RAS, 1992, 196 pp. [in Russian].

[3] M. W. Guinan, D. J. Steinberg, J. Phys. Chem. Solids, **35,** 1501 (1974).

[4] J. Lees, B. H. Williamson, Nature, **208,** 278 (1965).

[5] P. W. Mirwald, G. C. Kennedy, J. Geophys. Res. Ser. B, **84,** 6750 (1979).

[6] L. V. Al'tshuler, A. P. Petrunin, Sov. Phys. - Tech. Phys., **6,** 516 (1961).

[7] T. Neal, Phys. Rev. Ser. B, **14,** 5172 (1976).

[8] J. R. Asay, J. Appl. Phys., **46,** 197 (1975).

[9] R. G. McQueen, S. P. Marsh, J. W. Taylor, J. N. Fritz, W. J. Carter, - In: High Velocity Impact Phenomena (1970)/ Ed. R.Kinslow. - New-York: Academic Press, p.293-417; appendies on pp. 515-568.

[10] A. A. Bakanova, I. P. Dudoladov, Yu. N. Sutulov, Zh. Prikl. Mekh. Tekhn. Fiz. **2,** 117 (1974) [in Russian] (J. Appl. Mech. Techn. Phys. **15,** 241 (1974)).

[11] J. R. Asay, D. B. Hayes, J. Appl. Phys., **46,** 4789 (1975).

[12] L. V. Al'tshuler, A. A. Bakanova, R. F. Trunin, Zh. Eksp. Teor. Fiz. **42,** 91-104 (1962) [in Russian] (Sov. Phys. - JETP **15,** 65-74 (1962)).

[13] L. V. Al'tshuler, B. S. Chekin, Metrology of high pulse pressures, In: Proceed. 1-st All-Union symposium of pulse pressures, Moscow: VNIIFTRI, V. **1**, 5 (1974) [in Russian].

[14] A. C Mitchell, W. J. Nellis, J. Appl. Phys., **52,** 3363 (1981).

[15] S. B. Kormer, A. I. Funtikov, V. D. Ulrin, A. N. Kolesnikova, Zh. Eksp. Teor. Fiz. **42,** 686-701 (1962) [in Russian] (Sov. Phys. - JETP **15,** 477-478 (1962)).

[16] L. V. Al'tshuler, S. B. Kormer, M. I. Brazhnik, L. A. Vladimirov, M. P. Speranskaya, A. I. Funtikov, Zh. Eksp. Teor. Fiz. **38(4),** 1061-1073 (1960) [in Russian] (Sov. Phys. - JETP **11(4),** 766-775 (1960)).

[17] T. Neal, J. Appl. Phys., **46,** 2521 (1975).

[18] A. D. Sakharov, R. M. Zaidel', V. N. Mineev, A. G. Oleinik, Dokl. Akad. Nauk SSSR, **159,** 1019 (1965).

[19] G. M. Gandel'man, Zh. Eksp. Teor. Fiz., **51,** 147 (1966) [in Russian] (Sov. Phys. JETP **24,** 99 (1967)).

[20] L. V. Al'tshuler, A. A. Bakanova, Usp. Fiz. Nauk, **96,** 163 (1968) [in Russian] (Sov. Phys. - Usp., **11,** 678 (1969)).

[21] R. F. Trunin, G. V. Simakov, M. A. Podurets, B. N. Moiseev, L. V. Popov, Izv. Akad. Nauk SSSR, Ser. Fizika Zemli, **1,** 13 (1971) [in Russian] (Bull. Acad. Sci. USSR, Phys. Solid Earth, **1,** 8 (1971)).

[22] B. L. Glushak, A. P. Zharkov, M. V. Zhernokletov, V. Ya. Ternovoi, A. S. Filimonov, V. E. Fortov, Sov. Phys. - JETP, **69**, 739 (1989).

[23] C. E. Ragan C.E. Phys. Rev. Ser. A, **25,** 3360 (1982).

[24] C. E. Ragan C.E. Phys. Rev. Ser. A, **29,** 1391-1402 (1984).

[25] L. V. Al'tshuler, N. N. Kalitkin, L. V. Kuz'mina, B. S. Chekin, Zh. Eksp. Teor. Fiz. **72(1),** 317-325 (1977) [in Russian] (Sov. Phys. - JETP **45(1),** 167-171 (1977)).

[26] G. V. Sin'ko, Teprofiz. Vis. Temp., **21,** 1041 (1983).

[27] A. F. Nikiforov, V. G. Novikov, V. B. Uvarov, Dokl. Akad. Nauk SSSR, **267,** 615 (1982) [in Russian] (Sov. Phys. - Dokl. **27**).

[28] S. B. Kormer, A. I. Funtikov, V. D. Ulrin, A. N. Kolesnikova, Zh. Eksp. Teor. Fiz. **42,** 686-701 (1962) [in Russian] (Sov. Phys. - JETP **15,** 477-478 (1962)).

[29] V. A. Simonenko, N. P. Voloshin, A. S. Vladimirov, A. P. Nagibin, V. N. Nogin, V. A. Popov, V. A. Sal'nikov, Yu. A. Shoidin, Sov. Phys. - JETP, **61**, 869 (1985).

[30] V. E. Fortov, A. N. Dremin, A. A. Leont'ev, Teplofiz. Visok. Temper., **13,** 1072 (1975) [in Russian].

[31] D. A. Young, B. A. Alder, Phys. Rev. Ser. A, **3,** 1439 (1971).

[32] D. A. Young, Report UCRL-52352, Univ. of California, Livermore (1977).

[33] E. Morris, AWRE Report 067/64, UKAEA, London (1964).

[34] E. I. Gol'tsova, Teplofiz. Visok. Temper., **3,** 483 (1965) [in Russian].

[35] R. R. Boade, J. Appl. Phys., **39,** 5693-5702 (1968).

[36] L. V. Al'tshuler, A. V. Bushman, M. V. Zhernokletov, V. N. Zubarev, A. A. Leont'ev, V. E. Fortov, Zh. Eksp. Teor. Fiz. 78, 741-760 (1980) [in Russian] (Sov. Phys. - JETP 51(2), 373-383 (1980)).

[37] R. F. Trunin, A. B. Medvedev, A. I. Funtikov, M. A. Podurets, G. V. Simakov, A. G. Sevast'yanov, Zh. Eksp. Teor. Fiz. **95,** 631-641 (1989) [in Russian] (Sov. Phys. - JETP **68(2),** 356-361 (1989)).

[38] Ph. de Beaumont, J. Leygonie, In: Fifth Symp. on Detonation. - Washington: U.S.Government Printing Office, 430-439 (1970).

[39] N. N. Kalitkin, L. V. Kuz'mina, Preprint No. 35, Inst. of Applied Mathem. of USSR Acad. Sci., Moscow (1975) [in Russian].

[40] R. F. Trunin, M. A. Podurets, G. V. Simakov, L. V. Popov, B. N. Moiseev, Zh. Eksp. Teor. Fiz., **62(3),** 1043-1048 (1972) [in Russian] (Sov. Phys. - JETP **35(3),** 550-552 (1972)).

[41] L. V. Al'tshuler, A. A. Bakanova, A. V. Bushman, I. P. Dudoladov, V. N. Zubarev, Zh. Eksp. Teor. Fiz., **73(11),** 1866-1872 (1977) [in Russian] (Sov. Phys. - JETP **46(5),** 980-983 (1977)).

[42] A. D. Kirshenbaum, J. A. Cahill, A. V. Grosse, J. Inorg. Nucl. Chem., **22,** 33 (1961).

[43] E. E. Spil'rain, K. A. Yakimovich, E. E. Totoskii, D. L. Timrot, V. A. Fomin, *Teplofizicheskie svoistva shelochnikh metallov (Thermphysical Properties of Alkali Metals),* ed. by V. A. Kirillin, Moscow: Izdatel'stvo Standartov, 1970 [in Russian].

[44] H. D. Luedemann, G. C. Kennedy, J. Geophys. Res., **73,** 2795 (1968).

[45] I. N. Makarenko, A. M. Nikolaenko, S. M. Stishov, Zh. Eksp. Teor. Fiz., **74,** 2175 (1978) [in Russian] (Sov. Phys. - JETP, **47,** 1132 (1978)).

[46] A. A. Bakanova, I. P. Dudoladov, R. F. Trunin, Fizika Tverd. Tela, **7(6),** 1615-1622 (1965) [in Russian] (Sov. Phys. - Solid State, **7,** 1307 (1965)).

[47] *LASL Shock Hugoniot Data /* Ed. S.P.Marsh. - Berkeley: Univ. of California Press, 1980.

[48] I. I. Novikov, Yu. S. Trelin, T. A. Tsyganova, Teplofiz. Visok. Temper., **7,** 1220 (1969).

[49] E. I. Gol'tsova, Teplofiz. Visok. Temper., **4,** 360 (1966).

[50] V. V. Gogoleva, L. R. Fokin, Preprint No. IVTAN 1-061, Moscow: IVT AN SSSR, 1981 [in Russian] (Report Inst. of High Temper., USSR Acad. Sci.).

Appendix: Pictures to Report

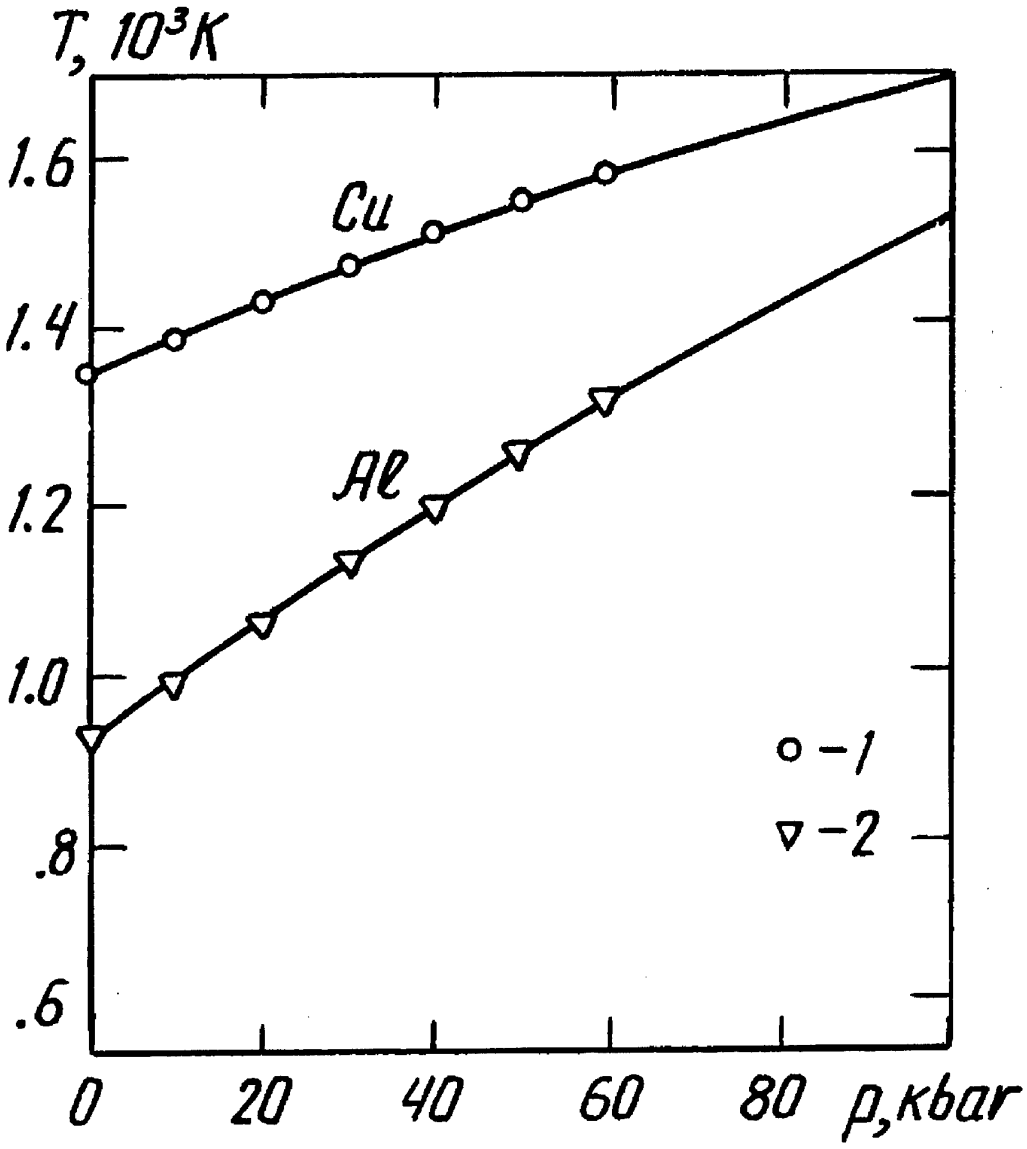

Fig. 1. Melting curves for aluminum and copper. Experimental data: 1 - [4], 2- [5].

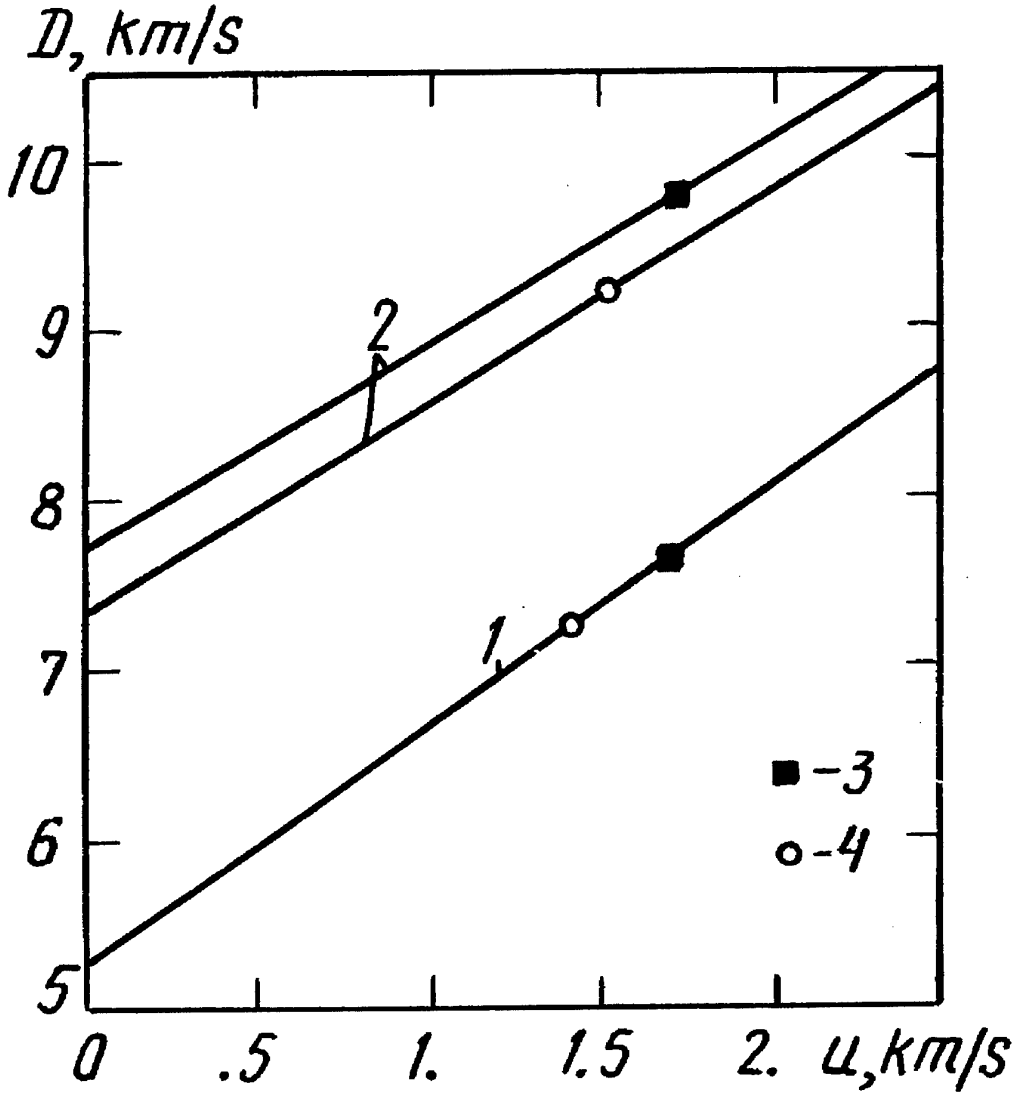

Fig. 2. Velocity of incident shock wave (1) and reflected shock waves (2) in aluminum. Experimental data: 3 - [6], 4 - [7].

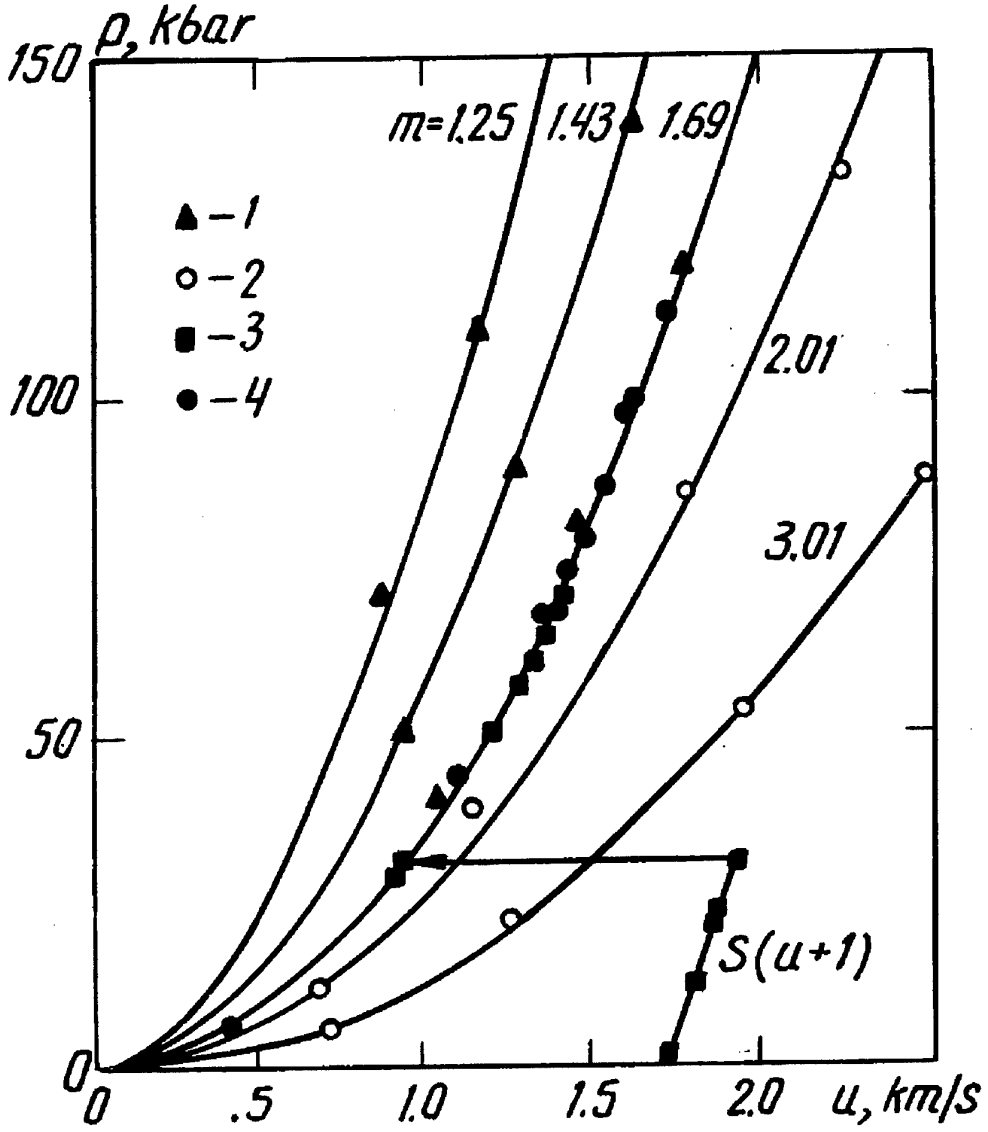

Fig. 3. Porous Hugoniots (m) and release isentrope (S) for aluminum. Experimental data: 1 - [9], 2 - [10], 3 - [8], 4 - [11].

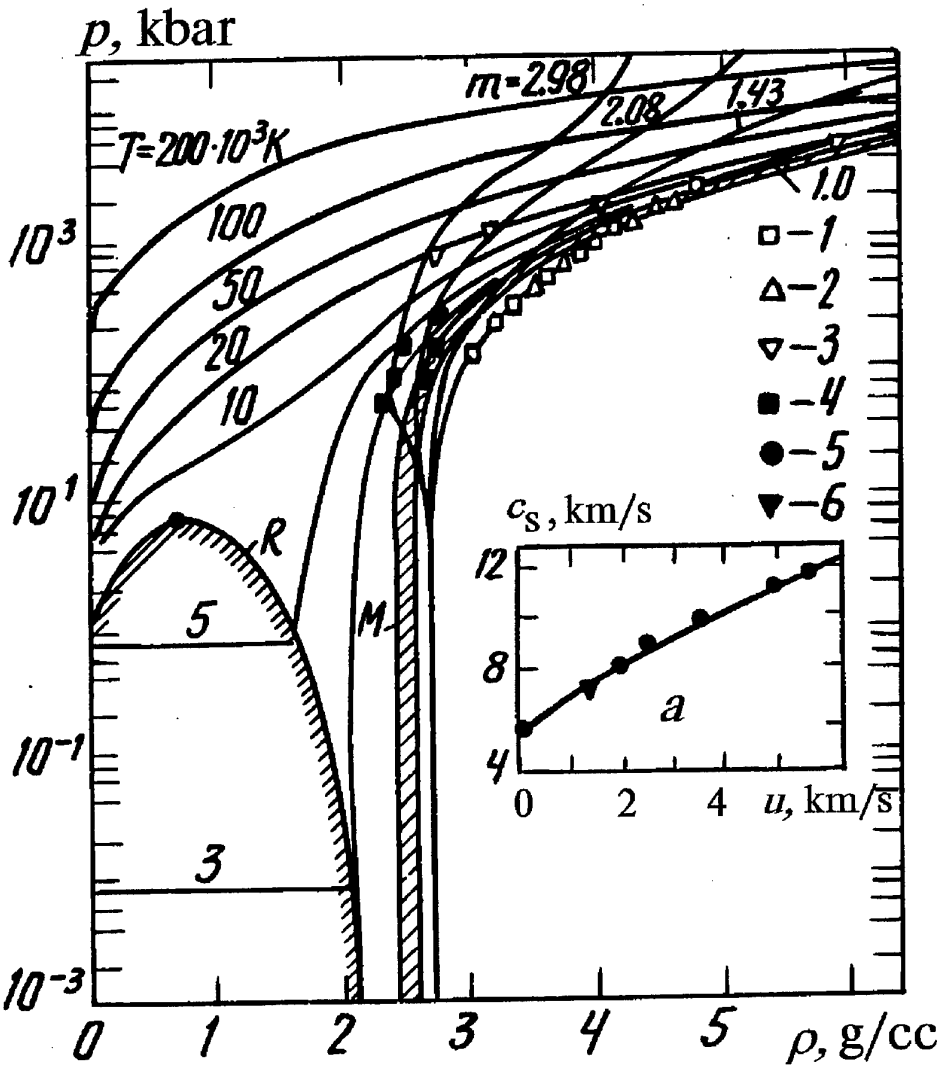

Fig. 4. Phase diagram for aluminum. T, isotherms; m, porous Hugoniots; M, melting region; R, liquid-vapor equilibrium curve. (a) The sound velocity in shocked aluminum. Experimental data: 1 - [12,13], 2 - [14], 3 - [15], 4 - [10], 5 - [16], 6 - [17].

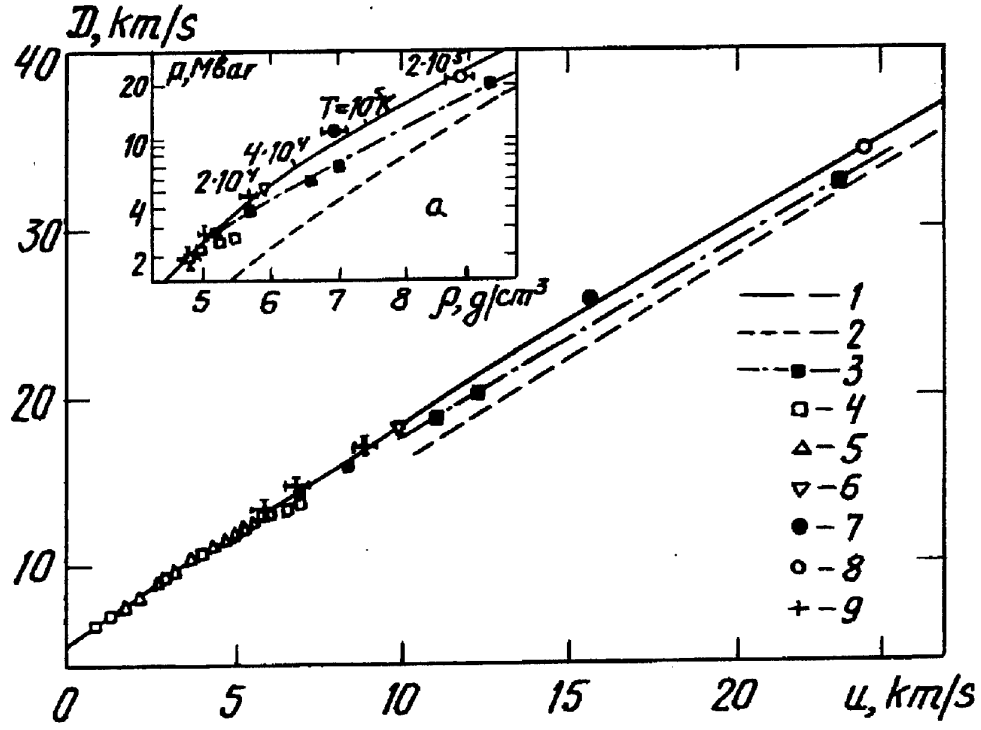

Fig. 5. Shock adiabat for aluminum at ultrahigh pressures. Calculations: 1 - this EOS, 2 - from Thomas - Fermi model with corrections [25], 3 - interpretation of nuclear-explosion data with quartzite standard, calculated by Thomas - Fermi model [25]. Experimental data: 4 - [12,13], 5 - [14], 6 - [28], 7 - [29], 8 - [23], 9 - [22].

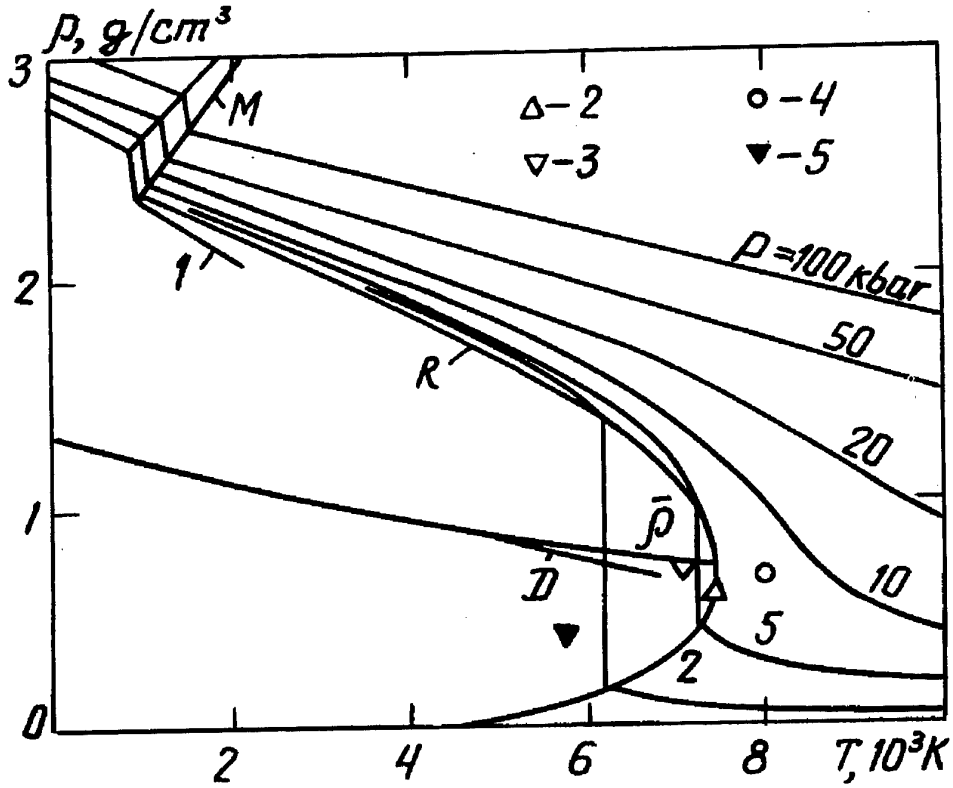

Fig. 6. Phase diagram for aluminum in the region of lower temperatures. P, isobars; M, melting region; R, liquid-vapor equilibrium curve; D, rectilinear diameter; $\bar{\rho}$, half-sum of liquid and vapor densities. 1 - data from measuring the liquid-metal density at p=1 bar [34]; evaluations of the critical-point parameters: 2 - [33], 3 - [31], 4 - [30], 5 - [32].

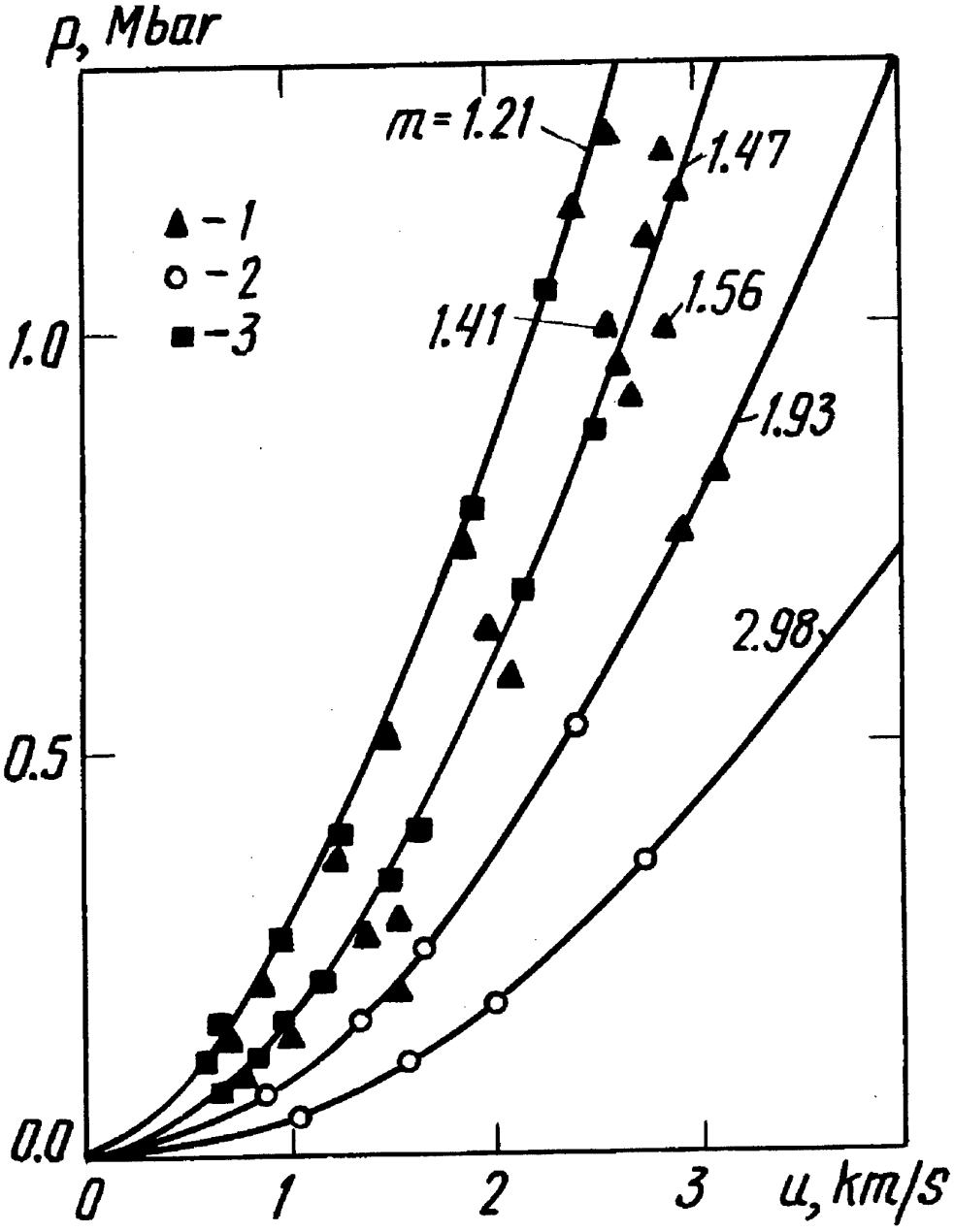

Fig. 7. Shock adiabats for porous copper. Designations are the same as in Fig. 3, except that the experimental data shown as 3 come from Ref. [35].

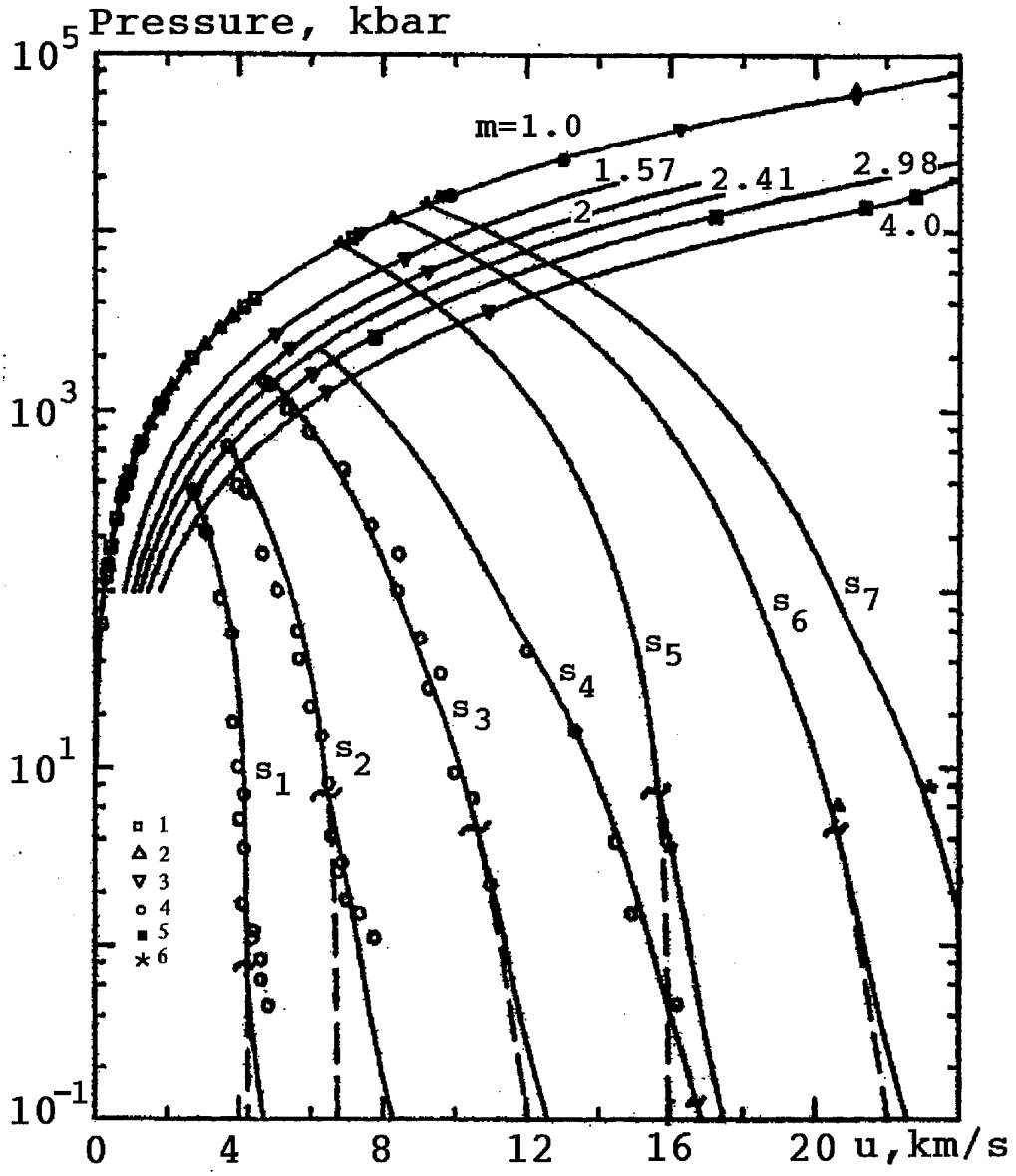

Fig. 8. Shock adiabats (m) and release isentropes (S) for copper. Calculations: solid lines, equilibrium states; dashed lines, metastable states. Experimental data: 1 - [12,13], 2 - [14], 3 - [15], 4 - [36], 5 - [37], 6 - [38].

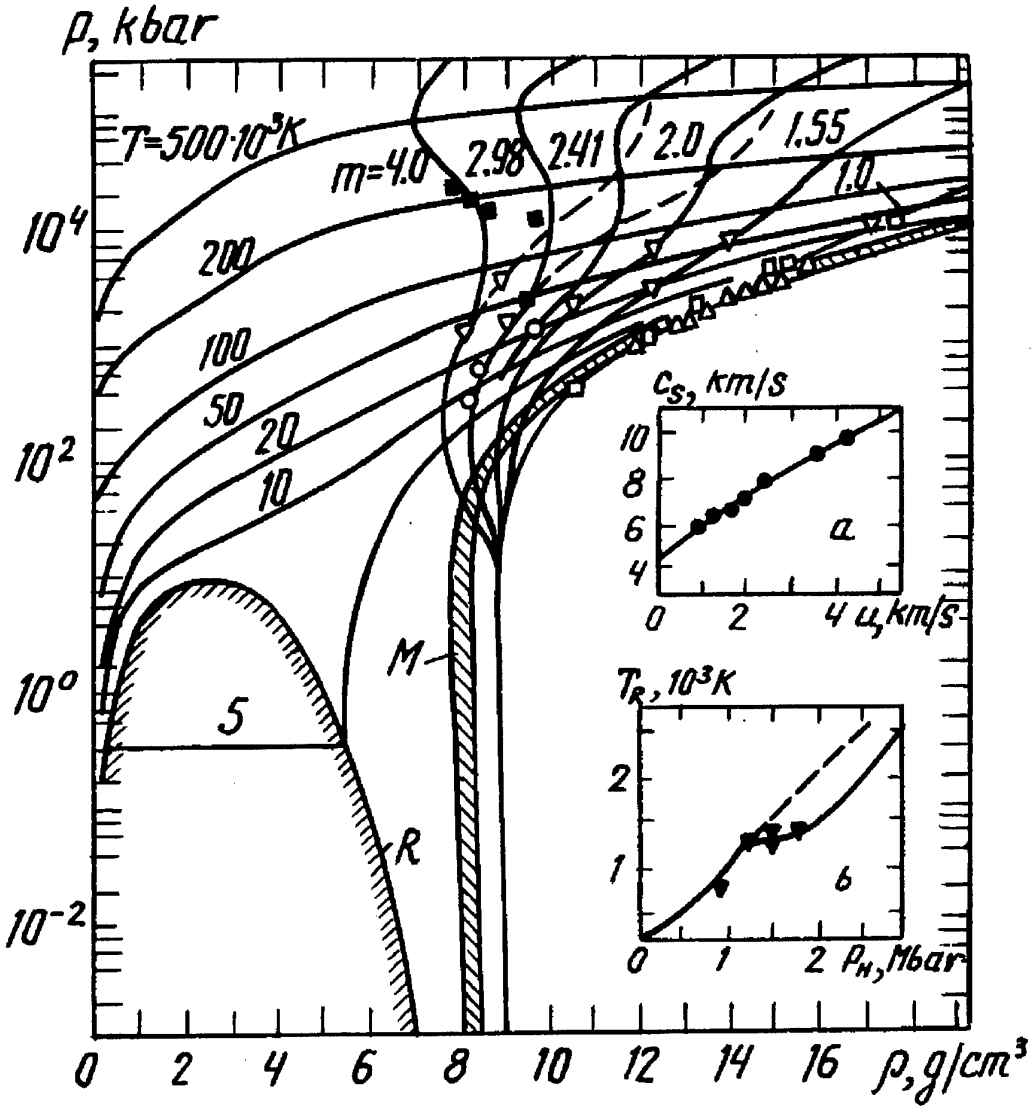

Fig. 9. Phase diagram for copper. Designations are the same as in Fig. 4, except that the experimental data shown: 4 - [37], 6 - [41]. The dashed lines represent the interpretation of shock adiabats from the corrected Thomas-Fermi model [39]. (a) Velocity of sound in shocked copper; (b) residual temperature in the isentropic release wave, the dashed line representing the calculation of Ref. [9] in which melting is ignored.

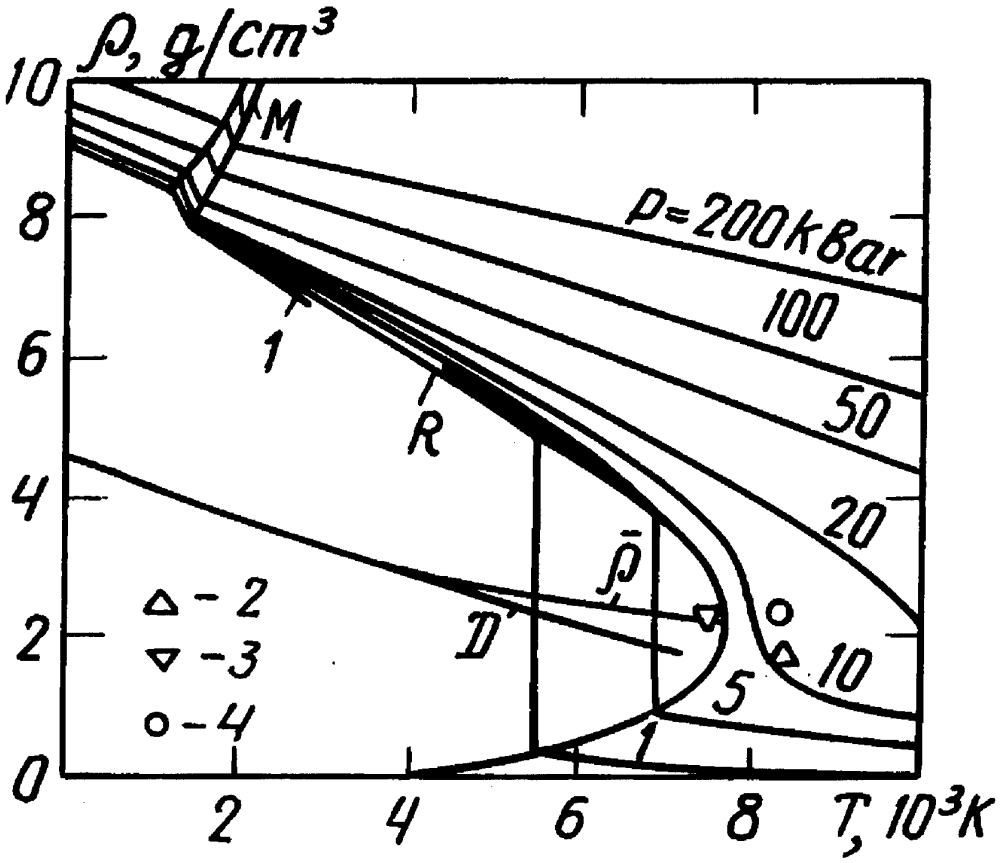

Fig. 10. Phase diagram for copper in the region of lower temperatures. Designations are the same as in Fig. 6, except that the data shown at 1 come from Ref. [42].

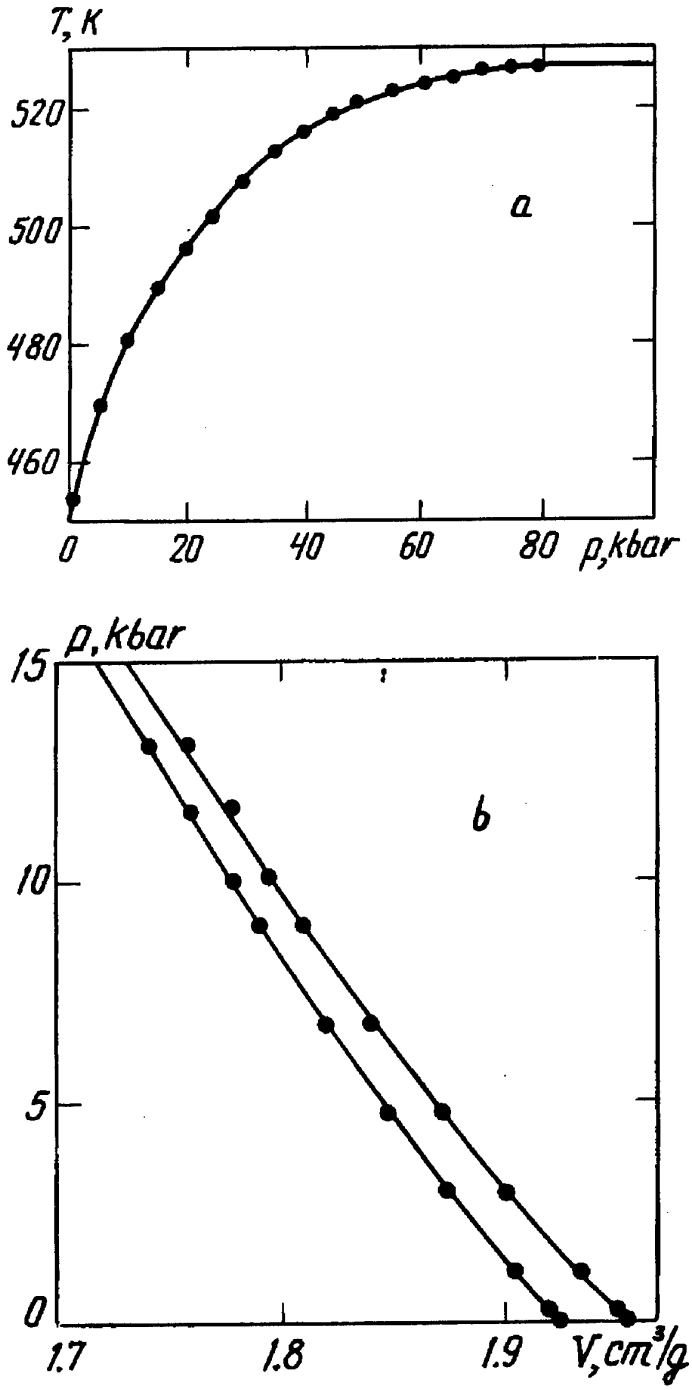

Fig. 11. Temperature (a) and density (b) on the lithium melting curve. Points represent the experimental data: (a) from Ref. [44], (b) from Ref. [45].

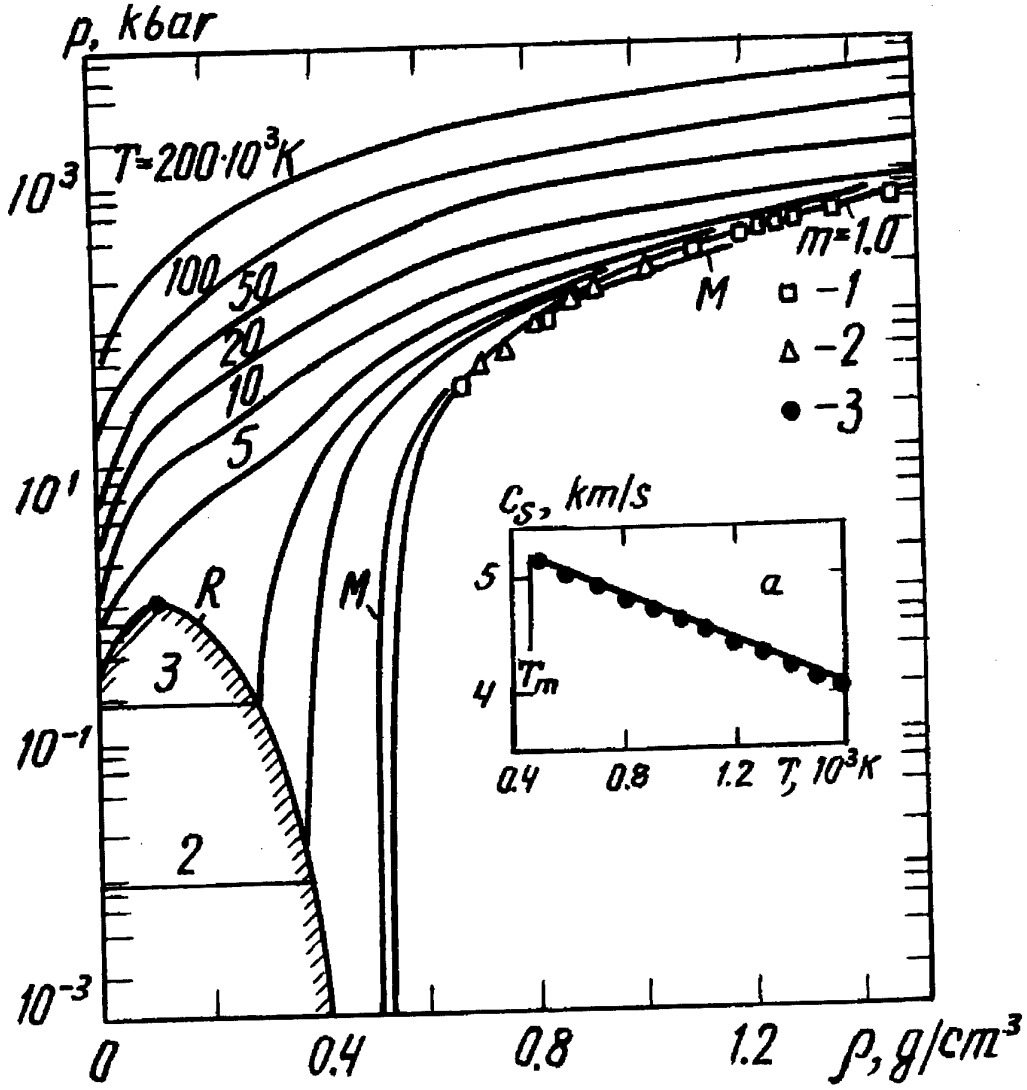

Fig. 12. Phase diagram for lithium. Designations are the same as in Fig. 4, except that the data: 1 - [46], 2 - [47], 3 - [48]. (a) velocity of sound in liquid lithium.

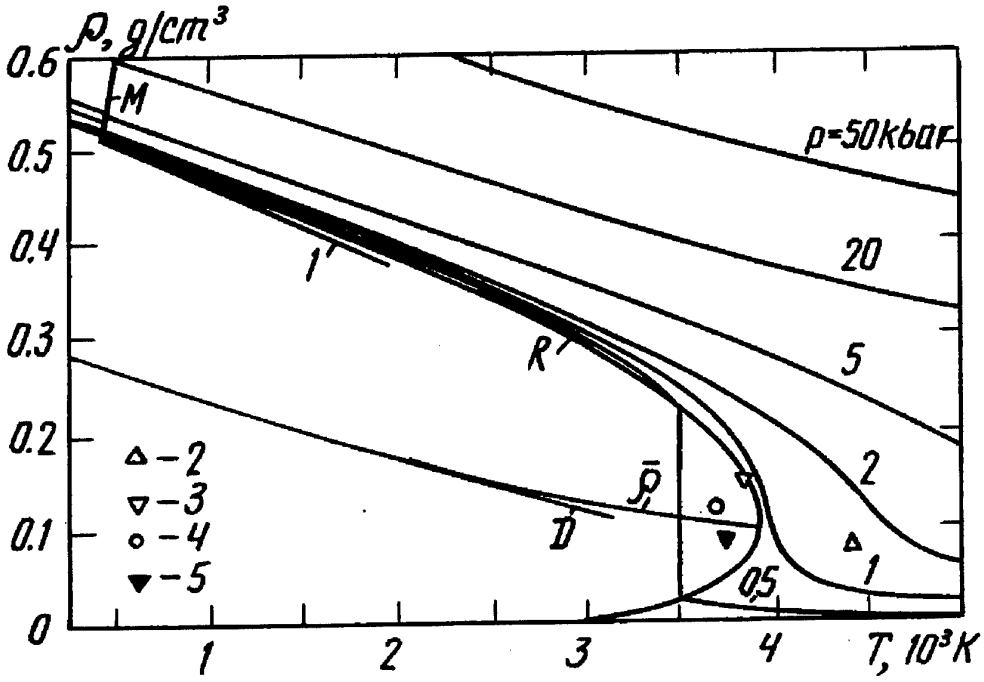

Fig. 13. Phase diagram for lithium in the region of lower temperatures. Designations are the same as in Fig. 6, except: 1 - [49], 4 - [50].